8-2019

# Development of Peptides for Enantioselective Hypervalent Iodine(III)-Mediated Chemistry and Functional Materials for Environmental Remediation

Maria I. Swasy
*Clemson University*, mswasy@g.clemson.edu

# DEVELOPMENT OF PEPTIDES FOR ENANTIOSELECTIVE HYPERVALENT IODINE(III)-MEDIATED CHEMISTRY AND FUNCTIONAL MATERIALS FOR ENVIRONMENTAL REMEDIATION

---

A Dissertation
Presented to
the Graduate School of
Clemson University

---

In Partial Fulfillment
of the Requirements for the Degree
Doctor of Philosophy
Chemistry

---

by
Maria I. Swasy
August 2019

---

Accepted by:
Dr. Daniel C. Whitehead, Committee Chair
Dr. Dev P. Arya
Dr. Leah Casabianca
Dr. Modi Wetzler

ABSTRACT

Within the field of asymmetric catalysis, many researchers have been inspired by the multifaceted structures and corresponding catalytic activity and selectivity of enzymes. One approach to mimicking the important characteristics of enzymes is to develop peptide-based catalysts for asymmetric transformations. Peptides containing even a small number of amino acids are able to provide an environment, rich with chiral information, that is adequate for the transfer of chirality. The overall goal of the presented research is to combine peptide-mediated asymmetric catalysis with hypervalent iodine (HI) chemistry in order to develop new and highly modular peptide catalysts for a variety of HI-mediated enantioselective transformations. HI compounds are recognized as valuable and attractive reagents due to their mild reactivity, high selectivity, and commercial availability as oxidants and electrophiles, while also reducing the overall negative environmental impact of these transformations. In particular, the emergence of catalytic and enantioselective processes with iodine(III) species is starting to make these compounds competitive with metal catalysts. Thus, one could imagine that the incorporation of an iodine(III) active site, such as an iodoarene moiety, into a peptide scaffold would result in asymmetric catalysts well suited for organic transformations such as the α-oxytosylation of propiophenone and oxylactonization of 5-oxo-5- phenylvaleric acid. While, these two reactions represent broadly studied catalytic iodine(III)-mediated transformations, they have yet to reach synthetically useful levels of enantioselectivty.

The second part of this dissertation pivots to focus on the implementation of functional materials for environmental remediation techniques, such as, the capture of

volatile organic compounds and pesticide degradation. Polyethylenimine (PEI) functionalized kaolinite clay was successfully prepared, characterized, and assessed for the remediation of volatile organic compounds (VOCs). A gas chromatographic vapor capture assay evaluated the capability of unmodified and modified clay material to capture representative aldehyde, carboxylic acid, and sulfur VOCs in a laboratory setting. Unmodified kaolinite clay was moderately effective at remediating these VOCs, while the amine functionalized kaolinite was exceptionally successful at selectively capturing organics in the vapor phase. Further, a series of amine-functionalized cellulose nanocrystal materials were successfully synthesized, characterized, and evaluated for the remediation of pesticide contaminants from organic and aqueous media. Their ability to degrade malathion in organic systems has been examined, resulting in up to 100% degradation of malathion into detectable lower molecular weight by-products. A poly(ethyleneimine)-grafted cellulose nanocrystal material was also effective at degrading malathion, deltamethrin, and permethrin in aqueous systems with 100%, 95%, and 50% reduction, respectively. Thus, these materials can potentially serve as a new and viable remediation technique based on their ability to effectively degrade various pesticides. The reusability of the amine-modified cellulose nanomaterial was also explored.

# DEDICATION

This dissertation is dedicated to my parents, Roger and Barbara W. Swasy for their never ending love, support, and dedication in support of my goals.

LIST OF ABBREVIATIONS

| | |
|---|---|
| Å | Angstrom |
| Aq | Aqueous |
| °C | Degrees centigrade |
| cat | Catalytic |
| COSY | Correlation Spectroscopy |
| d | doublet |
| DIPEA | Diethylisopropylamine |
| DMF | N, N'-Dimethylformamide |
| DMSO | Dimethylsulfoxide |
| equiv | Equivalent(s) |
| ee | Enantiomeric excess |
| EPA | Environmental Protection Agency |
| EtOAc | Ethyl acetate |
| g | Gram |
| GC | Gas Chromatography |
| HBTU | *O*-(Benzotriazol-1-yl)-*N*,*N*,*N*′,*N*′-tetramethyluronium hexafluorophosphate |
| HFIP | Hexafluoroisopropanol |
| h | hour(s) |
| HI | Hypervalent Iodine |
| HPLC | High pressure liquid chromatography |
| HRMS | High resolution mass spectrum or spectrometry |
| i-PrOH | Isopropanol |
| IR | Infrared spectroscopy |
| LUMO | Lowest unoccupied molecular orbital |
| MALDI | Matrix Assisted Laser Desorption/Ionization |
| MeOH | Methanol |
| Mg | Milligram |
| mol | Moles |
| mmol | Milli moles |
| mp | Melting point |
| MS | Mass spectrometry |
| m | multiplet |
| MW | Molecular Weight |
| m/z | Atomic mass units per charge |
| NMR | Nuclear Magnetic Resonance |
| NOE(SY) | Nuclear overhauser effect (spectroscopy) |
| NOx | Nitrogen Oxides |
| PAN | Peroxy acetyl nitrate |
| q | Quartet |
| rt | Room temperature |
| TFA | Trifluoroacetic acid |
| TFE | 2,2,2-Trifluoroethanol |
| t | triplet |

| | |
|---|---|
| THF | Tetrahydrofuran |
| $Et_3N$ | Triethyl amine |
| TLC | Thin layer chromatography |
| TOF | Time of Flight |
| VOCs | Volatile Organic Compounds |

TABLE OF CONTENTS

Page

LIST OF TABLES

LIST OF SCHEMES

Scheme

LIST OF FIGURES

# CHAPTER ONE

# INTRODUCTION AND REVIEW OF ASYMMETRIC PEPTIDE CATALYSIS AND HYPERVALENT IODINE CHEMISTRY

## *1.1.1. Introduction*

Organocatalysis is a synthetic technique used to facilitate chemical transformations through the use of substoichiometric amounts of metal-free organic reagents. Recently, hypervalent iodine (HI) compounds have emerged as valuable and versatile organocatalysts due to their ability to successfully catalyze a wide array of chemical reactions. The main attraction of HI compounds derives from their ability to act as viable alternatives to heavy metals due to their inexpensive cost, environmentally benign nature, and similar reactivity patterns in comparison to toxic transition metals. In the last decade, considerable attention has been focused on utilizing HI reagents and catalysts in several synthetically useful electrophilic and oxidative reactions. Nevertheless, a common difficulty has been promoting these types of transformations in a highly reactive and enantioselective fashion. Our strategy to impart enantiocontrol in these reactions is to attach the active iodane site to molecular architecture bearing chiral information, such as a short peptide sequence consisting of 5 to 6 amino acids residues. Peptides can serve as an advantageous source of ligands and organocatalysts for a variety of organic transformations. Their modularity and facile preparation following standard Fmoc-solid-phase peptide synthesis (SPPS) techniques facilitates the synthesis and evaluation of numerous catalyst structures in a timely manner. The intention of this chapter is to provide

an introduction to the flourishing fields of peptide-mediated asymmetric catalysis as well as hypervalent iodine chemistry.

*1.1.2. Asymmetric Synthesis*

There is an undeniable demand for methods focused on the synthesis of chiral compounds in their single enantiomeric form. Industries, such as, pharmaceutical, agrochemical, fragrance, materials, *etc*. have an increased need for synthetic protocols in which the formation of one stereoisomer is favored over the other. Of note, upwards of two-thirds of all pharmaceuticals are chiral, with many being prescribed as a single enantiomer. This, in addition to the importance of chirality in biological systems, makes the efficient production of enantiomerically pure compounds a prime goal in synthetic organic chemistry.[1-11]

Traditionally, enantiomerically pure compounds are acquired via chemical transformations of enantioenriched substrates or by the resolution of racemic mixtures. While successful, these approaches are not ideal due to the need for stoichiometric amounts of substrate and maximum yields around 50% of the preferred enantiomer, respectively.[2-4] The emergence of asymmetric catalysis offers a suitable and effective alternative by employing a chiral catalyst that controls the formation of one stereoisomer during the course of a reaction with a non-chiral substrate. The obvious advantage of this method over a non-catalytic alternative is the regeneration of substoichimetric amounts of the catalyst, resulting in decreased waste and higher atom economy.[2-6]

Asymmetric catalysis has the potential to yield a myriad of chiral products in high yields and enantiomeric excesses (*ee*). Regarded as the two most prevailing facets of

asymmetric catalysis, enzyme- and transition metal-mediated catalysis are widely applied for the generation of chiral organic products.[1-6] Nature has beautifully evolved enzymes with the ability to catalyze chemical transformations in a highly reactive and selective fashion. This can partially be attributed to their well-defined, folded structures. These folded structures help to orient the substrate of interest within the enzyme, creating a preorganized and thus highly stable transition state. The subsequent transformation is then promoted by a few amino acid catalytic residues that are embedded within the active site of the enzyme. Generally, chiral biological molecules are synthesized in living cells by enzymes by means of an asymmetric catalysis mechanism. Chemists also employ enzymes or even whole cells to synthesize these chiral compounds. Further, such biological catalysis is increasingly used on an industrial scale and is particularly preferred in hydrolytic reactions.[5,6,9]

Beyond biological catalysis, transition metal catalysts have proven to be exceptionally useful for asymmetric transformations. Historically, however, not all reported catalytic asymmetric transformations rivals the levels of selectivity characteristic of chiral information transfer in enzymatic catalysis. This reality was challenged in the early 1970s by William Knowles and co-workers, upon their disclosure detailing the use of rhodium complexes containing chiral phosphine ligands to catalyze the addition of $H_2$ selectively to one face of a prochiral olefinic substrate, so generating a new chiral C—H center. This method was later used for the commercial production of the anti-Parkinson drug, *L*-dopa, as well as many other laboratory and industrial scale processes. This as well as other noteworthy advances from Ryoji Noyori and K. Barry Sharpless were recognized

in 2001 with the Nobel Prize in Chemistry, for their work on catalytic asymmetric hydrogenation and catalytic asymmetric oxidation, respectively.[1-4] Collectively, their work toward highly enantioselective reactions benchmarked the synthetic utility and practicality of enantioselective catalysis in the context of synthetic organic chemistry. However, transition metal catalysis comes with its own unique issues as it has the potential to leave traces of toxic heavy metals in the product.

*1.1.3. Asymmetric Organocatalysis*

Defying the traditional view of using metal complexes or enzymes for efficient asymmetric catalysis, organocatalysts have emerged as a contending third option for highly selective catalytic transformations. Asymmetric organocatalysis is described as the use of small, purely organic molecules as catalysts to effect organic transformations in an enantioselective fashion.[9-12] The implementation of organocatalysts has not only enriched the field of asymmetric catalysis; it has also provided a highly attractive alternative. In comparison to enzymes, small organic catalysts tolerate a broader range of solvents and substrates. Organocatalysts are also generally less-toxic and less-sensitive towards oxidation and moisture as compared to organometallic reagents. [9-12]

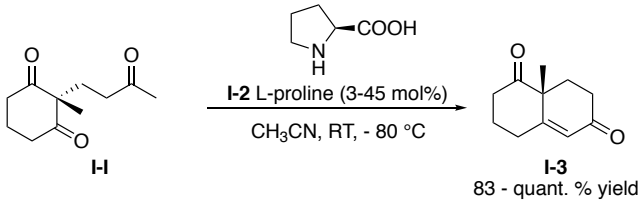


**Scheme 1.1.** Hajos-Parrish-Sauer-Wiechert protocol for the symmetric intramolecular reaction of di- and tri-ketones, such as, compound **I-I**.

The emergence of synthetically useful asymmetric organocatalysis can be benchmarked in 1971 by the concomitant reports of Eder *et al*. and Hajos and co-workers, wherein L-proline was employed as a catalyst for intramolecular asymmetric aldol reactions. The aptly named Hajos-Parrish-Eder-Sauer-Wiechert protocol was used to promote the cyclization of di- and tri-ketones to generate the corresponding diketones in high yield and enantiomeric excess (Scheme 1.1).[13-15] This pioneering work was followed by further examples of intramolecular aldol reactions, such as the D-proline-catalyzed aldol reaction toward the synthesis of erythromycin disclosed by Woodward.[16-18] Despite this discovery, over three decades passed before proline and proline derivatives were successfully applied as catalysts for intermolecular reactions. This application prompted the spectacular growth of these organocatalysts as one of the most widely applied and versatile scaffolds in the field. Barbas, Lerner, and List initially disclosed an intermolecular aldol reaction wherein acetone participated in an aldol condensation with aryl- and alkyl-substituted aldehyde acceptors. Upon the addition of 30 mol % proline (**I-2**), the desired aldol products were obtained in moderate to excellent yields (*i.e*. 54–97%) and enantioselectivities ranging from 60 to 96% *ee* (Scheme 1.2).[19] The significance of proline-catalyzed reactions was continually highlighted following numerous reports for asymmetric transformations beyond aldol condensations including Mannich reactions, amination, aminoxylation, and Michael additions. [17-25]

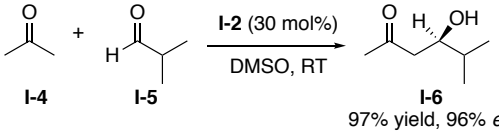


**Scheme 1.2.** Asymmetric intermolecular aldol reaction reported by List *et al.*

MacMillan also reported a method detailing the use of chiral imidazolidinone

**I-9**, for the iminium-type catalytic asymmetric Diels-Alder reaction between cyclopentadiene **I-7** and cinnamaldehyde **I-8** (Scheme 1.3). This report, in conjunction with L-proline catalysis, helped to launch the field of asymmetric organocatalysis as well as reinforce these strategies as viable synthetic routes by providing thoroughly investigated mechanistic insight. Today many synthetic chemistry groups are actively working in this field, resulting in numerous examples of powerful and noteworthy examples of organocatalysts, such as, cinchona alkaloids, MacMillan's imidazolidinones, Jacobsen's thiourea catalysts, DMAP catalysts reported by Fu *et al.,* and Shi and Yang's catalysts for asymmetric epoxidations.[26-38]

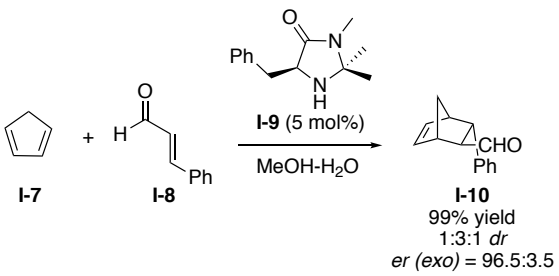


**Scheme 1.3.** Asymmetric Diels-Alder reaction catalyzed by imidazolidinone **I-7**.

*1.1.4. Peptides in Asymmetric Catalysis*

Within the field of asymmetric catalysis, many have been inspired by the multifaceted structures and corresponding catalytic activity and selectivity of enzymes.[39-42] The individual building blocks of peptides, *i.e.* amino acids, have provided routes to several attractive organic transformations in asymmetric synthesis, as both auxiliary scaffolds and catalysts. Landing in the middle of the catalyst size gamut, peptides composed of two to ten amino acids have emerged as simple, yet still well-defined chiral catalysts for various enantioselective methods.[43-49]

One of the first examples was reported in the early 1980s when Inoue and co-workers demonstrated the use of a diketopiperazine cyclo(Phe-His) dipeptide for the

catalytic cyanation of benzaldehyde (Scheme 1.4A).[50] Soon after, the Juliá-Collona epoxidation was disclosed, wherein polymers of leucine or alanine were employed as asymmetric catalysts for the epoxidation of chalcones (Scheme 1.4B). Mechanistic investigations for this transformation ultimately revealed two possible enantioinduction models: 1) transfer of chiral information via H-bond interactions between the substrate the N-terminal amide protons of the polypeptide α-helix, or 2) an H-bond promoted binding between the peroxide nucleophile and the peptide. Regardless, the peptide is able to transfer chirality to the chalcone by means of a non-covalent mechanism.[51,52] Despite this intriguing work, the use of peptides as asymmetric catalysts remained rather dormant for almost two decades. In 1998, Miller et al. disclosed a methylimidazole-containing peptide catalyst for the asymmetric kinetic resolution of alcohols, ultimately, providing excellent enantioselectivities (Scheme 1.4C).[53] This contribution from Miller's group helped establish the use of peptides as asymmetric catalysts as an intriguing area research. Throughout the past 30 years, an array of new and exciting peptide catalyst structures have been reported, and cannot be thoroughly reviewed here.[53-56] Therefore, a brief summary of select reactions are discussed below.

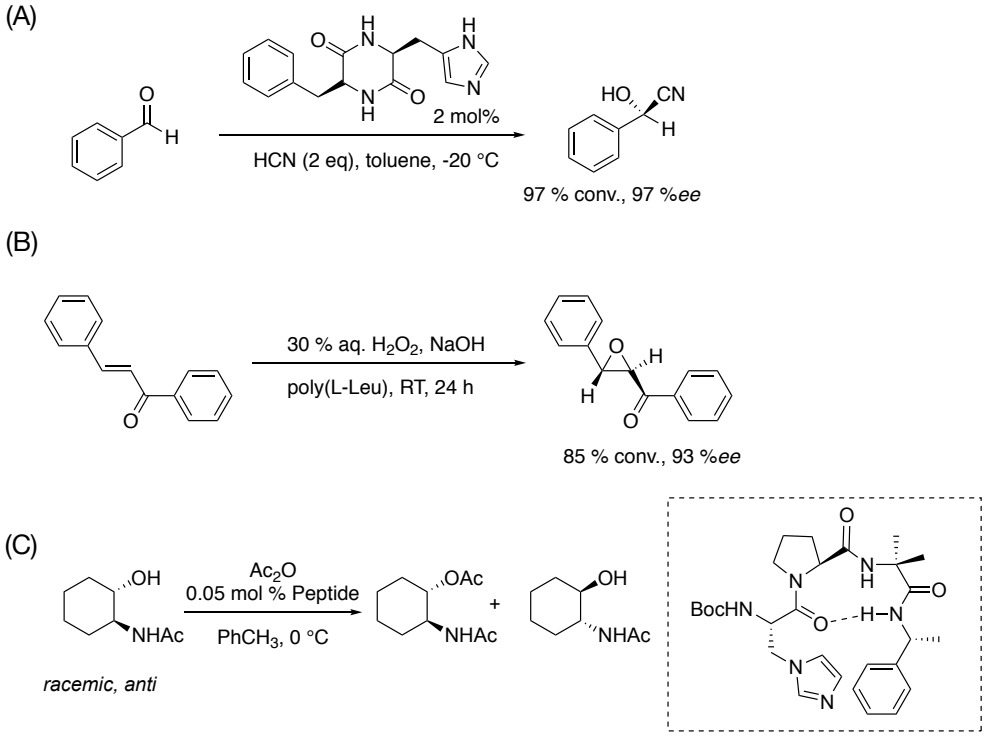


**Scheme 1.4.** Initial reports for asymmetric peptide catalyzed reactions: (A) The asymmetric cyanation of benzaldehyde to a cyanohydrine (B) the enantioselective epoxidation of chalcones. (C) Peptide-mediated kinetic resolution of alcohols.

*Peptide-Mediated Asymmetric Epoxidations*

Beyond Juliá and Colonna's disclosure of poly(alanine) and poly(leucine) catalysts, many have reported improved reaction conditions and solid-supported peptide catalysts for asymmetric epoxidations. Originally, this epoxidation protocol only tolerated substrates that were not sensitive to the highly basic conditions provided by the triphasic reaction system of an organic solvent, an aqueous basic oxidant, and an insoluble homo-oligopeptide.[51,52] Thus, there was a need for milder and more environmentally benign reaction conditions that also tolerate a wider substrate scope.[57] Initially, the scope of this reaction was expanded to include enones substituted with one aromatic moiety, such as subtrate **I-11**, when Roberts and coworkers employed a biphasic system of an urea-$H_2O_2$ terminal oxidant in THF (Scheme 1.5A).[58] Previously, substrates such as enolizable ketones and other aqueous base-sensitive starting materials could not be used in the presence of excess oxidant and NaOH base. This resin-bound peptide catalyst **I-12** could also be recycled following a regeneration protocol consisting of washing with 4 M NaOH and a small addition of fresh catalyst (10% of the original catalyst weight). Itsuno *et al*. also reported a recyclable solid-supported polyamino acid for

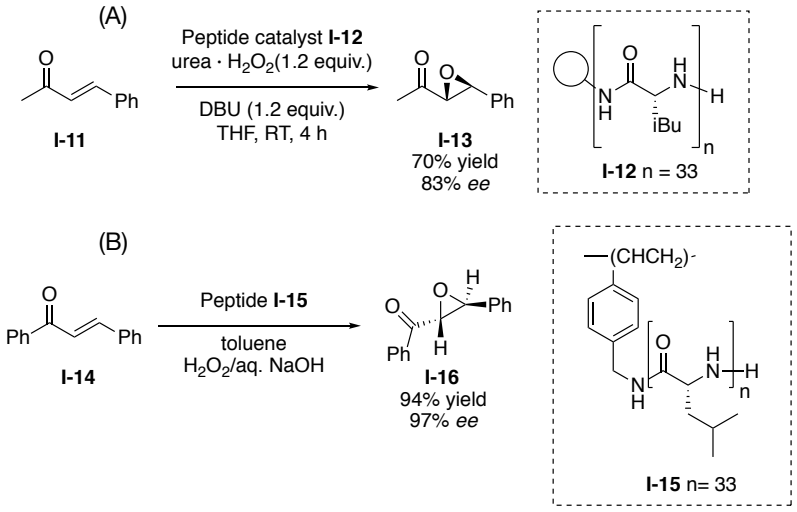


**Scheme 1.5.** Polymer supported peptide catalysts for the asymmetric epoxidation of alkenes reported by (A) Roberts *et al.* and (B) Itsuno *et al*.

the enantioselective epoxidation of chalcones and α, β-unsaturated carbonyl compounds.[59] They prepared poly(L-leucine) cross-linked with amino methylated polystyrene, which provided the desired enantioenriched epoxide product **I-16** in 94% yield and 97% *ee* (Scheme 1.5B). The resin-supported catalyst could be recovered and reused for up to 12 cycles, while maintaining a 94% *ee* of product **I-16**.

Later, peptide oxidation catalyst **I-18** was reported by Miller and co-workers. This catalyst was designed around a known $\beta$-turn peptide sequence to include an aspartic acid residue necessary for formation of the reactive peracid **I-18'**. This protocol tolerated a variety of urethane-substituted olefins, such as **I-17**, which in the presence of DIC, hydrogen peroxide, and DMAP was easily converted to epoxide **I-19** in a 99% yield (Scheme 1.6).[56] Lastly, a resin supported oligo-L-Leu-peptide **I-21** was disclosed by Kudo for the enantio- and diastereoselective epoxidation of $\alpha,\beta$-unsaturated aldehydes (**I-20**). The introduction of a sterically bulky and hydrophobic amino acid residue, such as 3-(1-pyrenyl)alanine, led to increased rate and enantioselectivity in aqueous media (Scheme 1.7) .It was also noted that peptide catalyst **I-21** promoted an asymmetric epoxidation that resulted in opposite enantioselectivity to that of the traditional Juliá–Colonna reaction.[60-62]

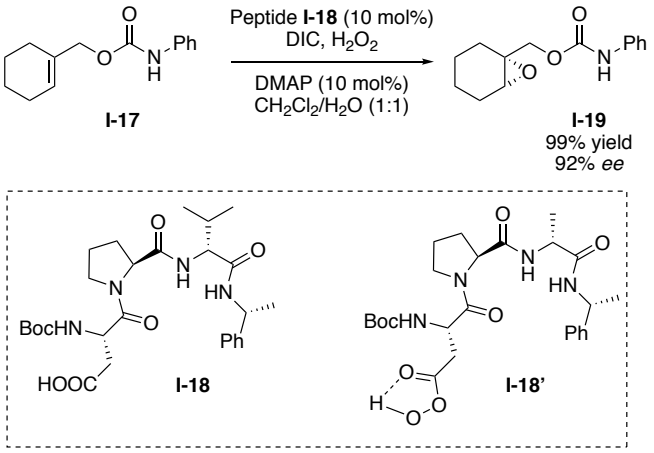


**Scheme 1.6.** $\beta$-turn peptide-mediated asymmetric epoxidation reported by Miller et al. This reaction proceeds via reactive peracid peptide intermediate **I-18'**.

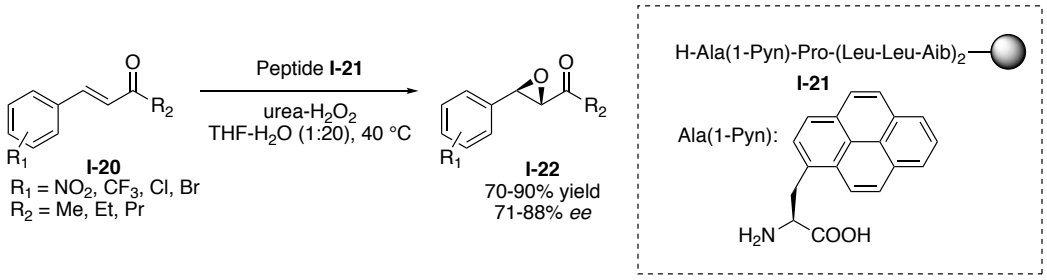


**Scheme 1.7.** Resin-supported peptide **I-21** for the asymmetric epoxidation of enones bearing electron withdrawing groups on the aryl moiety.

*Peptide-Mediated Enantioselective Aldol Reactions*

Asymmetric aldol reactions, whether intra- or intermolecular, represent an essential route to the formation of carbon-carbon bonds. Enzymatic transformations promoted by aldolases of Type I and Type II exist in nature whereby Type I reacts via an enamine pathway while the latter proceeds via the coordination of Zn (II) ions. Therefore, enamine catalysis has served as an effective mechanistic pathway for peptide catalyzed enantioselective aldol reactions. Short peptide catalysts consisting of 2-4 amino acid residues in length, as well as a secondary amine at the N-terminus, have been successfully employed as effective catalysts for asymmetric aldol condensations. The first peptide-catalyzed aldol reaction was reported in 2003 by Reymond and co-workers, wherein, the reaction between acetone and *p*-nitrobenzaldehyde proceeded in the presence of a proline-based peptide and a mixture of acetone and DMSO in excellent yields and moderate enantioselectivities.[63] Further, this disclosure examined various classes of peptide catalysts.

Specifically, class IA and IB contain primary amines, while class IIA and IIB contain secondary amines (Figure 1.1).[63] It was found that class IIB peptide catalysts, containing N-terminal prolines as the secondary amine substituent, performed the best in terms of yield and enantioselectivity (Scheme 1.8A). Similarly, di- and tri-peptides have also been successful as enantioselective catalysts for aldol reactions between *p*-nitrobenzaldehyde and acetone, generating the desired product in up to 91% yield and 77% *ee*. The substrate scope for this reaction was expanded to unmodified ketones and aldehydes in aqueous media. In this case, di-peptide **I-26,** containing a proline and a serine amino acid residue, furnished the desired β-hydroxy ketone **I-25** in 87% yield and 77% *ee* in DMSO (Scheme 1.8B).[64]

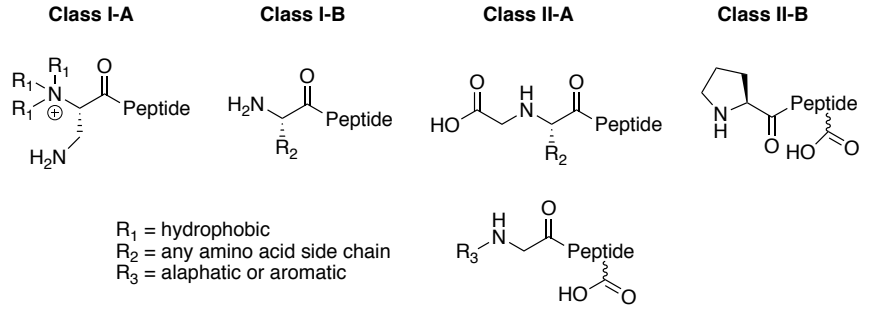


**Figure 1.1.** Classes of peptides for asymmetric aldol reactions reported by Reymond and co-workers.

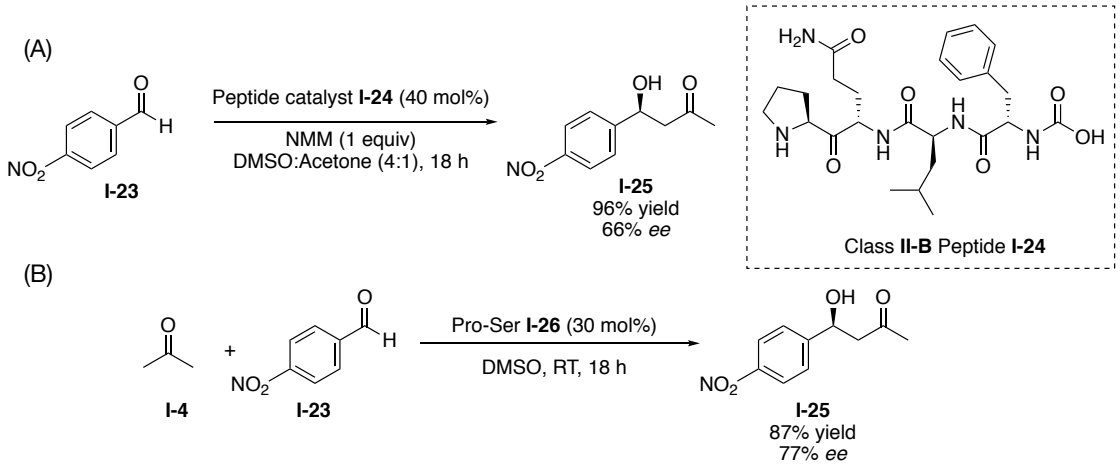


**Scheme 1.8.** Peptide catalyzed enantioselective aldol reactions of *p*-nitrobenzaldehyde and acetone reported by (A) Reymond and (B) Martin and List.

A regioselective direct aldol transformation was realized by Gong *et al*. with the use of a proline based catalyst, H-Pro-Phe-Phe-Phe-OMe (**I-28**) (Scheme 1.9). They explored the reaction between hydroxy acetone and various electron-deficient aromatic aldehydes in the presence of di-, tri-, tetra-, penta- and hexa-peptide catalysts.[65] Tetra peptide **I-28** proved the most effective, providing the desired aldol regioisomer in 82 yield, and 82 %*ee*. Recyclable, solid-supported peptides have also been reported for the direct asymmetric aldol reaction of acetone with various aldehydes. For example, Kudo reported a recyclable polyethylene glycol grafted on cross-linked polystyrene (PEG-PS)-immobilized peptide/ zinc chloride aqueous catalyst system. In the presence of a 20 mol % loading of the peptide catalyst, H-*D*-Pro-Tyr-Phe-(PEGPS), 20 mol % $ZnCl_2$, $H_2O$/THF (1:1), at 0° C, nitro- and chloro-substituted benzaldehydes and ketones smoothly reacted to furnish the desired aldol adduct in up to 100% yields and 84% *ee*.[66]

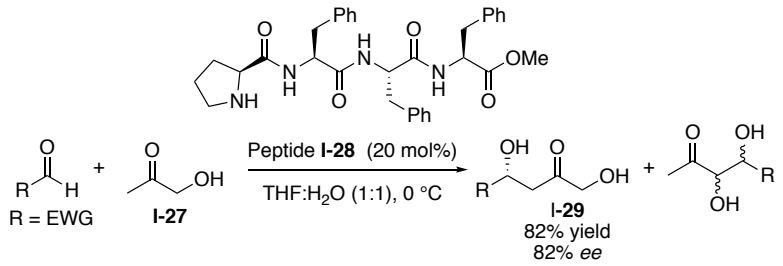


**Scheme 1.9.** Proline-based tetra-peptide (**I-28**) for the regioselective aldol reaction of electron-deficient aromatic aldehydes and hydroxy-acetone.

Later, Wennemers *et al*. reported a 'catalyst-substrate co-immobilization' strategy for probing peptides from split-and-mix libraries for catalytic activity applications in bimolecular reactions.

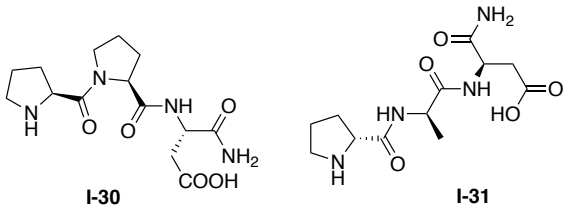


**Figure 1.2.** Wennemer's peptide catalysts discovered from a split-and-mix library.

These efforts led to the discovery of catalysts structures **I-30** and **I-31** for the aldol reaction of acetone with various aldehydes (Figure 1.2). With as little as 1 mol % loading of peptide catalyst **I-30**, the (*S*)-aldol product was accessed, while, 10 mol % of **I-31** provided the (*R*)-counterpart in up to 91% *ee*. [67,68] Recently, Kokotos *et al*. reported a Pro-Glu(O*t*Bu)-O*t*Bu catalyst that promoted the aldol condensation of a variety of cyclic/acyclic ketones and substituted benzaldehydes in the presence of MeCN, $H_2O$, and 20 mol % 4-nitrobenzoic acid. The proposed transition state model (Figure 1.3) consists of the dipeptide activation of a ketone substrate via enamine formation, with concomitant activation of the electrophile by means of H-bonding from the amide proton.[70]

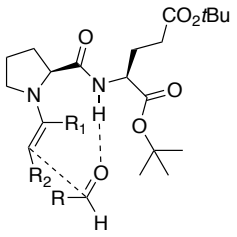


**Figure 1.3.** Putative transition state model of dipeptide ketone activation.

*Michael or 1,4-Conjugate Addition Reactions*

Often, the enantioselective 1,4-addition of α, β-unsaturated carbonyl or nitrile compounds with enolate ions or enamines requires the use of chiral auxiliaries, phase-transfer catalysts, or chiral imines/enamines. Amino acid and small peptide catalysts have also served as efficient enantioselective catalysts for Michael additions. For example, the asymmetric addition of various nitroalkanes to cyclic enones was promoted by an L-proline catalyst to generate the Michael addition product (**I-32**) in moderate yields and enantioselectivities (Scheme 1.10). This transformation likely occurs via an iminium

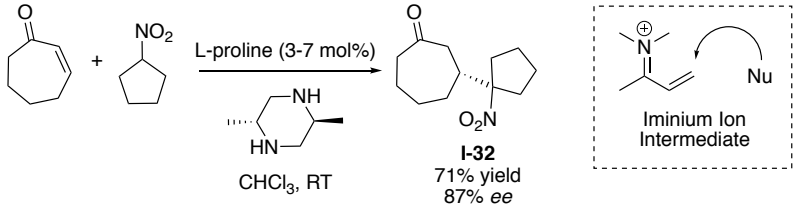


**Scheme 1.10.** L-proline catalyzed Michael addition of nitroolefins to cyclic enones via an iminium ion intermediate.

ion intermediate that forms following conversion of the carbonyl moiety (Scheme 1.10). Further, the chiral diamine, trans-2,5-dimethylpiperazine, functions as a basic and stereodefining additive that led to increase *ee* values.[64]

Beyond proline, Martin and List initially reported peptide catalyst scaffolds for the asymmetric addition of acetone and *trans*-β-nitrostyrene. Cordova also prepared a small suite of alanine containing di- and tripeptides catalysts for the asymmetric Michel addition of ketones to nitroolefins, generating the desired nitroketone product in high stereoselectivities up to 68:1 dr and 97% *ee* (Scheme 1.11).[71]

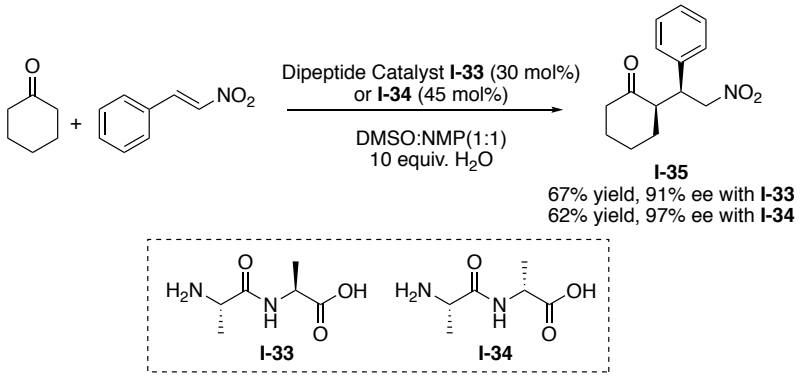


**Scheme 1.11.** Cordova and co-workers di-peptide catalyzed asymmetric Michael addition.

In 2009, Wennemers *et al*. also employed tri-peptides as asymmetric catalysts for the 1, 4-addition of aldehydes to *trans*-nitroolefins. Notably, all hit peptide scaffolds, such as **I-36**, included a D-Pro-Pro amino acid motif, known to nucleate a secondary turn structure and improve stereoselectivity and catalytic activity (Figure 1.4).[72,73] The correlation between peptide secondary structure and increased levels of enantioinduction was supported by Miller's β-turn peptides containing a τ-(benzyl)-His residue

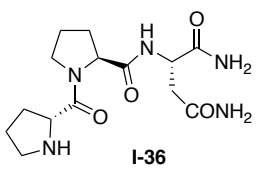


**Figure 1.4.** D-Pro-Pro containing peptide for 1,4-conjugate additions.

(*i.e.* **I-38**), which promoted the conjugate addition of azides to α,β-unsaturated compounds (Scheme 1.12). Upon treatment with 2.5 mol% of peptide catalyst **I-38** and $TMSN_3$, substrate **I-37** was converted to its corresponding azide product (**I-39**) in 97% yield and 63% *ee*.[74,75]

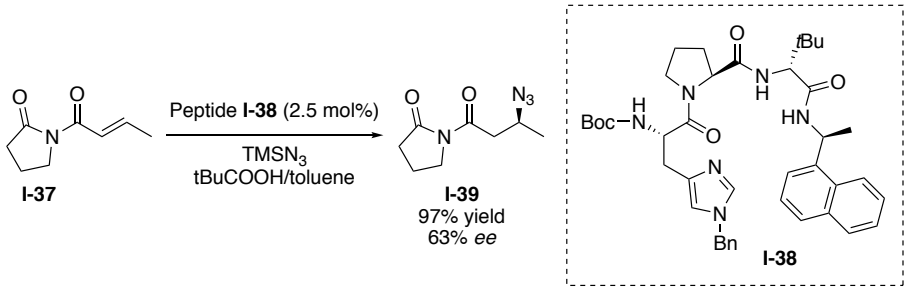


**Scheme 1.12.** Asymmetric addition of azides to α,β-unsaturated compounds, promoted by β-turn peptide **I-38**.

*Kinetic Resolutions and Desymmetrizations Promoted by Peptide Catalysts*

Peptides have also been utilized as catalysts for the kinetic resolution of racemic mixtures and the desymmetrization of *meso* compounds.[76,77] Currently, most peptide-based approaches for kinetic resolution center around bromination and acylation reactions. In 2010, Miller's group communicated the dynamic kinetic resolution (DKR) of biaryl atropisomers following a bromination reaction. More specifically, this method takes advantage of molecules that contain a mode of chirality known as atropisomerism. Briefly, atropisomers are compounds that contain an axis of chirality about a bond with hindered rotation. Energy differences, due to steric strain, result in a barrier of rotation that is high enough to allow for isolation of individual conformers. Treatment of biphenols, such as compound **I-40,** with 10 mol% of peptide catalyst **I-41**, *N*-bromophthalimide (NBP), in a

3 % acetone/DCM solvent system resulted in successful DKR, yielding the resolved product **I-42** in up to 94% *ee* (Scheme 1.13).[53,77]

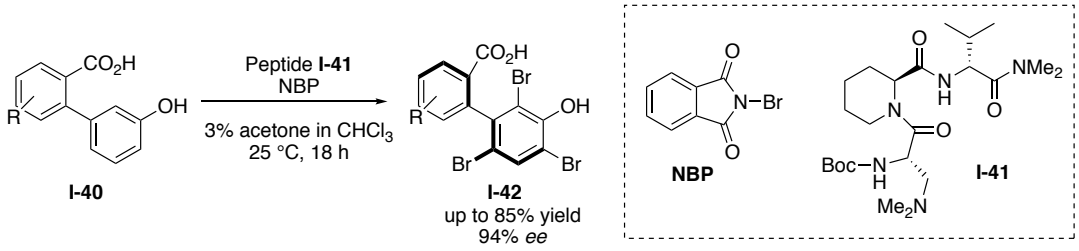


**Scheme 1.13.** Kinetic resolution of atropisomer (**I-40**) via a peptide-mediated asymmetric bromination.

Miller and co-workers continued to make impressive strides to fortify peptides as powerful and versatile asymmetric catalysts. Their efforts have resulted in various peptide-mediated acylation reactions for the kinetic resolution of racemic mixtures of alcohols.[56] For instance, peptides containing a nucleophilic, alkylated histidine residue at the N-terminus react via an acyl transfer (*i.e.* reactive intermediate **I-50**); wherein, chirality is induced via interactions such as hydrogen bonding, pi-stacking, ion pairing, *etc*. between the peptide backbone amides and amino acid side chains that stabilize the transition state of one enantiomer over the other. *Meso*-diols, such as **I-43**, can undergo desymmetrization employing a 5 mol % loading of peptide catalyst **I-44,** which upon selective acylation of one alcohol, results in product **I-45** in 80% yield and excellent enantioselectivity (Scheme 1.14A). Additional peptides, such as **I-47**, that were designed around amino acid sequences that adopt a β-hairpin secondary structure in solution also served as efficient catalysts for the kinetic resolution of amino alcohols by means of enantioselective acylation (**I-46**) (Scheme 1.14B).[78]

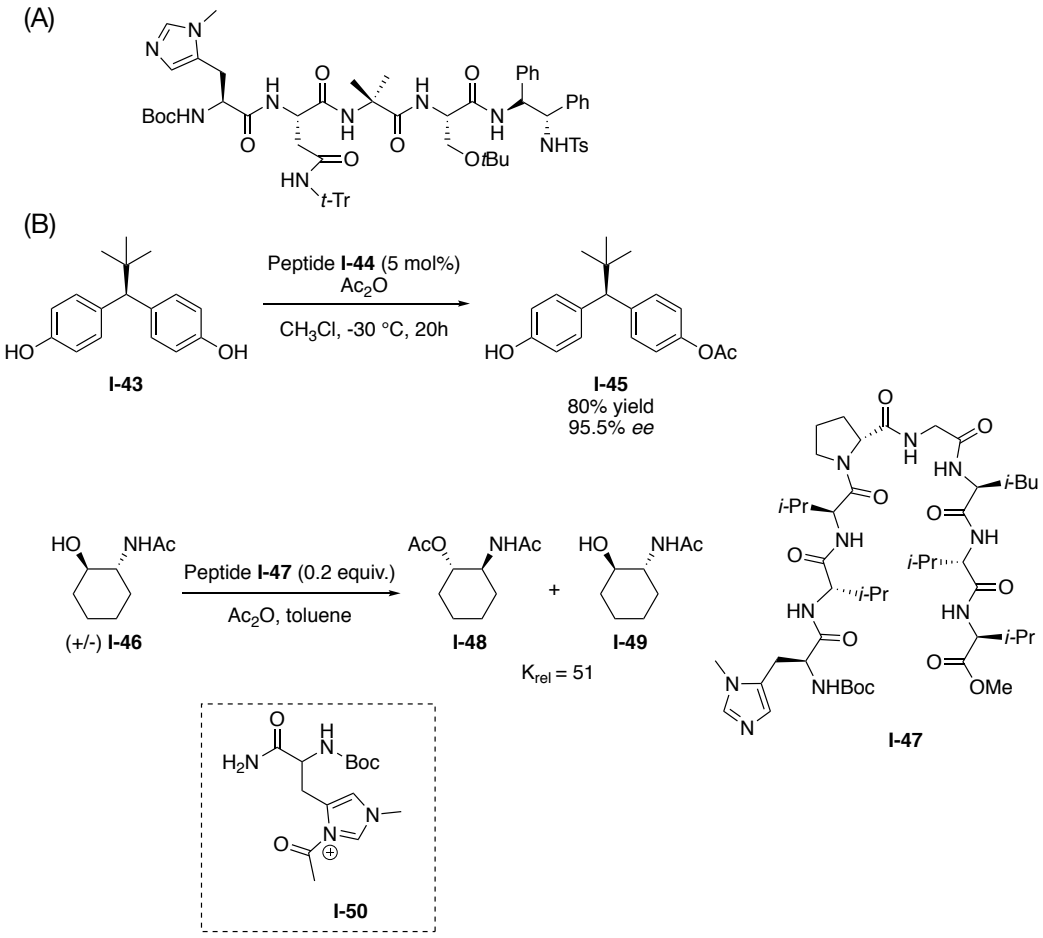


**Scheme 1.14.** Alkyl-histidine based peptides reported by Miller's group for the kinetic resolution of racemic alcohols via an acyl-transfer mechanism.

Other noteworthy asymmetric peptide-mediated organocatalytic reactions not discussed above include: phosphorylations and Acyl-Pictet Spengler reactions (Scheme 1.15 A and B).[74,79]

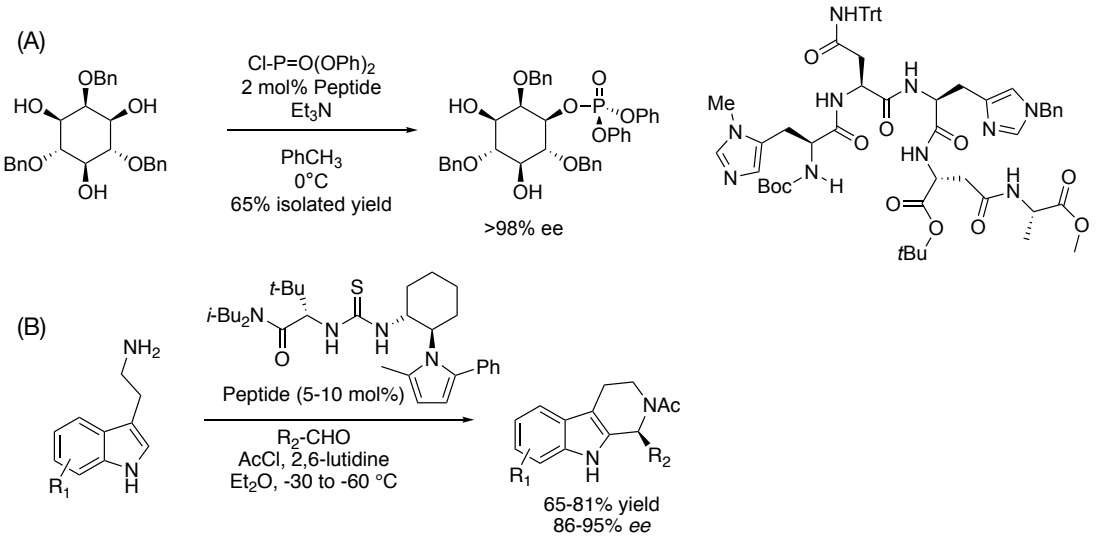


**Scheme 1.15.** Peptide-catalyzed asymmetric (A) phosphorylation and (B) acyl-Pictet Spangler transformations.

Ultimately, rendering a catalytic reaction highly enantioselective remains an important and yet challenging task in chemical synthesis. However, many reports detailing the success of peptide scaffolds as highly reactive and enantioselective catalysts support the importance and potential of this area of asymmetric organocatalysis. Further, major advantages of peptide-mediated asymmetric catalysis over conventional approaches toward catalyst design are apparent when one considers their modularity, ease of preparation, and the ability to evaluate a multitude of catalyst structures in a timely manner. The ease of preparation and modularity is facilitated by access to a large number of natural and unnatural amino acid building blocks as well as well-known solid-phase-peptide synthesis (SPPS) techniques. Furthermore, peptide structures can be iteratively modified

by simply replacing a single amino acid residue in order to alter the reactivity and/or enantioselectivty. The main disadvantage is highlighted by the infinite number of amino acid sequences available, leading to increased screening demands.

It can be imagined that a catalytic residue can easily be incorporated into a chiral peptide backbone in order to generate asymmetric peptide catalysts. In other words, chiral information can be installed onto a well-established catalyst framework via a chiral peptide scaffold. Hypervalent iodine catalysis represents such an area in which many effective and widely applicable catalytic structures have been explored, yet many of these reactions have yet to succumb to synthetically useful levels of enantioselectivity. The study described in this thesis sought to develop iodoarene-containing peptide catalysts for asymmetric hypervalent iodine (III)-mediated organic transformations. Therefore, the remainder of this introduction will focus on the development and application of hypervalent iodine reagents in a stoichiometric, catalytic, and asymmetric fashion.

## *1.2. Hypervalent Iodine Chemistry*

### *1.2.1. Iodine*

French chemist Bernard Courtois first noticed the purple-black metallic sheen of crystalline iodine in 1811 when he treated seaweed with an excess of sulfuric acid and collected the resulting crystals arising from the condensed vapor. Since this discovery, iodine has been found to be biologically and chemically important, playing a vital role in stimulating cell and tissue growth. Moderate iodine deficiencies can lead to multifocal autonomous growth of the thyroid, resulting in thyrotoxicosis. Severe deficiencies can cause hypothyroidism, leading to impaired somatic growth and motor development in

children. Iodine also represents a significant element in organic synthesis. For example, the bond dissociation energy of a C-I bond is around 55 kcal/mol, positioning organoiodine compounds as important intermediates that can easily be formed or undergo facile cleavage. Thus, they have been utilized in a variety of reactions such as Hofmann's alkylation of amines, the Wurtz coupling reaction, and Williamson ether synthesis.[80]

*1.2.2. Hypervalent Iodine Compounds*

Over the past 200 years, it has also been realized that iodine-containing compounds can serve as versatile reagents in organic synthesis, leading to synthetically valuable products. In comparison to other halogens, iodine's unique properties can be attributed to it being the largest, least electronegative, and most polarizable nonradioactive nonmetal. Due to its large size and high degree of polarizability, iodine displays polyvalent bonding that differs from other light main-group elements, existing in an expanded octet as well as a number of different oxidation states (–1, +1, +3, +5, +7), much like transition metals. The most predominant structural arrangement of an iodine (III) compound consists of a central iodine atom bonded between two heteroatom ligands and an aryl functionality (aryl-λ3-iodanes) within a pseudotrigonal bipyramidal geometry (Figure 1.5). The equatorial aryl group and the central iodine atom engage in a classical two-center two-electron (2c-2e) covalent σ-bond. In contrast, the bonding between the orbitals of the two apically positioned heteroatom ligands and the central

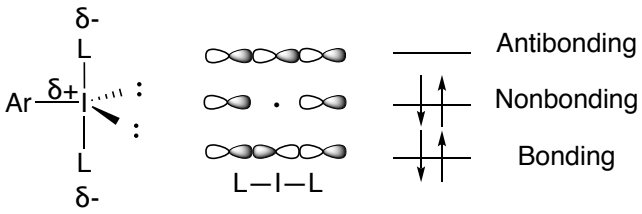


**Figure 1.5.** Hypervalent iodine(III) structure and molecular orbital bonding.

iodine atom necessitate a 3c-4e hypervalent bond. The molecular orbital diagram of this 3c-4e bond shows that the lower energy molecular orbitals (bonding and nonbonding) are completely filled, creating a node, and thus a partial positive charge, on the central iodine atom (Figure 1.5). Consequently the presence of a more electropositive central atom is energetically favorable for a hypervalent species. In general, the rich chemistry of hypervalent iodine can primarily be attributed to its inherently strong electrophilic character.[80-85]

The first polyvalent iodine compound was reported in 1886 by the German chemist Conrad Willgerodt, who synthesized (dichloroiodo)benzene from iodobenzene and chlorine gas.[86] Since then, a multitude of synthetically useful and commercially available polyvalent I(III) and I(V) compounds have been realized (Figure 1.6). Representative examples include, (diacetoxyiodo)benzene (PIDA) which is commonly used to oxidize

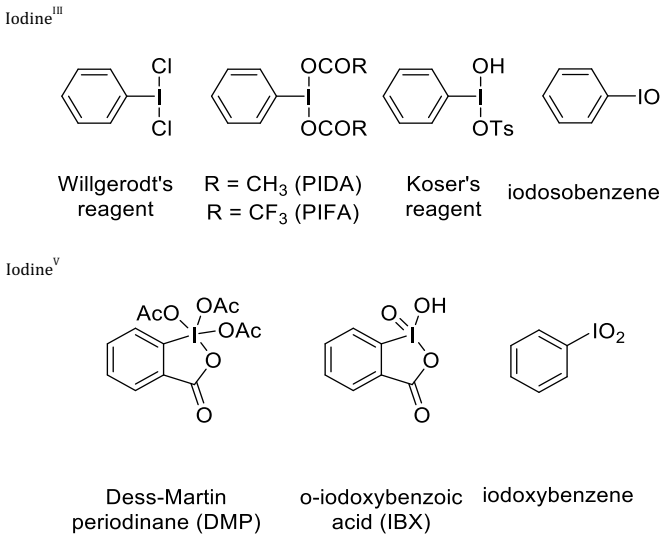


**Figure 1.6.** Examples of commonly recognized and employed polyvalent I(III) and (V) reagents.

carbonyl compounds, hydroxy(tosyloxy)iodobenzene (HTIB or Koser's reagent) often used to functionalize the α-carbons of carbonyls and Dess-Martin periodinane (DMP) used for mild oxidation of primary and secondary alcohols to aldehydes and ketones respectively.[80-88]

### *1.3. Hypervalent Iodine Reagents in Organic Transformations*

#### *1.3.1. Stoichiometric Applications*

In the last three decades, considerable attention has been focused on utilizing organohypervalent iodine reagents in several synthetically useful reactions. While traditionally being recognized as selective oxidants and electrophiles, HI reagents have also proven useful in the formation of carbon-carbon bonds, carbon-heteroatom bonds, and rearrangement reactions.

A representative example of HI reagents being applied to effect the oxidation of alcohols to their corresponding carbonyl products under simple, selective, and mild conditions includes the use of iodoxybenzene (IBX) and its DMP derivative for the oxidation of 1,2-diols. It was first reported in 1994, by Santagostino, that IBX could be used to oxidize alcohols in DMSO.[89] Since then, IBX has been used to prepare α-ketols and α-diketones from glycol starting materials (Scheme 1.16A). DMP also shows useful reactivity towards 1, 2-diols,

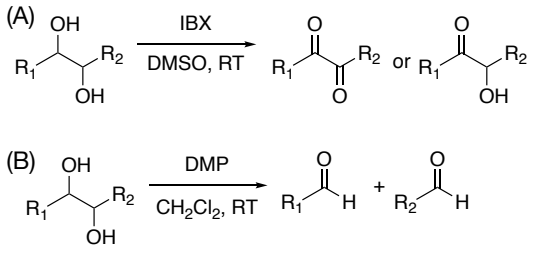


**Scheme 1.16.** 1,2-diol oxidation with A) IBX or B) DMP.

typically producing the C-C bond cleavage product of the glycol (Scheme 1.16B).[90,91]

The formation of carbon-carbon bonds is undoubtedly a useful organic transformation. When HI reagents are used to effect such a transformation, it typically proceeds via the generation of a carbon-centered reactive intermediate (free radicals, carbocations, carbenes, *etc*.) followed by trapping with an organic substrate or by a ligand coupling mechanism. Kita *et al.* reported the successful intramolecular carbon-carbon bond coupling reaction of phenolic compound **I-51** in the presence of PIFA and solid acid additive MK10 (Scheme 1.17A). This transformation gives rise to the spirodienone derivative **I-52** and represents an important synthetic step toward Discorhabdin natural products and other related alkaloids.[92] Further, an intermolecular carbon-carbon bond formation example is the oxidation of 2-alkylnapthols in the presence of PIFA and an allyl silane or silyl enol ether nucleophile (Scheme 1.17B).[85] Other functionalities, such as fluoride ions, alcohols, amides, and electron-rich aromatic rings, can also serve as appropriate nucleophiles for C-C bond formation reactions.

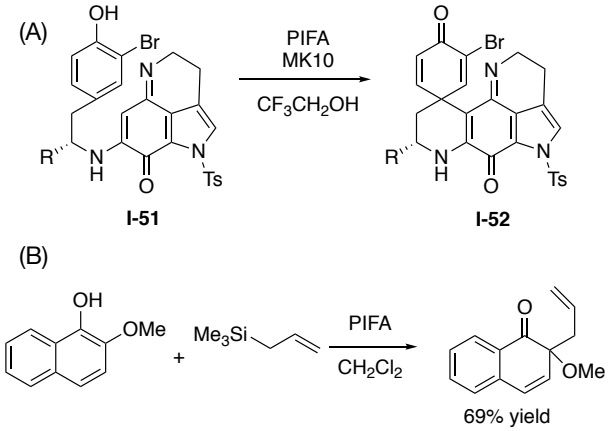


**Scheme 1.17.** Stoichiometric application of PIFA promoted carbon-carbon bond formation examples.

Lastly, the literature is also rich with examples of HI reagents being applied to carbon-heteroatom bond formation reactions with a high tolerance for a variety of substrates. Many of these cases include the halogenation of carbonyl compounds. The Fluoro-Pummerer reaction involves the α-fluorination of sulfur- and selenium-containing carbonyl substrates. The corresponding mono- and di-substituted *α*-fluoro sulfides or selenides are generated in the presence of (difluoroiodo)toluene in good to excellent yields (Scheme 1.18).[93-95] There are a plethora of other hypervalent iodine mediation reactions in the literature; however, the focus of this dissertation is on asymmetric organocatalytic processes. Therefore, the author directs the reader to reviews pertaining to the synthesis and application of HI reagents by Wirth, Zhdankin, Varvoglis, and Koser.[82-85, 96, 97]

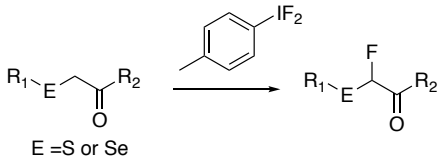


**Scheme 1.18.** HI-mediated fluorination of sulfur or selenium compounds.

*1.3.2. Hypervalent Iodine Reagents and Catalysts in Asymmetric Organic Transformations*

There are numerous publications describing the use of substoichiometric quantities of PhI to catalyze organic transformations in the presence of a terminal oxidant to promote the *in situ* regeneration of the iodine(III) species. Considerable progress has been made toward the development of iodoarene catalysts with the use of easily accessible and economical co-oxidants, such as, Oxone, $H_2O_2$, *m*CPBA, *etc*. However, much of previously developed hypervalent iodine chemistry has yet to yield highly reactive and enantioselective chiral HI catalysts.[98, 99] Typically, asymmetric hypervalent iodine compounds are synthesized by attaching chiral information via a chiral acid or alcohol in

proximity to the iodine center following ligand exchange or by inclusion of axial chirality through the backbone of the iodoarene (Figure 1.7).

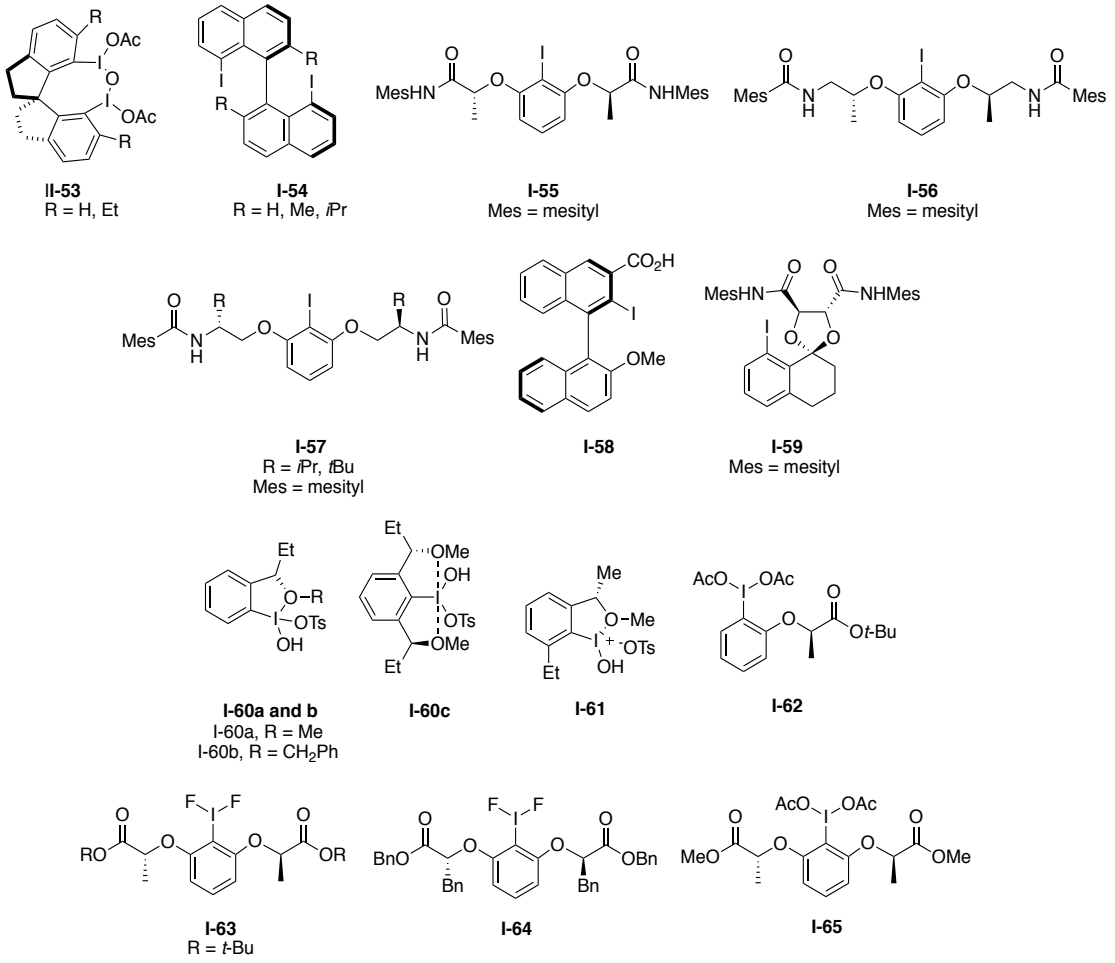


**Figure 1.7.**Select examples of chiral hypervalent iodine reagents applied to a variety of iodine(III)-mediated asymmetric organic transformations.

As previously mentioned, most of the I(I) precatalysts are then oxidized *in situ* to their hypervalent I(III) counterpart by means of an appropriate terminal oxidant. Such chiral HI-mediated transformations include, but are not limited to, asymmetric oxidative dearomatizations, functionalization of alkenes, rearrangements, and $\alpha$-functionalizations. Select examples of each transformation are briefly detailed below as well as in Chapter 2 of this thesis.

In 2008, the first chiral I(III) catalysts were reported by Kita *et al*. for the asymmetric oxidative dearomatization of phenolic derivatives by means of spirolactonization. This disclosure represents one of the most versatile and useful chiral HI-mediated transformations as it gives access to dearomatized products that can be incorporated into stereochemically and structurally complex molecules.[100]

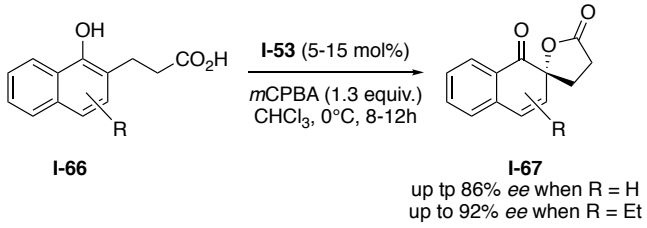


**Scheme 1.19.** Oxidative dearomatization of substituted phenolic carboxylic acid substrates.

The rigid spirocyclic backbone of catalyst **I-53**, proved essential to yield dearomatized compounds **I-67** in enantioselectivities up to 92% *ee* (Scheme 1.19). The addition of steric bulk on the arene in the *ortho*/*ortho'* positions with respect to the iodine moiety (*i.e*. R = Et in **I-53**) led to increased selectivity. More recently, this same group has developed a binaphthyl-based chiral I(III) prereagent **I-54** for the spirocyclization of napthol carboxylic acids upon treatment with *m*CPBA.[101]

A major breakthrough in this field came when a library of $C_2$-symmetric chiral iodoarene reagents were reported by Ishihara *et al*. This family of chiral pre-catalysts was examined in the oxidative *o*-lactonization of naphthols, similar to the transformation reported by *Kita et al*. (Scheme 1.20).[102] Naphthol derivatives were converted to spirocyclic lactones **I-68** in the presence of 10 mol % of chiral (*R*,*R*)-**I-55** and *m*CPBA as co-oxidant for the in situ generation of the I(III) catalyst. High levels of enantioselectivity were promoted by intramolecular interactions between iodine(III) atom and the two oxygen atoms at the carbonyl groups, and the hydrogen-bonding interactions between the iodine(III) ligands and the NH from the amide groups. This methodology was further leveraged for the dearomatization of phenols followed by the reaction with various dienophiles for the synthesis of enantioenriched Diels-Alder adducts. In this case, it was noted that the chiral iodine precatalyst **I-56** engaged in intramolecular H-bonding with achiral alcohol additives (MeOH, HFIP) resulting in excellent enantioselectivities (*i.e*. 99% *ee*) and lower catalyst loadings.[102]

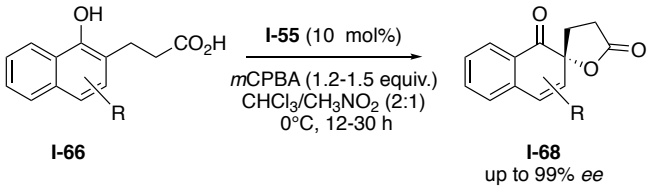


**I-66** **I-68** up to 99% *ee*

**Scheme 1.20.** $C_2$-symmetric iodoarene **I-55** for the catalytic oxidative *o*-lactonization of **I-66** to **I-68**.

Other groups have made thoughtful modifications to previously disclosed catalysts in hopes to generate new and more selective chiral iodine precatalyst scaffolds. For example, Ciufolini *et al*. reported structural changes to the chiral center located next to the amide NH moiety in compound **I-56**. The altered precatalyst, **I-57**, containing *i*Pr or *t*Bu moieties resulted in increased hydrogen-bonding and thus increased catalytic activity compared to that seen with **I-56** in Ishihara's reports.[103] Further, there was no longer a need for an achiral alcohol additive and the oxidative cyclization of phenolic derivatives **I-69** was done in the presence of 1.3 equiv. of *m*CPBA to afford spirocyclic compounds such as **I-70** in 98% *ee* (Scheme 1.21). The incorporation of binaphthyl backbones into various chiral HI precatalysts was explored by Quideau and co-workers, resulting in I(I)-structure **I-58**.[104] Upon *in situ* oxidization of the iodobiarene in the presence of *m*CPBA, its reactive I(III)-reagent counterpart promoted the hydroxylative naphthol dearomatization to afford the desired α-hydroxylation products in moderate enantioselectivities (*i.e*. 50% *ee*). Lastly, the Harned group has more recently disclosed new chiral HI pre-catalyst **I-59** for the asymmetric oxidation of a various phenols. Once again *m*CPBA (2.2 equiv) was utilized as a co-oxidant for the *in situ* generation of the active I(III)-catalyst, which allowed for the oxidation of phenols **I-71** to chiral *p*-quinols

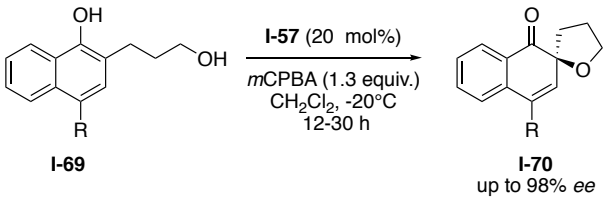


**Scheme 1.21.** Catalytic I(III)-mediated transformation of phenol derivative **I-69** to **I-70**.

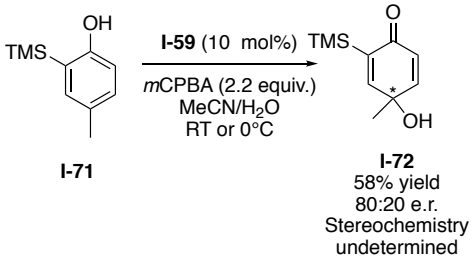


**Scheme 1.22.** Harned and co-workers synthesis of hydroxylated quinones.

**I-72** in moderate to good yields (Scheme I-22). While, low levels of enantioselectivities (*i.e.* <60% *ee*) were observed, this report represents the first time chiral hypervalent iodine(III) catalysts were examined for this particular reaction.[105]

In 1997, Wirth *et al*. disclosed three new chiral hypervalent iodine(III) compounds **I-60a-c** (Figure 1.7), for the asymmetric dioxytosylation of styrene.[106] This seminal work detailed the synthesis and investigation of these reagents for the enantioselective synthesis of di-oxytosylated **I-74**, resulting in a low selectivity of only 21% *ee*. However, their efforts did eventually lead to the discovery of HI reagent **I-61**, which promoted the desired alkene deoxygenation in up to 65% *ee (*Scheme 1.23*)*.[107, 108]

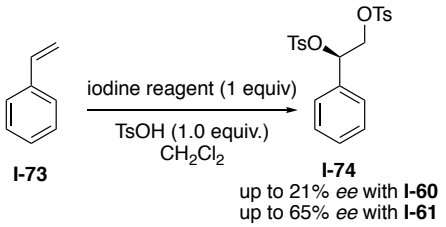


**Scheme 1.23.** Enantioselective dioxytosylation of styrene with HI reagents.

Progress in this area continued with the exploration of chiral HI reagents for the diacetoxylation of alkenes. Fujita and co-workers developed reaction conditions that included chiral HI reagent **I-62** in combination with a Lewis acid co-reagent for the

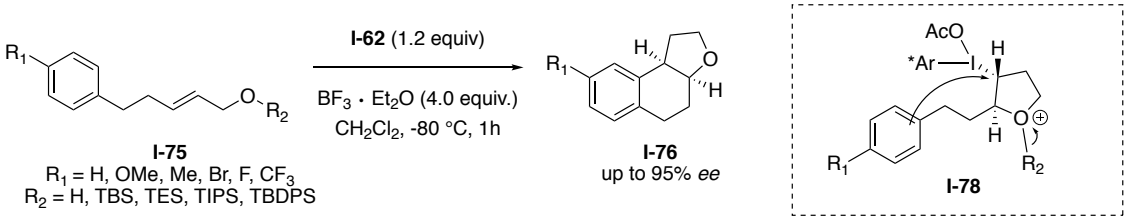


**Scheme 1.24.** Intramolecular oxyarylation of silyoxy-olefins reported by Fujita *et al*.

intramolecular oxyarylation of alkenes **I-75** to **I-76** (Scheme 1.24). It is proposed that the silyoxy substituent on **I-75** serves as a Lewis acid to activate iodoarene **I-62**, which can subsequently add to one enantiotopic face of the alkene substrate. Notably, high levels of

enantioselectivity were not achieved with reagents lacking the silyoxy moiety. This reaction also tolerated substrates with silyl-protected amines.[109]

Difluorination reactions are also accessible via chiral HI reagents and catalysts. For example, Nevado and colleagues reported the lactate-derived I(III) reagent (**I-63)** for the asymmetric aminofluorinaion of substituted styrene and alkene substrates via the chiral difluoroiodonium salt **I-63**.[110] Jacobsen *et al*. also applied $C_2$-symmetric chiral iodine precatalysts, such as **I-64**, for the I(III)-mediated 1,2-difluorination, 1,1-difluorination and fluorolactonization of alkenes using pyr•HF as a nucleophilic fluoride source. These reactions produced the desired products in excellent enantioselecitivities, up to 93, 97, and 96% *ee*, respectively.[111]

Lastly, precatalyst **I-55** was utilized for the enantioselective diacetoxylation of styrene derivatives. The *in situ* activation of the I(I) precatalyst to its active I(III) counterpart was achieved following exposure to peracetic acid. The oxidized hypervalent catalyst promoted the synthesis of a variety of vicinal diacetoxylation products (**I-79**) (Scheme 1.25). Muñiz and Ishihara *et al*. reported that increased levels of selectivity are promoted by intramolecular hydrogen bonding interactions between the amide moieties in the iodoarene catalyst and the acetoxy ligands on the active I(III) center represented by complex **I-80** (Scheme 1.25).[112]

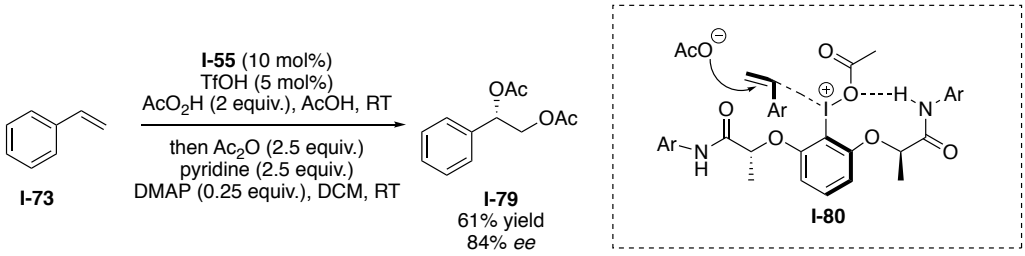


**Scheme 1.25.** Catalytic asymmetric diacetoxylation of styrene promoted by the *in situ* oxidation of **I-55** to its active I(III) counterpart.

Chiral HI reagents have also proven useful for stereoselective oxidative rearrangement reactions. For instance, Wirth *et al*. used I(III) reagent **I-55** to transform α,β-unsaturated carbonyls **to** their corresponding α-arylated carbonyls in up to 97% *ee*.[106] This same approach was also applied to asymmetric oxidative rearrangements of 1,1-disubstituted olefins **I-81** using HI reagent **I-65** (Scheme 1.26). This reaction proceeds via the formation of a conformationally restricted cyclic iodonium-intermediate **I-83**, allowing the generation of the desired enantioenriched α-arylated ketone products.[113] Typically, access to α-arylated ketones requires the use of transition metals such palladium or nickel. Therefore, chiral HI reagents have once again been demonstrated as attractive metal-free alternatives for synthetically useful transformations.[114, 115]

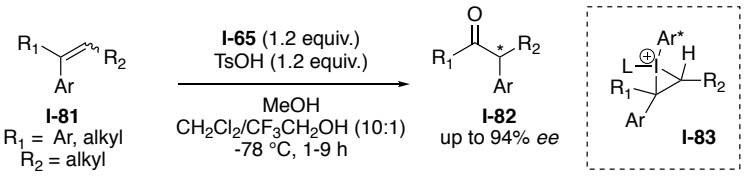


**Scheme 1.26.** Oxidative rearrangement of disubstituted alkenes.

### *1.4. Objectives and Conclusions*

Information obtained from research in the field of hypervalent iodine chemistry has revealed their utility as very versatile and mild reagents that can replace toxic heavy metal-containing reagents, thus providing more environmentally friendly reaction conditions. Nonetheless, this area of research is still in its infancy and many efforts are being put forth to realize highly reactive and enantioselective derivatives, poising HI reagents as suitable candidates for incorporation into a chiral peptide scaffold.

Further, traditional approaches toward catalyst design often rely on timely step-by-step modifications of an initial "hit" structure. Therefore, we envisaged that the modularity and facile preparation of short peptide sequences would aid in the development of a library of iodoarene-containing peptide scaffolds. A major objective of the work described in this thesis was to prepare libraries of peptide precatalysts bearing iodo arenes following Fmoc-SPPS protocols and to screen these peptide libraries in catalytic hypervalent I(III)-mediated reactions to probe their ability to impart enantiocontrol in the reaction.

### *1.5. References*

1. Kagan, H .B.; Gopalaiah, K. Early history of asymmetric synthesis: who are the scientists who set up the basic principles and the first experiments? *New J. Chem.* **2011**, *35*, 1933-1937.

2. Trost, B. M. Asymmetric catalysis: An enabling science. *Proc. Natl. Acad. Sci. USA*. **2004**, *101*, 5348–5355.

3. Farina, V.; Reeves, J.T.; Senanayake, C. H.; Song, J. J.; Asymmetric Synthesis of Active Pharmaceutical Ingredients. *Chem. Rev.* **2006,** *106*, 2734- 2793.

4. Noyori, R. Asymmetric Catalysis in Organic Synthesis. Wiley, New York (1994).

5. Davidi, D.; Longo, L. M.; Jabłonska, J.; Milo, R.; Tawfik, D. S. A Bird's-Eye View of Enzyme Evolution: Chemical, Physicochemical, and Physiological Considerations. *Chem. Rev.* **2018**, *118*, 8786-8797.

6. *Comprehensive Asymmetric Catalysis*; Jacobsen, E. N., Pfaltz, A., Yamamoto, H., Eds.: Springer-Verlag: Berlin Heidelberg, 1999; Vols. I–III.

7. Dalko, P. I.; Moisan, L. Enantioselective organocatalysis. *Angew. Chem., Int. Ed.* **2001**, *40*, 3726–3748.

8. Dalko, P.I.; Moisan, L. In the Golden Age of Organocatalysis. *Angew. Chem., Int. Ed.* **2004**, *43*, 5138.

9. Berkessel, A.; Groger, H. Asymmetric Organocatalysis. WileyVCH, Weinheim, 2005.

10. Dalko, P.I. Enantioselective Organocatalysis: Reactions and Experimental Procedures. Wiley- VCH, Weinheim, 2007.

11. Seayad, J.; List, B. Asymmetric organocatalysis. *Org. Biomol. Chem.* **2005**, *3*, 719.

12. Groger, H.; Wilken, J. The application of l-proline as an enzyme mimic and further new asymmetric syntheses using small organic molecules as chiral catalysts. *Angew. Chem., Int. Ed.* **2001**, *40*, 529–532.

13. Hajos, Z. G.; Parrish, D. R., *Ger. Pat.*, July 29, 1971.

14. Eder, U.; Sauer, G.; Wiechert, R., *Ger. Pat.,* Oct 7, 1971.

15. Eder, U.; Sauer, G.; Wiechert, R., New Type of Asymmetric Cyclization to Optically Active Steroid CD Partial Structures. *Angew. Chem. Int. Ed. Engl.*, **1971**, *10*, 496.

16. Woodward, R. B.; Logusch, E.; Nambiar, K. P.; Sakan, K.; Ward, D. E.; Au-Yeung, B. W.; Balaram, P.; Browne, L. J.; Card, P. J.; Chen, C. H. Asymmetric total synthesis of erythromycin. 3. Total synthesis of erythromycin. *J. Am. Chem. Soc.* **1981**, *103*, 3215-3217.

17. Xua, L. W.; Lu, Y. Primary amino acids: privileged catalysts in enantioselective organocatalysis. *Org. Biomol. Chem.* **2008**, *6*, 2047–2053.

18. Mukherjee, S.; Yang, J. W.; Hoffmann, S.; List, B. Asymmetric Enamine Catalysis *Chem. Rev.* **2007**, *107*, 5471−5569.

19. List, B.; Lerner, R. A.; Barbas, C. F. Proline-Catalyzed Direct Asymmetric Aldol Reactions *J. Am. Chem. Soc.* **2000**, *122*, 2395-2396.

20. Movassaghi, M.; Jacobsen, E. N. The simplest enzyme. *Science* **2002**, *298*, 1904–1905.

21. Cobb, A. J. A.; Shaw, D. M.; Longbottom, D. A.; Gold, J. B.; Ley, S. V. Organocatalysis with proline derivatives: improved catalysts for the asymmetric Mannich, nitro-Michael and aldol reactions *Org. Biomol. Chem.* **2005**, *3* , 84–96.

22. Vignola, N.; List, B. Catalytic Asymmetric Intramolecular α-Alkylation of Aldehydes *J. Am. Chem. Soc.* **2004**, *126*, 450–451.

23. Tang, Z.; Jiang, F.; Yu, L.; Cui, X.; Gong, L.; Mi, A.; Jiang, Y.; Wu, Y. Novel Small Organic Molecules for a Highly Enantioselective Direct Aldol Reaction *J. Am. Chem. Soc.* **2003**, *125*, 5262–5263.

24. Notz, W.; Tanaka, F.; Barbas, C. F. Enamine-Based Organocatalysis with Proline and Diamines: The Development of Direct Catalytic Asymmetric Aldol, Mannich, Michael, and Diels–Alder Reactions *Acc. Chem. Res.* **2004**, *37*, 580–591.

25. List, B. Proline Catalyzed Asymmetric Reactions. *Tetrahedron* **2002**, *58*, 5573-5590.

26. Morrison, J.; Mosher, H. *Asymmetric Organic Reactions;* Prentice-Hall: Englewood Cliff, **1971**.

27. O'Donnell, M. J. The Enantioselective Synthesis of α-Amino Acids by Phase-Transfer Catalysis with Achiral Schiff Base Esters *Acc. Chem. Res.* **2004**, *37*, 506.

28. Lygo, B.; Andrews, B. Asymmetric Phase-Transfer Catalysis Utilizing Chiral Quaternary Ammonium Salts: Asymmetric Alkylation of Glycine Imines. *Acc. Chem. Res.* **2004**, *37*, 518.

29. Jew, S.-S.; Jeong, B.-S.; Yoo, M.-S.; Huh, H.; Park, *H.-G. Cinchona*-based phase-transfer catalysts for asymmetric synthesis. *Chem. Commun.* **2001**, 46, 1244.

30. Ahrendt, K. A.; Borths, C. J.; MacMillan, D. W. C. Ahrendt, K. A.; Borths, C. J.; MacMillan, D. W. C. New Strategies for Organic Catalysis: The First Highly Enantioselective Organocatalytic Diels–Alder Reaction. *J. Am. Chem. Soc.* **2000**, *122*, 4243.

31. Jen, W. S.; Wiener, J. J. M.; MacMillan, D. W. C. New Strategies for Organic

Catalysis: The First Enantioselective Organocatalytic 1,3-Dipolar Cycloaddition. *J. Am. Chem. Soc.* **2000**, *122*, 9874.

32. Paras, N. A.; MacMillan, D. W. C. New Strategies in Organic Catalysis: The First Enantioselective Organocatalytic Friedel–Crafts Alkylation. *J. Am. Chem. Soc.* **2001**, *123*, 4379-4371.

33. Vachal, P.; Jacobsen, E. N. Structure-Based Analysis and Optimization of a Highly Enantioselective Catalyst for the Strecker Reaction. *J. Am. Chem. Soc.* **2002**, *124*, 10012.

34. Joly, G. D.; Jacobsen, E. N. Thiourea-Catalyzed Enantioselective Hydrophosphonylation of Imines: Practical Access to Enantiomerically Enriched α-Amino Phosphonic Acids. *J. Am. Chem. Soc.* **2004**, *126*, 4102.

35. Wenzel, A. G.; Jacobsen, E. N. Asymmetric Catalytic Mannich Reactions Catalyzed by Urea Derivatives: Enantioselective Synthesis of $\beta$-Aryl-$\beta$-Amino Acids. *J. Am. Chem. Soc.* **2002**, *124*, 12964.

36. Fu, G. C. Asymmetric Catalysis with "Planar-Chiral" Derivatives of 4-(Dimethylamino)pyridine. *Acc. Chem. Res.* **2004**, *37*, 542-547.

37. Wang, Z.; Tu, Y.; Frohn, M.; Shi, Y. A Dramatic pH Effect Leads to a Catalytic Asymmetric Epoxidation. *J. Org. Chem.* **1997**, *62*, 2328.

38. Wang, Z.; Tu, Y.; Frohn, M.; Zhang, J.; Shi, Y. An Efficient Catalytic Asymmetric Epoxidation Method. *J. Am. Chem. Soc.* **1997**, 11224.

39. *Enzyme Catalysis in Organic Synthesis: A Comprehensive Handbook*; Drauz, K., Waldmann, H., Eds.: Wiley-VCH Verlag GmbH: Weinheim, Germany, 2002; Vols. I–III.

40. Breslow, R. Biomimetic chemistry and artificial enzymes: catalysis by design. *Acc. Chem. Res.* **1995**, *28*, 146–153.

41. Murakami, Y.; Kikuchi. J.; Hiseada, Y.; Hayashida, O. Artificial enzymes. *Chem. Rev.* **1996**, *96*, 721–758.

42. Kirby, A. J. Enzyme mechanisms, models and mimics. *Angew. Chem., Int. Ed. Engl.* **1996**, *35*, 707–724.

43. Akabori, S.; Sakurai, S.; Izumi, Y.; Fujii, Y. An Asymmetric Catalysts. *Nature* **1956**, *178*, 323-324.

44. Gilbertson, S. R.; Collibee, S. E.; Agarkov, A. Asymmetric Catalysis with Libraries of Palladium β-Turn Phosphine Complexes *J. Am. Chem. Soc.* **2000**, *122*, 6522-6523.

45. Gilbertson, S. R.; Wang, X.; Hoge, G. S.; Klung, C.; Schaefer, J. Synthesis of Phosphine–Rhodium Complexes Attached to a Standard Peptide Synthesis Resin. *Organometallics* **1996**, *15*, 4678-4680.

46. Luchaco-Cullis, C. A.; Mizutani, H.; Murphy, K. E.; Hoveyda, A. H. Modular Pyridinyl Peptide Ligands in Asymmetric Catalysis: Enantioselective Synthesis of Quaternary Carbon Atoms Through Copper-Catalyzed Allylic Substitutions. *Angew. Chem., Int. Ed. Engl.* **2001**, *40*, 1456-1460.

47. Jarvo, E. R.; Miller, S. J. Amino acids and peptides as asymmetric organocatalysts *Tetrahedron* **2002**, 58, *2481-2495*.

48. Berkessel, A. The Discovery of Catalytically Active Peptides through Combinatorial Chemistry. *Curr. Opin. Chem. Biol.* **2003**, *7*, 409-419.

49. Blank, J. T.; Miller, S. J. Studies of folded peptide-based catalysts for asymmetric organic synthesis. *Biopolymers* **2006**, *84*, 38-47.

50. Oku, J.; Inoue, S. Asymmetric cyanohydrin synthesis catalyzed by synthetic dipeptides, 2. *Makromol. Chem.* **1979**, *180*, 1089.

51. Juliá, S.; Masana, J.; Vega, J. C. "Synthetic Enzymes" Highly Stereoselective Epoxidation of Chalcone in a Triphasic Toluene-Water-Poly[(S)-alanine] System. *Angew. Chem. Int. Ed. Engl.* **1980**, *19*, 929-931.

52. Colonna, S.; Molinari, H.; Banfi, S.; Juliá, S.; Masana, J.; Alvarez, A. Synthetic enzymes—4 : Highly enantioselective epoxidation by means of polyaminoacids in a triphase system: influence of structural variations within the catalysts *Tetrahedron* **1983**, *39*, 1635-1641.

53. Miller, S. J.; Copeland, G. T.; Papaioannou, N.; Horstmann, T. E.; Ruel, E. M. Kinetic Resolution of Alcohols Catalyzed by Tripeptides Containing the *N*-Alkylimidazole Substructure *J. Am. Chem. Soc.* **1998**, *120*, 1629–1630.

54. Jarvo, E. R.; Copeland, G. T., Papaioannou, N.; Bonitatebus, P. J.; Miller, S. J. *J. Am. Chem. Soc.* **1999**, *121*, 1638–11643.

55. Wennemers, H. Asymmetric catalysis with peptides. *Chem. Commun.* **2011**, *47*, 12036- 12041.

56. Miller, S. J. In Search of Peptide-Based Catalysts for Asymmetric Organic Synthesis *Acc. Chem. Res.* **2004**, *37* , 601–610.

57. Bérubé, C.; Barbeau, X.; Lagüe, P.; Voyer, N. Revisiting the Juliá–Colonna enantioselective epoxidation: supramolecular catalysis in water. *Chem. Commun.* **2017**, *53*, 5099-5102.

58. Bentley, P. A.; Bergeron, S.; Cappi, M. W.; Hibbs, D. E.; Hursthouse, M. B. Nugent, T. C.; Pulido, R.; Roberts, S. M.; Wu, L. E. Asymmetric epoxidation of enones employing polymeric α-aminoacids in non-aqueous media *Chem. Commun.* **1997**, 739-740.

59. Itsuno, S.; Sakakura, M.; Ito, K. Polymer-Supported Poly(amino acids) as New Asymmetric Epoxidation Catalyst of Unsaturated Ketones *J. Org. Chem.* **1990**, *55*, 6047-6048.

60. Kudo, K., Akagawa, K., & Hirata, T. Asymmetric Epoxidation of Enones by Peptide-Based Catalyst: A Strategy Inverting Juliá–Colonna Stereoselectivity. *Synlett* **2015**, *27,* 1217–1222.

61. Akagawa, K.; Kudo, K. Asymmetric Epoxidation of α, β-Unsaturated Aldehydes in Aqueous Media Catalyzed by Resin-Supported Peptide- Containing Unnatural Amino Acids. *Adv. Synth. Catal.* **2011**, *353*, 843–847.

62. Akagawa, K.; Kudo, K. Asymmetric Epoxidation of α,β-Unsaturated Aldehydes in Aqueous Media Catalyzed by Resin-Supported Peptide- Containing Unnatural Amino Acids. *Adv. Synth. Catal.* **2011**, *353*, 843-847.

63. Kofoed, J.; Nielsen, J.; Reymond, J. L. Discovery of new peptide-based catalysts for the direct asymmetric aldol reaction. *Bioorg. Med. Chem. Lett.* **2003**, *13*, 2445-2447.

64. Martin, H. J.; List, B. Mining Sequence Space for Asymmetric Aminocatalysis: N-Terminal Prolyl-Peptides Efficiently Catalyze Enantioselective Aldol and Michael Reactions. *Synlett* **2003**, *12*, 1901-1902.

65. Tang, Z.; Yang, Z.H.; Cun, L.F.; Gong, L.Z.; Mi, A.-Q.; Jiang, Y.Z. Small Peptides Catalyze Highly Enantioselective Direct Aldol Reactions of Aldehydes with Hydroxyacetone: Unprecedented Regiocontrol in Aqueous Media. *Org. Lett.* **2004**, *6*, 2285-2287.

66. Akagawa, K.; Sakamoto, S.; Kudo, K. Direct Asymmetric Aldol Reaction in Aqueous Media Using Polymer-Supported Peptide. *Tetrahedron Lett.* **2005**, *46*, 8185-8187.

67. Krattiger, P.; McCarthy, C.; Pfaltz, A.; Wennemers, H. Catalyst-Substrate Co-Immobilization: A Strategy for Catalysts Discovery in Split-and-Pool-Mix Libraries. *Angew. Chem., Int. Ed.* **2003**, *42*, 1722-1724.

68. Krattiger, P.; Kovasy, R.; Revell, J. D.; Ivan, S.; Wennemers, H. Increased Structural Complexity Leads to Higher Activity: Peptides as Efficient and Versatile Catalysts for Asymmetric Aldol Reactions. *Org. Lett.* **2005**, *7*, 1101-1103.

69. Bisticha, A.; Triandafillidi, I.; Kokotos, C. G. tert-Butyl esters of peptides as organocatalysts for the asymmetric aldol reaction. *Tetrahedron: Asymmetry* **2015**, *26,* 102–108.

70. Dziedzic, P.; Zou, W.; Háfren, J.; Córdova, A. The small peptide-catalyzed direct asymmetric aldol reaction in water. *Org. Biomol. Chem.* **2006**, *4*, 38-40.

71. Xu, Y.; Zou, W.; Sunden, H.; Ibrahem, I.; Cordova, A. Small Peptide-Catalyzed Enantioselective Addition of Ketones to Nitroolefins *Adv. Synth. Catal.* **2006**, *348*, 418 – 424.

72. Wiesner, M.; Neuburger, M.; Wennemers, H. Tripeptides of the Type H-D-Pro-Pro-Xaa-NH2 as Catalysts for Asymmetric 1,4-Addition Reactions: Structural Requirements for High Catalytic Efficiency. *Chem.: Eur. J.* **2009**, *15,* 10103–10109.

73. Grünenfelder, C. E.; Kisunzu, J. K.; Wennemers, H. Peptide-Catalyzed Stereoselective Conjugate Addition Reactions of Aldehydes to Maleimide *Angew. Chem. Int. Ed.* **2016**, *55*, 8571.

74. Sculimbrene, B. R.; Miller, S. J. Discovery of a Catalytic Asymmetric Phosphorylation through Selection of a Minimal Kinase Mimic: A Concise Total Synthesis of d-*myo*-Inositol-1-Phosphate *J. Am. Chem. Soc.* **2001**, *123*, 10125–10126.

75. Linton, B. R.; Reutershan, M. H.; Aderman, C. M.; Richardson, E. A.; Brownell, K. R.; Ashley, C. W.; Miller, S. J. Asymmetric Michael addition of α-nitro-ketones using catalytic peptides. *Tetrahedron Lett.* **2007**, *48,* 1993–1997.

76. Gustafson, J. L.; Lim, D.; Miller, S. J. Dynamic kinetic resolution of biaryl atropisomers via peptide-catalyzed asymmetric bromination. *Science* **2010**, *328*, 1251-1255.

77. Akagawa, K.; Higuchi, J.; Yoshikawa, I.; & Kudo, K. Kinetic Resolution of Ansa Cyclophanes by Peptide-Catalyzed Aldol/Retro-Aldol Reactions. *Eur. J. Org. Chem.* **2018**, 5278-5281.

78. Lewis, C. A.; Gustafson, J. L.; Chiu, A.; Balsells, J.;Pollard, D.; Murry, J.; Reamer R. A.; Hansen, K. B.; Miller, S. J. A case of remote asymmetric induction in the peptide-catalyzed desymmetrization of a bis(phenol). *J. Am. Chem. Soc.* **2008**, *130*, 16358-16365.

79. Taylor, M. S.; Jacobsen, E. N. Highly Enantioselective Catalytic Acyl-Pictet–Spengler Reactions. *J. Am. Chem. Soc.* **2004**, *126*, 10558.

80. Stang, P. J.; Zhdankin, V. V. Organic Polyvalent Iodine Compounds. *Chem. Rev.* **1996**, *96*, 1123.

81. Musher, J. I. The Chemistry of Hypervalent Molecules. *Angew. Chem. Int. Ed.* **1969**, *8*, 54-68.

82. Stang, P. J.; Zhdankin, V. V. Recent Developments in the Chemistry of Polyvalent Iodine Compounds. *Chem. Rev.* **2002**, *102*, 2523.

83. Stang, P. J.; Zhdankin, V. V. Chemistry of Polyvalent Iodine. *Chem. Rev.* **2008,** *108*, 5299.

84. "Hypervalent Iodine Chemistry. Modern Developments in Organic Synthesis": *Topics in Current Chemistry*, Vol. 224 (Ed.: T. Wirth), Springer, Berlin, **2003**.

85. Zhdankin, V. V. *Hypervalent Iodine Chemistry Preparation, Structure and Synthetic Applications of Polyvalent Iodine Compounds*, Wiley, Chichester, **2014**.

86. Willgerodt, C. Ueber einige aromatische Jodidchloride. *J. Prakt. Chem.* **1886**, *33*, 154-160.

87. Dess, D. B.; Martin, J. C. Readily accessible 12-I-5 oxidant for the conversion of primary and secondary alcohols to aldehydes and ketones *J. Org. Chem.* **1983**, *48*, 4155.

88. Dess, D. B.; Martin, J. C. A useful 12-I-5 triacetoxyperiodinane (the Dess-Martin periodinane) for the selective oxidation of primary or secondary alcohols and a variety of related 12-I-5 species *J. Am. Chem. Soc.* **1991**, *113*, 7277.

89. Frigerio, M.; Santagostino, M. A mild oxidizing reagent for alcohols and 1,2-diols: o-iodoxybenzoic acid (IBX) in DMSO. *Tetrahedron Lett.* **1994**, *35,* 8019–8022.

90. Frigerio, M.; Santagostino, M.; Sputore, S.; Palmisano, G. Oxidation of Alcohols with o- Iodoxybenzoic Acid in DMSO: A New Insight into an Old Hypervalent Iodine Reagent. *J. Org. Chem.* **1995**, *60,* 7272–7276.

91. Frigerio, S. M.; Santagostino, M.; Sputore, S.; Palmisano, G. Hypervalent Iodine Oxidants: Structure and Kinetics of the Reactive Intermediates in the Oxidation of Alcohols and 1,2-Diols by *o*-Iodoxybenzoic Acid (IBX) and Dess–Martin Periodinane. A Comparative 1H-NMR Study. *J. Org. Chem.* **1996**, *61*, 9272.

92. Tohma, H.; Harayama, Y.; Hashizume, M.; Iwata, M.; Kiyono, Y.; Egi, M.; Kita, Y. The First Total Synthesis of Discorhabdin A. *J. Am. Chem. Soc.* **2003**, *125*, 11235-11240.

93. Motherwell, W. B.; Greaney, M. F.; Tocher, D. A. Fluorination of α-phenylsulfanyl esters using difluoroiodotoluene. *J. Chem. Soc., Perkin Trans.* **2002**, *1*, 2809-2815.

94. Motherwell, W. B.; Greaney, M. F.; Tocher, D. A. Fluorination of sulfanyl amides using difluoroiodoarene reagents. *J. Chem. Soc. Perkin Trans.*, **2002**, *1*, 2816-2826.

95. Arrica, M. A.; Wirth, T. Fluorinations of α-Seleno Carboxylic Acid Derivatives with Hypervalent (Difluoroiodo)toluene. *Eur. J. Org. Chem.* **2005**, 395-403.

96. Wirth, T.; Hirt, U. H. Hypervalent Iodine Compounds: Recent Advances in Synthetic Applications. *Synthesis* **1999**, *8*, 1271-1287.

97. Wirth, T.; Ochiai, M. Ed. Hypervalent Iodine Chemistry, Springer: Berlin (Germany), 2003, Vol. 224, pp 5-68.

98. Hirt, U. H.; Schuster, M. F. H.; French, A. N.; Wiest, O. G.; Wirth. T. Chiral Hypervalent Organo-Iodine(III) Compounds. *Eur. J. Org. Chem.* **2001**, *2001*, 1569- 1579.

99. Moriarty, R. M. Organohypervalent iodine: development, applications, and future directions. *J. Org. Chem.* **2005**, *70*, 2893-2903.

100. Dohi, T.; Maruyama, A.; Takenaga, N.; Senami, K.; Minamitsuji, Y.; Fujioka, H.; Caemmerer, S.; Kita, Y. A Chiral Hypervalent Iodine(III) Reagent for Enantioselective Dearomatization of Phenols. *Angew. Chem. Int. Ed.* **2008**, *47*, 3787-3790.

101. Dohi, T.; Kita, Y. Hypervalent iodine reagents as a new entrance to organocatalysts. *Chem. Comm.* **2009**, 2073-2085.

102. Uyanik, M.; Ishihara, K. Conformationally-Flexible Chiral Hypervalent Organoiodine Catalysts for Enantioselective Oxidative Transformations. *J. Synth. Org. Chem. Jpn.* **2012**, *70*, 1116.

103. Liang, H.; Ciufolini, M. A. Chiral Hypervalent Iodine Reagents in Asymmetric Reactions. *Angew. Chem. Int. Ed.* **2011**, *50*, 11849-11851.

104. Ozanne-Beaudenon, A.; Quideau, S. Regioselective Hypervalent-Iodine(III)-Mediated Dearomatizing Phenylation of Phenols through Direct Ligand Coupling. *Angew. Chem. Int. Ed.* **2005**, *44*, 7065-7069.

105. Harned, A. M. Asymmetric oxidative dearomatizations promoted by hypervalent iodine(III) reagents: an opportunity for rational catalyst design? *Tet. Lett.* **2014**, *55*, 4681–4689.

106. Singh, F. V.; Wirth, T. Hypervalent iodine-catalyzed oxidative functionalizations including stereoselective reactions. *Chem. Asian J.* **2014**, *9*, 950.

107. Romero, R. M.; Wçste, T. H.; MuÇiz, K. Vicinal Difunctionalization of Alkenes with Iodine(III) Reagents and Catalysts. *Chem. Asian J.* **2014**, *9*, 972.

108. Drutu, I.; Njardarson, J. T.; Wood, J. L. Reactive Dienes: Intramolecular Aromatic Oxidation of 3-(2-Hydroxyphenyl)-propionic Acids. *Org. Lett.* **2002**, *4*, 493- 496.

109. Fujita, M.; Ookubo, Y.; Sugimura, T. Asymmetric cycloetherification based on a chiral auxiliary for 4-acyloxy-1-butene substrates during oxidation with iodosylbenzene via a 1,3-dioxan-2-yl cation. *Tetrahedron Lett.* **2009**, *50*, 1298.

110. Kong, W.; Feige, P.; de Haro, T.; Nevado, C. Regio- and enantioselective aminofluorination of alkenes. *Angew. Chem.* **2013**, *125*, 2529.

111. Banik, S. M.; Medley, J. W.; Jacobsen, E. N. Catalytic, Diastereoselective 1,2-Difluorination of Alkenes. *J. Am. Chem. Soc.* **2016**, *138*, 5000–5003.

112. Haubenreisser, S.; Wöste, T. H.; Martínez, C.; Ishihara, K.; Muñiz, K. h Structurally Defined Molecular Hypervalent Iodine Catalysts for Intermolecular Enantioselective Reactions. *Angew. Chem. Int. Ed.* **2016**, *55*, 413.

113. Ueno, M.; Nabana, T.; Togo, H. Novel Oxidative α-Tosyloxylation of Alcohols with Iodosylbenzene and *p*-Toluenesulfonic Acid and Its Synthetic Use for Direct Preparation of Heteroaromatics. *J. Org. Chem.* **2003**, *68*, 6424.

114. Rçben, C.; Souto, J. A.; Gonz.lez, Y.; Lishchynskyi, A.; MuÇiz, K. Enantioselective metal-free diamination of styrenes. *Angew. Chem. Int. Ed.* **2011**, *50*, 9478.

115. Souto, J. A.; Gonz.lez, Y.; Iglesias, A; Zian, D.; Lishchynskyi, A.; MuÇiz, K. Iodine(III)-promoted intermolecular diamination of alkenes. *Chem. Asian J.* **2012**, *7*, 1103.

Chapter Two

# FUNCTIONAL PEPTIDES FOR ENANTIOSELECTIVE HYPERVALENT IODINE(III)-MEDIATED CHEMISTRY

## *2.1. Introduction: Hypervalent Iodine(III)-Mediated Reactions of Interest*

As previously described in Chapter One of this thesis, the research detailed by Ochai, Kita, Togo, and Yamamoto leading to the *in situ* generation of a Koser-type species from an iodoarene compound in the presence of a co-oxidant has laid the groundwork for many other hypervalent iodine-mediated reactions to be conducted in a catalytic fashion. Further efforts toward rendering such iodoarene catalysts enantioselective have positioned chiral hypervalent iodine (HI) catalysts as synthetically useful compounds to effect fundamental asymmetric organic transformations.[1-10] Two such reactions are the α-oxytosylation of propiophenone and the oxidative cyclization of 5-oxo-5-phenylvaleric acid (Scheme 2.1).

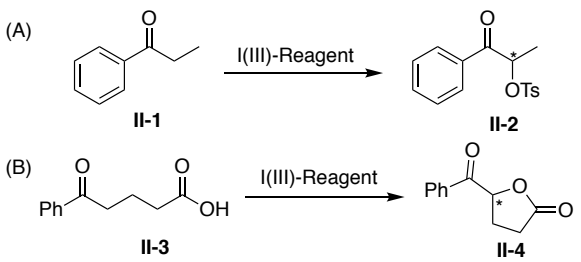


**Scheme 2.1.** Hypervalent I(III)-mediated organic transformations of interest. A) α-oxytosylation of propiophenone B) oxidative cyclization of 5-oxo-5-phenylvaleric acid.

### *The α-Oxytosylation of Propiophenone*

The α-functionalization of carbonyl compounds is a central component of any organic chemist's synthetic tool box. Specifically, the α-oxytosylation reaction effectively installs a new stereocenter, equipped with an excellent leaving group, in the α-position

relative to the carbonyl moiety. This valuable product, in turn, can be utilized in nucleophilic displacement reactions, providing a facile method to access a wide variety of α-substituted ketones.

Koser *et al.* first disclosed the use of a stoichiometric amount of PhI(OH)(OTs) or HTIB as an oxidant for the generation of α-oxytosyl ketones in moderate to good yields (40 – 100%).[1] This methodology was later expanded to other oxysulfonyl moieties (Scheme 2.2).[1-3] The use of HI reagents renders this transformation environmentally more moderate in comparison to the traditionally employed thallium-mediated process. Moriarty was also successful in promoting the indirect α-oxytosylation of ketones in excellent yields (78 – 92%) by using trimethylsilyl enol ethers as a ketone substitute and HTIB in $CH_2Cl_2$ at RT.[5] An increase in reactivity was later noticed by Togo and Nabana with the implementation of substituted [hydroxy(tosyloxy)iodo]arenes. Specifically, arenes bearing trifluoromethyl moieties produced the desired α-oxytosylated propiophenone product in a 96% yield.[11]

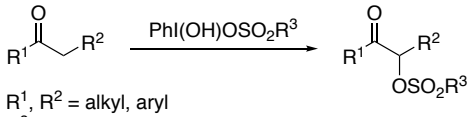


$R^1$, $R^2$ = alkyl, aryl
$R^3$ = Me, *p*-Tol

**Scheme 2.2.** Representative α-functionalization of ketones in the presence of [hydroxy(organosulfonyloxy)iodo] arenes, first reported by Koser et. al.

Previously, the use of stoichiometric amounts of HI reagents had been essential for mediating such transformations; however, within the last few decades, considerable attention has been focused on applying these reagents in a catalytic fashion.[12, 13] A major breakthrough in this field came when Ochai and Kita concurrently reported the use of a terminal oxidant for the *in situ* generation of the HI(III) species.[14, 15] More specifically, Ochai and coworkers demonstrated the α-acetoxylation of ketones using iodobenzene as

the precatalyst, and *meta*-chloroperoxybenzoic acid (*m*CPBA) as the terminal oxidant, resulting in moderate isolated yields of 43 – 63% (Scheme 2.3 A). Kita *et al.* also employed *m*CPBA as a suitable co-oxidant to perform the catalytic oxidative spirocyclization of phenols (Scheme 2.3 B).

Yamamoto and Togo extended this work when they established the *in situ* generation of a Koser-type reagent by exposing an iodoarene compound to *m*CPBA and *para*-toluenesulfonic acid monohydrate (*p*TSA·$H_2O$), thus providing the oxidized, catalytically active aryl-iodo(III) species. Using these conditions, a variety of α-oxytosylketones were accessed in moderate to good yields of 63 – 88% (Scheme 2.3 C).[16] This work represents considerable progress toward the development of iodoarene catalysts as viable alternatives to transition metal catalysts.[17]

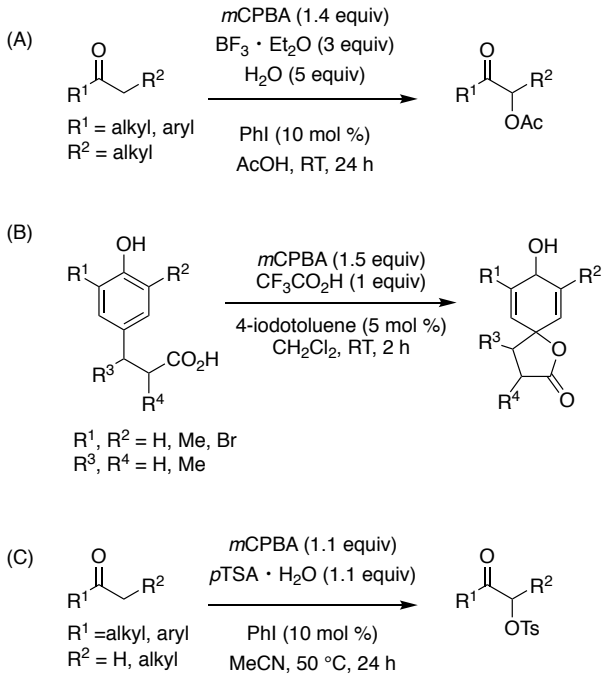


**Scheme 2.3.** Representative catalytic α-functionalization of ketones.

*The Asymmetric α-Oxytosylation of Propiophenone*

The scope of this transformation was further broadened following reports of the attempted asymmetric α-functionalization of carbonyl compounds, achieved by attaching chiral information in the *ortho* position relative to the iodoarene moiety. Initially, Koser and Wirth independently published *ortho*-substituted iodoarene structures; however, it was Wirth that first implemented chiral iodanes for the enantioselective α-oxytosylation of ketones in 1998.[2]

Since then, extensive research and time has been put into rendering these reactions highly enantioselective. Figure 2.1 represents a series of the most selective catalysts (**II-5** – **II-8**) reported thus far for the direct enantioselective α-oxytosylation of propiophenone. Catalyst structures **II-5**, **II-6**, and **II-8** represent iodoarene structures developed by Wirth

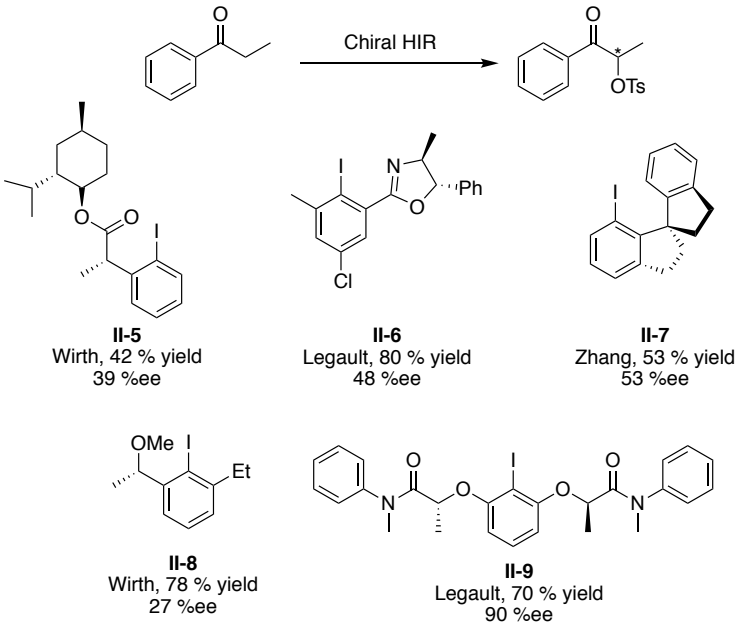


**Figure 2.1.** Current catalyst structures for the α-oxytosylation of propiophenone, pictured with their corresponding author, product yield, and enantioselectivity.

and Legault that position the chiral information in the *ortho* position on the iodoarene relative to the iodine moiety.[12,18-19] These three catalysts were able to achieve enantioselectivities for the α-oxytosylation of propiophenone in 39, 48, and 27% ee, respectively. Zhang disclosed catalyst **II-7**, an axially chiral aryl-iodo compound, capable of effecting the α-oxytosylation of propiophenone in 53% *ee*.[20] The most recent catalyst structure **(II-9)** was reported by Legault in 2015, in which the α-oxytosylated product was generated as its *(S)*-enantiomer in 90% *ee* and a 70% yield. This is impressive considering

that the highest levels reported prior to that disclosure were not greater than 55% *ee*.[21,22] It is important to note that the direct α-oxytosyation of propiophenone was not achieved, rather Legault employed a (*Z*)-enol acetate derivative of the propiophenone starting material (Scheme 2.4). Additionally, accessing the $C_2$-symmetric catalyst **II-9** requires a synthetic protocol consisting of five linear synthetic steps, with a majority requiring column purification. The reaction also requires the rather tedious, slow addition of the enol acetate starting material over a 13 h time period using a syringe pump. Finally, only one catalytic example was reported in the manuscript, and the substrate scope was explored using a stoichiometric loading of **II-9**. This may suggest a lack of catalytic utility upon application to substrates other than the (Z)-enol acetate congener of propiophenone. Nevertheless, the asymmetric variant of the α-oxytosylation of propiophenone has yet to succumb to synthetically useful levels of enantioselectivity when using iodoarene chiral catalysts.

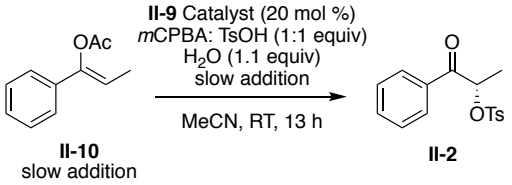


**Scheme 2.4.** Conditions for Legault's **II-9** catalyzed α -oxytosylation of enol acetate **II-10**.

*Oxidative Lactonization of Keto-Acids*

Hypervalent I(III)-mediated chemistry can also be applied to the oxidative cyclization of keto acids to their corresponding lactones. The ability to efficiently access varying lactone products represents a significant transformation due to the prevalence of this moiety in nature as well as their utility in synthetic and medicinal communities.[23,24] For example, the lactone motif is present in innumerable natural products with select aryl-substituted γ-lactones demonstrating interesting biological activities such as human

neutrophil elastase (HNE) and chitin synthase inhibition, as well as anti-inflammatory properties.[25-29]

Lactones can be synthesized via their carboxylic acid starting materials upon a direct oxidative C-O coupling reaction. Many of the previously reported coupling reactions involve the use of metal oxidants under harsh conditions. Additionally, these reactions often have a limited substrate scope, low product yields, and/or result in undesired side reactions such as ring oxidations and decarboxylations.[30-33] Alternatively, HI reagents could serve as mild alternatives to these traditionally required metal oxidants while also promoting direct lactone formation. Koser initially reported the use of HTIB in $CH_2Cl_2$ for the synthesis of oxytosyl-substituted lactones from various alkenoic acids in moderate yields.[2] Similarly, Moriarty also employed HTIB in refluxing $CH_2Cl_2$ for the oxylactonization of carboxylic acids.[34] Nearly two decades later, Wirth *et al.* demonstrated that aryl-λ3–iodanes, such as PIDA, PIFA, and HTIB, could promote the lactonization of 4-aryl-4-pentenoic acids.[35] Kita and co-workers presented a direct lactonization route, involving a benzylic C-H bond abstraction in the presence of a stoichiometric amount of (diacetoxyiodo)benzene, PIDA, and KBr for the synthesis of aryl lactones from their corresponding carboxylic acids. Methoxy-, nitro-, fluoro-, bromo- and phenyl-substituted aryl functionalities were all tolerated under these conditions producing the desired cyclic ether product in moderate to good yields (61 – 91 %).[7,15]

Great strides were made when the catalytic HI-mediated oxylactonization was realized by Ishihara and co-workers in 2009 with the *in situ* generation of HTIB from iodobenzene in the presence of a substoichiometric amount of tosic acid (TsOH) and *m*CPBA as a stoichiometric co-oxidant (Scheme 2.5A).[36] Soon after, tetrabutylammonium iodide was employed, as the pre-catalyst for the oxylactonization of various carboxylic acids, and was efficiently oxidized to its I(III)-catalytic state upon treatment with aqueous hydrogen peroxide (Scheme 2.5B).[37] Currently, most of the research surrounding this reaction of interest is focused on rendering it highly enantioselective.

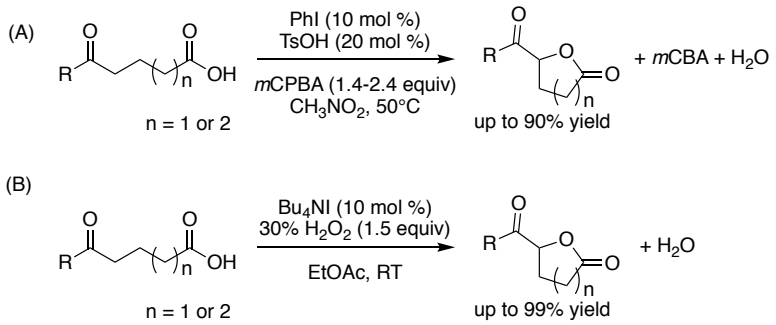


**Scheme 2.5.** Notable work by Ishihara and co-workers for the HI-mediated catalytic oxidative lactonization of carboxylic acids.

*The Asymmetric Oxidative Cyclization of 5-oxo-5-Phenylvaleric Acid*

In comparison to the asymmetric α-oxytosylation of propiophenone, even less success has been realized with the enantioselective oxidative cyclization of 5-oxo-5-phenylvaleric acid. Moran reported catalyst structures **II-11** and **II-12**, which promoted the highest levels of enantioselectivity, 12% *ee* and 47% *ee*, respectively (Figure 2.2).[38] Additionally, the yields for the reaction are fairly low, providing the lactone in only 31% and 47% yields, respectively. Further efforts were made by Ishihara and Wirth, yet these studies were also unsuccessful, resulting in enanatioselectivities no greater than 3% *ee*.[2,36,37] While these catalyst structures represent the most successful compounds for the two catalytic hypervalent I(III)-mediated asymmetric processes of interest, they only represent one approach to catalyst design. The major disadvantages of traditional catalyst design stems from lengthy synthetic protocols to prepare just one structure and the typically time consuming, step-by-step modification required to generate derivatives of an initial "hit" scaffold.[39] Furthermore, all of the catalysts described above position the chiral information in the *ortho* position relative to the iodine atom. Having only one position relative to the active I(III) site where chiral information can be communicated may represent a limiting factor in developing a highly reactive and enantioselective catalyst.

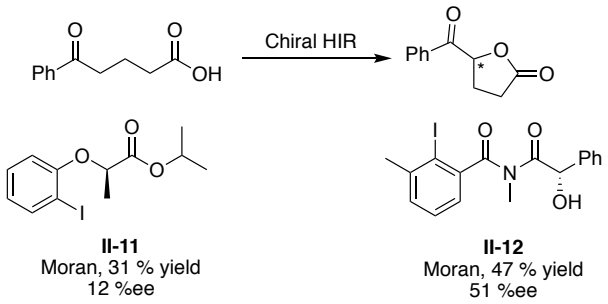


**Figure 2.2.** Catalyst structures for the oxidative cyclization of 5-oxo-5-phenylvaleric acid, pictured with their corresponding author, product yield, and enantioselectivity.

### *2.2. Hypervalent Aryl-Iodo Peptides for Asymmetric Catalysis*

Another potential mode for installation of chiral information onto a catalyst framework is the use of a chiral peptide scaffold.[39-41] Thus, we were intrigued by the possibility of short-chain peptides serving as viable alternatives to the previously described low molecular weight HI catalysts. Specifically, we hypothesized that the unique reactivity of hypervalent iodine in conjunction with the structural complexity and chiral space provided by short peptides ultimately might allow for the construction of catalysts suitable for enantioselective iodine(III)-mediated organic transformations.

The initial search for a synthetically useful HI peptide based catalyst centered around three initial scaffolds (Figure 2.3). Peptide catalysts possessing only a few amino acid residues have been shown to adopt a secondary structure suitable for the transfer of chirality.[42-49] Thus, Scaffolds A and B were both designed around a known β-turn secondary structure induced by a proline-D-alanine sequence.[45,46] More specifically, this sequence nucleates the β-turn via hydrogen bonding between the carbonyl oxygen of one residue with the amide proton of an amino acid three residues down the chain. One could hypothesize that the inclusion of this type of secondary structure would impart some rigidity into the peptide scaffold, possibly enhancing the enantioselectivity.[50-56] Scaffold C serves as a necessary linear comparison, as it possesses no amino acid residue sequence that is known to induce a secondary structure. Further Scaffold C, was designed using peptidic ligands published by Hoveyda and Snapper as inspiration.[39-42] The active iodoarene site (highlighted in blue) can easily be incorporated into Scaffolds B and C by capping the N-terminus of the peptides with commercially available 2-iodobenzoic acid

(2-IBA). The iodo-aryl portion in Scaffold A can be installed by inserting the commercially available Fmoc-4-iodophenyl alanine residue into the middle of the growing peptide sequence.

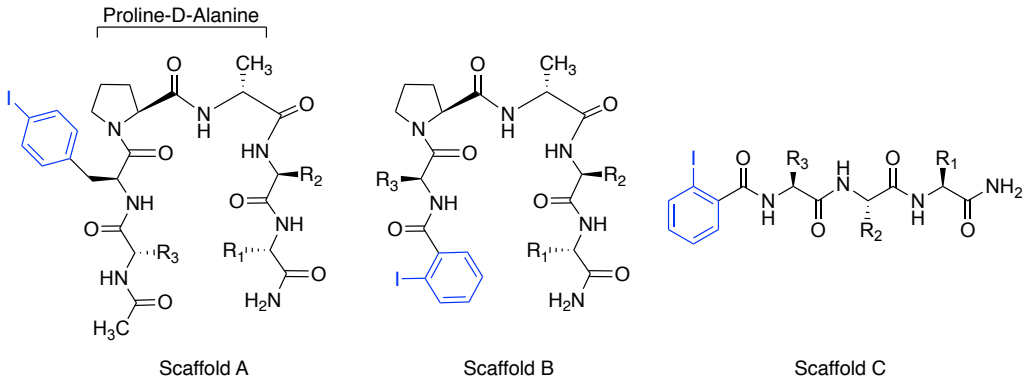


**Figure 2.3.** Peptide pre-catalyst scaffolds A-C, iodoarene sites are highlighted in blue. Scaffolds A and B contain a proline-D-alanine sequence, known to nucleate a β-turn secondary structure. Scaffold C will serve as a linear comparison, with no known secondary structure.

*Fmoc-Solid Phase Peptide Synthesis:*

Solid-Phase Peptide Synthesis (SPPS) was developed for the purpose of providing a rapid, simplified, and effective route to prepare oligopeptides. Briefly, it involves a heterogeneous reaction mixture composed of an insoluble resin-bound peptide chain, a soluble activated amino acid derivative and an appropriate solvent. This method of linking an amino acid to an insoluble support, then condensing it with a second amino acid followed by a third, and thus stepwise elongating the peptide chain was a monumental development in the field of peptide synthesis.

Fluorenylmethyloxycarbonyl- (Fmoc) SPPS is the most frequently used methods to prepare short peptide sequences. It features a base labile α-amino Fmoc-protecting group along with acid labile α-R-side chain protecting groups and peptide resin linkages. Our

group specifically used a Rink amide MBHA resin that is pre-loaded with an Fmoc-protected amine. After peptide assembly this resin yields C-terminal amide peptides, an attractive attribute due to the desire to synthesize a peptide library that will not exist in the typically charged state of free C-terminal carboxylate anions.[57,58]

Peptides in this study were assembled in disposable fritted syringes using the following general sequence. Following swelling of the resin in DCM, the base-labile group was removed with triple treatments of 20% (v/v) 4-methylpiperidine in DMF thus revealing the free amine available for amino acid coupling. Amino acid couplings were achieved by double two-minute treatments of the deprotected resin with 5 equiv of the coupling reagent O-(1*H*-6-Chlorobenzotriazole-1-yl)-1,1,3,3-tetramethyluronium hexafluorophosphate (HCTU), *N*,*N*-diisopropylethylamine (DIPEA), and the desired Fmoc-protected amino acid residue. This deprotection followed by coupling sequence was then repeated until the desired peptide sequence was assembled on the resin. The resin-bound, protected peptide sequence was then be cleaved and side-chain deprotected by treatment with a trifluoracetic acid (TFA) cleavage cocktail (TFA:$H_2O$:tri-*iso*-propylsilane, 95:4.5:0.5, v/v) and isolated upon evaporation of the TFA cocktail and precipitation with ice-cold diethyl ether (Figure 2.4). The successful preparation of all isolated peptide sequences were confirmed via MALDI-TOF mass spectrometry analysis.

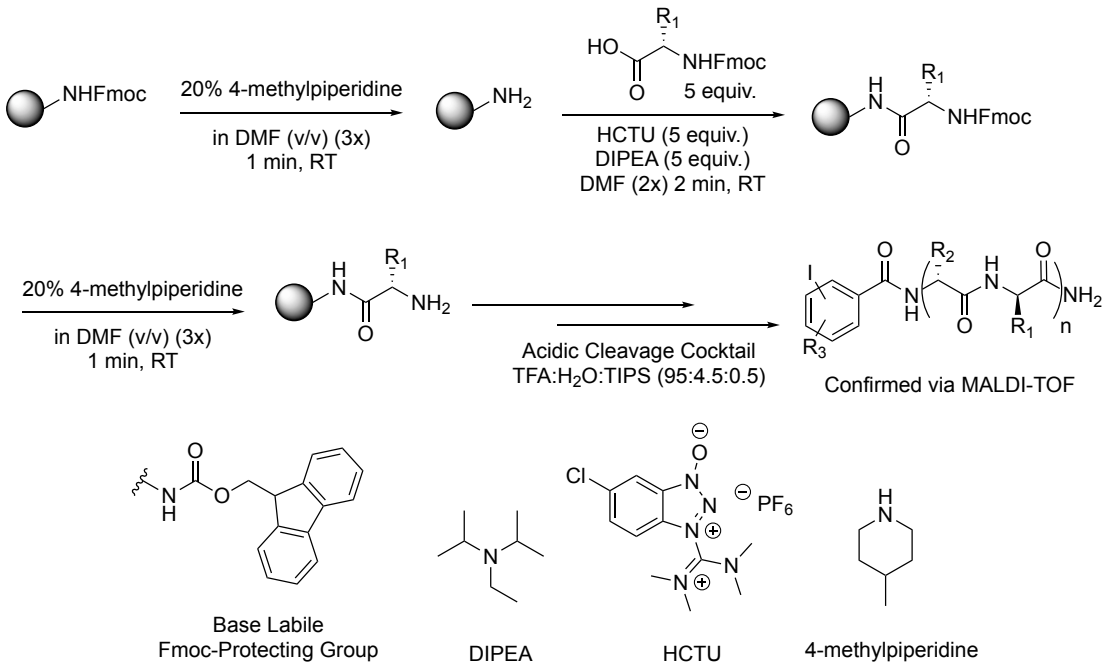


**Figure 2.4.** General Fmoc-SPPS scheme with corresponding reagents. Synthetic route to access iodoarene containing peptide precatalysts.

## *2.3. Results and Discussion*

### *1st Generation Peptide Catalyst Screening Results for the α-Oxytosylation of Propiophenone*

An initial 420-member iodoarene peptide catalyst library was prepared and screened as potential enantioselective catalysts for the α-oxytosylation of propiophenone. Briefly, this library resulted from the synthesis of amino acid sequences that were determined at random with varying commercial available Fmoc-protected amino acids, including basic, acid, polar, aromatic, and non-polar side chains. Cysteine, methionine, and arginine were not incorporated into the iodoarene peptides due to their highly susceptibility toward oxidation, which would complicate the study of our reactions of interest.[57,58]

This initial library consisted of 90 peptides of Scaffold A, 280 from Scaffold B, and only 50 from linear Scaffold C. Throughout the screening process, it was quickly realized that linear peptides from Scaffold C were not promoting selective reactions, therefore, the focus shifted mainly to the synthesis of bent peptides of Scaffold A and B. These aryl-iodo peptides were screened utilizing the reaction conditions previously disclosed by Togo. Namely, 3 equiv. of *m*CPBA was used as the co-oxidant and 3 equiv. of *p*TSA·$H_2O$ was used as the nucleophile in MeCN at RT for 24 hours (Scheme 2.6).[11,16] The success of enantioinduction for each catalyst was determined by means of chiral HPLC analysis and reported as % enantiomeric excess (% *ee*), calculated by taking the difference of the two enantiomeric peak areas divided by the sum of the peak areas, multiplied by a factor of 100. No attempts to quantify reaction yields were made due to the small scale and the desire conduct rapid screening of a large library of peptide structures.

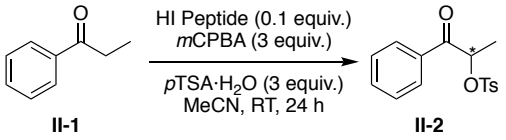


**Scheme 2.6.** Reaction screening conditions for the α-oxytosylation of propiophenone.

From this large screen, only two "hit" peptide structures emerged, **II-13** and **II-14** (Figure 2,5). For optimization purposes a "hit" peptide was taken to be a pre-catalyst capable of effecting the oxytosylation of propiophenone with levels of enantioselectivity above 20% *ee*. Peptide structure **II-13**, with an amino acid sequence of 2-IBA-Ile-Pro-D-Ala-Asp-Gln, successfully catalyzed the α-oxytosylation of propiophenone to generate the desired product with 48% *ee*. Catalyst **II-14**, with the primary sequence of 2-IBA-hPhe-Pro-D-Ala-Phg-Asp, produced the α-oxytosylated ketone with in 23% *ee*.

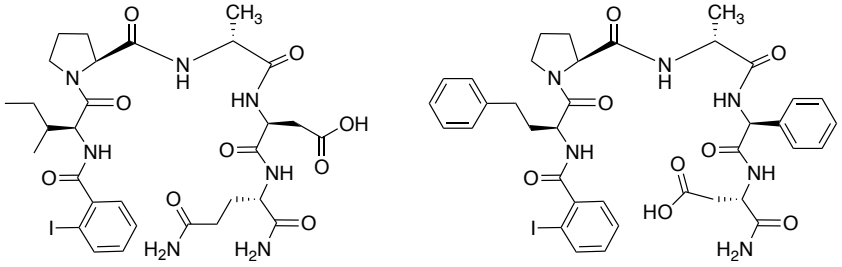

**II-13**
2-IBA-Ile-Pro-D-Ala-Asp-Gln
48% *ee*

**II-14**
2-IBA-hPhe-Pro-D-Ala-Phg-Asp
23% *ee*

**Figure 2.5.** Two lead peptide structures emerging from initial 420-member iodoarene peptide catalyst library screen for the α-oxytosylation of propiophenone.

*1st Generation Peptide Catalyst Screening Results for the Oxidative Cyclization of 5-oxo-5-Phenylvaleric Acid*

For the oxylactonization of 5-oxo-5- phenylvaleric acid, a much smaller library of peptide structures were screened. Namely, 100 precatalysts, pulled from Scaffold A and Scaffold B libraries, were assessed using almost identical conditions to those of the α-oxytosylation of propiophenone but at elevated temperatures,

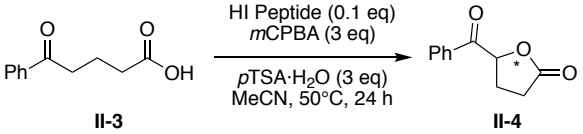


**II-3** **II-4**

**Scheme 2.7.** Reaction screening conditions for the oxidative cyclization of 5-oxo-5-phenylvaleric acid.

*i.e*. 3 equiv. of *m*CPBA, 3 equiv. of *p*TSA·$H_2O$ in MeCN at 50 ˚C for 24 hours (Scheme 2.7). Unfortunately, levels of stereoinduction greater than 18% *ee* were not realized from this 1st generation peptide library screen for the oxylactonization reaction of interest. (Figure 2.6).

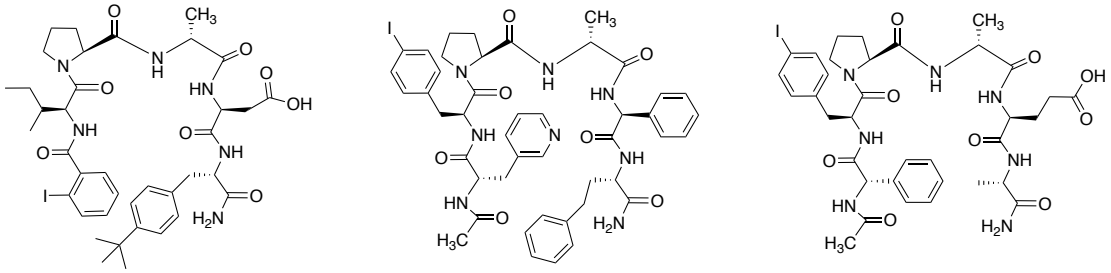

**II-15**
2-IBA-Ile-Pro-D-Ala-Asp-tPhe
10% *ee*

**II-16**
3-Pya-4-I-Phe-Pro-D-Ala-Phg-hPhe
18% *ee*

**II-17**
Phg-4-I-Phe-Pro-D-Ala-Glu-Ala
16% *ee*

**Figure 2.6.** Three lead peptide structures emerging from the initial 100-member iodoarene peptide catalyst library screen for the oxidative lactonization of 5-oxo-5-phenylvalaric acid.

Despite the low levels of enantioselectivity, three lead peptide structures were realized as a result of their ability to catalyze the reaction of interest and impart a modest degree of enantioinduction. More specifically, peptide **II-15**, with an amino acid sequence of 2-IBA-Ile-Pro-D-Ala-Asp-tPhe, produced the lactonization product (**II-4**) in 10% *ee*. Further, precatalysts **II-16** and **II-17** with primary structures from scaffold A, generated **II-4** in 18 and 16% *ee*, respectively. For optimization purposes, peptide structure **II-16** will be referred to as the "hit" peptide from this 1st generation library screen for the oxidative lactonization of 5-oxo-5-phenylvalaric acid.

*"Hit" Precatalyst Peptide Primary Structure Optimization*

Following the completion of the 1st generation peptide library screening campaign, efforts were focused on optimizing the amino acid sequences of our best "hit" peptide precatalysts **II-12**, **II-13**, and **II-16**. Peptide derivatives of each "hit" scaffold were iteratively optimized in

positions *i*, *i+4*, and *i+5* for peptides sequences from scaffold A and *i+1*, *i+4*, *i+5* for "hits' from scaffold B (Figure 2.7). Positions *i+2* and *i+3* were not altered in order to preserve the β-turn secondary structure nucleated by the Pro-D-Ala sequence. Also, the active iodoarene sites, namely the 4-iodo-phenylalanine residue and the 2-iodoarene cap

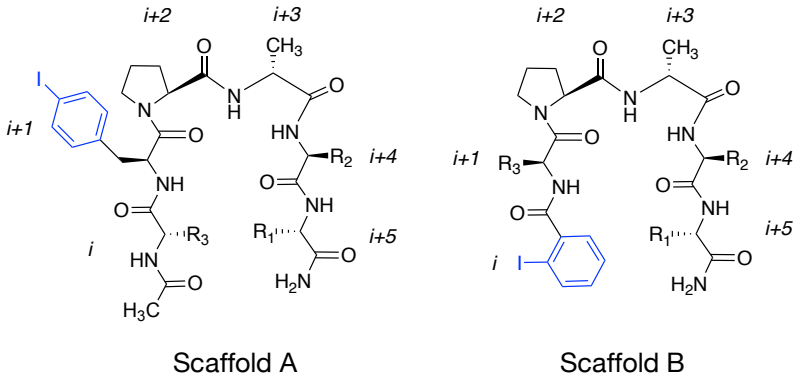


**Figure 2.7.** Generic peptide structures of Scaffold A and B with amino acid residue positions available for iterative optimization indicated as *i*, *i+1*, *i+2*, *i+3*, *i+4*, and *i+5*.

on scaffold A and B, respectively, were not varied. Peptide derivatives were synthesized using 31 different Fmoc-protected L-amino acids with R-side chains. The modularity of using short peptide sequences is highlighted by the ability to swap out an amino acid residue for one of similar or vastly different chemistry such as alkyl, aryl, acidic, basic and or polar character (Figure 2.8).

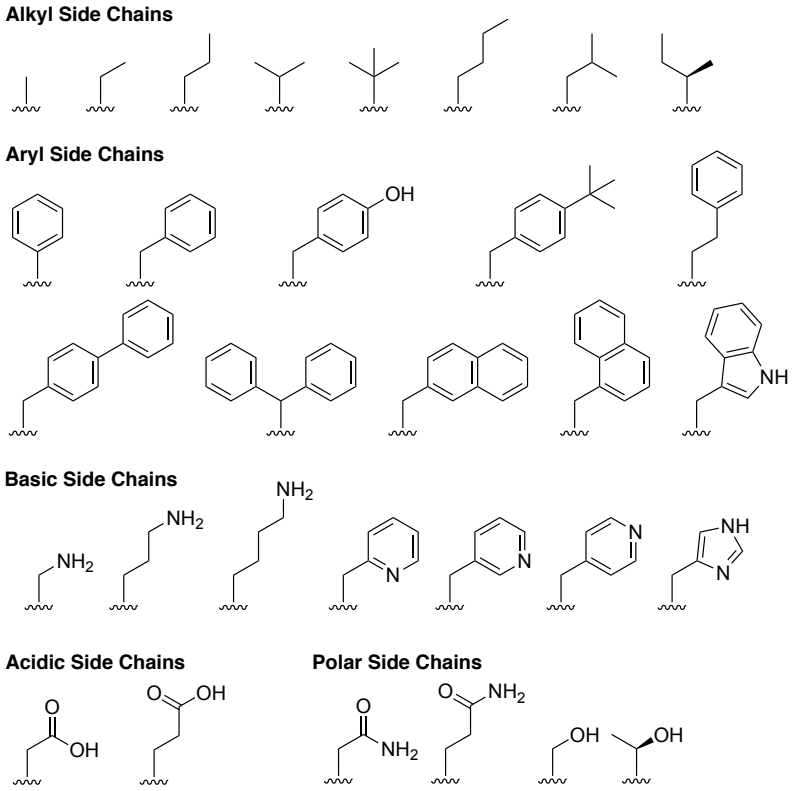


**Figure 2.8.** Available amino acid residue R-side chains.

Peptide structure **II-12** was fully modified at the *i+1*, *i+4*, *i+5* amino acid residue positions, resulting in an additional 90 precatalysts to screen in the α-oxytosylation of propiophenone. Structure **II-13** was only modified at positions *i+4* and *i+5* resulting in 60 additional catalyst structures. Despite this effort that resulted in a 150-member 2nd generation iodoarene peptide library, enantioselectivities greater than the initial "hits" of 48 and 23% *ee*, respectively, were not achieved for the α-oxytosylation of propiophenone.

Similarly, the systematic replacement of amino acid residue positions *i* and *i+4* on peptide **II-16**, resulted in a new 2nd generation library of 60 peptides that were screened for their enantioselectivity in the lactonization of 5-oxo-5-phenylvaleric acid. Three new peptide structures emerged **II-18**, **II-19**, and **II-20**, generating the desired lactonization product in -22, -20, and -24% *ee*, respectively. The levels of enantioinduction obtained

with these new precatalysts are only slightly increased from the previous -18% *ee* seen from the 1st generation **II-16** aryl-iodo peptide.

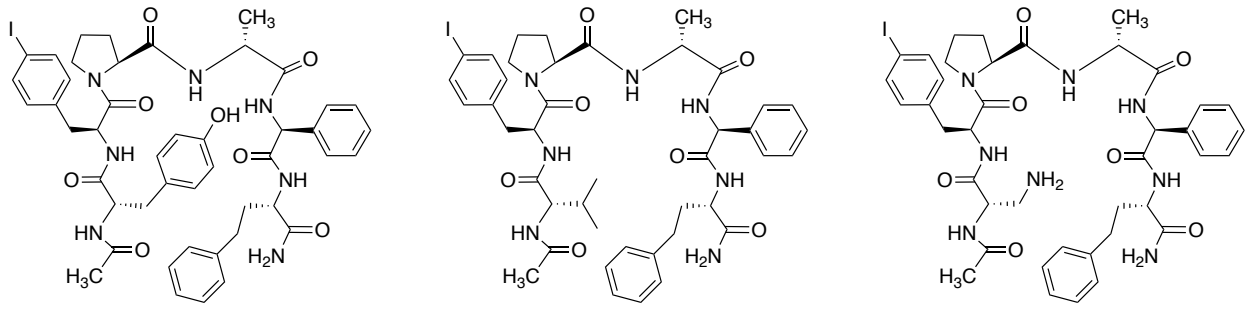

**II-18**
Tyr—4-I-Phe-Pro-D-Ala-Phg-hPhe
-22% *ee*

**II-19**
Val-4-I-Phe-Pro-D-Ala-Phg-hPhe
-20% *ee*

**II-20**
Dap-4-I-Phe-Pro-D-Ala-Glu-Ala
-24% *ee*

**Figure 2.9.** Peptide precatlayst structures emerging from the 2nd generation screen for oxidative lactonization of 5-oxo-5-phenylvalaric acid.

### *2.4. Conclusions and Future Directions*

With their ease of preparation, modularity, and accessible secondary structure (*e.g.* β-turn),1st and 2nd generation iodoarene peptide scaffold libraries were synthesized and screened for catalytic activity and enantioinduction in two test reactions hinging on hypervalent iodine catalysis. The results obtained for the α-oxytosylation of propiophenone and for the oxidative cyclization of 5-oxo-5-phenylvaleric acid clearly demonstrate that our iodoarene peptides have the potential to serve as asymmetric catalysts for I(III)-mediated processes. It is also worth highlighting that "hit" peptide **II-13** was able to impart levels of enantioselectivity on par with the current most successful chiral HI catalysts, for the α-oxytosylation transformation, reported by Wirth, Legault, and Zhang

(**II-5-II-8**).

Nonetheless, the overall aim of this research is to develop chiral hypervalent iodine peptide catalysts that ensure exceptionally high levels of enantioselectivty; thus, it is noticeable that despite the large number of peptides screened (>650) we were unable to break the 50% *ee* selectivity barrier for our two reactions of interest. The natural progression of this work was to investigate and improve upon the initial "hit" peptide scaffolds by iteratively optimizing selective amino acid residues in hopes that a new, more selective peptide would emerge. The likelihood of this approach being successful is not unreasonable due to the vast amount of chiral space provided and explored by our peptide library as well as similar approaches bearing highly reactive and enantioselective catalysts in the past.[59] In our case, this approach was unsuccessful; therefore, investigations into the mode of stereoinduction will be considered as well as the structure-enantioselectivity relationship of our iodoarene peptide catalysts.

### *2.5. Experimental Methods*

#### *2.5.1. General Materials and Methods*

All chemicals were purchased from commercial suppliers and used without further purification. Following isolation, synthesized products were purified by flash column chromatography using silica gel SDS 60 C.C. 40- 63 microns. $^{1}H$ and $^{13}C$ NMR spectra were collected on a 500 MHz Bruker NMR spectrometer at ambient temperature. Chemical shifts are reported in parts per million (ppm) and referenced to residual solvent peaks (i.e. δ 7.28 ppm for $^{1}H$ NMR, 77 ppm for $^{13}C$ NMR) in $CDCl_3$. Data is presented as follows: chemical shift, integration, multiplicity (s = singlet, d = doublet, t = triplet, q = quartet, br

= broad, m = multiplet), and coupling constants (*J*) are given in Hz. All synthesized peptides were characterized via MALDI-TOF mass spectrometry.

Enantiomeric excess (% *ee*) of products were **II-2** and **II-4** determined using chiral high performance liquid chromatography (HPLC). Chiral samples were run on an Agilent 1260 Infinity system equipped with a diode array detector (G4212-60008), and an Agilent 1260 Infinity auto sampler. The chiral stationary column used was a Chiralpak-AD (250mm X 4.6 mm). The mobile phase consisted of *iso*-propyl alcohol/hexanes mixture (50:50). The flow rate was set at 1 mL/min and the elution of analytes was monitored at 254 nm.

*2.5.2. Fmoc-SPPS Synthetic Methods:*

Following standard Fmoc-SPPS protocols, iodoarene peptide precatalysts were prepared on solid support using the commercially available Rink Amide MBHA resin (200 mg, 0.3–0.8 meq/g, 200-400 mesh). Rink Amide MBHA resin comes pre-loaded with an Fmoc-protected amine for the preparation of C-terminal amide peptides. Therefore, amino acid residues were built on the solid support beginning at the C-terminus. Peptides from Scaffold A were N-caped with an acetate group while peptides from Scaffolds B and C were N-capped with the appropriate iodobenzoic acid. Double amino acid couplings were achieved using a 5 equiv. excess of the appropriate Fmoc-amino acid, HCTU as the coupling agent, and DIPEA in DMF as the solvent. Fmoc-deprotections were completed upon treatments with a basic solution of 20% 4-methylpiperidine in DMF. The fully assembled aryl-iodo peptide were cleaved from the resin and side-chain deprotected using a standard trifluoroacetic acid (TFA) cleavage cocktail and isolated following evaporation

of the TFA solution followed by precipitation with ether and centrifugation. All peptide precatalyst structures were confirmed via MALDI-TOF MS analysis (See Appendix A for full table of synthesized peptides). A step-wise procedure for the Fmoc-solid-phase synthesis of peptide **II-13** is described below.

*Resin Swelling:* The Rink Amide MBHA resin (200 mg) was added to the barrel of a 10 mL fritted syringe and swelled by a 4 mL DCM wash, followed by soaking for 5 min in an additional 5 mL of DCM. The residual DCM was purged from the syringe and the resin was washed with DMF (3 x 4 mL).

*Fmoc-Deprotection:* The initial Fmoc-deprotection of the Rink Amide resin was performed by means of three sequential one-min treatments with 2 mL of a 20% 4-methylpiperidine in DMF solution. The deprotected resin was then washed three times with 5 mL of DMF, resulting in a free amine ready for the first amino acid coupling.

*Amino acid couplings:* Peptide **II-13** was assembled on the solid-support beginning at the C-terminus. Therefore, 5 equiv. (relative to resin loading) of Fmoc-L-Gln, HCTU, and DIPEA were added to a 3 mL screw-top vial. The solids were then dissolved in 1 mL of DMF. This prepared mixture was then taken up into the fritted syringe, containing the resin, and agitated for 2 min. This first coupling mixture was then ejected into a waste container. The resin was subsequently treated with a second aliquot of the Fmoc-L-Gln amino acid mixture for 2 min. Following this double amino acid coupling procedure, the resin was once again washed with DMF (3 x 5 mL). The $N_{\alpha}$-Fmoc group was then removed following the previously described Fmoc-deprotection protocol in order to achieve the next amino acid residue coupling of an Fmoc-L-Asp residue. This deprotection-coupling pattern was

repeated until the desired amino acid residues were assembled as follows: Resin-Gln-Asp-D-Ala-Pro-Ile-2-IBA.

*N-terminal Acetate Capping:* Where appropriate (Scaffold A), the fully assembled peptide, was N-capped with an acetate group following double, 5 min treatments with a 4 mL aliquot of a 5% acetic anhydride in DMF solution. After the allotted time for the double treatment, the solution was ejected from the syringe and the resin was washed with DMF (3 x 5 mL).

*Peptide Cleavage and Isolation:* Following N-terminal capping of the resin-bound peptide, the resin was washed with DCM (3 x 5 mL), and de-swelled with methanol (3 x 5 mL). The resin was dried in a vacuum oven at room temperature for 24 h. The resin-bound peptide was then cleaved and the acid-labile R-side chains were deprotected via a 2 h treatment with an acidic cleavage cocktail of trifluoroacetic acid: $H_2O$: tri-*iso*-propylsilane (95:4.5:0.5). Following evaporation of the cleavage cocktail and precipitation with ice cold ether, the peptide was isolated as a white powdery solid and characterized by MALDI-TOF mass spectrometry: (*m*/*z*) calcd for $C_{30}H_{42}NaIN_7O_4$ $[MNa]^+$ 794.1981, found 794.1976.

### *2.5.3. Screening Reaction Protocols:*

Chiral HPLC analyses of the crude reaction mixtures were completed to determine enantiomeric excesses for the α-oxytosylation of propiophenone and the oxidative lactonization of 5-oxo-5-phenylvaleric acid. Pure racemic samples were first prepared following protocols found in section ***2.5.4.*** of this chapter and used as chiral HPLC standards to determine the retention times of product enantiomers.

*General Procedure for the α-Oxytosylation of Propiophenone*

Iodoarene peptide precatalysts were evaluated in the asymmetric α-oxytosylation of propiophenone using the following representative procedure: A 3 mL screw-capped vial was charged with propiophenone (4 μL, 0.01 mmol, 1.0 equiv), *p*TSA·$H_2O$ (17.1 mg, 0.03 mmol, 3 equiv), *m*CPBA (19.1 mg, 0.03 mmol, 3 equiv), the appropriate iodoarene peptide precatayst (0.01 mmol, 0.1 equiv) and a small stir bar. The reagents were dissolved in 1 mL of acetonitrile and the reaction was stirred for 24 h at RT. Following the allotted reaction time, the crude solution was concentrated by rotary evaporation and prepared for chiral HPLC analysis.

***General Procedure for the Oxidative Cyclization of 5-oxo-5-Phenylvaleric Acid***

Iodoarene peptide precatalysts were evaluated in the asymmetric oxylactonization of 5-oxo-5-phenylvaleric acid using the following representative procedure: a 3 mL screw-capped vial was charged with 5-oxo-5-phneylvaleric acid (1.9 mg, 0.01 mmol, 1.0 equiv), *p*TSA·$H_2O$ (17.1 mg, 0.03 mmol, 3 equiv.), *m*CPBA (19.1 mg, 0.03 mmol, 3 equiv), the appropriate iodoarene peptide precatayst (0.01 mmol, 0.1 equiv) and a small stir bar. The reagents were dissolved in 1 mL of acetonitrile and the reaction was stirred for 24 h at 50 ˚C. Due to the two enatiomeric product peaks eluting around the same retention time as residual *p*TSA·$H_2O$ all crude reaction mixtures were washed with a saturated sodium bicarbonate solution (2X). The aqueous layer was extracted twice with ethyl acetate and the combined organic layers were washed once more with sat. aq. $NaHCO_3$ followed by sat. aq. brine.

### *2.5.4. Synthesis of Racemic Products*

The corresponding racemic products from our two reactions of interest were synthesized and purified to serve as chiral HPLC standards for the determination of each enantiomeric peak retention times.

*General procedure for α-oxytosylation of propiophenone,* ***II-2****.*

A flame dried, 100 mL round-bottom flask was charged with propiophenone **II-1** (132 µL, 1 mmol, 1.0 equiv), *para*-toluenesulfonic acid monohydrate (0.571 g, 3 mmol, 3 equiv), *meta*-chloroperoxybenzoic acid (0.702 g, 3 mmol, 3 equiv), and 4-iodotoluene (0.637 g, 1.5 mmol, 1.5 equiv). The reagents were dissolved in 10 mL of acetonitrile and the resulting solution was allowed to stir under $N_2$ at 50 ˚C for 24 h. The reaction mixture was concentrated by rotary evaporation, followed by dilution in DCM, and the organics were washed three times with an aqueous saturated sodium bicarbonate solution. The combined organic layers were dried over sodium sulfate, filtered, and concentrated by rotary evaporation. The crude product was purified by column chromatography on silica gel (20:80 EtOAc:hexanes) to give a light brown solid **II-2** (0.274 g, 94%). $R_f$= 0.22 (20:80 EtOAc:hexanes) $^1$H NMR (500 MHz, $CDCl_3$): δ 7.90, 7.88 (2H, d, J= 7.0 Hz), 7.78, 7.76 (2H, d, J = 8.3 Hz), 7.62-7.59 (1H, t, J= 7.4 Hz), 7.55-7.49 (2H, m), 7.29-7.27 (2H, t, J= 8.0 Hz), 5.82-5.78 (1 H, q, J= 7.0 Hz), 2.424 (3 H, s), 1.62, 1.60 (3 H, d, J= 7.0 Hz) ppm. $^{13}$C NMR (125 MHz, $CDCl_3$): δ 194.8, 144.9, 133.8, 133.6, 130.2, 129.8, 128.8, 128.7, 128.6, 128.5, 127.9, 76.6, 21.6, 18.7 ppm.

*General procedure for oxylactonization of 5-oxo-5-phenylvaleric acid,* ***II-4.***

The substrate 5-oxo-5-phenylvaleric acid, **II-3**, (0.192 g, 1 mmol, 1.0 equiv), *m*CPBA (0.702 g, 3 mmol, 3.0 equiv), *p*TSA·$H_2O$ (0.571 mg, 3 mmol, 3.0 equiv), and 4-iodotoluene (0.637 g, 1.5 mmol, 1.5 equiv) were dissolved in MeCN (10 mL) and stirred for 24 h at 50 ˚C under nitrogen in a flame dried round-bottom flask. Following rotary evaporation, the reaction mixture was diluted in DCM and washed three times with aqueous saturated sodium bicarbonate. The organic layers were collected and dried over anhydrous sodium sulfate, filtered, and concentrated by rotary evaporation. The crude product was purified via silica gel column chromatography (20:80 EtOAc:hexanes) to give a white solid **II-4** (0.176 g, 92%) $^1$H NMR (500 MHz, $CDCl_3$): 8.00 (2H, d, J = 7.4), 7.67 (1H, t, J 7.4 Hz), 7.54 (2H, t, J = 7.6 Hz), 5.85-5.82 (1H, m), 2.62-2.48 (4H, m) ppm. $^{13}$C NMR (125 MHz, $CDCl_3$): 19.3, 176.2, 134.3, 133.6, 129.0, 128.9, 78.3, 26.8, 25.0 ppm.

### *2.6. Supplementary Information*

Appendix A contains this chapter's corresponding chiral HPLC chromatograms, $^1$H and $^{13}$C NMR spectra as well as all a catalog of the libraries of synthesized 1$^{st}$ and 2$^{nd}$ generation peptides and their corresponding MALDI-TOF characterization data.

### *2.7. References*


1. Moriarty, R. M.; Vaid, R. K.; Koser, G. F. [Hydroxy(organosulfonyloxy)iodo]arenes in Organic Synthesis. *Synlett* **1990**, 365-383.
2. Wirth, T.; Hirt, U. H. Hypervalent Iodine Compounds: Recent Advances in Synthetic Applications. *Synthesis* **1999**, *8*, 1271-1287.
3. Wirth, T.; Ochiai, M. Ed. Hypervalent Iodine Chemistry, Springer: Berlin (Germany), 2003, Vol. 224, pp 5-68.
4. Hirt, U. H.; Schuster, M. F. H.; French, A. N.; Wiest, O. G.; Wirth. T. Chiral Hypervalent Organo-Iodine(III) Compounds. *Eur. J. Org. Chem.* **2001**, *2001*, 1569- 1579.
5. Moriarty, R. M. Organohypervalent iodine: development, applications, and future directions. *J. Org. Chem.* **2005**, *70*, 2893-2903.
6. Zhdankin, V. V.; Stang, P. J. Recent Developments in the Chemistry of Polyvalent Iodine Compounds. *Chem. Rev.* **2002**, *102*, 2523-2584.
7. Tohma, H.; Kita, Y. Hypervalent Iodine Chemistry; Wirth, T. Ed.; Springer: Berlin, 2003; pp 209.
8. Varvoglis, A. Hypervalent Iodine in Organic Synthesis; Academic Press: London, 1997.
9. Varvoglis, A. Commentary: organic hypervalent iodine chemistry spanning three centuries—a historical overview. *Tetrahedron* **2010**, *66*, 5739-5744.

10. Wirth, T. Hypervalent Iodine Chemistry; Ochiai, M., Ed.; Springer: Berlin (Germany), 2003, Vol. 224, pp 5-68.

11. Nabana, T.; Togo, H. Reactivities of Novel [Hydroxy(tosyloxy)iodo]arenes and [Hydroxy(phosphoryloxy)iodo]arenes for α-Tosyloxylation and α-Phosphoryloxylation of Ketones. *J. Org. Chem.* **2002**, *67*, 4362–4365.

12. Wirth, T. Catalytic Enantioselective α-Oxysulfonylation of Ketones Mediated by Iodoarenes. *Eur. J. Org. Chem.* **2008**, *2008*, 5315-5328.

13. Altermann, S. M.; Richardson, R. D.; Page, T. K.; Schmidt, R. K.; Holland, E.; Mohammed, U.; Paradine, S. M.; French, A. N.; Richter, C.; Bahar, A. M.; Witulski, B.; Wirth, T. Catalytic Enantioselective α-Oxysulfonylation of Ketones Mediated by Iodoarenes. *Eur. J. Org. Chem.* **2008**, *2008*, 5315-5328.

14. Ochiai, M.; Takeuchi, Y.; Katayama, T.; Sueda, T.; Miyamoto, K. Iodobenzene-catalyzed alpha-acetoxylation of ketones in situ generation of hypervalent (diacyloxyiodo)benzenes using m-chloroperbenzoic acid. *J. Am. Chem. Soc.* **2005**, *127*, 12244-12245.

15. Dohi, T.; Maruyama, A.; Yoshimura, Y.; Morimoto, K.; Tohma, H.; Kita, Y. Versatile hypervalent-iodine(III)-catalyzed oxidations with m-chloroperbenzoic acid as a cooxidant. *Angew. Chem., Int. Ed.* **2005**, *44*, 6193-6196.

16. Yamamoto, Y.; Togo, H. PhI-catalyzed α-tosyloxylation of ketones with *m*-chloroperbenzoic acid and *p*-toluenesulfonic acid. *Synlett* **2006**, 798-800.

17. Dohi, T.; Kita, Y. Hypervalent iodine reagents as a new entrance to organocatalysts. *Chem. Comm.* **2009**, 2073-2085. .

18. Guilbault, A.-A.; Basdevant, B.; Wanie, V.; Legault, C. Y. Catalytic Enantioselective α-Tosyloxylation of Ketones Using Iodoaryloxazoline Catalysts: Insights on the Stereoinduction Process. *J. Org. Chem.* **2012**, *77*, 11283-11295.

19. Guilbault, A.-A.; Legault, C. Y. Drastic Enhancement of Activity in Iodane-Based α-Tosyloxylation of Ketones: Iodine(III) Does the Hypervalent Twist. *ACS Catalysis* **2012**, *2*, 219-222.

20. Yu, J.; Cui, J.; Hou, X. S.; Liu, S. S.; Gao, W. C.; Jiang, S.; Tian, J.; Zhang, C. Enantioselective α-tosyloxylation of ketones catalyzed by spirobiindane scaffold-based chiral iodoarenes. *Tet. Asym.* **2011**, *22*, 2039-2055.

21. Basdevant, B.; Legault, C. Y. Enantioselective Iodine(III)-Mediated Synthesis of α- Tosyloxy Ketones: Breaking the Selectivity Barrier. *Org. Lett.* **2015**, *17*, 4918- 4921.

22. Basdevant, B.; Legault, C. Y. Study of the Reactivity of [Hydroxy(tosyloxy)iodo]benzene Toward Enol Esters to Access α-Tosyloxy Ketones. *J. Org. Chem.* **2015**, *80*, 6897-6902.

23. Collins, I. Saturated and Unsaturated Lactones. *J. Chem. Soc., Perkin Trans. 1.* **1998**, *11*, 1869-1888.

24. Donnelly, D. M. X.; Meegan, M. J. Comprehensive Heterocyclic Chemistry; Katritzky, A. R., Ed.; Pergamon: New York, 1984; Vol. 4, p 657.

25. Devon, T. K.; Scott, A. I. In Handbook of Naturally Occurring Compounds; Academic Press: New York, 1975; Vol. 1, 249.

26. Katzenellenbogen, J. A.; Rai, R.; Dai, W. Enol lactone derivatives as inhibitors of human neutrophil elastase and trypsin-like proteases. *Bioorg. Med. Chem. Lett.* **1992**, *2*, 1399.

27. Hwang, E.-I.; Yun, B.-S.; Kim, Y.-K.; Kwon, B.-M.; Kim, H.-G.; Lee, H.-B.; Jeong, W.J.; Kim, S.-U. Chaetoatrosin A, a Novel Chitin Synthase II Inhibitor Produced by *Chaetomium atrobrunneum* F449. *J. Antibiot.* **2000**, *53*, 248-255.

28. Husain, A.; Khan, M. S. Y.; Hasan, S. M.; Alam, M. M. 2-Arylidene-4-(4-phenoxy-phenyl)but-3-en-4-olides: synthesis, reactions and biological activity. *Eur. J. Med. Chem.* **2005**, *40*, 1404.

29. Lambert, J. D.; Rice, J. E.; Hong, J.; Hou, Z.; Yang, C. S. Synthesis and biological activity of the tea catechin metabolites, M4 and M6 and their methoxy-derivatives. *Bioorg. Med. Chem. Lett.* **2005**, *15*, 873-876.

30. Brauman, J. I.; Pandell, A. J. Mechanism of Permanganate Oxidation of Tertiary Hydrogen to Hydroxyl. *J. Am. Chem. Soc.* **1970**, *92*, 329-335.

31. Nagarajan, A.; Porchezhiyan, V.; Srinivasaramanujam; Balasubramanian, T. R. Synthesis of γ-Phenyl-γ-butyrolactone. *Ind. J. Chem.* **1985**, *24B*, 1202.

32. Irie, H.; Maruyama, J.; Shimada, M.; Zhang, Y.; Kouno, I.; Shimamoto, K.; Ohfune, Y. Use of Potassium Peroxodisulfate for Benzylic Oxidation and Oxidative Coupling of Benzoylacetates. *Synlett* **1990**, 421.

33. Jevric, M.; Taylor, D. K.; Greatrex, B. W.; Tiekink, E. R. T. DDQ induced oxidative cyclisations of 1,2-dihydronaptho[2,1-b]furans. *Tetrahedron* **2005**, *61*, 1885-1891.

34. Moriarty, R. M.; Vaid, R. K.; Hopkins, T. E.; Vaid, B. K.; Prakash, O. Conversion of h lactones to the higher homologous α, β-unsaturated lactones v/a hypervalent iodine oxidation of 1-trimethylsilyloxy-2-oxa[n.1.0] cycloalkanes. *Tetrahedron Lett*. **1990**, *31*, 197-200.

35. Farooq, U.; Schäfer, S.; Shah, A. A.; Freudendahl, D. M.; Wirth, T. Synthesis of New Enantiomerically Pure Organoiodine Catalysts and Their Application in the α-Functionalization of Ketones. *Synthesis* **2010**, 1023-1029.

36. Uyanik, M.; Yasui, T.; Ishihara, K. Hypervalent iodine-catalyzed oxylactonization of ketocarboxylic acids to ketolactones. *Bioorg. Med. Chem. Lett.* **2009**, *19*, 3848-3851.

37. Uyanik, M.; Okamoto, H.; Yasui, T.; Ishihara, K. Quaternary ammonium (hypo)iodite catalysis for enantioselective oxidative cycloetherification. *Science* **2010**, *328*, 1376-1379.

38. Rodriguez, A.; Moran, W. J. Chiral Aryl Iodide-Catalyzed Enantioselective α-Oxidation of Ketones. *Synthesis* **2012**, *44*, 1178-1182.

39. Hoveyda, A. H. Catalyst discovery through combinatorial chemistry. *Chem. Biol.* **1998**, *5*, 187-191.

40. Hoveyda, A. H.; Hird, A. W.; Kacprzynski, M. A. Small peptides as ligands for catalytic asymmetric alkylations of olefins. Rational design of catalysts or of searches that lead to them? *Chem. Commun.* **2004**, 1779-1785.

41. Kuntz, K. W.; Snapper, M. L.; Hoveyda, A. H. Combinatorial catalyst discovery. *Curr. Opin. Chem. Biol.* **1999**, *3*, 313-319.

42. Shimizu, K. D.; Snapper, M. L.; Hoveyda, A. H. High-throughput strategies for the discovery of catalysts. *Chem. Eur. J.* **1998** , *4* , 1885-1889.

43. Oku, J.; Inoue, S. Asymmetric cyanohydrin synthesis catalyzed by synthetic dipeptides, 2. *Makromol. Chem.* **1979**, *180*, 1089.

44. Berkessel, A. The discovery of catalytically active peptides through combinatorial chemistry. *Curr. Opin. Chem. Biol.* **2003**, *7*, 409-419.

45. Miller, S. J. In Search of Peptide-Based Catalysts for Asymmetric Organic Synthesis. *Acc. Chem. Res.* **2004**, *37* , 601–610.

46. Blank, J. T.; Miller, S. J. Studies of folded peptide-based catalysts for asymmetric organic synthesis. *Biopolymers* **2006**, *84*, 38-47.

47. Dalko, P. I.; Moisan, L. Enantioselective organocatalysis. *Angew. Chem., Int. Ed.* **2001**, *40*, 3726–3748.

48. Jarvo, E. R.; Miller, S. J. Amino acids and peptides as asymmetric organocatalysts. *Tetrahedron* **2002**, 58, 2481-2495.

49. Wennemers, H. Asymmetric catalysis with peptides. *Chem. Commun.* **2011**, *47*, 12036- 12041.

50. Wilmot, C. M.; Thornton, J. M. Analysis and prediction of the different types of beta-turn in proteins. *J. Mol. Biol.* **1988**, *203*, 221-231.

51. Hutchinson, E. G.; Thornton, J. M. A revised set of potentials for beta-turn formation in proteins. *Protein Sci.* **1994**, *3*, 2207-2216.

52. Haque, T. S.; Little, J. C.; Gellman, S. H. Stereochemical requirements for β-hairpin formation: model studies with four-residue peptides and depsipeptides. *J. Am. Chem. Soc.* **1996**, *118*, 6975-6985.

53. Haque, T. S.; Little, J. C.; Gellman, S. H. Insights on β-hairpin stability in aqueous solution from peptides with enforced type i 'and type ii 'β-turns. *J. Am. Chem. Soc.* **1997**, *119*, 2303–2304.

54. Liang, G.-B.; Rito, C. J.; Gellman, S. H. Thermodynamic analysis of .beta.-turn formation in Pro-Ala, Pro-Gly, and Pro-Val model peptides in methylene chloride. *J. Am. Chem. Soc.* **1992**, *114*, 4440-4442.

55. Metrano, A. J.; Abascal, N. C.; Mercado, B. Q.; Paulson, E. K.; Miller, S. J. Structural studies of β-turn-containing peptide catalysts for atroposelective quinazolinone bromination. *Chem. Commun. (Camb).* **2016**, *52*, 4816-4819.

56. Ravi, A.; Venkataram Prasad, B. V.; Balaram, P. Cyclic peptide disulfides. Solution and solid-state conformation of Boc-Cys-Pro-Aib-Cys-NHMe with a disulfide bridge from Cys to Cys, a disulfide-bridged peptide helix. *J. Am. Chem. Soc.* **1983**, *105*, 105-109.

57. Fields, G. B.; Noble, R. L. Solid phase peptide synthesis utilizing 9-fluorenylmethoxycarbonyl amino acids. *J. Pept. Protein Res.* **1990**, *35*, 161-214.

58. Chan, W. C.; White, P. D. *Fmoc Solid Phase Peptide Synthesis: A Practical Approach*; Oxford University Press: Oxford, UK, 2000.

59. Davie, E. A.; Mennen, S. M.; Xu, Y.; Miller, S. J. Asymmetric catalysis mediated by synthetic peptides. *Chem. Rev.* **2007**, *107*, 5759-5812.

# CHAPTER THREE

# HYPERVALENT IODOARENE PEPTIDES FOR THE $\alpha$-OXYTOSYLATION OF 1-INDANONE

## *3.1. Introduction*

After the evaluation of a library consisting of 420 different peptide catalysts, no significant breakthroughs were realized; therefore, it was crucial to begin exploring the underlying nuances of the enantioinduction observed for the two reactions of interest. The initial, "hunt-and-peck" approach that we applied early-on has been successful in the past, with many examples of groups screening large pools of potential catalysts, finding an initial "hit" scaffold, and then optimizing the catalyst structure from the primary lead. Nonetheless, the α-oxytosylation of propiophenone and the oxidative cyclization of 5-oxo-5-phenylvaleric acid did not succumb to this approach in our early efforts.

In order to postulate what may be the foundation for the observed low levels of enantiocontrol, one must consider the proposed mechanistic pathways for the iodine(III)-mediated α-oxytosylation of propiophenone (Figure 3.1). Currently, two mechanistic pathways have been suggested, both commencing with the acid-catalyzed enolization of the ketone followed by its reaction with a Koser-type I(III) reagent.[1-5] If the reaction proceeds via pathway 1, pictured on the left, the enol oxygen atom will attack the electrophilic I(III) center of the Koser-type reagent to generate an iodo-enolate (**III-1**). Upon the loss of a water molecule and subsequent nucleophilic attack by a tosylate anion, the desired α-oxytosylated product can be achieved by an $S_N2$' displacement reaction. If the reaction does proceed by this pathway, it can be suggested that low levels of enantioselectivity could be caused by

the large distance between the chiral information on the iodoarene and the newly forming α-stereocenter. This obstacle would add to the difficulty associated with effectively controlling the stereoinduction process.[3-5] Alternatively, if pathway 2 is operative, the I(III) reagent will undergo nucleophilic attack by the α-carbon of the enol to generate a C-I bonded intermediate (**III-2**). This species can then eject water and subsequently undergo $S_N2$ displacement by the tosylate anion to generate the α-functionalized ketone.

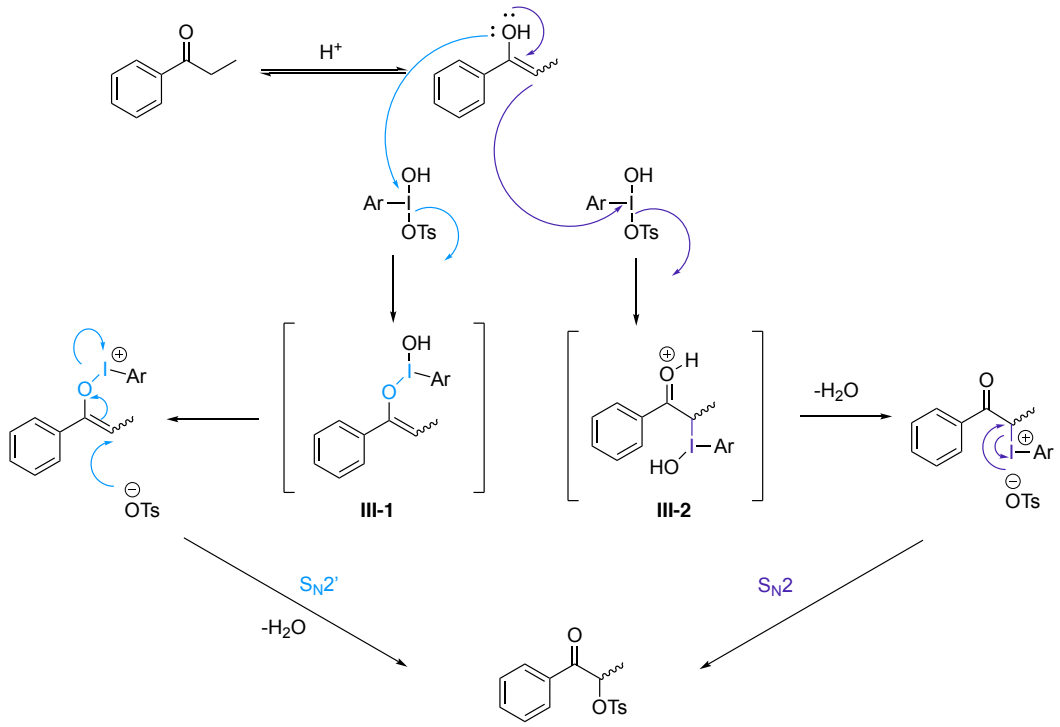


**Figure 3.1.** Two possible mechanistic pathways for the I(III)-mediated α-oxytosylation of propiophenone.

Regardless of which pathway the reaction proceeds through, both begin with an acid-catalyzed enolization of the ketone that results in a mixture of (E/Z) enol stereoisomers. Specifically, there are two mechanistic obstacles to overcome in terms of achieving high levels of enantioselectivity. The iodoarene peptide catalyst must deliver the iodine active site to only one enantiotopic pi face of the enol ether as well as selectively add to the (E)- or (Z)-enol. In other words, even if the peptide catalyst can exclusively select one pi face of the enol to deliver the tosylate in an $S_N2'$ fashion the overall enantioselectivity will only be as good as the (E/Z)-enol ratio. This is also the case if the α-carbon of the (E/Z) enol mixture traps the (III) reagent through the C-I bonded intermediate (**III-2**). The enantioselectivity of the reaction will depend on the relative ratio of the two enol geometries.

There is experimental evidence that supports the concern that the enol geometry plays a pivotal role in the overall reaction enantioselectivity. Under conventional acid promoted equilibria, the (Z/E) ratio of the enol tautomers is 63:37 in the presence of trimethyl orthoformate and a catalytic amount of tosic acid (Scheme 3.1 A).[4] It can reasonably be suggested that a similar distribution of (Z)- and (E)-enols (E/Z= ~60:40) might be present at equilibrium under the acidic reaction conditions for the catalytic $\alpha$-oxytosylation reaction (*i.e.* 3 equiv. each

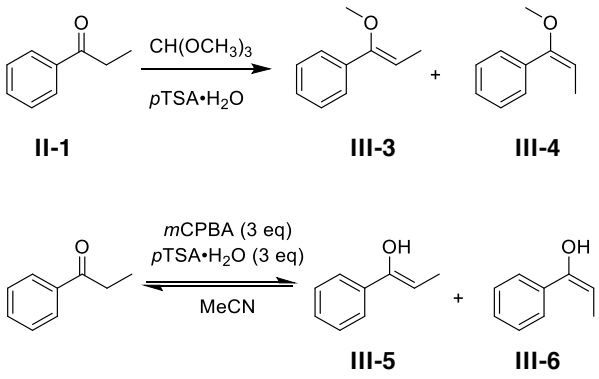


**Scheme 3.1. A)** Experimental (Z)-methyl enol ether and (E)-methyl enol ether Z/E ratio = 63:37 **B)** Theoretical (Z)-enol and (E)-enol ; Z/E ratio = ~ 60:40 in iodoarene peptide catalyzed system .

of *m*CPBA and *p*TSA·$H_2O$) (Scheme 3.1 B). This represents a need to not only understand the effect that the enol geometry has on the enantioinduction process but to also devise a strategy to control the (E/Z) enol ratio of the starting material.

As is well appreciated, the enol geometry of the starting material following acid-catalyzed tautomerization presents a significant challenge. Therefore, this chapter will focus on the implementation of a stereochemically restricted starting material in place of propiophenone for the I(III)-mediated α-oxytosylation reaction. These efforts ultimately led to various "hit" peptide scaffolds, thus the this chapter will also focus on optimization of reaction conditions with the ultimate goal to achieve increased levels of enantioselectivity. In conjunction, the observations gleaned from the efforts help to shed light on the catalyst and reaction condition requirements for this system.

### *3.2. Results and Discussion*

#### *3.2.1. Controlling the Enol Geometry*

One way to quickly address the issue of fluxional enol geometry was to investigate ketone substrates that only adopt one enol geometry owing to the presence of an additional ring. For instance, 1-indanone (**III-7**) can be used as an alternative starting material for the

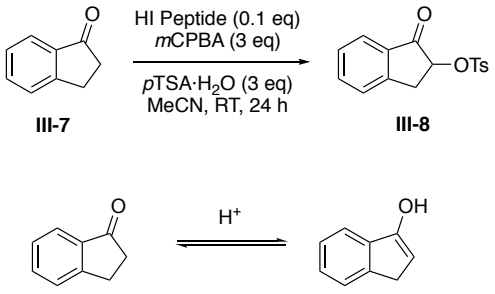


**Scheme 3.2.** A) Iodoarene peptide-mediated α-oxytosylation of 1-indanone. B) Acid-catalyzed tautomerization of 1-indanone, resulting in only the E-enol.

α-oxytosylation of ketones. In the presence of the previously described reaction conditions (3 equiv. *m*CPBA, 3 equiv. *p*TSA·$H_2O$, RT, 24 h) the acid catalyzed enolization of this alternative starting material will result solely in the (E)-enol stereoisomer (Scheme 3.2). Screening this substrate would provide the opportunity to evaluate the enantioselectivity of the catalysts in the absence of the potentially confounding (E/Z)-enol isomerization event.

An initial screen consisting of 50 random iodoarene peptides pulled from libraries of Scaffold A and B, resulted in a "hit" peptide, **III-10**, with a primary sequence of 2-IBA-Orn-Pro-D-Ala-Ile-Tle (Figure 3.2). This catalyst, emerging from Scaffold B, provided the α-oxytosylated product, **III-8**, in 48% *ee*. This exciting result encouraged the iterative optimization of "hit" peptide structure **III-10**.

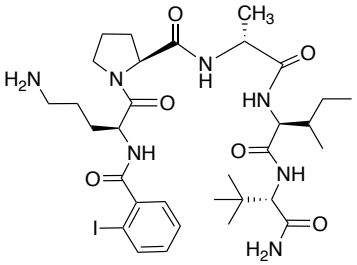

**II-10**
2-IBA-Orn-Pro-D-Ala-Ile-Tle
48% *ee*

**Figure 3.2.** "Hit" peptide **III-10** for the α-oxytosylation of 1-indaone.

*3.2.2. Optimization of "Hit" Peptide Structure **III-10***

The iterative optimization of amino acid residues in positions *i+1*, *i+4*, *i+5* was completed by synthesizing peptide derivatives using the 31 different Fmoc-protected L-amino acids previously described in Chapter 2 of this thesis (Figure 3.3). Once again, methionine, cysteine, and arginine amino acids were not used due to the potential difficulties associated with these residues in conventional Fmoc-SPPS. Further, no attempts to optimize positions *i+2* or *i+3* were made in order to maintain the Pro-D-Ala β-turn sequence. Pleasingly,

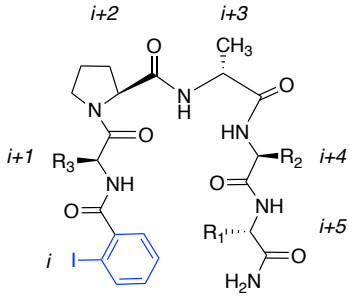

**Figure 3.3.** Generic peptide structures of Scaffold B with amino acid residue positions available for iterative optimization indicated as *i*, *i+1*, *i+2*, *i+3*, *i+4*, and *i+5*.

eight additional "hit" peptides were discovered upon screening the second generation library as catalysts for the enantioselective $\alpha$-oxytosylation of 1-indanone . These "hit" precatalyst structures **III-11** – **III-18** gave the desired product **III-8** in >30% *ee* (Figure 3.4).

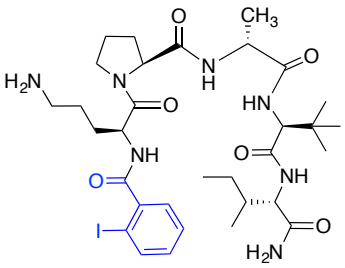

**III-11**
2-IBA-Orn-Pro-D-Ala-Tle-Ile
40% *ee*

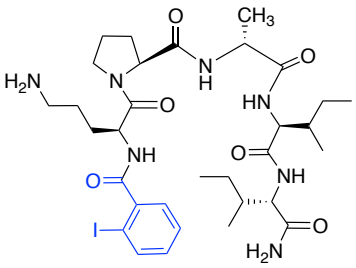

**III-12**
2-IBA-Orn-Pro-D-Ala-Ile-Ile
32% *ee*

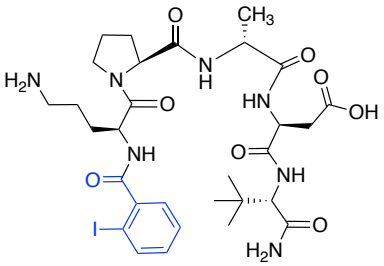

**III-13**
2-IBA-Orn-Pro-D-Ala-Asp-Tle
32% *ee*

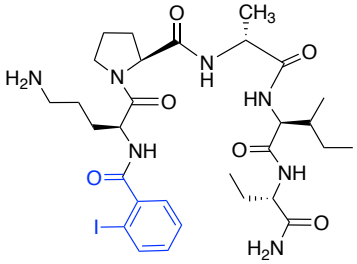

**III-14**
2-IBA-Orn-Pro-D-Ala-Ile-Abu
30% *ee*

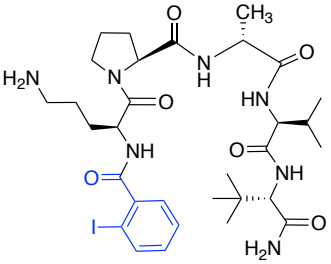

**III-15**
2-IBA-Orn-Pro-D-Ala-Val-Tle
38% *ee*

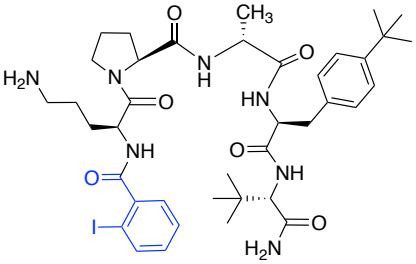

**III-16**
2-IBA-Orn-Pro-D-Ala-tPhe-Tle
40% *ee*

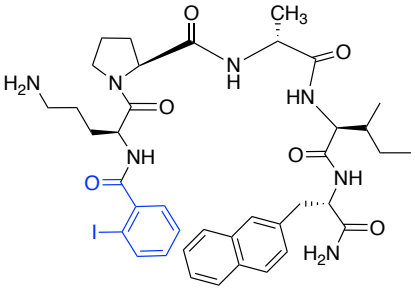

**III-17**
2-IBA-Orn-Pro-D-Ala-Ile-2-Nap
30% *ee*

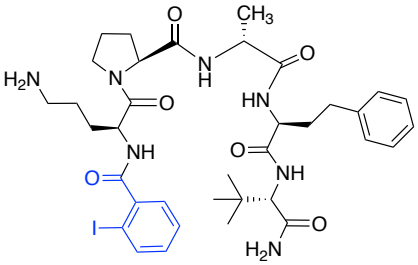

**III-18**
2-IBA-Orn-Pro-D-Ala-hPhe-Tle
37% *ee*

**Figure 3.4.** "Hit" peptides for the α-oxytosylation of 1-indanone from  from the iterative optimization of peptide **III-10**.

Overall, it was noticed that all the "hit" peptides contain sterically bulky alkyl and/or aromatic R-side chains in positions *i+4* and *i+5*, such as Ile, Tle, and hPhe. Further, when position *i+1* was optimized, no additional "hit" peptides emerged following this iteration. This potentially suggests that the *i+1* position, containing the ornithine residue, plays a critical role in the selectivity of the reaction. Further comparisons between other basic amino acid residues, such as lysine (Lys), diamino propionic acid (Dap), and histidine (His) in the *i+1* position, revealed lower levels of enantioselectivity (Figure 3.5). For example, peptides **III-10**, **III-19** and **III-20** all contain amine-terminated alkyl side chains, yet they display different levels of stereoinduction. It is possible that the number of methylene units between the $\alpha$-carbon of the *i+1* amino acid residue and the side chain amine significantly influences the observed % *ee*. It was also interesting to compare peptides structures resulting from modifications at the *i+1* position that promoted the lowest levels of selectivity. In addition to Dap-containing peptide **III-20**, eight additional peptides gave **III-8** in ≤5% *ee* (Figure 3.6, Structures III-23-29). Not including precatalysts **III-20**, **III-26**, and **III-27**, the peptides that generated product **III-8** all have aromatic side chains, such as, Phe, tPhe, Bip, Tyr, 1-Nap, and 2-Nap in the *i+1* position. This observation highlights the need for further

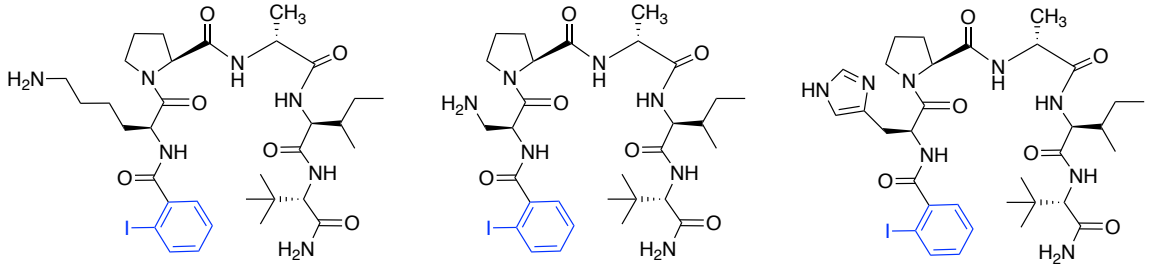

**III-19**
2-IBA-Lys-Pro-D-Ala-Ile-Tle
14% *ee*

**III-20**
2-IBA-Dap-Pro-D-Ala-Ile-Tle
5% *ee*

**III-21**
2-IBA-His-Pro-D-Ala-Ile-Tle
14% *ee*

**Figure 3.5.** Comparison of peptide structures with basic amino acid residues in the *i+1* position.

investigations into the possible intermolecular interactions between the peptide and substrate of interest. There are numerous possibilities for hydrogen bonding, pi-stacking, ion pairing, *etc*. interactions that could aid or hinder the enantioselectivty of the transformation.

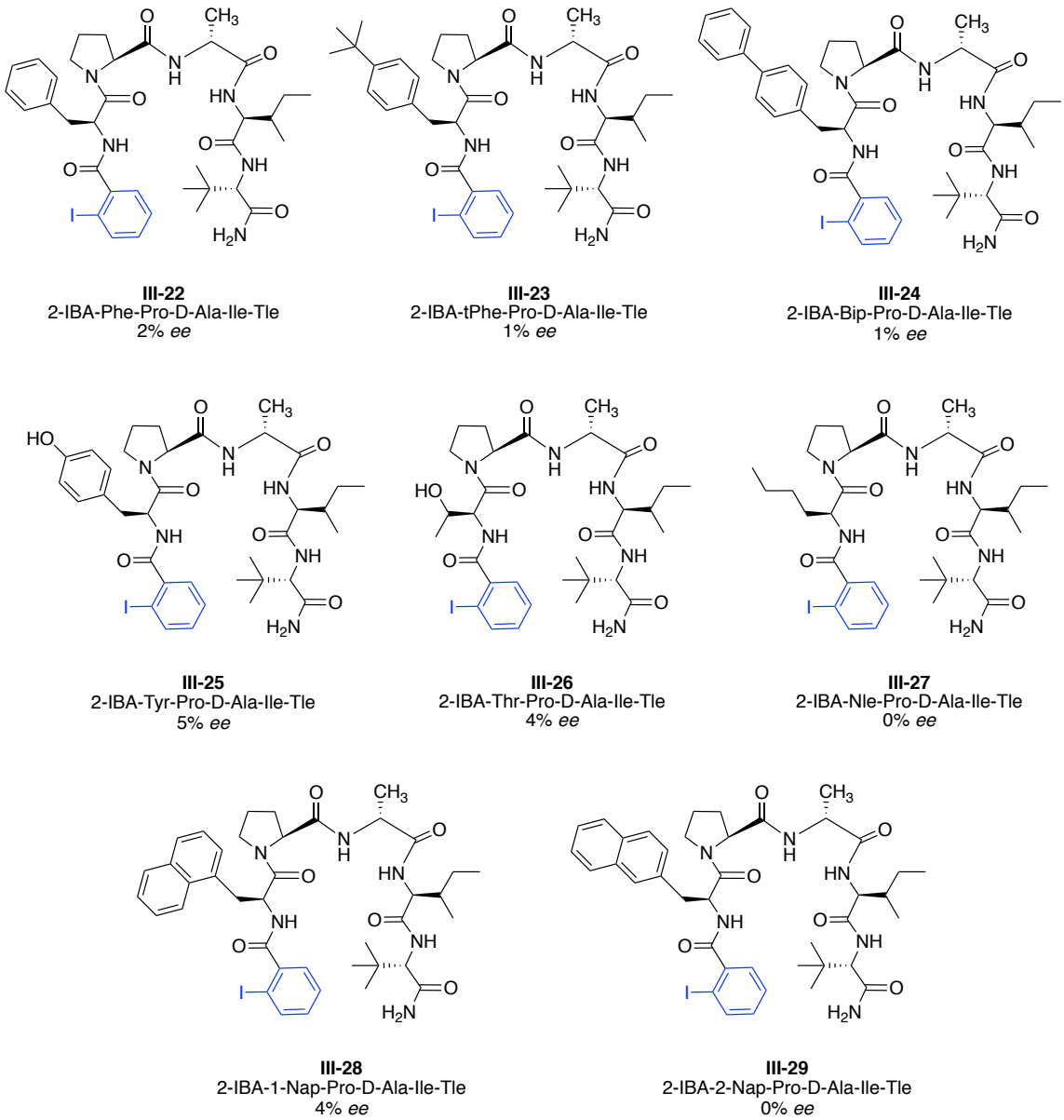

**III-22**
2-IBA-Phe-Pro-D-Ala-Ile-Tle
2% *ee*

**III-23**
2-IBA-tPhe-Pro-D-Ala-Ile-Tle
1% *ee*

**III-24**
2-IBA-Bip-Pro-D-Ala-Ile-Tle
1% *ee*

**III-25**
2-IBA-Tyr-Pro-D-Ala-Ile-Tle
5% *ee*

**III-26**
2-IBA-Thr-Pro-D-Ala-Ile-Tle
4% *ee*

**III-27**
2-IBA-Nle-Pro-D-Ala-Ile-Tle
0% *ee*

**III-28**
2-IBA-1-Nap-Pro-D-Ala-Ile-Tle
4% *ee*

**III-29**
2-IBA-2-Nap-Pro-D-Ala-Ile-Tle
0% *ee*

**Figure 3.6.** Peptides from *i+1* iterative modification of parent **III-10** that gave product **III-8** in ≤5% *ee* α-oxytosylation of 1-indanone

*3.2.3. Reaction Condition Optimization*

The promising results arising from this most recent peptide library screening in the $\alpha$-oxytosylation of 1-indanone prompted a reaction condition optimization campaign. Initially, factors such as oxidant, solvent, time, and temperature were probed. First, an oxidant screen was conducted in which various potential co-oxidants at various equivalents were explored in place of *m*CPBA (3 equiv). Reports predominantly feature *m*CPBA as a suitable co-oxidant for the catalytic $\alpha$-oxytosylation of propiophenone.[6-17] In fact, the utilization of *m*CPBA as a co-oxidant for the *in situ* oxidation of I(I) species to its I(III) derivative reported by Ochai and Kita, is regarded as a pioneering moment in hypervalent iodine chemistry.[6,7] Previously, the stoichiometric application of an hypervalent iodoarene ($ArIX_2$) reagent would produce at least an equimolar amount of the reduced iodoarene (ArI), as well as the two ligands (X). These by-products not only represent waste but also the free ligands would often end up incorporated into the product. An ideal co-oxidant for the transformation would also be inert to the substrate and desired product, or the rate of regeneration for the I(III) catalyst should be faster than any undesired side reactions. Ultimately, the catalytic application of iodoarene reagents ($ArIX_2$) is made possible by the *in situ* oxidation of the I(I)-precatalyst to the I(III)-catalyst, subsequent reaction with the substrate, which upon release of the iodoarene I(I) must be successfully reoxidized *in situ* to continue the catalytic cycle (Figure 3.7).[17]

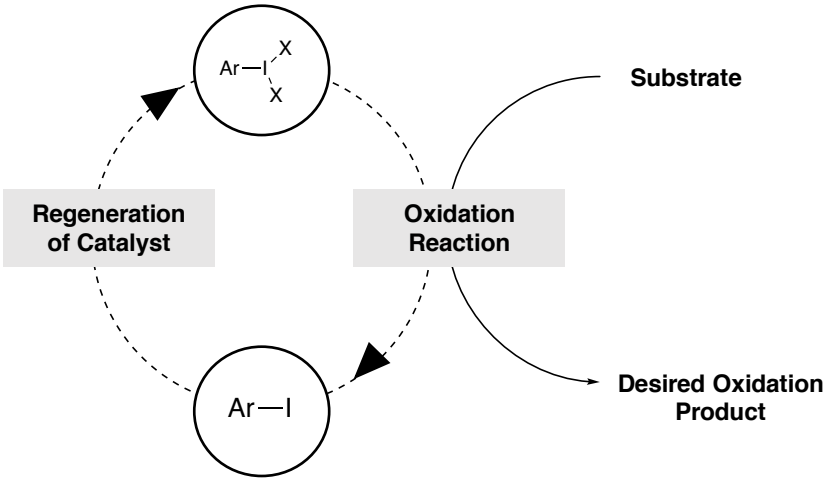


**Figure 3.7.** General catalytic cycle for the *in situ* oxidation of an I(I) precatalyst to its active I(III) counterpart.

We sought to explore various oxidants such as, peroxides, Oxone® ($2KHSO_5 \bullet KHSO_4 \bullet K_2SO_4$), Triazox (2-hydroperoxy-4,6-diphenyl-1,3,5-triazine), and $NaBO_3 \cdot 4H_2O$. Often, altering the terminal oxidant from *m*CPBA to a different reagent, such as $H_2O_2$•Urea or $H_2O_2$, resulted in no product; in these instances "NP is used to denote that the desired **III-8** product was not detected via chiral stationary-phase HPLC analysis (Table 3.1 A, Entries 6-8). Presumably, reagents that resulted in no product (Entries 6-8) did not serve as appropriate oxidants for the *in situ* oxidation of the I(I) precatalyst peptide **III-10** to its active I(III) catalytic derivative. Employing Oxone®, sodium perborate tetrahydrate, and Triazox all resulted in an observed decrease in the reaction enantioselectivity. For example, applying 3, 1.5, or 6 equiv of Oxone® all led to decreased enantioselectivities of 22, 20, and 25% *ee*, respectively (Table 3.1 A, Entries 1-3). This was surprising due to the many successful examples of the use of Oxone® as a co-oxidant in I(III)-mediated

reactions.[18-24] Sodium perborate ($NaBO_3$) is an inorganic oxidant that has been used to prepare $ArIX_2$ reagents in the past; though, it has often been deemed unsatisfactory for the *in situ* oxidation of I(I) precatalysts due to its poor solubility in organic solvents.[17] Triazox was explored due to its ease of synthesis from 2-chloro-4,6-diphenyl-1,3,5-triazine (CDPT) as a bench-stable, water-free oxidant.[25] Nonetheless, the use of $NaBO_3{\cdot}4H_2O$ and Triazox did not promote increased enantioselectivity (Table 3.1, Entries 10-15). Further, decreasing or increasing the equivalents of *m*CPBA also resulted in decreased enantioselectivities, displaying 23 and 16% *ee* for 1.5 and 6 equiv, respectively (Table 3.1, Entries 16-18).

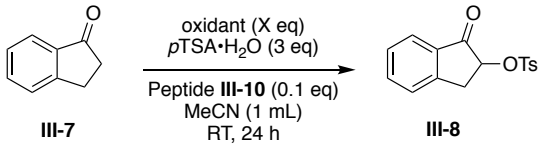


**III-7** **III-8**

**Table 3.1 A:** Oxidant Screen

| Entry | Oxidant (eq) | Solvent | % *ee* of **III-8**[a] |
|---|---|---|---|
| 1 | Oxone (3) | Dry MeCN | 22 |
| 2 | Oxone (1.5) | Dry MeCN | 20 |
| 3 | Oxone (6) | Dry MeCN | 25 |
| 4 | $H_2O_2$•Urea (3) | Dry MeCN | 13 |
| 5 | $H_2O_2$•Urea (1.5) | Dry MeCN | 9 |
| 6 | $H_2O_2$•Urea (6) | Dry MeCN | NP |
| 7 | 30% $H_2O_2$ (3) | Dry MeCN | NP |
| 8 | 30% $H_2O_2$ (1.5) | Dry MeCN | NP |
| 9 | 30% $H_2O_2$ (6) | Dry MeCN | 6 |
| 10 | $NaBO_3$•$4H_2O$ (3) | Dry MeCN | 13 |
| 11 | $NaBO_3$•$4H_2O$ (1.5) | Dry MeCN | 14 |
| 12 | $NaBO_3$•$4H_2O$ (6) | Dry MeCN | 15 |
| 13 | Triazox (3) | Dry MeCN | 26 |
| 14 | Triazox (1.5) | Dry MeCN | 14 |
| 15 | Triazox (6) | Dry MeCN | 24 |
| 16 | *m*CPBA (3) | Dry MeCN | 50 |
| 17 | *m*CPBA (1.5) | Dry MeCN | 23 |
| 18 | *m*CPBA (6) | Dry MeCN | 16 |

[a]Determined by Chiral HPLC

Throughout the oxidant screen, varying reaction solubilities were noted. For example, *m*CPBA is fully soluble in the reaction medium upon addition of MeCN solvent but, Oxone® and $NaBO_3{\cdot}4H_2O$ were not fully solubilized until after sonication . Therefore, 1,2-dimethoxyethane (DME) and 1,4-dioxane were explored as alternative solvents due to their use in the literature as successful solvents for Oxone®-promoted enantioselective oxidation reactions.[26,27] Unfortunately, these alternative solvents did not prove effective: in all cases decreased enantioselectivities or no reaction turnover was observed (Table 3.1 B). Lastly, *m*CPBA (3 equiv) in DME and 1,4-dioxane was examined to serves as a control, and in both instances, decreased enantioselectivities were observed (Table 3.1 B, Entries 1 and 6).

**Table 3.1 B:** Oxidant Screen

| Entry | Oxidant (eq) | Solvent | % *ee* of **III-8**[a] |
|---|---|---|---|
| 1 | *m*CPBA (3) | DME | 19 |
| 2 | Oxone (3) | DME | 0 |
| 3 | $H_2O_2$•Urea (3) | DME | NP |
| 4 | $NaBO_3$•$4H_2O$ (3) | DME | NP |
| 5 | Triazox (3) | DME | 18 |
| 6 | *m*CPBA (3) | 1,4-dioxane | 27 |
| 7 | Oxone (3) | 1,4-dioxane | NP |
| 8 | $H_2O_2$•Urea (3) | 1,4-dioxane | 9 |
| 9 | $NaBO_3$•$4H_2O$ (3) | 1,4-dioxane | 8 |
| 10 | Triazox (3) | 1,4-dioxane | 15 |

[a]Determined by Chiral HPLC

After determining that *m*CPBA (3 equiv) served as the best co-oxidant for the *in situ* oxidation of the iodoarene peptides to their active I(III) species for the catalytic and enantioselective α-oxytosylation of 1-indanone, a solvent screen was conducted. First, other polar aprotic solvents such as DCM, EtOAc, THF, ether, and acetone were explored. In all cases, except with ether, lowered enantioselectivities, in comparison to MeCN, were noticed. The use of ether resulted in no detectable **III-8** product, presumably due to poor reagent solublitly (Table 3.2 A, Entries 1-5). The addition of molecular sieves to dry MeCN generated the desired III-8 producted in an increasd 65% *ee*.

Next, polar protic solvents were probed, including MeOH, EtOH, and nitromethane. Polar protic solvents would undoubtedly increase the solubilty of the reagents and so possibly increase the reactivity and selectivity of the reaction. Contrary to this, the use of MeOH and EtOH as solvents in our system, significantly decreased the enantioselectivity, providing **III-8** in only 12 and 18% *ee*, respectively (Table 3.2A, Entries 8 and 7). Conversely, the use of nitromethane resulted in a 53% *ee* (Table 3.2 A, Entry 10).

Further, protic fluorinated solvents, such as TFE and HFIP, are documented as useful solvents for the stablilization of anions, in comparison to other alcohols, thus serving as useful solvents in reactions with anionic intermediates. Therefore, they are often applied to enantioselective reactions in hopes that this stablization will support increased levels of enantioselectivity. In our case, increased levels of enantioselectivity were not observed (Table 3.2 A, Entries 6 and 7). Lastly, nonpolar solvents were examined. Hexanes, toluene, chloroform, and DME did not proove advantageous for the α-oxytosylation of 1-indanone.

In all cases, decreases in reaction enantioselectivity was observed, especially in chloroform, which gave the α-oxytosylated product in only 4% *ee* (Table 3.2 A, Entries 12-15). Poor solubility of the reagents in all the nonpolar solvents was noted throughout the course of the reaction. While, no attempts were made to quantify reaction yields, the intensity of the enantiomeric product peaks on the HPLC chromatograms can give an indication as to the overall reaction yield. With the nonpolar solvents, very little product was detected in comparison to the other solvents.

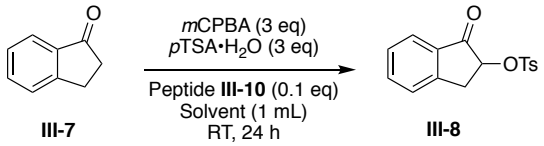


**Table 3.2 A:** Solvent Screen

| Entry | Solvent | % *ee* of **III-8**[a] |
|---|---|---|
| 1 | DCM | 23 |
| 2 | EtOAc | 22 |
| 3 | THF | 19 |
| 4 | Ether | NP |
| 5 | Acetone | 16 |
| 6 | MeOH | 12 |
| 7 | EtOH | 18 |
| 8 | TFE | 22 |
| 9 | HFIP | 36 |
| 10 | Nitromethane | 53 |
| 11 | Dry MeCN, 4Å Mol Sieves | 65 |
| 12 | Hexanes | 17 |
| 13 | Toluene | 20 |
| 14 | Chloroform | 4 |
| 15 | DME | 13 |

[a]Determined by Chiral HPLC

Additionally, co-solvent systems were explored, yet, none led to increased levels of stereoinduction of the desired $\alpha$-oxytosylated product (Table 3.2 B). For example, aprotic polar solvents MeCN and DCM were used in a 1:1 ratio with DCM, EtOAc, ether, HFIP, and TFE to probe wheter mixed solvent systems of similair or different polarity would affect the observed product enantioselectivity. The largest hit to the reaction enantioselectitivy was seen with co-solvent systems of MeCN/MeOH and MeCN/EtOH, wherein, the addition of these polar protic solvents generated **III-8** in only 6% *ee* (Table 3.2 B, Entries 6 and 7). Mixed solvent systems of ether and MeCN or DCM did generate the desired product in 21 and 17% *ee*, respectively, whereas, ether alone did not (Table 3.2 B, Entries 3 and 8). Based on the results observed from this solvent screens, dry MeCN with 4 Å molecular sieves was determined to be the best solvent system for the α-oxytosylation of 1-indanone. This could suggest that the presence of water is negatively influencing the reaction selectivity.

**Table 3.2 B:** Mixed Solvent Screen

| Entry | Solvent (Ratio) | % *ee* of **III-8**[a] |
|---|---|---|
| 1 | MeCN/DCM (1:1) | 27 |
| 2 | MeCN/EtOAc (1:1) | 28 |
| 3 | MeCN/Ether (1:1) | 21 |
| 4 | MeCN/HFIP (1:1) | 34 |
| 5 | MeCN/TFE (1:1) | 15 |
| 6 | MeCN/MeOH (1:1) | 6 |
| 7 | MeCN/EtOH (1:1) | 6 |
| 8 | DCM/EtOAc (1:1) | 22 |
| 9 | DCM/TFE (1:1) | 37 |
| 10 | DCM/Ether (1:1) | 17 |
| 11 | DCM/HFIP (1:1) | 25 |
| 12 | DCM /TFE (1:1) | 25 |

[a]Determined by Chiral HPLC

Simultaneously, a time screen was conducted in order to probe the relationship between reaction time and enantioselectivity. When 1-indanone is treated with *m*CPBA, *p*TSA•$H_2O$, a catalytic amount of **III-10** in MeCN at RT, no significant increase or decrease in selectivity was noticed. With regards to overall enantioselectivity and completing screening reactions in a timely and logistically simple fashion, a 24 h reaction time was deemed the most appropriate (Table, 3.3, Entry 8).

**Table 3.3**: Time Screen

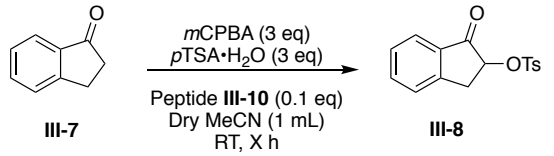


**III-7** **III-8**

| Entry | Time (h) | % *ee* of **III-8**[a] |
|---|---|---|
| 1 | 0 | 46 |
| 2 | 2 | 48 |
| 3 | 4 | 43 |
| 4 | 6 | 48 |
| 5 | 8 | 50 |
| 6 | 10 | 46 |
| 7 | 12 | 53 |
| 8 | 24 | 56 |
| 9 | 36 | 41 |
| 10 | 48 | 46 |

[a]Determined by Chiral HPLC

The effect of temperature on the $\alpha$-oxytosylation of **III-7** was next investigated. Often, altering the reaction temperature will promote increased levels of steroinduction. For example, some temperature-dependent asymmetric transformations will experience greater stereoinduction at lower temperatures. It is proposed that at lower temperatures, the formation of one product enantiomer over the other will be favored due to an enhanced Boltzman distribution bias for the lower energy enantiomeric complex in the transition state.[28] There are also reports of increased % *ee* with increased temperatures, as is the case with asymmetric addition of diethylzinc to

benzaldehyde, asymmetric borane reduction of ketones, and in Rh(I) complex-catalyzed hydrogenation of unsaturated amino acids.[30-37]

In the context of asymmetric hypervalent iodine chemistry, Ogasawara, Dohi, and co-workers, recently applied this approach to the asymmetric dearomatizing spirolactonization of 3-(1-hydroxy-2-naphthyl)propionic acid. Their axially-chiral diodo-tertalin catalysts garnered higher reaction yields and enantioselectivities at 0 °C and even better results at –20 °C, providing the desired product in 64 and 73% *ee*, respectively.[38] Therefore, we first conducted the $\alpha$-oxytosylation of 1-indanone at lowered temperatures ranging from –50 to 10 °C. Unfortunately, only decreased enantioselectivities were realized (Table 3.4, Entries 1-8). The freezing point of MeCN is –45° C, so at –40 °C a mixed solvent system of MeCN/DCM (1:1) was employed as well as dry DCM at –50°C. It was quickly realized that decreasing the reaction temperature significantly decreased the observed levels of enantioselectivity (Table 3.4, Entries 8). It is possible that longer reaction times may be necessary at these lower temperatures in order for the transformation to reach completion. Additional studies are being conducted to explore this possibility.

Further, even slight increases in reaction temperature decreased enantioselectivity. For example, at RT a 65% *ee* of **III-8** was obtained but at 40 °C only a 22% *ee* was achieved. It can be suggested that increasing the temperature may also increase the overall rate of the reaction, thus decreasing the selectivity.

**Table 3.4**: Temperature Screen

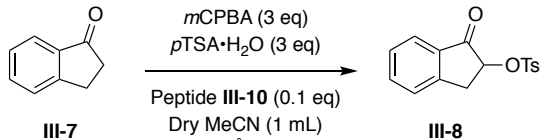


III-7 III-8

| Entry | Temp (°C) | Solvent | % *ee* of III-8[a] |
|---|---|---|---|
| 1 | -50 | Dry DCM | 19 |
| 2 | -40 | Dry MeCN/Dry DCM | 15 |
| 3 | -40 | Dry MeCN | 18 |
| 4 | -30 | Dry MeCN | 14 |
| 5 | -20 | Dry MeCN | 8 |
| 6 | -10 | Dry MeCN | 10 |
| 7 | 0 | Dry MeCN | 15 |
| 8 | 10 | Dry MeCN | 28 |
| 9 | 20 | Dry MeCN | 41 |
| 10 | 30 | Dry MeCN | 43 |
| 11 | RT | Dry MeCN | 65 |
| 12 | 40 | Dry MeCN | 22 |
| 13 | 45 | Dry MeCN | 27 |
| 14 | 50 | Dry MeCN | 26 |
| 15 | 55 | Dry MeCN | 28 |
| 16 | 60 | Dry MeCN | 28 |
| 17 | 70 | Dry MeCN | 34 |
| 18 | 80 | Dry MeCN | 38 |

[a]Determined by Chiral HPLC

Additives are often employed in asymmetric organocatalytic reactions with the intent of reducing the reaction time, improving the overall yield, and/or increasing the enantioselectivity.[39,40] There are numerous examples wherein the introduction of an additive to an organocatalytic system substantially increases the reactivity and/or the selectivity of the transformation; such as, the addition of water to proline-catalyzed aldol reactions will typically result in higher yields and enantioselectivities.[41-44] In general, an additive can activate the substrate, promote the formation of a favorable transition state, block side-reactions, and/or aid in the regeneration of the catalysts.[39,40]

There are not many mechanistic studies fully detailing the role of additives. Further, it is difficult to predict which additive(s) will prove effective in a given reaction. Therefore, various additives were explored using the established optimized conditions for the $\alpha$-oxytosylation of 1-indanone (**III-7**). Namely, treatment of 1-indanone with 3 equiv of *m*CPBA as the co-oxidant, 3 equiv of *p*TSA·$H_2O$ as the nucleophile, 4 Å molecular sieves in dry MeCN at RT for 24 h (Table 3.5). Throughout, this additive screen, the focus was on changes to the observed enantioselectivty of product **III-8**, once again no attempts to quantify reaction yield were made.

First, the addition of alcohols, capable of hydrogen bonding, such as MeOH, EtOH, HFIP, and TFE were investigated. Previously, the addition 10 and 25 equiv of MeOH and EtOH to the hypervalent iodine-mediated asymmetric oxidative dearomatization of phenols was explored by Ishihara and co-workers. In this study, it was suggested the presence of MeOH as a protic polar solvent increased the reaction rate of the oxidation as well as improved the enantioselectivity of the reaction by functioning as a ligand on the I(III) chiral

catalysts.[45] Reactions containing MeOH and EtOH did not generate **III-8** in enantioselectivities higher than 65% *ee*. It was noted that as the equivalents of each alcohol was increased from 10 to 25, the selectivity also increased, with 25 equiv. of MeOH resulting in 50% *ee* (Table 3.5, Entries 1-4). Further, fluorinated alcohols HFIP and TFE were investigated due to their noted reactivity and stereoinduction benefits in hypervalent iodine processes.[46-52] These also did not serve as effective additives for increased stereocontrol (Table 3.5, Entries 5-8). The addition of DCE (2 and 5 equiv), as a non-polar additive, led to a decreased selectivity, producing **III-8** in 30 and 38% *ee*, respectively (Table 3.5, Entries 12 and 13). Lastly, the use of acid additives for the $\alpha$-oxytosylation of 1-indanone was explored. Boron trifluoride diethyl etherate ($BF_3 \cdot Et_2O$) has been readily applied as an activator to promote the oxidation of stoichiometric amounts of hypervalent iodine reagents as well as a Lewis acid additive in catalytic I(III)-mediated processes.[4, 53-56] It was quickly apparent that care needed to be taken when using $BF_3 \cdot Et_2O$ because when directly added to the reaction, no product was detected via HPLC analysis (Table 3.5, Entry 9). Therefore, $BF_3 \cdot Et_2O$, *m*CPBA, *p*TSA·$H_2O$, and the peptide was allowed to stir for 30 min prior to the dropwise addition of the 1-indanone substrate dissolved in MeCN. Using this protocol, product **III-8** was detected upon the addition of 2 and 5 equiv of $BF_3 \cdot Et_2O$ but only at 18 and 23% *ee*, respectively. (Table 3.5, Entries 10 and 11). Further, inorganic and organic acids also proved ineffective, as the addition of 10 equiv. of HCl and TFA yielded **III-8** in 48 and 45 % *ee* (Table 3.5, Entries 12 and 13).[57, 58]

**Table 3.5**: Additive Screen

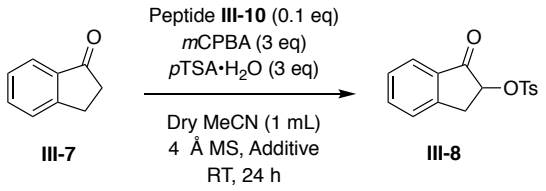


III-7 III-8

| Entry | Additive (equiv) | % *ee* of **III-8**[a] |
|---|---|---|
| 1 | EtOH (10) | 30 |
| 2 | MeOH (10) | 31 |
| 3 | EtOH (25) | 48 |
| 4 | MeOH (25) | 50 |
| 5 | EtOH (50) | 20 |
| 6 | MeOH (50) | 14 |
| 7 | EtOH (100) | 17 |
| 8 | MeOH (100) | 7 |
| 9 | HFIP (10) | 36 |
| 10 | HFIP (25) | 34 |
| 11 | TFE (10) | 44 |
| 12 | TFE (25) | 46 |
| 12 | $BF_3 \cdot Et_2O$ (2) | NP |
| 14[b] | $BF_3 \cdot Et_2O$ (2) | 18 |
| 15[b] | $BF_3 \cdot Et_2O$ (5) | 23 |
| 16 | DCE (2) | 30 |
| 17 | DCE (5) | 38 |
| 18 | HCl (10) | 48 |
| 19 | TFA (10) | 45 |

[a]Determined by Chiral HPLC; [b]1-indanone was added after reagents were allowed to stir for 30 min.

Upon analysis of the results obtained from the various reaction conditions employed during the aforementioned optimization experiments, it was apparent that very slight changes, such as a small increase in temperature or solvent switch, had the potential to greatly impact the overall enantioselectivty of the reaction. These data also suggest that the presence of water may hinder the enantioselectivity of the process.

*3.2.4 Non-Polar Co-Solvent System Screens*

Despite the numerous reaction conditions explored in hopes of achieving increased levels of enantioselectivity for the α-oxytosylation of 1-indanone, the mere addition of molecular sieves to the reaction led to a substantial increase from 48 to 65% *ee* for product **III-8**. This may suggest that a more non-polar solvent system may be appropriate for stereoinduction. Previously, we have only examined non-polar solvents, such as hexanes and toluene, on their own. Therefore, it was deemed prudent to explore mixed solvent systems of MeCN/hexanes and MeCN/toluene. Various ratios of MeCN and hexanes or toluene were evaluated; however, decreased enantioselectivities of product III-8 were observed in all cases (Table 3.6.).

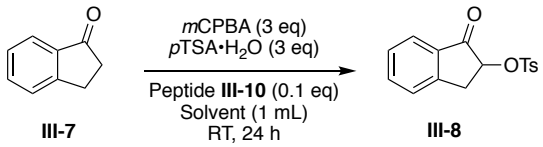


**Table 3.6:** Non-Polar Mixed Solvent Screen

| Entry | Solvent (Ratio) | % *ee* of **III-8**[a] |
|---|---|---|
| 1 | MeCN/Hexanes (1:1) | 22 |
| 2 | MeCN/Toluene (1:1) | 22 |
| 3 | MeCN/Hexanes (9:1) | 28 |
| 4 | MeCN/Toluene (9:1) | 27 |
| 5 | MeCN/Hexanes (1:9) | 15 |
| 6 | MeCN/Toluene (1:9) | 14 |
| 7 | MeCN/Hexanes (3:1) | 28 |
| 8 | MeCN/Toluene (3:1) | 26 |
| 9 | MeCN/Hexanes (1:3) | 22 |
| 10 | MeCN/Toluene (1:3) | 24 |

[a]Determined by Chiral HPLC

*3.2.5. Alternative Nucleophiles for the α-Oxytosylation of Ketones*

Each HI-mediated asymmetric α-functionalization reaction screened thus far has utilized *p*TSA·$H_2O$ as the nucleophile. Previously, Levitre *et al*. reported the catalytic and stoichiometric application of chiral non-$C_2$-symmetric iodoarenes(III) for the asymmetric oxygenation of propiophenone. In this report, the enantioselective α-sulfonylation of ketones was achieved upon treatment with 1-naphthalenesulfonic acid (**III-30**) or methane sulfonic acid (**III-31**), *m*CPBA, and an hypervalent iodine compound.[59] Therefore, we sought to apply these nucleophiles in conjunction with our iodoarene peptides to not only

expand the utility of this method but also probe whether these nucleophiles would lead to higher levels of stereoinduction.

Hit peptide **III-10** in addition to a handful of other peptides from the same peptide library were screened using the same reaction conditions as applied to the previous peptide screening reactions, except **III-30** or **III-31** were applied in 3 equiv rather than *p*TSA·$H_2O$ (Scheme 3.3). The structures for the screened peptides are depicted in Figure 3.8 along with their corresponding primary sequences. The success of the enantioinduction for each catalyst was determined by means of chiral stationary-phase HPLC analysis (Table 3.6). In general, the desired α-functionalized product, either **III-32** or **III-33**, was detected; suggesting that our iodoarene peptides can serve as suitable catalysts for various other ketone α-sulfonylation reactions. The exception to this includes the lack of product detected when peptide **III-34** was applied to the α-sulfonylation of 1-indanone with 1-napthelene sulfonic acid (Table 3.6, Entry 10). Moreover, no distinct trends were uncovered. For example, peptide **III-28** gave moderate % *ee* for **III-8**, **III-32**, and **III-33**. On the other hand, peptide **III-27** produced **III-32** in 25% *ee* but generated in **III-8** and **III-33** in only 9 and 3 % *ee*, respectively.

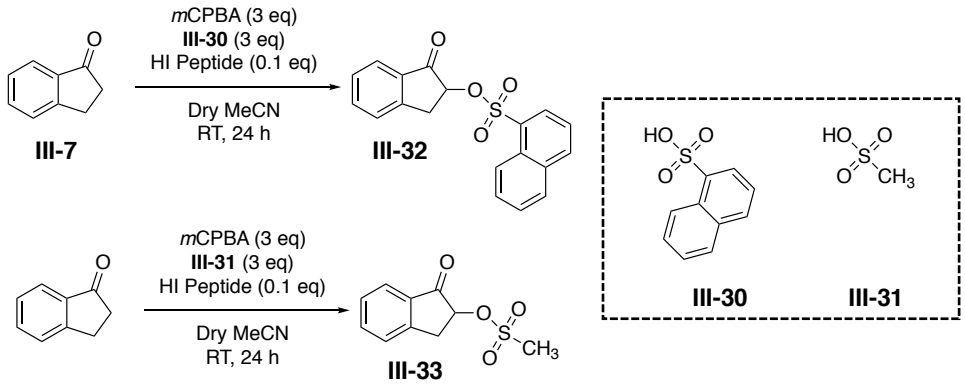


**Scheme 3.3.** The α-sulfonylation of 1-indanone, using **III-30** and **III-31** as the nucleophile.

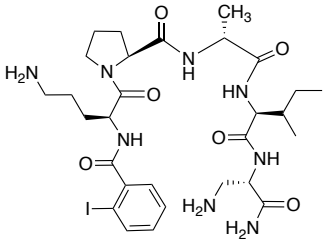

**III-32**
2-IBA-Orn-Pro-D-Ala-Ile-Dap

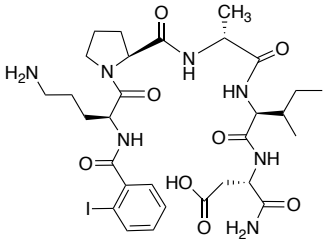

**III-33**
2-IBA-Orn-Pro-D-Ala-Ile-Asp

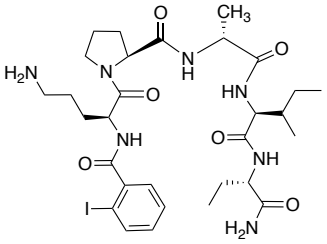

**III-34**
2-IBA-Orn-Pro-D-Ala-Ile-Abu

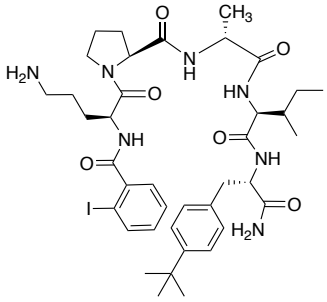

**III-35**
2-IBA-Orn-Pro-D-Ala-Ile-tPhe

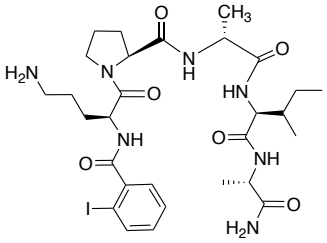

**III-36**
2-IBA-Orn-Pro-D-Ala-Ile-Ala

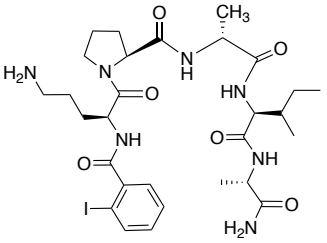

**III-37**
2-IBA-Orn-Pro-D-Ala-Ile-Phg

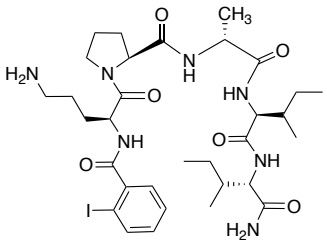

**III-38**
2-IBA-Orn-Pro-D-Ala-Ile-Ile

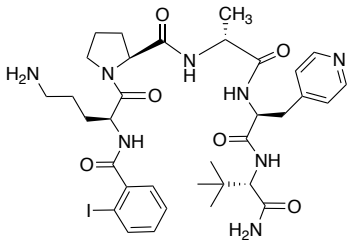

**III-39**
2-IBA-Orn-Pro-D-Ala-4-Pya-Tle

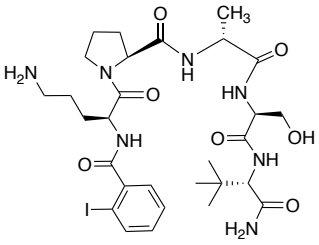

**III-40**
2-IBA-Orn-Pro-D-Ala-Ser-Tle

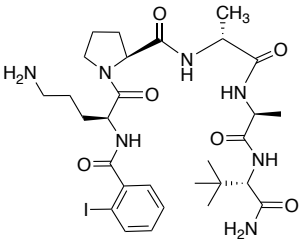

**III-41**
2-IBA-Orn-Pro-D-Ala-Ala-Tle

**Figure 3.8.** Peptides screened in α-sulfonylation of 1-indanone reactions.

**Table 3.7**: Alternative Nucleophiles for the α- Functionalization of 1-Indanone

| Entry | Peptide Catalyst | % *ee* of **III-32**[a] | % *ee* of **III-33**[a] | % *ee* of **III-8**[a] |
|---|---|---|---|---|
| 1 | **III-10** | 11 | 28 | 48 |
| 2 | **III-26** | 19 | 35 | 21 |
| 3 | **III-27** | 9 | 25 | 3 |
| 4 | **III-28** | 22 | 21 | 30 |
| 5 | **III-29** | 21 | 15 | 26 |
| 6 | **III-30** | 15 | 20 | 27 |
| 7 | **III-31** | 24 | 23 | 25 |
| 8 | **III-32** | 23 | 24 | 32 |
| 9 | **III-33** | 12 | 20 | 26 |
| 10 | **III-34** | 16 | 18 | 33 |
| 11 | **III-35** | 17 | 15 | 35 |

[a]Determined by Chiral HPLC

*3.2.6. Catalyst Loading*

In order to examine the limits of our hypervalent iodoarene peptide catalyzed system, we sought to perform a catalyst loading experiment. Using the optimized conditions, *i.e.* 3 equiv. *m*CPBA, 3 equiv *p*TSA·$H_2O$, 4 Å molecular sieves, in dry MeCN at RT for 24 h, 0.05, 0.1, 0.2, 0.3, 0.4, 0.5, and 1 equiv of peptide **III-10** were used in the α-oxytosylation of 1-indanone (Table 3.8). Typically, one would expect to observe a positive linear relationship between the catalyst loading and the observed enantioselectivity.[60, 61] This was not the case, as the amount of peptide catalyst was increased, the % *ee* of product **III-8** decreased.

**Table 3.8**: Catalyst **III-10** Loading Experiment

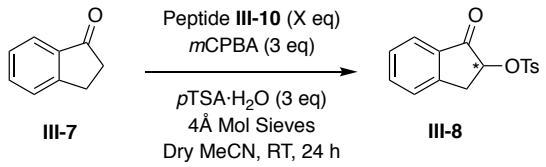


**III-7** **III-8**

| Entry | Peptide **III-10** (equiv) | % *ee* of **III-8**[a] |
|---|---|---|
| 1 | 0.05 | 64 |
| 2 | 0.1 | 66 |
| 3 | 0.2 | 43 |
| 4 | 0.3 | 34 |
| 5 | 0.4 | 32 |
| 6 | 0.5 | 31 |
| 7 | 1 | 27 |

[a]Determined by Chiral HPLC

Often, observed non-linear effects in asymmetric catalysis can be attributed to bi-functional catalysis.[59, 60] Peptide **III-10** may be promoting a side-reaction as well as the desired α-oxytosylation of 1-indanone. More specifically, the amine moiety on the ornithine amino acid residue in position *i + 1* may be functioning as a nucleophile and promoting iminium or enamine formation via the condensation of the peptide and the 1-indanone substrate, and thus a potential and undesired side reaction.

In order to evaluate this possibility, 1-indanone and a stoichiometric amount of **III-8** were allowed to react in deuterated MeCN for 24 h at RT. This reaction mixture was monitored via $^{1}$H NMR in order to follow the α-proton of 1-indanone. Throughout the reaction no indication of iminium or enamine formation was observed as no shifts or changes in splitting were observed in NMR spectrum for the α-proton of 1-indanone. An additional experiment was conducted, wherein equimolar amounts 1-indanone, peptide **III-10**, and trifluoroacetic acid-*d* were allowed to stir in deuterated MeCN for 24 h at RT. The addition of acid to the mixture was thought appropriate due to the acidic nature of the α-oxytosylation reaction of ketones. After 12h and 24 h, a slight shift in the α-proton of 1-indanone resonance peaks of 1-indanone as well as the emergence of a slight shoulder to the right of the peak. Further, when comparing a pure sample of peptide **III-10** to the mixture of peptide, acid, and 1-indanone, it is observed that the peak associated with the *δ* protons of ornithine (~3 ppm) is altered (Figure 3.9). This observance possibly suggests bi-functional catalysis between the amine side chain of ornithine and the 1-indanone substrate.

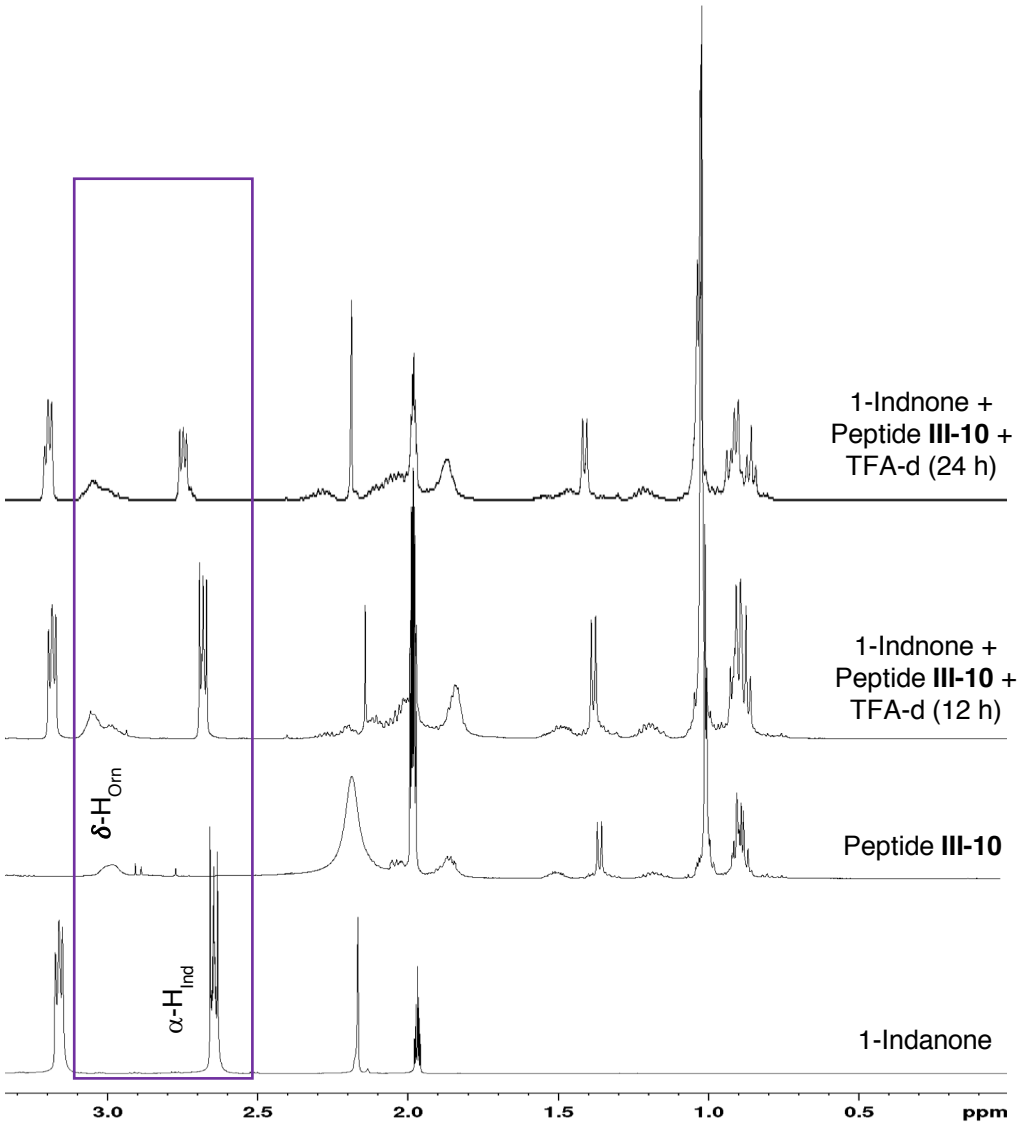


**Figure 3.9.** 1H NMR overlays of 1-indanone, peptide **III-10**, and a mixture of them with TFA-*d* at 12 and 24 h.

### *3.3. Conclusions*

These data further support the ability of our iodoarene-containing peptides to create a chiral environment that can impart moderate enantiocontrol onto hypervalent iodine-mediated organic transformations in a mild, straightforward, and environmentally friendly manner. Switching ketone substrates from propiophenone to the cyclic congener, 1-indanone, proved fortuitous as "hit" peptide **III-10** was realized following an initial screen of only 50 peptides. Further, following the iterative optimization of this scaffold, an additional eight "hit" peptides emerged that generated the α-oxytosylated ketone product **III-8** in >30% *ee* ( >65:35 er).

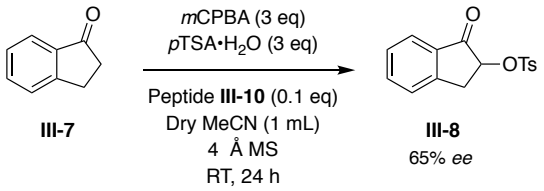


**Scheme 3.4.** Optimized reaction conditions for the α-oxytosylation of 1-indanone.

It was also realized, after the optimization of various reaction conditions such as, oxidant, time, temperature, solvent, *etc*., that the treatment of 1-indanone (**III-7**), with *m*CPBA (3 equiv), *p*TSA·$H_2O$ (3 equiv), 10 mol% **III-10** peptide, 4 Å molecular sieves, in dry MeCN for 24 h gave the desired α-oxytosylated product **III-8** in 65% *ee* and 23 % yield (Scheme 3.4). Further, upon application of these optimized conditions to propiophenone, only 24% *ee* of **III-8** was observed in 27 % yield (Scheme 3.5). This in combination with the success of the peptide library formulated around the initial "hit" **III-10** for the α-oxytosylation of 1-indanone suggests

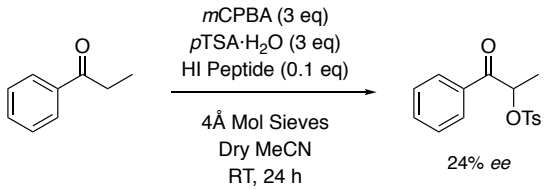


**Scheme 3.5.** The α-oxytosylation of propiophenone under optimized reaction conditions.

that the (Z/E)-ratio of the key enol intermediate may profoundly influence the overall enantioselectivity of these reactions. Further experiments are required in order to verify this hypothesis, such as the treatment of pure samples of the (E)- and (Z)-enol of propiophenone with a stoichiometric amount of the oxidized **III-10** peptide.

Ultimately, information gleaned from the research detailed in this thesis suggests that hypervalent aryl-iodo peptides can serve as versatile and mild precatalysts for HI-mediated organic transformations. Nonetheless, this area of research is still in its infancy and many efforts are being put forth to realize highly reactive and enantioselective peptide catalysts. This is highlighted by the inability to realize synthetically useful levels of enantioselectivty following a reaction optimization campaign of over 100 different conditions. While this is an inherent difficulty in asymmetric catalysis, as there is a small energy difference (1 to 2 kcal/mol) that typically separates an inactive or nonreactive catalyst from a highly selective and reactive one, it also supports the need for further mechanistic studies. It is clear that additional research is needed in order to fully understand the intricacies behind the interactions of the peptide and substrate, the mode of enantioinduction, and the true mechanism of the hypervalent I(III)-mediated α-oxytosylation of ketones.

### *3.4. Future Directions*

One of the clearest next steps is to screen precatalysts from the current iodoarene peptide library, consisting of over 800 different structures, in other HI enantioselective transformations. Theoretically, these peptides should prove useful in any I(III)-mediated transformation, given the correct *in situ* oxidation conditions. The literature is rich with

catalytic and asymmetric I(III)-promoted organic reactions. For example, given the success of our previously screened α-functionalization reactions, other nucleophiles should prove accessible , such as, acetic acid or diphenylphosphate, for the asymmetric α-oxygenation and α-phosphorylation of propiophenone and 1-indanone, respectively (Scheme 3.6 A and B).[59, 62] Additionally, Wang and co-workers have recently published the use of chiral HI reagents for the enantioselective oxidative fluorination of β-keto esters with trihydrofluoride-triethylamine ($3HF•Et_3N$), as a nucleophilic fluoride source.[63] There is potential for our iodoarene peptides to serve as successful chiral catalysts in this fluorination reaction, as well (Scheme 3.6 C).

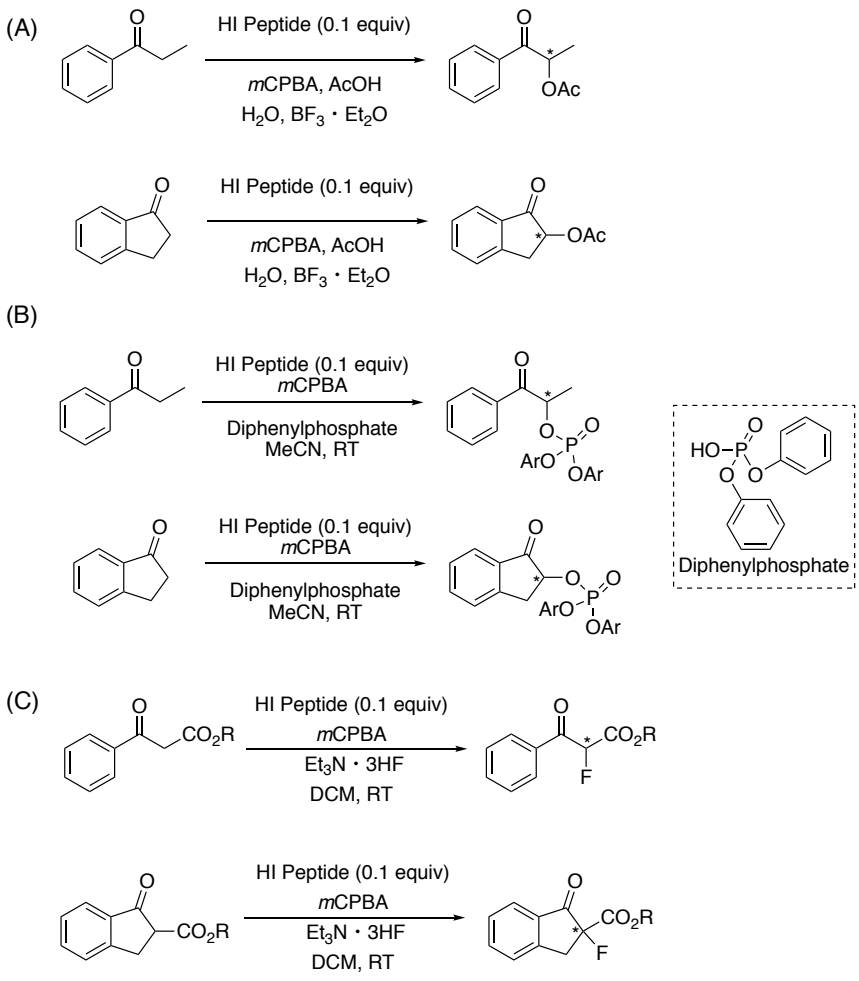


**Scheme 3.6.** Potential future enantioselective HI-mediated transformations.

### *3.5. Experimental*

#### *3.5.1. General Materials and Methods*

Enantiomeric excess (% *ee*) of product **III-8** was determined via chiral stationary-phase high performance liquid chromatography (HPLC). Chiral samples were run on an Agilent 1260 Infinity system equipped with a diode array detector (G4212-60008), and an Agilent 1260 Infinity auto sampler. The chiral stationary column used was a Chiralpak-AD (250mm X 4.6 mm). The mobile phase consisted of *iso*-propyl alcohol/hexanes mixture (80:20). The flow rate was set at 1 mL/min and the elution of analytes was monitored at 254 nm, with enantiomeric retention times = 10.4 and 12.9 min.

#### *3.5.2. Screening Reaction Protocols*

Chiral stationary-phase HPLC analyses of the crude reaction mixtures were completed to determine % *ee* for the α-oxytosylation of 1-indanone. A pure racemic sample of 1-indanone was prepared following the procedure detailed in section *3.5.3.* of this chapter and used as HPLC standards to determine the retention times of product enantiomers.

*General Procedure for the α-Oxytosylation of 1-Indanone*

Iodoarene peptide precatalysts were evaluated in the asymmetric α-oxytosylation of 1-indanone using the following representative procedure: A 3 mL screw-capped vial was charged with 1-indanone (3.97 mg, 0.3 mmol, 1.0 equiv), *p*TSA·$H_2O$ (17.1 mg, 0.09 mmol, 3 equiv), *m*CPBA (77%) (20.2 mg, 0.03 mmol, 3 equiv), the appropriate iodoarene peptide precatayst (0.01 mmol, 0.1 equiv) and a small stir bar. The reagents were dissolved in 1 mL of acetonitrile and the reaction was stirred for 24 h at RT. Following the allotted reaction time, the crude solution was concentrated by rotary evaporation and prepared for

HPLC analysis. Samples were prepared for HPLC analysis by dissolving the samples in 0.2 mL of the HPLC solvent system of IPA/Hexanes (80/20) followed by filtration through micro-syringe filters into HPLC analysis vials.

### *3.5.3. Synthesis of Racemic Products*

The racemic product **III-8** expected from the α-oxytosylation of 1-indanone was synthesized and purified to serve as a chiral HPLC standard for the determination of each enantiomeric peak retention time.

*General procedure for the Synthesis of Racemic 1-oxo-2,3-dihydro-1H-inden-2-yl 4-methylbenzenesulfonate,* ***III-8***.

A flame dried, 100 mL round-bottom flask was charged with 1-indanone **II-7** (1 g, 7.58 mmol, 1.0 equiv), *para*-toluenesulfonic acid monohydrate (4.32 g, 22.7 mmol, 3 equiv), 77% *meta*-chloroperoxybenzoic acid (5.1 g, 22.7 mmol, 3 equiv), and 4-iodotoluene (5 g, 22.7 mmol, 1.5 equiv). The reagents were dissolved in 20 mL of acetonitrile and the resulting solution was allowed to stir under $N_2$ at 50 ˚C for 24 h. The reaction mixture was concentrated by rotary evaporation, followed by dilution in DCM, and the organics were washed three times with an aqueous saturated sodium bicarbonate solution. The combined organic layers were dried over sodium sulfate, filtered, and concentrated by rotary evaporation. The crude product was purified by column chromatography on silica gel (20:80 EtOAc:hexanes) to give a beige solid **III-8** (2.1 g, 92%). $R_f$ = 0.21 (20:80 EtOAc:hexanes) $^1$H NMR (500 MHz, $CDCl_3$): δ 7.95 (2H, d, J = 8.3), 7.75 (1H, d, J = 7.6 Hz), 7.67 (1H, td, J = 7.5, 1.2 Hz), 7.46-7.40 (4H, m), 5.15 (1H, dd, J = 7.9, 4.8 Hz), 3.68 (1H, dd, J = 17.1, 7.9), 3.30 (1H, dd, J = 17.2, 4.7), 2.49 (3H, s) ppm. $^{13}$C NMR (125 MHz, $CDCl_3$): δ 197.6,

150.0, 145.2, 136.4, 133.6, 133.2, 129.9, 128.5, 128.3, 126.7, 124.7, 33.9, 21.8 ppm.

### *3.5.4. Synthesis of Racemic Products for Alternative Nucleophiles*

*General procedure for the Synthesis of Racemic, 1-oxo-2,3-dihydro-1H-inden-2-yl naphthalene-1-sulfonate,* ***III-32***.

The substrate 1-indanone **II-7** (0.132 g, 1 mmol, 1.0 equiv), Oxone (0.46 g, 3 mmol, 3 equiv), and 4-iodotoluene (0.65 g, 3 mmol, 3 equiv) were all added to a dry 100 mL round-bottom flask. A separate solution of 1-napthelene sulfonic acid (0.62 g, 3 mmol, 3 equiv) was prepared by slowly adding 20 mL MeCN to the reagent under $N_2$. This solution was then added dropwise to the contents of the round-bottom flask. The reaction was allowed to stir under $N_2$ at 50 ˚C for 48 h. Following concentration of the reaction mixture by rotary evaporation and dilution in DCM, the crude mixture was washed three times with an aqueous saturated sodium bicarbonate solution. The combined organic layers were dried over sodium sulfate, filtered, and concentrated by rotary evaporation. The crude product was purified by column chromatography on silica gel (20:80 EtOAc:hexanes) to give a light brown solid **III-32** (0.301 g, 89%). $R_f$ = 0.18 (20:80 EtOAc:hexanes) $^1$H NMR (500 MHz, $CDCl_3$): δ 8.75 (1H, dd, J = 8.7, 0.75 Hz), 8.40 (1H, d, 1.2 Hz), 8.20 (1H, d, 8.3 Hz), 8.00 (1H, d, 8.2 Hz), 7.72 -7.67 (2H, m), 7.66-7.60 (2H, m), 7.40 (2H, d, J = 7.5 Hz), 5.19 (1H, dd, J = 7.9, 4.8 Hz), 3.57 (1H, dd, J = 17.2, 8.0 Hz), 3.22 (1H, dd, J = 17.2, 8.0 Hz) ppm. $^{13}$C NMR (125 MHz, $CDCl_3$): δ 197.2, 149.8, 136.3, 135.7, 134.2, 133.6, 131.6, 130.3, 128.8, 128.6, 128.4, 127.4, 126.6, 125.4, 124.9, 124.7, 123.9, 78.5, 33.7 ppm.

*General procedure for the Synthesis of Racemic 1-oxo-2,3-dihydro-1H-inden-2-yl methanesulfonate,* ***III-33***.

Racemic compound **III-33** was prepared on the same scale and following the same synthetic protocol as described for compound **III-32** except methane sulfonic acid (0.288 g, 3 mmol, 3 equiv) was used as the nucleophile. The reaction mixture was also washed with an aqueous solution of sodium bicarbonate and extracted with DCM. The crude product was purified by column chromatography on silica gel (20:80 EtOAc:hexanes) to give brown solid **III-33**: (0.194 g, 86%). $R_f$= 0.24 (20:80 EtOAc:hexanes) $^1$H NMR (500 MHz, $CDCl_3$): δ 7.81 (1H, d, J = 7.7 Hz), 7.72 (1H, t, J = 7.5 Hz), 7.51-7.46 (2H, m), 5.39 (1H, dd, J = 8.1, 4.8), 3.74 (1H, dd, J = 17.1, 8.2), 3.35 (1H, s), 3.34-3.30 (1H, m) ppm. $^{13}$C NMR (125 MHz, $CDCl_3$): δ 198.9, 150.1, 136.6, 133.5, 128.6, 126.8, 124.8, 79.1, 39.6, 33.7 ppm.

*General Procedure for the α-Functionalization of 1-Indanone Screening*

In order to evaluate iodoarene peptide catalysts in the α-sulfonylation of 1-indanone, a similar protocol as detailed in section 3.5.2 of this thesis was applied. Briefly, a 3 mL screw-capped vial was charged with 1-indanone (3.97 mg, 0.3 mmol, 1.0 equiv), *m*CPBA (19.1 mg, 0.03 mmol, 3 equiv), the iodoarene peptide precatalyst (0.01 mmol, 0.1 equiv) and a small stir bar. The sulfonic acid, either 1-naphthalenesulfonic acid **III-30** (18.72 mg, 0.09 mmol, 3 equiv) or methane sulfonic acid **III-31** (8.64 mg, 0.09 mmol, 3 equiv), was added to a separate 3 mL vial and dissolved in 1 mL of MeCN. This solution was then added dropwise to the vial containing the substrate, peptide precatalyst and *m*CPBA. And the reaction was stirred for 24 h at RT. Following the allotted reaction time, the crude solution was concentrated by rotary evaporation and prepared for chiral HPLC

analysis. Samples were prepared for HPLC analysis by dissolving the samples in 0.2 mL of the HPLC solvent system followed by filtration through micro-syringe filters into HPLC analysis vials.

Both reactions, employing 1-naphthalenesulfonic acid **III-30** and methane sulfonic acid **III-31** were analyzed using a IPA/Hexanes (50/50) HPLC solvent system on a Chiral Pak OJ column with enantiomeric RT = 26.2 and 28.8 min and RT = 23.4 and 33.6 for chiral products **III-32** and **III-33**, respectively.

### *3.6. Supplementary Information*

Appendix B contains this chapter's corresponding chiral HPLC chromatograms, $^{1}H$ and $^{13}C$ NMR spectra as well as all a catalog of the libraries of synthesized peptides and their corresponding MALDI-TOF characterization data.

### *3.7. Acknowledgements*

My sincere thanks and gratitude to my undergraduate army. Without them, the number of synthesized iodoarene peptides and subsequent screening reactions, described in Chapter 2 and 3, of this thesis would not have been possible. Funding for this research was provided by the National Science Foundation (grant number CHE-1664920).

### *3.8. References*


1. Mizukami, F.; Ando, M.; Tanaka, T.; Imamura, J. The Acetoxylation of *p*-Substituted Acetophenones and β-Diketones with (Diacetoxyiodo)benzene. *Bull. Chem. Soc. Jap.* **1978**, *51*, 335-336.

2. Guilbault, A.-A.; Basdevant, B.; Wanie, V.; Legault, C. Y. Catalytic Enantioselective α-Tosyloxylation of Ketones Using Iodoaryloxazoline Catalysts: Insights on the Stereoinduction Process. *J. Org. Chem.* **2012**, *77*, 11283-11295.

3. Beaulieu, S.; Legault, C. Y. Mechanistic Insights on the Iodine(III)-Mediated α-Oxidation of Ketones. *Chem. Eur. J.* **2015**, *21*, 11206-11211.

4. Basdevant, B.; Legault, C. Y. Study of the Reactivity of [Hydroxy(tosyloxy)iodo]benzene Toward Enol Esters to Access α-Tosyloxy Ketones. *J. Org. Chem.* **2015**, *80*, 6897-6902.

5. Basdevant, B.; Legault, C. Y.Enantioselective Iodine(III)-Mediated Synthesis of α-Tosyloxy Ketones: Breaking the Selectivity Barrier. *Org. Lett.* **2015,** *17*, 4918-4921.

6. Dohi, T.; Maruyama, A.; Yoshimura, M.; Morimoto, K.; Tohma, H.; Kita, Y. Versatile Hypervalent-Iodine(III)-Catalyzed Oxidations with *m*-Chloroperbenzoic Acid as a Co-oxidant. *Angew. Chem., Int. Ed.* **2005**, *44*, 6193-6196.

7. Ochiai, M.; Takeuchi, Y.; Katayama, T.; Sueda, T.; Miyamoto, K. Iodobenzene-Catalyzed α-Acetoxylation of Ketones. In Situ Generation of Hypervalent

(Diacyloxyiodo)benzenes Using *m*-Chloroperbenzoic Acid. *J. Am. Chem. Soc.* **2005**, *127*, 12244-12245.

8. Yamamoto, Y.; Togo, H. PhI-catalyzed α-tosyloxylation of ketones with *m*-chloroperbenzoic acid and *p*-toluenesulfonic acid. *Synlett* **2006**, 798-800.

9. Dohi, T.; Maruyama, A.; Minamitsuji, Y.; Takenaga, N.; Kita, Y. First hypervalent iodine(III)-catalyzed C–N bond forming reaction: catalytic spirocyclization of amides to *N*-fused spirolactams. *Chem. Commun.* **2007**, *12*, 1224-1226.

10. Richardson, R. D.; Page, T. K.; Altermann, S.; Paradine, S. M.; French, A. N.; Wirth, T. Enantioselective α-oxytosylation of ketones catalysed by iodoarenes. *Synlett* **2007**, 538-542.

11. Akiike, J.; Yamamoto, Y.; Togo, H. Efficient conversion of ketones to α-tosyloxyketones with *m*-chloroperbenzoic acid and p-toluenesulfonic acid in the presence of catalytic amount of IL-supported PhI in [emim]OTs. *Synlett* **2007**, 2168-2172.

12. Yamamoto, Y.; Kawano, Y.; Toy, P. H.; Togo, H. PhI- and polymer-supported PhI-catalyzed oxidative conversion of ketones and alcohols to α-tosyloxyketones with *m*-chloroperbenzoic acid and *p*-toluenesulfonic acid. *Tetrahedron* **2007**, *63*, 4680-4687.

13. Moroda, A.; Togo, H. Iodobenzene-Catalyzed Preparation of 3,4Dihydro1 H -2,1-benzothiazine 2,2-Dioxides from 2Aryl N -methoxyethanesulfonamides with *m* -Chloroperoxybenzoic Acid. *Synthesis* **2008**, 1257-1261

14. Kawano, Y.; Togo, H. Iodoarene-Mediated One-Pot Preparation of 2,4,5-Trisubstituted Oxazoles from Ketones. *Synlett* **2008**, 217-220.

15. Kawano, Y.; Togo, H. Iodoarene-catalyzed one-pot preparation of 2,4,5-trisubstituted oxazoles from alkyl aryl ketones with *m*CPBA in nitriles. *Tetrahedron* **2009**, *65*, 6251-6256.

16. Ishiwata, Y.; Togo, H. Ion-supported PhI-catalyzed cyclization of N-methoxy-2-arylethanesulfonamides with *m*CPBA. *Tetrahedron Lett*. **2009**, *50*, 5354-5357.

17. Dohi, T.; Kita, Y. Hypervalent iodine reagents as a new entrance to organocatalysts. *Chem. Comm.* **2009**, 2073-2085.

18. Thottumkara, A. P.; Bowsher, M. S.; Vinod, T. K. In Situ Generation of *o*-Iodoxybenzoic Acid (IBX) and the Catalytic Use of It in Oxidation Reactions in the Presence of Oxone as a Co-oxidant. *Org. Lett.* **2005**, *7*, 2933-2936.

19. Schulze, A.; Giannis, A. Oxidation of Alcohols with Catalytic Amounts of IBX. *Synthesis* **2006**, 257-260.

20. Tanaka, A.; Togo, H. 4-$MeC_6H_4I$-Mediated Efficient α-Tosyloxylation of Ketones with Oxone® and *p*-Toluenesulfonic Acid in Acetonitrile. *Synlett* **2009**, *20*, 3360-3364.

21. Uyanik, M.; Akakura, M.; Ishihara, K. 2-Iodoxybenzenesulfonic Acid as an Extremely Active Catalyst for the Selective Oxidation of Alcohols to Aldehydes, Ketones, Carboxylic Acids, and Enones with Oxone. *J. Am. Chem. Soc*. **2009**, *131*, 251-262.

22. Uyanik, M.; Fukatsu, R.; Ishihara, K. IBS-Catalyzed Oxidative Rearrangement of Tertiary Allylic Alcohols to Enones with Oxone. *Org. Lett*. **2009**, *11*, 3470-3473.

23. Ojha, L. R.; Kudugunti, S.; Maddukuri, P. P.; Kommareddy, A.; Gunna, M. R.; Dokuparthi, P.; Gottam, H. B.; Botha, K. K.; Parapati, D. R.; Vinod, T. K. Benzylic carbon oxidation by an in situ formed o-iodoxybenzoic acid (IBX) derivative. *Synlett* **2009**, 117-121.

24. Yakura, T., Omoto, M., Yamauchi, Y., Tian, Y., & Ozono, A. Hypervalent iodine oxidation of phenol derivatives using a catalytic amount of 4-iodophenoxyacetic acid and Oxone® as a co-oxidant. *Tetrahedron* **2010**, *66*, 5833–5840.

25. Yamada, K.; Igarashi, Y.; Betsuyaku, T.; Kitamura, M.; Hirata, K.; Hioki, K.; Kunishima, M. An Isolable and Bench-Stable Epoxidizing Reagent Based on Triazine: Triazox. *Org. Lett.* **2018**, *20*, 2015-2019.

26. Jakka, K.; Liu,J.; Zhao, C-G. Facile epoxidation of alpha,beta-unsaturated ketones with cyclohexylidenebishydroperoxide. *Tetrahedron Lett*. **2007**, *48*, 1395–1398.

27. Dalpozzo, R.; Lattanzi, A.; Pellissier. H. Applications of Chiral Three-membered Rings for Total Synthesis: A Review. *Curr. Org. Chem*. **2017**, *21*, 1143-1191.

28. Otera, J.; Sakamoto, K.; Tsukamoto, T.; Orita, A. Temperature-Effected Tuning of Enantioselectivity in Asymmetric Catalysis. *Tetrahedron Lett*. **1998**, *39*, 3201-3204.

29. Ojima,I.; Kogure, T.; Yoda, N. Asymmetric hydrogenation of prochiral olefins catalyzed by rhodium complexes with chiral pyrrolidinodiphosphines. Crucial factors for the effective asymmetric induction. *J. Org. Chem*. **1980**, *45*, 4728-4739,

30. Sinou, D. Hydrogenation asymetrique a l'aide du complexe DIOXOP-Rh(I) voie dihydro ou voie insaturee. *Tetrahedron Lett*. **1981**, *22*, 2987-2990.

31. Muchow, G. ; Vannoorenberghe, Y.; Buono, G. Use of alkaloids and amino alcohols in catalytic asymmetric induction: Temperature effect on the addition of diethylzinc to benzaldehyde. *Tetrahedron Lett*. **1987**, *28*, 6163-6166.

32. Brunel, J. M.; Pardigon, O.; Faure, B.; Buono, G. Enantioselective borane reduction of ketones catalysed by a chiral oxazaphospholidine–borane complex. *J. Chem. Soc., Chem. Commun*. **1992**, *3*, 287-288.

33. Brunel, J. M.; Maffei, M.; Bouno, G. Enantioselective reduction of ketones with borane, catalyzed by (*S*)-(−)-proline or (*S*)-(+)-prolinol. *Tetrahedron: Asymmetry* **1993**, *4*, 2255-2260.

34. Stone, G. B. Oxazaborolidine catalyzed borane reductions of ketones: a significant effect of temperature on selectivity. *Tetrahedron: Asymmetry* **1994**, *5*, 465-472.

35. Dubois, L.; Fiaud, J. C.; Kagan, H. B. Enantioselective borane reduction of acetophenone catalysed by oxazaborolidines derived from chiral diethanolamines. *Tetrahedron: Asymmetry* **1995**, *6,* 1097-1104.

36. Chiodi, O.; Fotiadu, F.; Sylvestre, M.; Bouno, G. Enantioselective reduction of ketones by borane catalysed by oxazaphospholidine oxides. *Tetrahedron Lett*. **1996**, *37*, 39-42.

37. Lautens, M.; Rovis, T. A New Route to the Enantioselective Synthesis of Cycloheptenols. Temperature Effects in the Asymmetric Reductive Ring Opening of [3.2.1] Oxabicycloalkenes. *J. Am. Chem. Soc.* **1997**, *119*, 11090-11091.

38. Ogasawara, M.; Sasa, H.; Hu, H.; Amano, Y.; Nakajima, H.; Takenaga, N.; Nakajima, K.; Kita, Y.; Takahashi, T.; Dohi, T. Atropisomeric Chiral Diiododienes (Z,Z)-2,3-Di(1-iodoalkylidene)tetralins: Synthesis, Enantiomeric Resolution, and Application in Asymmetric Catalysis. *Org. Lett.* **2017**, *19*, 4102-4105.

39. Escorihuela, Jorge; Burguete, M. Isabel; Luis, Santiago V. New advances in dual stereocontrol for asymmetric reactions. *Chem. Soc. Rev.* **2013**, *42*, 5595-5617.

40. Hong, L.; Sun, W.; Yang, D.; Li, G.; Wang, R. Additive Effects on Asymmetric Catalysis. *Chem. Rev.* **2016**, *116*, 4006-4123.

41. Raj, M.; Singh, V. K. Organocatalytic Reactions in Water. *Chem. Commun.* **2009**, 6687– 6703.

42. Brogan, A. P.; Dickerson, T. J.; Janda, K. D. Enamine-Based Aldol Organocatalysis in Water: Are They Really ″All Wet″? *Angew. Chem., Int. Ed.* **2006**, *45*, 8100– 8102

43. Blackmond, D. G.; Armstrong, A.; Coombe, V.; Wells, A. Water in Organocatalytic Processes: Debunking the Myths. *Angew. Chem., Int. Ed.* **2007**, *46*, 3798– 3800.

44. Hayashi, Y. In Water or in the Presence of water? *Angew. Chem., Int. Ed.* **2006**, *45*, 8103– 8104.

45. Uyanik, M.; Yasui, T.; Ishihara, K. Hydrogen Bonding and Alcohol Effects in Asymmetric Hypervalent Iodine Catalysis: Enantioselective Oxidative Dearomatization of Phenols. *Angew. Chemie Int. Ed.* **2013***, 125,* 9385–9388.

46. Colomer, I.*;* Batchelor-McAuley, *C.;* Odell, *B.;* Donohoe, *T. J.;* Compton*, R. G.* Hydrogen Bonding to Hexafluoroisopropanol Controls the Oxidative Strength of Hypervalent Iodine Reagents. *J. Am. Chem. Soc.* **2016** *138*, 8855-8861.

47. Shuklov, I. A.; Dubrovina, N. V.; Börner, A. Fluorinated Alcohols as Solvents, Cosolvents and Additives in Homogeneous Catalysis. *Synthesis* **2007**, *2007,* 2925– 2943.

48. Berkessel, A.; Adrio, J. A.; Hüttenhain, D.; Neudörfl, J. M. Unveiling the "Booster Effect" of Fluorinated Alcohol Solvents: Aggregation-Induced Conformational Changes and Cooperatively Enhanced H-Bonding. *J. Am. Chem. Soc.* **2006**, *128*, 8421– 8426

49. Berkessel, A.; Adrio, J. A. Dramatic Acceleration of Olefin Epoxidation in Fluorinated Alcohols: Activation of Hydrogen Peroxide by Multiple H-Bond Networks. *J. Am. Chem. Soc.* **2006**, *128*, 13412– 13420.

50. Ratnikov, M. O.; Tumanov, V. V.; Smit, W. A. Lewis Acid Catalyst Free Electrophilic Alkylation of Silicon-Capped π Donors in 1,1,1,3,3,3-Hexafluoro-2-propanol. *Angew. Chem. Int.* **2008**, *47*, 9739– 9742.

51. Li, G.-X.; Qu, J. Friedel–Crafts alkylation of arenes with epoxides promoted by fluorinated alcohols or water. *Chem. Commun.* **2010**, *46*, 2653– 2655.

52. Colomer, I.; Coura Barcelos, R.; Donohoe, T. J. Catalytic Hypervalent Iodine Promoters Lead to Styrene Dimerization and the Formation of Tri- and Tetrasubstituted Cyclobutanes. *Angew. Chem. Int.* **2016**, *55*, 4748– 4752.

53. Izquierdo, S.; Essafi, S.; del Rosal, I.; Vidossich, P.; Pleixats, R.; Vallribera, A.; Ujaque, G.; Lledos, A.; Shafir, A. Acid Activation in Phenyliodine Dicarboxylates: Direct Observation, Structures, and Implications. *J. Am. Chem. Soc.* **2016**, *138*, 12747-12750.

54. Dohi, T.; Ito, M.; Morimoto, K.; Iwata, M.; Kita, Y. Oxidative cross-coupling of arenes induced by single-electron transfer leading to biaryls by use of organoiodine(III) oxidants. *Angew. Chem. Int.* **2008**, *47*, 1301-1304.

55. Fujita, M.; Mori, K.; Shimogaki, M.; Sugimura, T. Total synthesis of (12*R*)- and (12*S*)-12- hydroxymonocerins: stereoselective oxylactonization using a chiral hypervalent iodine(III) species. *RSC Adv.* **2013**, *3,* 17717.

56. Ochiai, M.; Takeuchi, Y.; Katayama, T.; Sueda, T.; Miyamoto, K. Iodobenzene-catalyzed alpha-acetoxylation of ketones. in situ generation of hypervalent

(diacyloxyiodo)benzenes using m-chloroperbenzoic acid. *J. Am. Chem. Soc.* **2005**, *127*, 12244-12245.

57. Erkkilä, A.; Majander, I.; Pihko, P. M. Iminium Catalysis. *Chem. Rev.* **2007**, *107*, 5416– 5470.

58. Mukherjee, S.; Yang, J. W.; Hoffmann, S.; List, B. Asymmetric Enamine Catalysis. *Chem. Rev.* **2007**, *107*, 5471– 5569.

59. Levitre, G.; Dumoulin, A.; Retailleau, P.; Panossian, A.; Leroux, F. R.; Masson, G. Asymmetric α-Sulfonyl- and α-Phosphoryl-Oxylation of Ketones by a Chiral Hypervalent Iodine(III). *J. Org. Chem.* **2017**, *82*, 11877-11883.

60. Guillaneux, D.; Zhao, S-H.; Samuel, O.; Rainford, D.; Kagan, H. B. Nonlinear Effects in Asymmetric Catalysis. *J. Am. Chem. Soc.* **1994**, *116*, 9430-9439.

61. Avalos, M.; Babiano, R.; Cintas, P.; Jimenez, J. L.; Palacios, J. C. Nonlinear stereochemical effects in asymmetric reactions. *Tetrahedron: Asymmetry* **1997**, *8*, 2297.

62. Ochiai, M.; Takeuchi, Y.; Katayama, T.; Sueda, T.; Miyamoto, K. Iodobenzene-catalyzed alpha-acetoxylation of ketones. in situ generation of hypervalent (diacyloxyiodo)benzenes using m-chloroperbenzoic acid. *J. Am. Chem. Soc.* **2005**, *127*, 12244-12245.

63. Wang, Y.; Yuan, H.; Lu, H.; Zheng, W-H. Development of Planar Chiral Iodoarenes Based on [2.2]Paracyclophane and Their Application in Catalytic Enantioselective Fluorination of β-Ketoesters. *Org. Lett.* **2018**, *20*, 2555–2558.

# Chapter Four

# INVESTIGATIONS OF THE SOLUTION PHASE STRUCTURE OF IODOARENE PEPTIDES AND ITS RELATIONSHIP TO ENANTIOSELECTIVITY

## *4.1. Introduction*

### *4.1.1. Structure/Enantoselectivity Relationship of Aryl-Iodo Peptides*

Despite the prevalence of short peptide sequences in nature as toxins, hormones, and neurotransmitters in addition to their application in medicinal chemistry, nanosciences, and asymmetric catalysis, there is still much to learn about their structures. Thus far, the research detailed in this thesis has demonstrated the utility of iodoarene peptides to catalyze I(III)-mediated organic transformations, such as the α-functionalization of ketones and the oxylactonization of keto-carboxylic acids. Additionally, a few peptide structures have generated the desired chiral product with moderate enantioselectivities (>30% *ee*). Intriguingly, all of our "hit" peptides have exclusively emerged from peptide Scaffolds A and B. These scaffolds both possess the same Pro-D-Ala amino acid residue sequence that putatively nucleates a β-turn secondary structure. During the design of these peptide scaffolds, it was hypothesized that the inclusion of this type of secondary structure would impart some rigidity into the peptide scaffold in solution, thus enhancing the stereoselectivity of the catalytic process. In fact, it was quickly realized that the linear peptides from Scaffold C were not generating the desired products with even slight degrees of enantioselectivity; therefore, the focus quickly shifted to the synthesis of peptides only from Scaffold A and B (Figure 4.1).

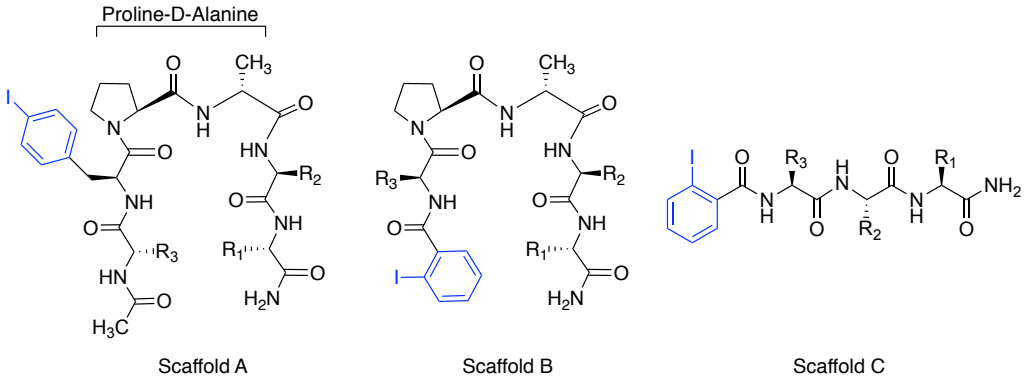


**Figure 4.1.** Peptide pre-catalyst scaffolds A-C.

This shift clearly increased the likelihood of "hit" peptides emerging solely from these scaffolds; nonetheless, it is interesting to delve deeper into the structural features of our iodoarene peptide catalysts and their ability to impart enantiocontrol onto a given reaction.

In order to quickly probe the influence of the Pro-D-Ala amino acid residue sequence, the linear counterpart to "hit" peptide **III-10**, was prepared and screened under standard conditions in the α-oxytosylation of 1-indanone (Scheme 4.1). Precatalyst peptide **IV-1**, generated the desired product **III-8** in only 7% *ee*. This suggests that the inclusion of the Pro-D-Ala sequence in the peptide sequence does influence the enantioselectivity of the reaction.

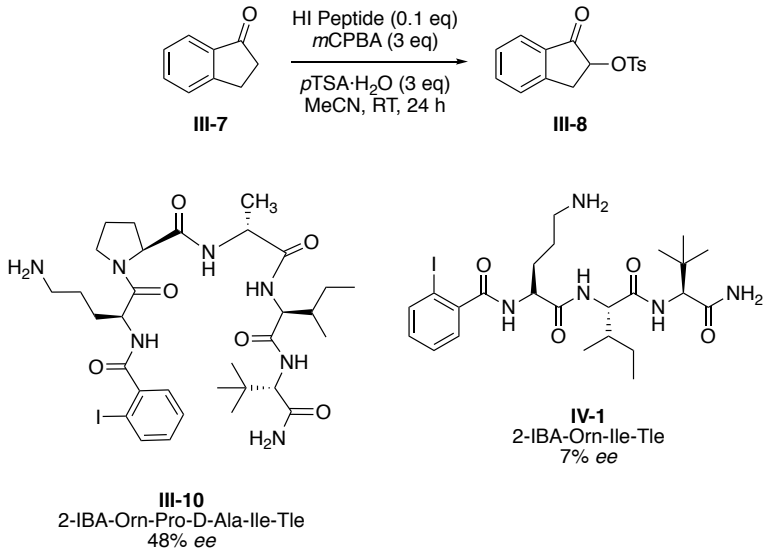


**Scheme 4.1.** The *α*-oxytosylation of 1-indanone, comparison of bent and linear peptides I**II-10** and **IV-1**.

4.1.2. The β -Turn

Proteins contain a wide array of secondary and tertiary structure elements on their surface as well as buried in protein–protein interfaces. Reverse turns, such as *β*-, *γ*-, and *α*-turns, represent one such class of protein secondary structure, wherein, following a chain reversal, a globular portion of the protein is created. These chain reversals are local features in proteins, and thus, have been extensively studied and mimicked using peptides.[1-4]

In folded proteins, the β-turn is the most commonly observed nonrepetitive reverse turn motif, and thus, amino acid sequences have been identified as being predisposed to adopt this secondary structure in peptide sequences. As previously discussed, it has been suggested that the incorporation of secondary structure into a short peptide sequence can impart rigidity into the peptide structure.[103] Simply, a β-turn is a

portion of the protein consisting of four consecutive residues where the peptide chain folds back on itself by nearly 180 degrees. Also, stabilization of this turn is provided by intraturn hydrogen bond interactions between the backbone CO(*i*) and the backbone NH(*i+3*) (Figure 4.2). In addition to the added conformational support, the incorporation of a β-turn into a short peptide sequence can also facilitate advantageous interactions between the catalytic site and other amino acid residue side chains and backbone amides. While, the most commonly observed β-turns display the aforementioned H-bond interactions between the *i* and *i* + 3 residues, they can further be classified as Type I/I' or II/II' based on the ϕ and ψ dihedral angles associated with amino acids *i* + 1 and *i* + 2. More simply stated, the main difference between Type I and II turns in the orientation of the amino acid residues in positions *i+1* and *i+2* (Figure 4.3).

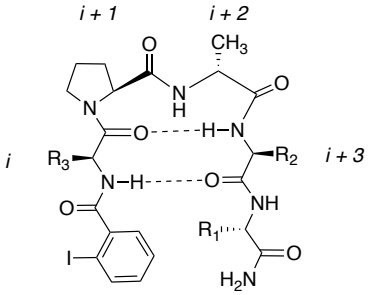


**Figure 4.2.** Expected H-bond interactions in peptide scaffold B.

In proteins, the most commonly observed β-hairpin turns are of type Type I' and II' that contain proline and glycine amino acid residues in the *i* + 1 and *i* + 2 positions, respectively. Nonetheless, a variety of other α- amino acid residues have been found to provide the necessary conformational restraints to promote the turn when located in the *i* + 2 position. For example, synthetic models that mimic type I' and II' turns typically incorporate a Gly, L-Ala, D-Ala, Aib, 1-Amino-1-cyclohexane carboxylic acid ($Ac_6c$), or 1-aminocyclooctane-1-carboxylic acid

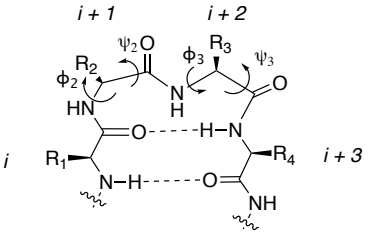


**Figure 4.3.** The ϕ and ψ dihedral angles associate with β-turns.

($Ac_8c0$) residue in the $i + 2$ position.[1-5] Nonetheless, proline's pyrrolidine ring provides the necessary conformational restraint, and thus is the most commonly observed turn inducing amino acid in the $i + 1$ position in peptides and proteins.[5]

*4.1.3. Previous Reports*

Many have sought to take advantage of this β-turn secondary structure when designing asymmetric peptide catalysts. There are numerous reports by Miller *et al.*, wherein the presence of a turn-inducing element greatly impacted the success of stereoinduction displayed by the peptide catalysts.[6-13] Examples of these β-turn-peptide catalyzed transformations include: the kinetic resolution of alcohols, the dynamic kinetic resolution of oxazol-5(*4H*)-ones, and the addition of allenoates to *N*-acyl imines (Figure 4.4). These peptides take advantage of a Pro-Xaa amino acid residue sequence, wherein Pro is D- or L-proline and Xaa is an achiral *α*-*α*-disubstituted amino acid.[20] In particular, Miller and coworkers incorporated a loop region, of either D-Pro-Aib or D-Pro-Aic, known to promote the desired β-turn secondary structure within short peptide sequences. They later verified the presence of the β-turn in an additional 35 peptide structures via solid-state characterization using X-ray crystallographic analysis. Additionally, select solid-state structures were also compared to their solution-phase conformations using 1D and 2D NMR experiments. Following the analysis of proton chemical shifts and $^1H$-$^1H$ NOESY interactions, they propose that sophisticated peptide confirmations in short peptide sequences may be vastly more accessible than previously suggested.

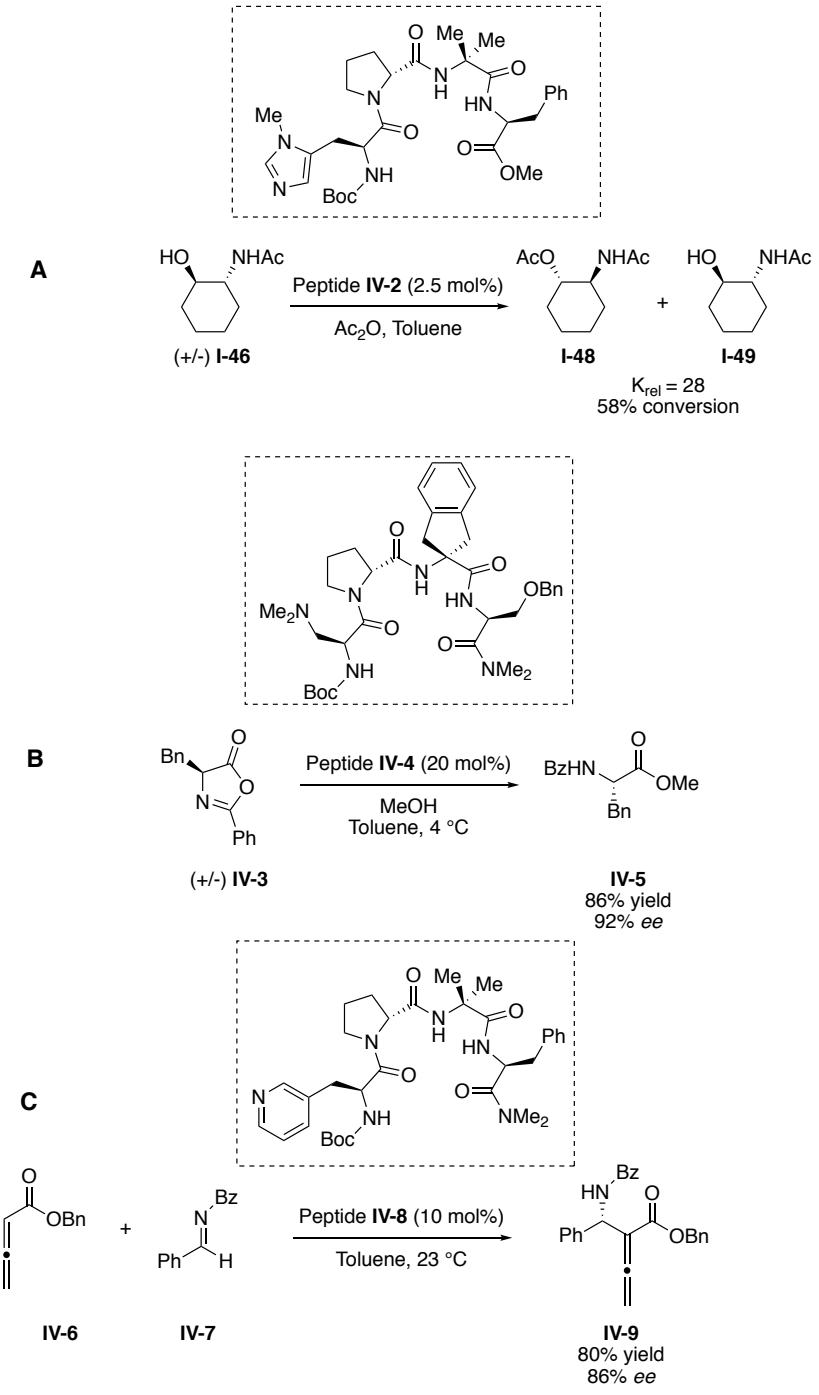


**Figure 4.4.** β-turn peptide-mediated asymmetric reactions reported by Miller *et al.*, including: A) The KR of alcohols, B) the DKR oxazol-5(*4H*)-ones, and C) the addition of allenoates to imines.

### *4.2. Results and Discussion*

#### *4.2.1. Solution-Phase Characterization*

Following the screening of nearly 850 peptide catalyst structures for the asymmetric α-oxytosylation of propiophenone and 1-indanone as well as the oxylactonization of 5-oxo-5-phenylvaleric acid, it became clear that a better understanding of the structure-function relationship of the iodoarene peptide precatalysts and their ability to impart enantiocontrol was needed. Specifically, we thought that a thorough understanding of the solution phase orientation of the pre-catalyst iodoarene peptide would prove critical for further catalyst optimization. Thus, solution-phase characterization of the secondary structure of our most selective peptide catalyst was completed by means of NMR spectroscopy. While the successful synthesis of peptides with the Pro-D-Ala sequence was confirmed by MALDI-TOF mass spectrometry, it was unclear as to whether or not they maintain the proposed β-turn secondary structure in the reaction solution. Briefly, solution-phase characterization was achieved by one and two dimensional NMR spectroscopy. One dimensional $^{1}$H NMR and 2D-COSY (correlated spectroscopy) was implemented to assign resonance peaks for individual protons.[15,16] Further, through space interactions of hit peptide **III-10** was examined with 2D-NOESY (2-D Nuclear Overhauser and Exchange Spectroscopy) in order to confirm the presence of the β-turn in solution. Finally, DMSO-$d_6$ titration $^{1}$H NMR experiments were conducted in order to probe how well the peptide catalysts adopted and maintained the β-turn.[17-21]

*4.2.2. $^{1}H$ NMR Characterization of Aryl-Iodo Peptides General Peptide Structure Characterization*

Solution-phase characterization of peptide **III-10** was achieved by $^{1}H$ NMR and 2D-COSY (correlation spectroscopy). This combination of techniques has been used previously to assign proton chemical shifts and identify through-bond interactions in short peptide structures.[15,16,23,24] Further, these NMR experiments were conducted in $CD_3CN$ at room temperature to mimic our acetonitrile solvent reaction conditions used for the α-oxytosylation of ketones. Figure 4.5 depicts the assigned amino acid residue proton chemical shifts for peptide **III-10**. In general, the aromatic protons on the iodoarene as well as all free amines and amide protons appear downfield between 9 and 6 ppm. Amino acid residue $\alpha$-protons appear between 5 and 3.5 ppm. The $\delta$ protons of proline are observed as split resonances around 3.9 and 3.8 ppm, while the $\delta$ protons of Orn are observed slightly upfield around 3 ppm as a broad peak. The remaining $\beta$- and $\gamma$-protons appear between 3 and 0 ppm. The methyl group of D-Ala is easily identified as a doublet around 1.3 ppm and the *t*-butyl group of Tle is observed as a strong singlet at 0.9 ppm.[14,15]

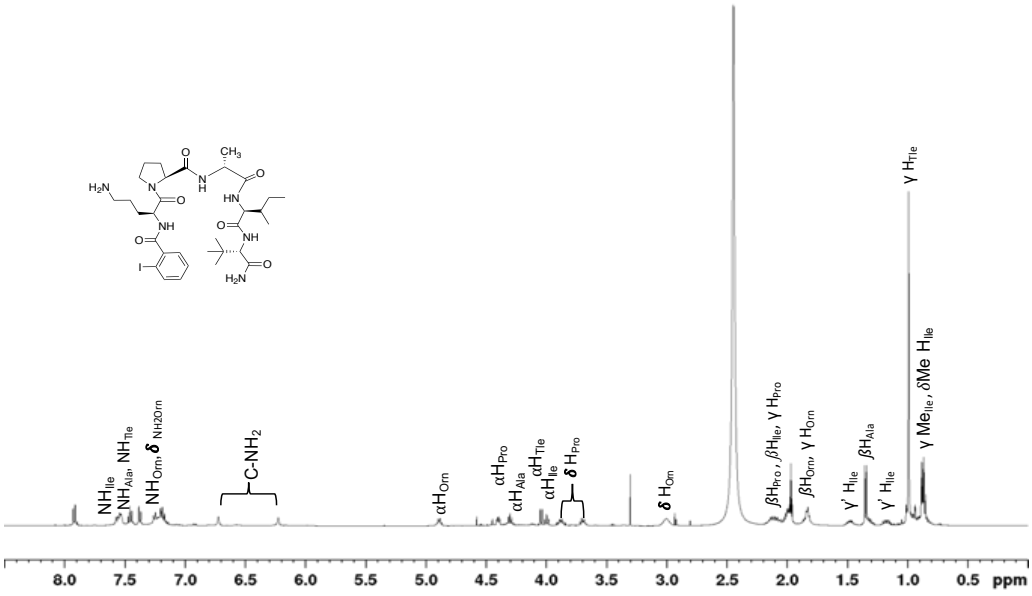


**Figure 4.5.** $^{1}$H NMR spectrum for peptide **III-10**.

Further, a 2D-COSY experiment aided in the assignment of these proton resonances. A COSY displays cross-peaks associated with [$^{1}$H,$^{1}$H]-correlations due to scalar (through-bond) couplings. For example, the amide proton on D-Ala will exhibit a cross-peak with its $\alpha$-proton, which will then display a cross-peak with the Ala methyl group peak at 1.3 ppm. Since the primary structure of the peptide is known, the COSY was used to identify individual amino acid residue spin systems by identifying characteristic cross peaks in the spectrum (See SI for spectrum).

*Verification of the β-Turn in Solution*

Next, in order to verify the presence of the *β*-turn in our reaction solvent, MeCN, a NOESY experiment was performed. A NOESY spectrum contains information related to the spatial proximity of protons in the structure of interest. More specifically, cross peaks arise due to dipolar couplings from interactions of spins close in space and hence only depend on the distance and not on the number of intervening bonds. As previously mentioned, it is suggested that the β-turn motif is nucleated by the D-Ala-Pro sequence and stabilized via the hydrogen bonding of a carbonyl oxygen of one residue with the amide proton of an amino acid three residues down the chain. If the peptide catalyst is maintaining the *β*-turn secondary structure in solution, diagnostic through-space NOE interactions will be observed (Figure 4.6). Interactions 1-3 are suggestive of a folded turn structure, while interaction 3 is indicative of Type II turns. Observation of NOE interaction 4 confirms that the proline amide has adopted the anticipated *s-trans* conformation. Lastly, if the amino acid residues in positions *i+1* and *i+4* are substituted with side-chain *β*-protons, as is the case with Orn and Ile in peptide **III-10**, the NOE interaction highlighted by 5 may be observed. Upon analysis of the NOESY spectrum for peptide **III-10**, all five NOE cross-peaks were observed (Figure 4.7). The presence of these diagnostic interactions in this solution phase

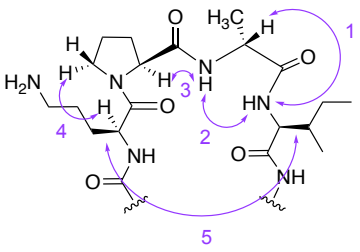


**Figure 4.6.** Expected NOE interactions for peptide **III-10.**

NMR study suggests that peptide **III-10** does exhibit a bent orientation, possibly a Type II β-turn, in the Orn-Pro-D-Ala-Ile region.

There is extensive literature describing the presence of a β-turn as the result of the D-Ala-Pro sequence. Therefore, it was not surprising that these initial solution-phase characterization efforts confirm the presence of the expected *β*-turn in our peptide scaffolds. Further experiments are necessary in order to determine whether or not this peptide maintains its bent structure in its oxidized hypervalent I(III)-state.

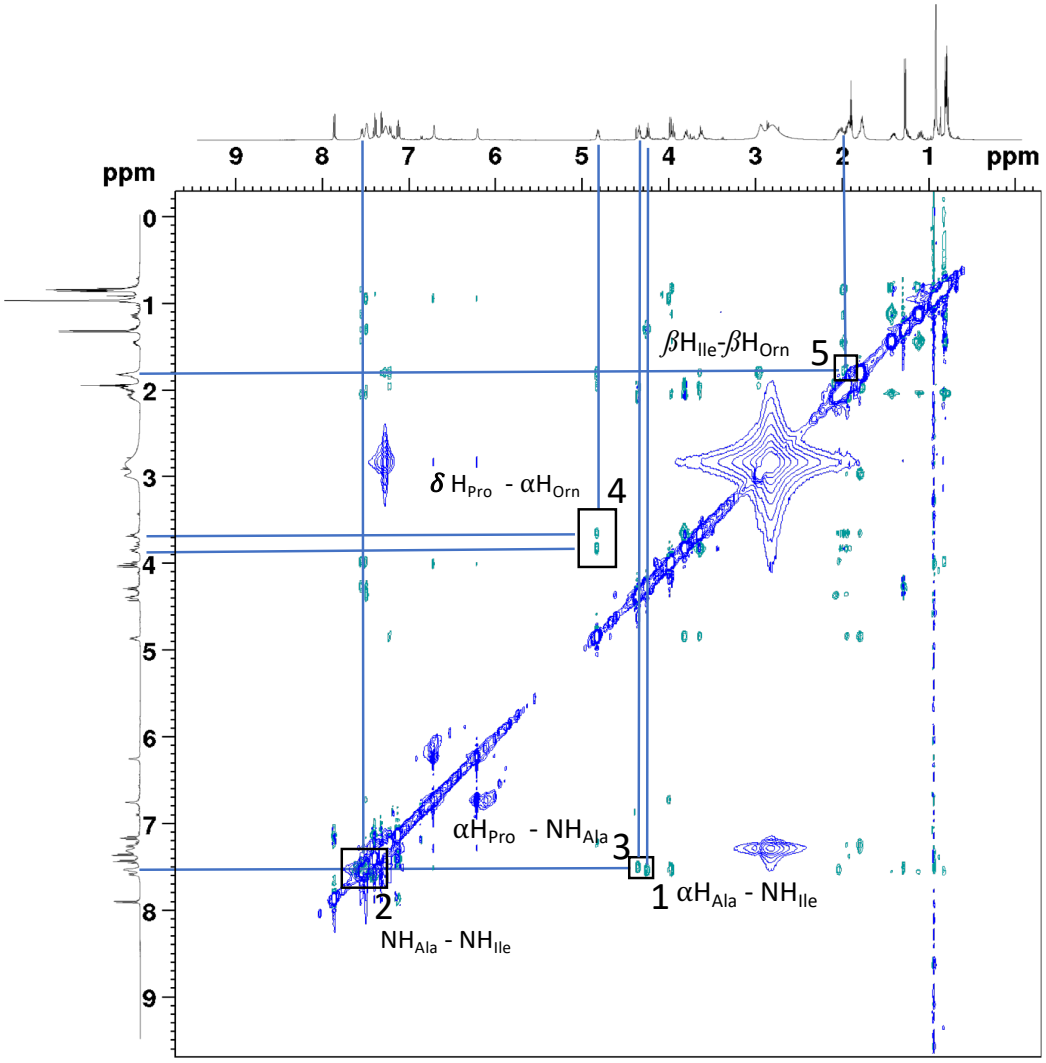


**Figure 4.7.** Identified NOE interactions characteristic of a turn secondary structure in peptide **III-10.**

*Probing the stability of the β-Turn: DMSO Titration Experiments*

Peptide scaffolds A and B were designed so that they would be predisposed to adopt a β-turn secondary structure. The aforementioned 2D-NOESY data confirms that our best peptide for the *α*-oxytosylation of 1-indanone (**III-10**), maintains its secondary structure in MeCN. Next, in order to further elucidate the role that the peptide structure plays in the observed enantioselectivity, DMSO-$d_6$ titration experiments on peptide catalysts showing high, moderate, and low levels of selectivity were performed by means of NMR spectroscopy. Briefly, when a peptide is dissolved in benzene-$d_6$ solution and then titrated with a strong H-bond accepting solvent, such as DMSO-$d_6$, the solvent exposed amide protons will exhibit a diagnostic downfield shift in the $^1$H NMR spectrum. However, in a typical β-turn, the *i+1* and *i+3* amide N-H protons are engaged in H-bonds with the *i+4* and *i+1* amide carbonyls, respectively, and are thus shielded from this shift. Figure 4.8 highlights the expected solvent-shielded N-H amide protons that would be engaged in hydrogen bonding interactions in the predicted β-turn, *i.e.* positions *i* and *i+3*.[26-28]

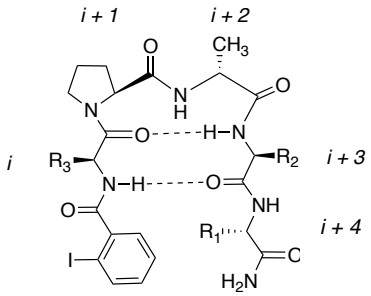


**Figure 4.8.** Solvent shielded protons in Scaffold B peptides.

Iodoarene peptides **III-10**, **IV-10**, and **IV-11** were chosen as representative peptides as they displayed the highest (48% *ee*), moderate (28% *ee*), and low levels (0% *ee*) of enantioselectivity in the initial screenings for the *α*-oxytosylation of 1-indanone, respectively (Figure 4.9). Solutions containing 0.025 mmol of each peptide and 0.2 mL of benzene-$d_6$ were prepared in NMR tubes. A baseline $^1$H NMR spectrum for each was

taken. Then following the sequential addition of 5 μL aliquots of DMSO-$d_6$, the chemical shifts of the amide protons were recorded. The observed amide protons shifts (ppm) were then plotted against the amount of DMSO-$d_6$ solvent added (μL) in order to observe the extent of the engagement of amide protons in hydrogen bonding either intramolecularly within the peptide or intermolecularly with the protic solvent.

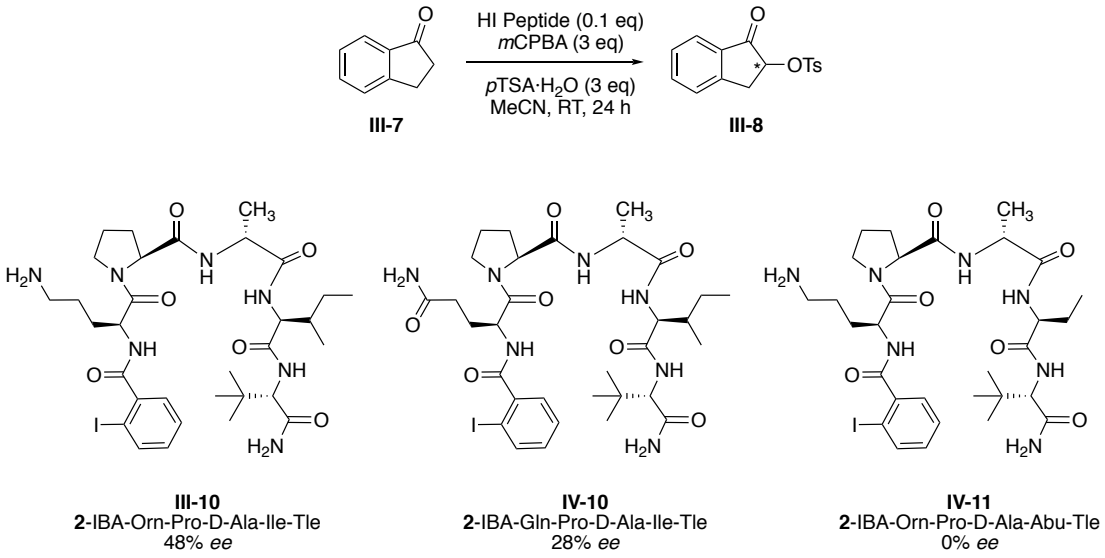


**Figure 4.9.** Peptides displaying high, moderate, and low levels of enantioselectivity for the α-oxytosylation of 1-indanone.

The resulting DMSO-$d_6$ dilution curves for peptides **III-10**, **IV-10**, and **IV-11** are depicted in Figure 4.10. Table 4.1 contains the calculated slopes as well as the overall change in chemical shift (Δ ppm) for curves corresponding to the amide protons in positions *i*, *i +2*, *i +3,* and *i +4.*

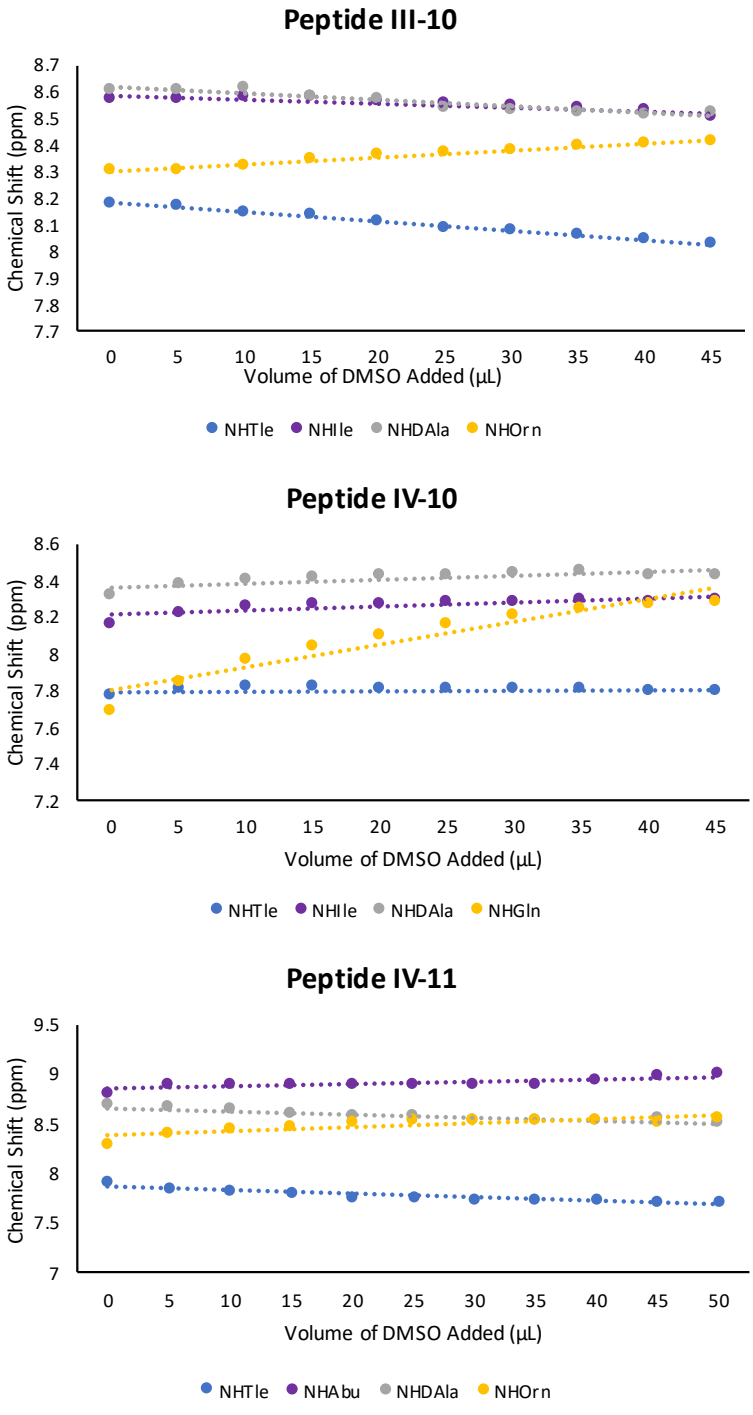


**Figure 4.10.** Dilution curves for peptides **III-10**, **IV-10**, and **IV-11**.

**Table 4.1. Slopes and Chemical Shifts of Amide Protons**

| Peptide | Slope of *i* Shift (Δppm) | Slope of *i+2* Shift (Δppm) | Slope of *i+3* Shift (Δppm) | Slope of *i+4* Shift (Δppm) |
|---|---|---|---|---|
| **III-10** | 0.0132 (0.1135) | 0.0122 (0.0845) | 0.0072 (0.0665) | 0.0172 (0.148) |
| **IV-10** | 0.0619 (0.5915) | 0.0102 (0.106) | 0.0114 (0.138) | 0.0003 (0.1765) |
| **IV-11** | 0.0202 (0.2795) | 0.0163 (0.181) | 0.012 (0.183) | 0.0174 (0.2035) |

If involved in the expected intramolecular hydrogen bonding network predicted for the β-turn, *i* and *i +3* amide protons should display little to no change in chemical shift upon the addition of increasing amounts of DMSO-$d_6$. Further, observation of a large change in chemical shift (~1 ppm) is characteristic of an amide proton that is not engaged in intramolecular H-bonding.[26-28] Upon analysis of the dilution curves, it can be suggested that peptides **III-10** and **IV-11** display strong intramolecular H-bonding in the expected positions. Both peptides contain an Orn residue in position *i* and an Ile or Abu amino acid residue in position *i+3,* respectively. It can be suggested that the H-bond network is slightly stronger in peptide **III-10**, due to the smaller slope and Δ ppm observed for the amides of interest (Table 4.1). On the other hand, the amide proton in position *i* of peptide **IV-10**, experiences a noticeable shift (~0.6 ppm), suggesting that it is involved in a weaker intramolecular H-bond as compared to the other two peptides. It is interesting to note, that the Tle amide proton (*i+4*) in peptide **IV-10**, is not sensitive toward the addition of DMSO, possibly suggesting an alternative strong H-bonding network in this peptide. Lastly, the amide protons in position *i+4* (Tle) in peptides **III-10**

and **IV-11** both display a slight up-field shift. This observation may be suggestive of an intermolecular H-bond association of these amides with benzene-$d_6$.[28]

### *4. 3. Conclusion*

A majority of all "hit" peptides have stemmed from peptide scaffolds A and B, which all possess the same D-Ala-Pro nucleated β-turn secondary structure (Figure 4.1). This observation suggested that the structural rigidity imparted by this secondary structure could be an important factor in the overall enantioselectivity of the reaction. Therefore, in an attempt to further our understanding of the relationship between catalyst structure and observed product enantioselectivity, a series of solution phase characterization experiments were conducted. First, noted NOESY interactions indicated that "hit" peptide **III-10** adopts the *β*-turn secondary structure in the reaction solvent (MeCN). Further, 1H NMR DMSO-$d_6$ titration experiments suggest that the extent of the *β*-turn may play a factor in enantioselectivity. For example, the ability to design a peptide scaffold that would position the catalytically active iodoarene site in close proximity to other functional groups, such as backbone amides, may play a significant role in achieving high levels of enantioselectivity. Lastly, there are other factors that need to be considered, such as, electronic and steric influences around the active I(III)-site, mechanism, and enol geometry. The influence of the proximity of the iodine center with respect to the peptide backbone is highlighted by screening peptide structures **IV-12** and **IV-13** in the *α*-oxytosylation of 1-indanone. These peptides have identical primary sequences to peptide **III-10** except for the location of the iodine moiety, with respect to

the peptide amide, on the arene ring (Figure 4.11). Reactions were performed under optimized conditions. Namely 1-indanone (**III-7**) was treated with *m*CPBA (3 equiv), *p*TSA•$H_2O$ (3 equiv), 10 mol% peptide **IV-12** or **IV-13**, 4 Å molecular sieves, in dry MeCN for 24 h to generate the α-oxytosylated product **III-8** in 0 and 25% *ee,* respectively. The observed drastic decreases in the enantioselectivty of these reactions clearly demonstrates the significance of the proximity of the active I(III)-center with regards to the peptide.

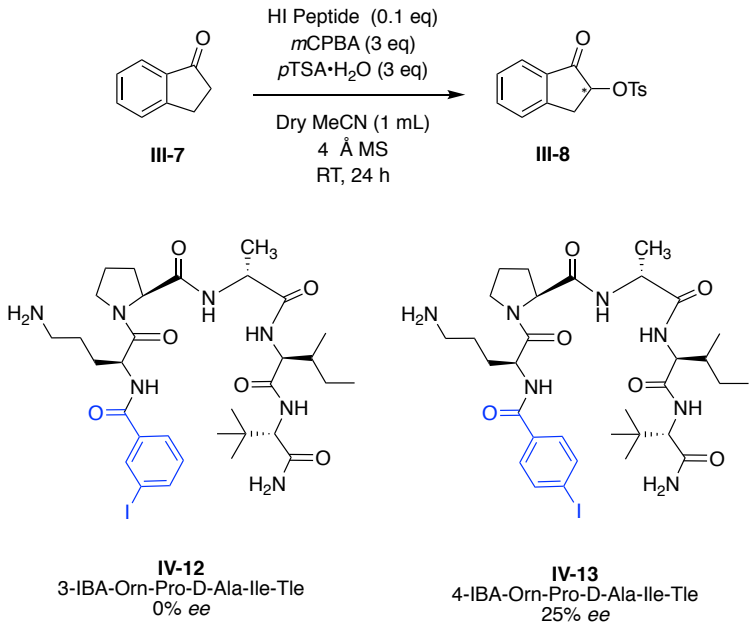


**Figure 4.11.** Results of screening peptides **IV-12** and **IV-13** in the *α*-oxytosyltion of 1-indanone.

### *4. 4. Future Directions*

Ultimately, there are numerous experiments that can be performed in order to truly understand the structure-function continuum for catalytic reactions. In order to fully understand the structural characteristics that promote highly enantioselective peptides, one must consider the orientation of the peptide backbone with respect to the iodoarene active site. This can be accomplished by examining the solution-phase and solid-state structure of the peptide catalysts in their oxidized I(III)-state. Presumably, this can be accomplished by conducting similar 1D and 2D NMR experiments as well as complementary solid-state X-ray crystallographic analysis of oxidized peptides. The I(I) peptides can be oxidized to their corresponding hydroxytosyloxy I(III) reagent upon treatment with 5 equiv *m*CPBA and 1 equiv *p*TSA•$H_2O$ in DCM for 48 h at elevated temperatures (Scheme 4.2).[29,30] Following reverse phase column purification, pure samples of the I(I) and I(III) peptides can be obtained. In order to obtain X-ray quality crystals, a systematic crystallizing solvent screen will be conducted. Ultimately, NMR solution state experiments and X-Ray analysis of these peptides will shed light on how the aryl-iodo active site interacts with the peptide backbone and if this interaction changes upon oxidation to the active I(III) state.

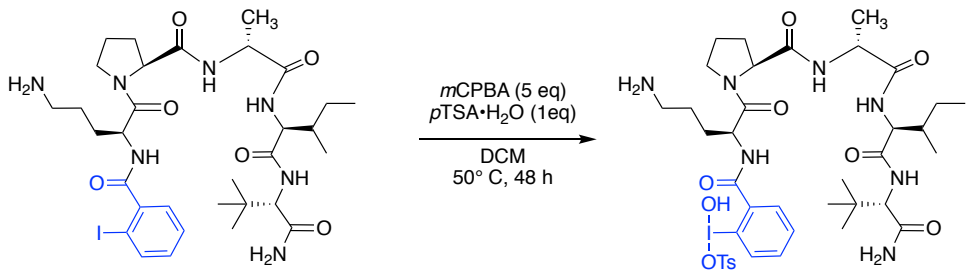


**Scheme 4.2.** Oxidation of I(I) peptide to its active I(III) congener.

Completion of the proposed solution-phase and solid-state characterization experiment will offer valuable information as to how the peptide sequence and its secondary structure influences the selectivity and reactivity of the I(III) catalyst. It will be especially interesting if trends can be gleaned upon comparison of peptide catalysts displaying high, moderate, and low levels of enantioselectivity.

### *4. 5. Experimental*

*General Remarks*

All NMR experiments were carried out on a Bruker Avance NEO NMR (500 MHz) spectrometer equipped with a broadband Prodigy $N_2$ cooled cryoprobe. Proton chemical shifts are reported in ppm (δ) relative to the residual NMR solvent: $CD_3CN$ (δ 1.94 ppm) or $C_6D_6$ (δ 7.16 ppm) NMR data are reported as follows: chemical shift (integration, multiplicity [singlet (s), doublet (d), doublet of doublets (dd), triplet (t), triplet of triplets (tt), quartet (q), multiplet (m)], coupling constants [Hz]). $^{13}C$ resonances are reported in ppm relative to residual solvent peaks for $CD_3CN$ (118.3 ppm) or $C_6D_6$ (128.1 ppm).NMR solvents, acetonitrile-$d_3$, benzene-$d_6$, and dimethylsulfoxide-$d_6$ were purchased from Cambridge Isotope Laboratories and used without further purification.

*DMSO- $d_6$ Titration Experiments*

NMR peptide samples were prepared by dissolving 0.025 mmol of the peptide of interest in 0.2 mL of benzene-$d_6$ in an NMR sample tube. $^1H$ NMR titration experiments were ran after the addition of 0, 5, 10, 15, 20, 25, 30, 25, 40, and 45 µL of DMSO-$d_6$. The

5 μL aliquots of DMSO-$d_6$ were added via micropipette to the NMR tube. In order to ensure homogeneity, the sample tube was equipped with a glass stopper and inverted. The sample tube was sealed with an NMR cap and the $^1$H NMR spectrum was recorded.

### *4. 6. Supplemental Information*

Peptide **2-IBA-Orn-Pro-D-Ala-Ile-Tle, III-10:** $^1$H NMR (500 MHz, $CDCl_3$): δ 7.92 (1H, m), 7.57-7.53 (3H, m), 7.47-7.44 (1H, m), 7.38 (1H, dd, J = 7.6, 1.7 Hz), 7.25 (1H, d, J = 7.8 Hz), 7.23-7.2 (3H, m), 6.72 (1H, s), 6.23 (1H, s), 4.91-4.87 (1H, m), 4.41-4.39 (1H, m), 4.32-4.27 (1H, m), 4.04 (1H, d, J = 8.3 Hz), 4.00 (1H, t, J = 8.2 Hz), 3.91-3.84 (1H, m), 3.72-3.67 (1H, m), 3.00 (1H, br), 2.16-2.00 (5H, m), 1.87-1.81 (4H, m), 1.52-1.44 (1H, m), 1.35 (3H, d, J = 7.13 Hz), 1.20-1.15 (1H, m), 1.00 (9H, s), 0.89-0.85 (6H, m) ppm.

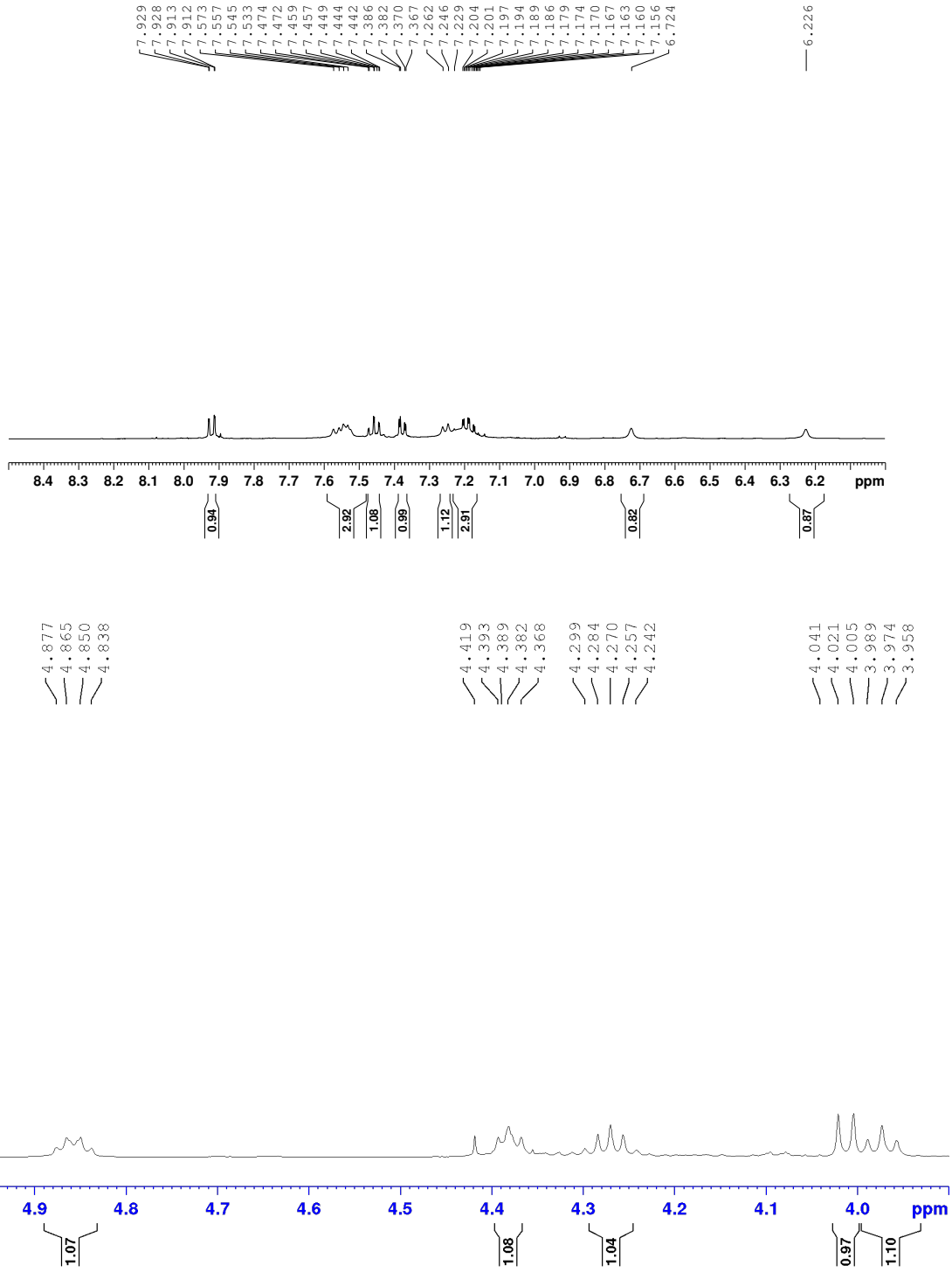
7.929
7.928
7.913
7.912
7.573
7.557
7.545
7.533
7.474
7.472
7.459
7.457
7.449
7.444
7.442
7.386
7.382
7.370
7.367
7.262
7.246
7.229
7.204
7.201
7.197
7.194
7.189
7.186
7.179
7.174
7.170
7.167
7.163
7.160
7.156
6.724
6.226
8.4 8.3 8.2 8.1 8.0 7.9 7.8 7.7 7.6 7.5 7.4 7.3 7.2 7.1 7.0 6.9 6.8 6.7 6.6 6.5 6.4 6.3 6.2 ppm
0.94
2.92
1.08
0.99
1.12
2.91
0.82
0.87
4.877
4.865
4.850
4.838
4.419
4.393
4.389
4.382
4.368
4.299
4.284
4.270
4.257
4.242
4.041
4.021
4.005
3.989
3.974
3.958
4.9 4.8 4.7 4.6 4.5 4.4 4.3 4.2 4.1 4.0 ppm
1.07
1.08
1.04
0.97
1.10

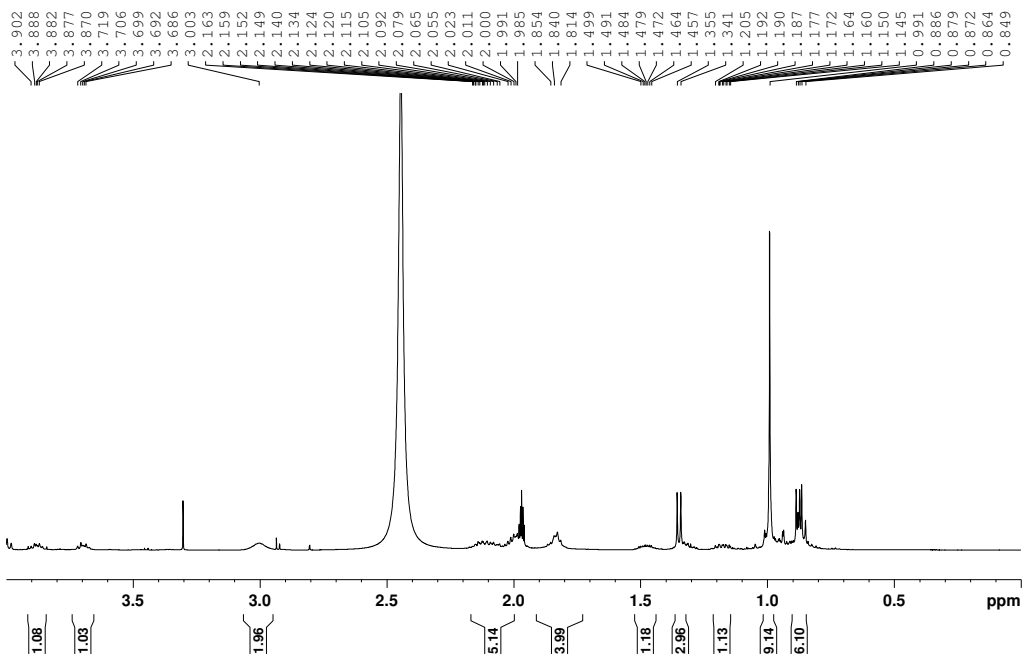
3.902
3.888
3.882
3.877
3.870
3.719
3.706
3.699
3.692
3.686
3.003
2.163
2.159
2.152
2.149
2.140
2.134
2.124
2.120
2.115
2.105
2.092
2.079
2.065
2.055
2.023
2.011
2.000
1.991
1.985
1.854
1.840
1.814
1.499
1.491
1.484
1.479
1.472
1.464
1.457
1.355
1.341
1.205
1.192
1.190
1.187
1.177
1.172
1.164
1.160
1.150
1.145
0.991
0.886
0.879
0.872
0.864
0.849
3.5
3.0
2.5
2.0
1.5
1.0
0.5
ppm
1.08
1.03
1.96
5.14
3.99
1.18
2.96
1.13
9.14
6.10

*COSY spectrum for peptide **III-10***

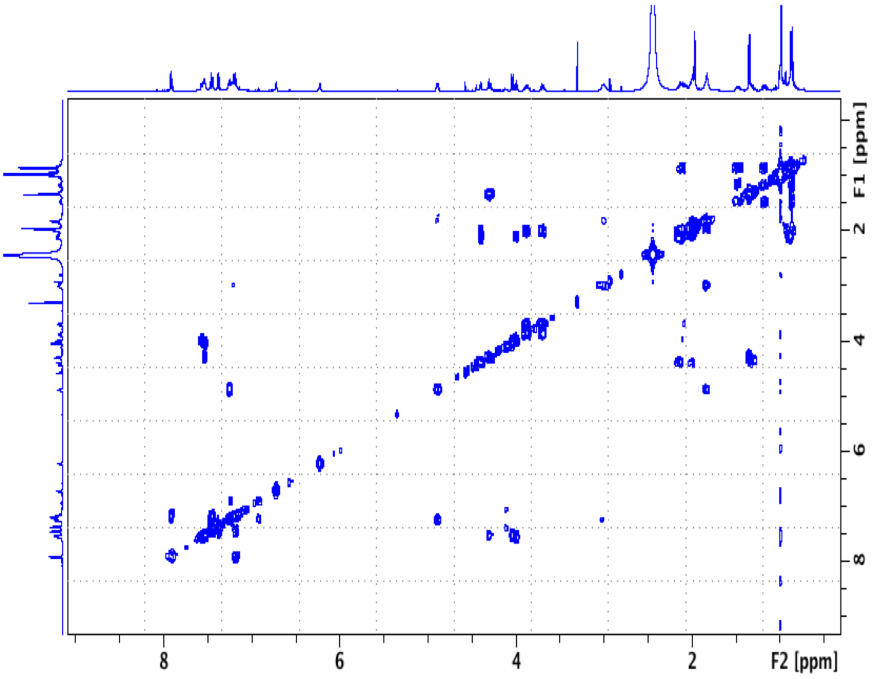


*DMSO-$d_6$ Titration Experiments*

$^1$H NMR spectra of the aromatic and amide regions of each DMSO-$d_6$ titration are included for peptides **III-10**, **IV-10**, and **IV-11**. Each spectrum, starting from the bottom, represents 0, 5, 10, 15, 20, 25, 30, 35, 40, and 45 µL additions of DMSO-d6 to the peptide sample that was prepared in benzene-$d_6$.

*DMSO-$d_6$ Titration Experiment Overlay for Peptide **III-10***

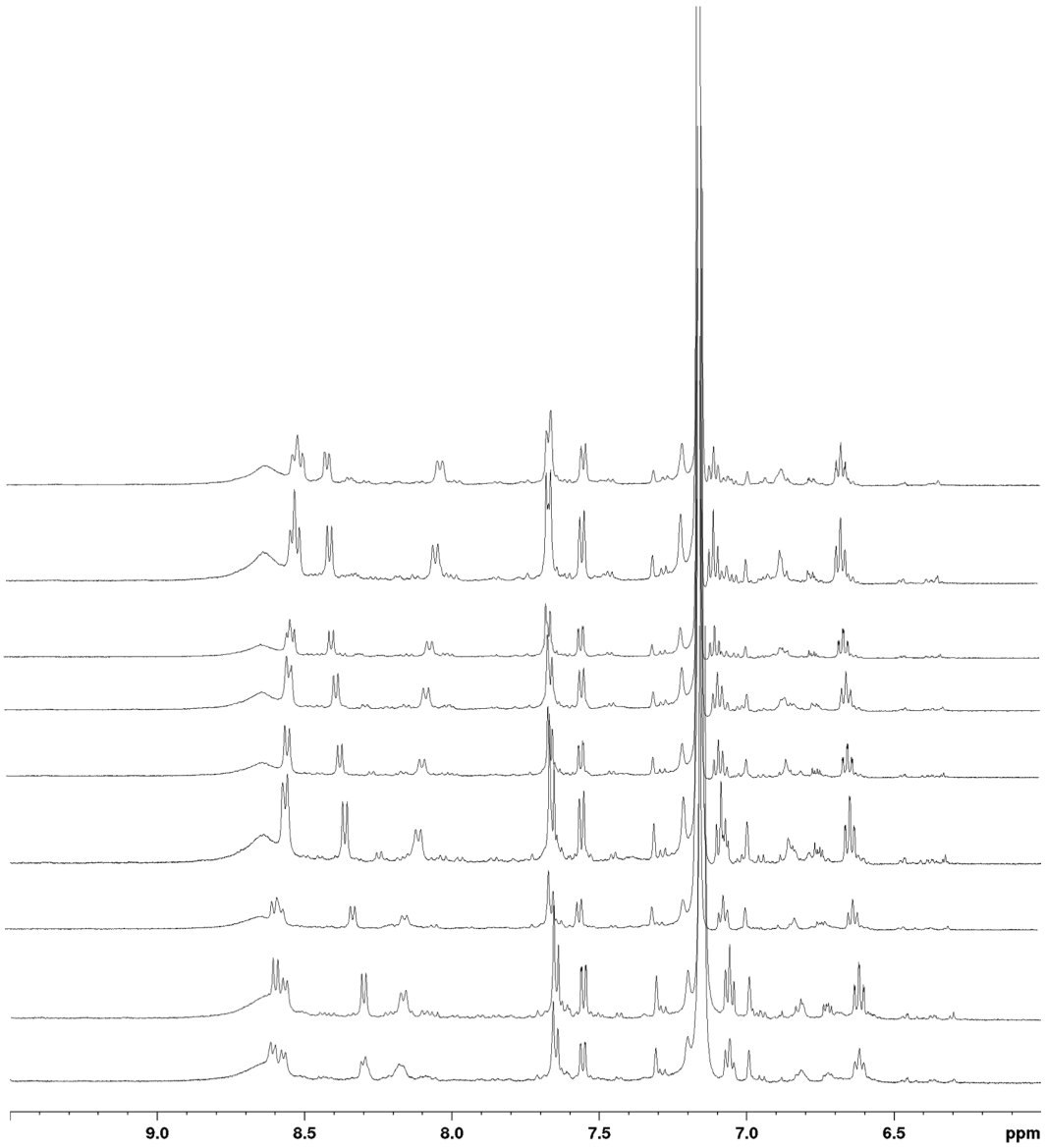

*DM SO-$d_6$ Titration Experiment Overlay for Peptide **IV-10***

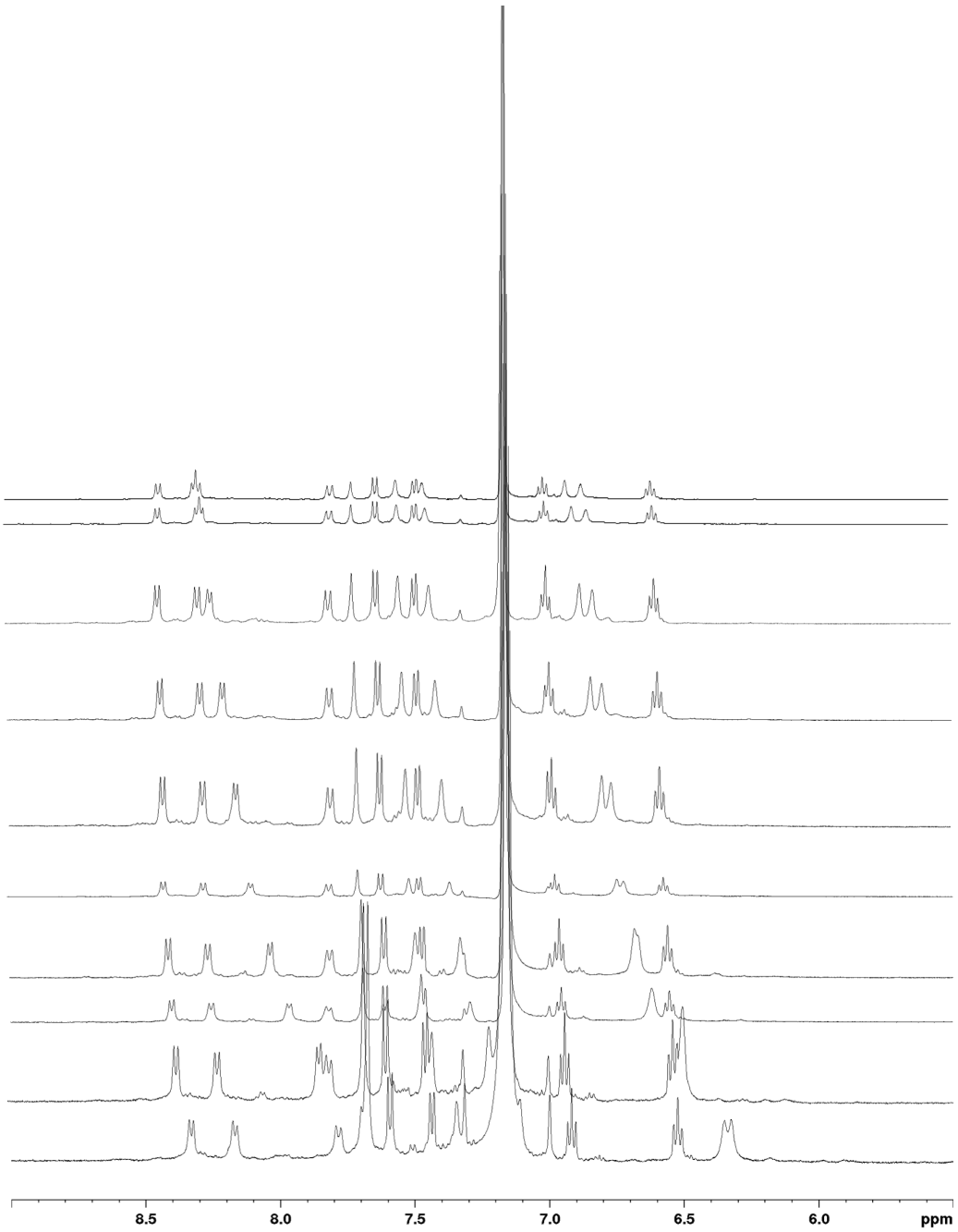

*DMSO-$d_6$ Titration Experiment Overlay for Peptide **IV-11***

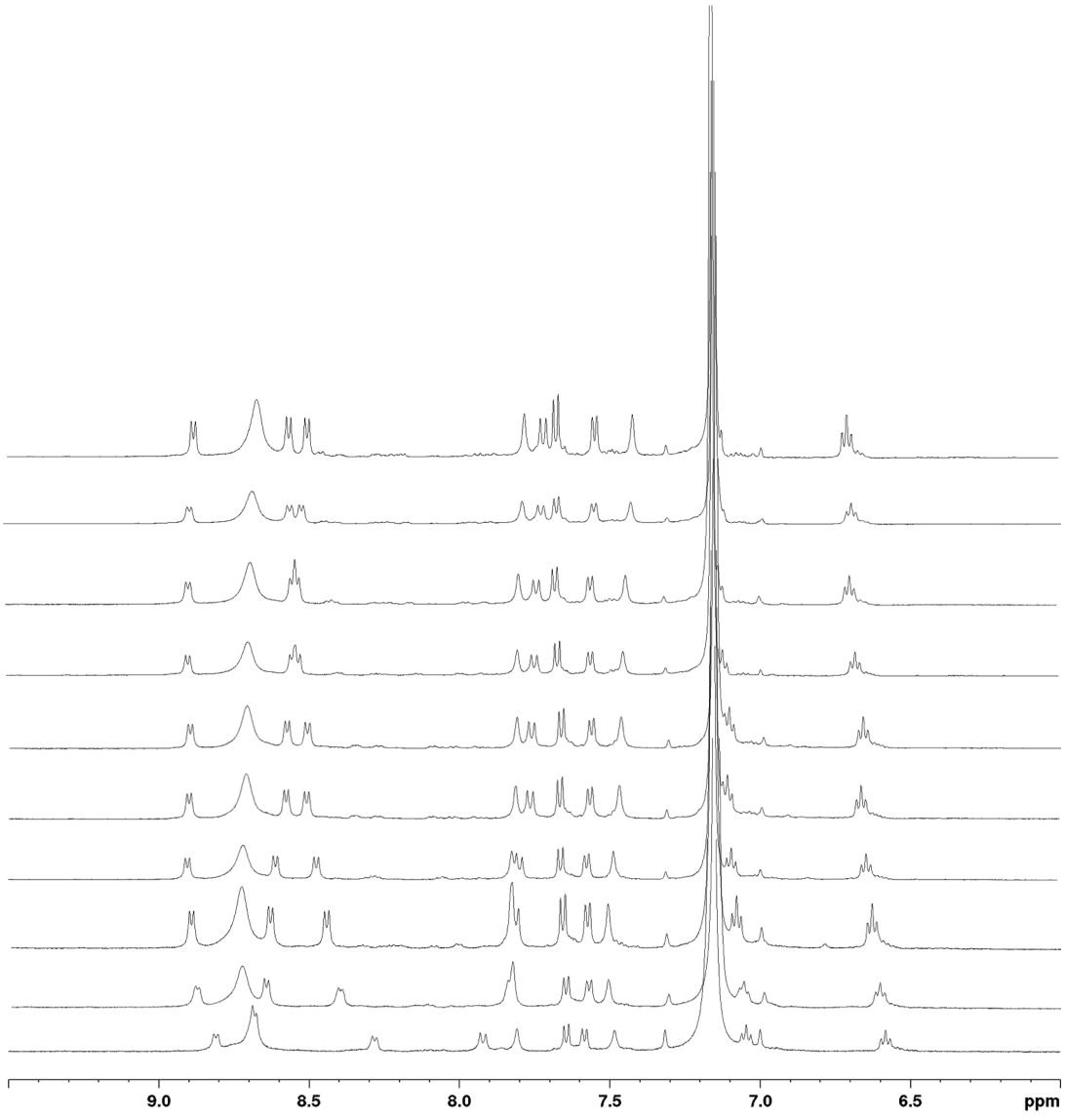

### *4.7. Acknowledgements*

Funding for this research was provided by The National Science Foundation (grant number CHE-1664920). All NMR experiments were performed on a 500 MHz Bruker Avance NEO NMR instrument funded by The National Science Foundation (grant number CHE-1725919). My sincere thanks and appreciation to Dr. Alex Kitaygorodskiy and Dr. Leah Casabianca for their assistance, guidance, and patience throughout these experiments.

### *4. 8. References*

1. Rose, G. D.; Gierasch, L. M.; Smith, J. A. Turns in peptides and proteins. *Adv. Protein. Chem.* **1985**, *37*, 1–109.
2. Hutchinson, E. G.; Thornton, J. A revised set of potentials for beta-turn formation in proteins. *Protein Sci.* **1994**, *3*, 2207–2216.
3. Nagai, U.; Sato, K. Synthesis of a bicyclic dipeptide with the shape of [beta]-turn central part. *Tetrahedron Lett.* **1985**, *26*, 647–650.
4. Metrano, A. J.; Abascal, N. C.; Mercado, B. Q.; Paulson, E. K.; Hurtley, A. E.; Miller, S. J. Diversity of Secondary Structure in Catalytic Peptides with *β*-Turn-Biased Sequences. *J. Am. Chem, Soc.* **2017** *139*, 492-516.
5. Wuethrich, K. NMR of Proteins and Nucleic Acids, Wiley 1986.
6. Cavanagh, J.; Fairbrother, W. J.; Palmer, A. G.; Skelton, N. J. Protein NMR Spectroscopy Principles and Practice, Academic Press 1996.

7. Koskinen, A. M. P.; Helaja, J.; Kumpulainen, E. T. T.; Koivisto, J.; Mansikkamäki, H.; Rissanen, K. Locked Conformations for Proline Pyrrolidine Ring: Synthesis and Conformational Analysis of cis- and trans-4-tert-Butylprolines. *J. Org. Chem.,* **2005**, *70,* 6447-6453.
8. Barrett, K. T.; Miller, S. J. Enantioselective Synthesis of Atropisomeric Benzamides through Peptide-Catalyzed Bromination. *J. Am. Chem. Soc.* **2013**, *135*, 2963–2966.
9. Han, S.; Miller, S. J. Asymmetric Catalysis at a Distance: Catalytic, Site-Selective Phosphorylation of Teicoplanin. *J. Am. Chem. Soc.* **2013**, *135*, 12414–12421.
10. Fowler, B. S.; Mikochik, P. J.; Miller, S. J. Peptide-Catalyzed Kinetic Resolution of Formamides and Thioformamides as an Entry to Nonracemic Amines. *J. Am. Chem. Soc.* **2010**, *132*, 2870–2871.
11. Saunders, L. B.; Cowen, B. J.; Miller, S. J. Pyridylalanine (Pal)-Peptide Catalyzed Enantioselective Allenoate Additions to N-Acyl Imines Proceed via an Atypical "Aza-Morita-Baylis-Hillman" Mechanism. *Org. Lett.* **2010**, *12*, 4800−4803.
12. Lewis, C. A.; Miller, S. J. Site-Selective Derivatization and Remodeling of Erythromycin A Using Peptide-Based Chiral Catalysts. *Angew. Chem., Int. Ed.* **2006**, *45*, 5616−5619.
13. Shugrue, C. R.; Miller, S. J. Phosphothreonine as a Catalytic Residue in Peptide-Mediated Asymmetric Transfer Hydrogenations of 8-Aminoquinolines. *Angew. Chem., Int. Ed.* **2015**, *54*, 11173−11176.

14. Mbofana, C. T.; Miller, S. J. Diastereo- and Enantioselective Addition of Anilide-Functionalized Allenoates to N-Acyl Imines Catalyzed by a Pyridylalanine-Based Peptide. *J. Am. Chem. Soc.* **2014**, *136*, 3285−3292.

15. Fiori, K. W.; Puchlopek, A. L. A.; Miller, S. J. Enantioselective Sulfonylation Reactions Mediated by a Tetrapeptide Catalyst. *Nat. Chem.* **2009**, *1*, 630−634.

16. Metrano, A. J.; Abascal, N. C.; Mercado, B. Q.; Paulson, E. K.; Miller, S. J. Structural Studies of β-Turn-Containing Peptide Catalysts for Atroposelective Quinazolinone Bromination. *Chem. Commun.* **2016**, *52*, 4816-4819.

17. Imperiali, B.; Fisher, S. L.; Moats, R. A.; Prins, T. J. A. Conformational Study of Peptides with the General Structure Ac-L-Xaa-Pro-D-Xaa-L-Xaa-NH2-Spectroscopic Evidence for a Peptide with Significant Beta-Turn Character in Water and in Dimethyl-Sulfoxide. *J. Am. Chem. Soc.* **1992**, *114*, 3182-3188.

18. Imperiali, B.; Kapoor, T. M. The Reverse Turn as a Template for Metal Coordination. *Tetrahedron* **1993** , *49* , 3501-3510.

19. Bax, A.; Davis, D. G. MLEV-17-Based Two-Dimensional Homonuclear Magnetization Transfer Spectroscopy. *J. Mag. Res.* **1985**, *65*, 355-360.

20. Fierman, M. B.; O'Leary, D. J.; Steinmetz, W. E.; Miller, S. J. Structure-Selectivity Relationships and Structure for a Peptide-Based Enantioselective Acylation Catalyst. *J. Am. Chem. Soc.* **2004**, *126*, 6967-6971.

21. Gilberston, S. R.; Chen, G.; Kao, J.; Beatty, A.; Campana, C. F. Structure of Phosphorus-Containing Peptide Ligands. X-Ray and NMR Structural Study of Free Ligand and Rhodium Complex. *J. Org. Chem.* **1997**, *62*, 5557-5566.

22. Vasbinder, M. M.; Jarvo, E. R.; Miller, S. J. Incorporation of peptide isosteres into enantioselective peptide-based catalysts as mechanistic probes. *Angew. Chem. Int.* **2001**, *40*, 2824-2827.

23. Bax, A.; Davis, D. G. Practical Aspects of Two-Dimensional Transverse NOE Spectroscopy. *J. Mag. Res.* **1985**, *63*, 207-213.

24. Bothner-By, A. A.; Stephens, R. L.; Lee, J.; Warren, C. D.; Jeanloz, R. W. Structure determination of a tetrasaccharide: transient nuclear Overhauser effects in the rotating frame. *J. Am. Chem. Soc*., **1984**, *106*, 811-813.

25. Venkatachalapathi, Y. V.; Balaram, H. Temperature dependence of peptide NH chemical shifts in benzene: Delineation of solvent-shielded and exposed amide protons. *Biopolymers* **1981**, *20*, 625-628.

26. Venkatachalapathi, Y. V.; Venkataram Prasad, B. V.; Balaram, H. Confromational analysis of small disulfide loops. Spectroscopic and theoretical studies on a synthetic cyclic tetrapeptide containing cystine. *Biochemistry* **1982**, *21*, 5502-5509.

27. Wuthrich, K.; Billeter, M.; Braun, W. Polypeptide secondary structure determination by nuclear magnetic resonance observation of short proton-proton distances. *J. Mol. Bio.* **1984**, *180*, 715-740.

28. Tremmel, P.; Geyer, A. Coupled Hydrogen-Bonding Networks in Polyhydroxylated Peptides. *Angew. Chem. Int.* **2004**, *43*, 5789–5791.

29. Zagulyaeva, A. A.; Yusubov, M. S.; Zhdankin, V. V. A General and Convenient Preparation of [Bis(trifluoroacetoxy)iodo]perfluoroalkanes and

[Bis(trifluoroacetoxy)iodo]arenes by Oxidation of Organic Iodides Using Oxone and Trifluoroacetic Acid. *J. Org. Chem.* **2010**, *75*, 2119-2122.

30. Watanabe, A.; Miyamoto, K.; Okada, T.; Asawa, T.; Uchiyama, M. Mechanistic Study on Aryl-Exchange Reaction of Diaryl-$\lambda^3$-iodane with Aryl Iodide. *J. Org. Chem.* **2018**, *83*,14262–14268.

CHAPTER 5

# MODIFIED KAOLINITE CLAY FOR THE CAPTURE OF VOLATILE ORGANIC COMPOUNDS

## *5.1. Introduction*

### *5.1.1. Volatile Organic Compounds*

In the late 1950s Haagen–Smit recognized the significance of anthropogenic organic compounds as they pertain to atmospheric chemistry through his pioneering studies on Los Angeles smog. This study highlighted how various volatile organic compounds (VOCs) and nitrogen oxides (NOx) react to generate tropospheric ozone via a photochemical process.[1-3] Since then, interest in emissions of VOCs into the atmosphere and their effects has amplified. VOCs can be defined as chemicals with low vapor pressures that are emitted into the atmosphere from either biogenic or anthropogenic sources. This class of compounds encompasses a wide range of reactive moieties, such as aldehydes, carboxylic acids, alcohols, amines, amides, and aromatic compounds (Figure 5.1).[4-6]

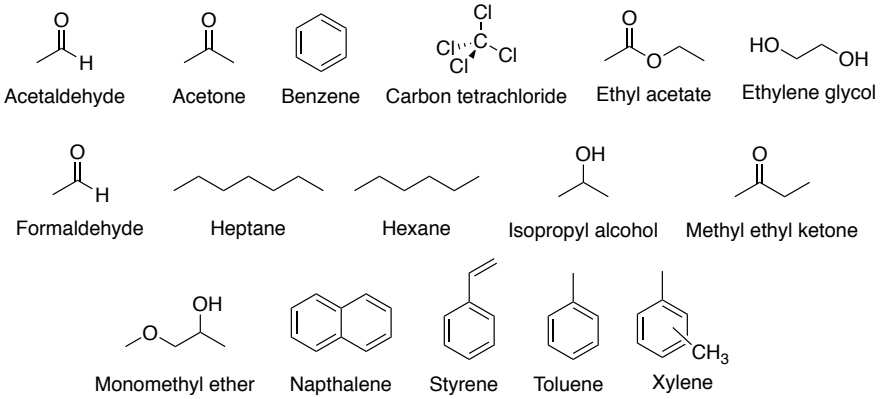


**Figure 5.1.** A selection of common volatile organic compounds.

While biogenic VOC emissions dominate world-wide, it is anthropogenic sources that result in the vast majority of volatile emissions and air pollution in urban areas.[4,5] VOCs from degreasers, lubricants, solvent thinners, fuels, and other heavily used

petrochemical and chemical industrial products constitute the majority of detected emissions.[7,8,10,11] For example, in population dense cities such as Boston and Los Angeles, non-methane VOCs are detected in the following ratios: alkanes, 40 – 45%; aromatic hydrocarbons, 20%; and oxygenates, 10 – 15%. The remaining 20 – 30% consists of alkenes and other unidentified VOCs.[3]

Among the different anthropogenic pollutants emitted into the troposphere, VOCs are particularly important because they represent the major contributors to two of the most serious air quality problems: photochemical smog and ground-level ozone.[2] Photochemical smog is composed of light-scattering liquid and solid particulates that result in the characteristic brown tinge associated with smog. Furthermore, chemicals such as ozone, NOx, and peroxyacetyl nitrate (PAN) are known to halt plant growth by delaying photosynthesis as well as play a negative role in climate change.[2,7,12]

In addition, several VOCs pose a threat to the health and well-being of humanity. For example, some VOCs detected in urban air such as 1,3-butadiene, benzene, acetaldehyde, and formaldehyde are known carcinogens.[7-9,12] Short term exposure to high concentrations of VOCs can cause many to experience eye-irritation, dizziness, and asthma attacks. Long-term exposure and the consequent accumulation of toxic VOCs can lead to liver and kidney damage and failure as well as cancer.[7] Furthermore, many volatile carbonyl compounds are notorious for their low, often unpleasant, odor thresholds (*i.e.* sometimes below 1 parts per billion).[8] It is evident that these daily VOC emissions are of great importance due to their potential toxicity and malodorous characteristics.

*5.1.2. Traditional Remediation Techniques*

The mounting concern surrounding environmental pollution has propelled the implementation of legislation and regulations pertaining to the control of organic aerosol pollutants worldwide. As a result, numerous chemical technologies have been developed and used to treat organic and toxic pollutants, including biological oxidation, chemical oxidation/incineration, and adsorption.[7-9]

Numerable reports of successful biological oxidation and degradation of VOCs using biofilters, bioscrubbers, biotrickling filters, and other bioreactors can be found in the literature. The main mechanism of remediation for these systems involves the conversion of pollutants to less-harmful compounds such as carbon dioxide and water upon treatment with microorganisms.[13] For example, biofiltration involves the flow of VOC-polluted air through a filter bed followed by diffusion into a biofilm where microorganism-assisted biological oxidation can occur.[14] Singh *et al*. disclosed the successful remediation of toluene-contaminated air upon treatment with a *Pseudomonas putida* (MTCC 102) inoculated polyurethane foam biofilter resulting in removal efficiencies of 68.2 to 99.9%.[15] Biofiltration can also be applied to hydrophilic and hydrophobic VOC mixtures. Specifically, Mohseni and Allen applied biofilters packed with wood chips and compost to treat methanol and α-pinene contaminated air. Notably, no microorganism inoculation was necessary. Rather, in this instance the microorganisms indigenous to the compost and wood chips were sufficient, resulting in 90 – 95% removal of the VOCs.[16]

Thermal oxidation/incineration is one of the more recognizable and commonly used methods for industrial gas waste treatment because it represents a universal method for the

disposal of gaseous organic effluent resulting in the breakdown of VOCs into less harmful by-products. Briefly, thermal oxidation involves an apparatus consisting of a single combustion chamber unit containing ceramic refractory blanket-lined oxidizers, which is connected to a propane or natural gas burner and a stack. Incineration is an attractive method because combustion of industrial gas effluent containing only carbon, hydrogen, and nitrogen-based VOCs will result in $CO_2$ and $H_2O$ as the main by-products. Conversely, if chlorinated and/or sulfur-containing compounds are in the mixture, the combustion products will consist of $CO_2$ and $H_2O$ as well as HCl and $SO_2$, respectively. These additional acidic by-products thus require removal by an added acid scrubber unit, resulting in increased costs.[17] In some cases, the addition of a catalyst to the thermal oxidant is required. Adsorption and subsequent reaction of VOCs onto the catalyst surface accelerates the oxidation as well as allows for lower operation temperatures between 320 and 540 ˚C compared to the 760 – 870 ˚C range required for traditional thermal oxidation. Commonly used catalysts contain chromium/nickel oxides and palladium and platinum metal.[18]

Lastly, adsorption, in the context of VOC remediation, refers to the ability of a solid sorbent to adsorb certain compounds selectively under mild conditions as well as to facilitate the recovery of the adsorbed organic compounds. Therefore, this approach has been widely applied in clean energy and environmental research. For instance, functional sorbents have been effectively used in the desulfurization and denitrogenation of ultra-clean transportation fuels, water purification, and air quality control.[19-26] For example, zeolites have been employed as sorbents for a variety of air remediation applications due

to their favorable pore size, surface area, and negatively charged framework. This charged framework makes zeolites an excellent platform for the addition of transition metal ions that are known to aid in the adsorption of sulfur from fossil fuels.[19] Yang *et al.* reported the use of $Cu^+$ and $Ag^+$ loaded zeolite Y for the adsorptive desulfurization of commercial diesel. Upon treatment with this material, the detectable sulfur content declined from 430 $ppm_w$ to below 1 $ppm_w$. Furthermore, the metal-anion doped zeolite was successfully regenerated by washing in dimethylformamide or carbon tetrachloride solvent to retain 100% of its remediation capacity upon reuse.[21] Mesoporous silica has also been widely implemented as an efficient desulfurization material for jet fuel.[22] Silica frameworks possess inherently high surface areas as well as pore sizes ranging from 2 – 4 nm and 4.5 – 30 nm in diameter for MCM-41 and SBA-15 mesoporous silica materials, respectively. These frameworks can be loaded with various metal ions or metal oxides, such as, $Ag^+$, $Pd^{2+}$, and cuprous oxide. Two such materials, specifically a $Pd^{2+}$ loaded SBA-15 and a $Ag^+$ loaded MCM-41 were reported by Wang and co-workers for the successful desulfurization of JP-5 jet fuel, demonstrating a sulfur saturation capacity of 16.0 mg S $g^{-1}$ and 32.1 mg S $g^{-1}$, respectively. Each material could also be regenerated by washing with solvent to maintain 50% of their adsorption capacity upon reuse.[24-26]

Metal-organic frameworks (MOFs) have also proven to be advantageous for the capture of VOCs and other airborne pollutants. MOFs are inherently amenable to chemical structure modifications that typically result in increased adsorption capacities. Numerable MOF structures have been investigated, under standard temperature pressure (STP) conditions, for their ability to adsorb, store, and remove $CO_2$.[27] Specifically, MOF

materials such as Cu-BTTri, CPO-27, HKUST-1, MIL-53, MOF-5, MIL-100, and YO-MOF, have all been evaluated based on their performance as it pertains to number of open metal sites, adaptable chemical structure, and ease of functionalization.[27-31] A magnesium doped MOF (Mg-MOF-74) was evaluated by Britt *et al*. for the capture of $CO_2$.[32] This material displayed an adsorption capacity of 8.9 wt% as well as $CO_2$ release at 80 ˚C. MOF adsorption capacities can be enhanced following a simple ethylene diamine modification. Following diamine-functionalization of a Mg(DOBDC) MOF, an improved $CO_2$ adsorption performance was noticed, namely 400 ppm $CO_2$ adsorption at 1 bar pressure. This same modification resulted in an en-$Mg_2$(dobpdc) MOF that displayed excellent sorption capacities of 16.7 wt % of CO2 in respect to the mass of the material. It was noted that the adsorption of $CO_2$ onto the free amines of the MOF produced carbamic acid, ultimately increasing the $CO_2$ adsorption capacity. Overall, while MOFs represent a promising material for air quality management they are not without their drawbacks. MOF-based formulations often exhibit poor selectivity, rather low capacities, high fabrication costs and difficulties with effective regeneration.[28,29]

Nanomaterials have also emerged as excellent sorbents for the mitigation of gaseous emissions due to their large surface-to-volume ratios, high chemical reactivity, and unique functionalities.[33-37] Carbon nanotubes (CNTs) have been applied as sorbents for the remediation of toxic gas pollutants from ambient air. CNTs are simply graphene sheets of hexagonally-oriented carbon atoms surrounding a tube axis and can be categorized as single wall carbon nanotubes (SWCNTs) or multiwall carbon nanotubes (MWCNTs).[38] There are numerous reports of CNTs successfully capturing environmental pollutants such

as dioxin. The two arene rings on dioxin display a strong attraction to the surface of CNTs as well as the porous wall, resulting in an increased and bifunctional adsorption. Long and Yang also disclosed the use of CNTs for the mitigation of NOx emissions from fossil fuel combustion. The uptake efficiency of NOx was reported as 78 mg $g^{-1}$ CNTs at room temperature.[39] A manganese oxide material with gold NPs grown into the pores has also proved highly efficient for the removal of VOCs and oxides of nitrogen and sulfur from air at room temperature. This catalytic material was able to remove and degrade common indoor air pollutants such as acetaldehyde, toluene, and hexane. They report a free radical promoted VOC degradation mechanism. Specifically, the presence of the gold NPs lowers the barrier of radical formation, in turn allowing VOC degradation to occur on the surface of the material.[40]

Previously, our group has demonstrated successful VOC remediation using biodegradable functionalized nanoparticles (NPs).[41,42] This initial interest in nanomaterials was motivated by the ease of functionalization via coating techniques or chemical modification in order to improve surface and prevent aggregation. The first generation NPs studied in our group were comprised of poly(D, L-lactic acid)-poly(ethylene glycol)-poly(ethyleneimine) (*i.e.* PDLLA-PEG-PEI) block copolymers that facilitated capture of aldehyde and carboxylic acid VOCs from gaseous mixtures. These NP materials showed reduction of aldehyde and carboxylic acid vapors greater than 80% and 76%, respectively, with reductions of up to 98% in some cases. Additionally, the NPs were effective in selectively capturing target aldehyde and carboxylic acid contaminants even when challenged by comparable or more volatile non-targeted vapors. While NPs are an effective

platform, these first generation materials proved to be relatively expensive, somewhat unstable, and potentially difficult to scale-up. Consequently, we pivoted our focus to poly(amine) functionalization of cheaper and easier to manipulate natural materials such as micro- and nano-crystalline cellulose and clay materials.[43]

*5.1.3. Natural Clay Materials as a Viable Alternative*

Just as nanoparticles are known for their high surface areas, clays and modified clays have been used as materials for numerous industrial applications due to their abundant availability, inexpensive cost, and large degree of surface area available for sorption. Furthermore, the sorption of polar and non-polar gases using phyllosilicate clay minerals has been explored by numerous groups.[44-53] Previous studies have employed clay minerals for the removal of $H_2S$ from systems that mimic environmental conditions.[46,47] For example, activated carbon-sepiolite pellets were used for the adsorption of ammonia and $H_2S$. Bentonite clay can also be treated with either aqueous iron chloride or copper chloride solutions to prepare modified bentonite materials as adsorbents for $H_2S$ gas.[47] This study showed that the iron and copper ions improved the natural adsorption capabilities of the bentonite clay by increasing its surface area. Lastly, clay minerals were assessed for the adsorption of chlorobenzene and trichloroethylene, wherein the successful hexadecyltrimethylammonium modification of montmorillonite clay led to increased adsorption.

Considering the underscored issues displayed by the nanoparticle materials as well as the established literature, inexpensive and naturally abundant kaolinite (Kao) clay was identified as a desirable alternative. More specifically, one can take advantage of the

mesoporous channels that aid in the electrostatic capture of contaminants along with their potential for surface-functionalization with amine groups suitable for chemical capture.[48] Polymeric modifications to Kao clay have proved effective for $CO_2$ capture. Simple acid and base Kao pore modifications followed by PEI (polyethylenimine) immobilization onto the clay resulted in new materials exhibiting $CO_2$ sorption capacities approaching 112 mg $CO_2$ $g^{-1}$ sorbent at 75 ˚C under dry conditions.[53]

Based on the promising results of our previous reports on PDDLA-PEG-PEI NPs as efficient sorbents for the selective capture of aldehyde and carboxylic acid vapors, we knew that the free amines of PEI were necessary to promote covalent or ionic capture of the respective VOCs. Applying this information, we set out to combine the efficient and selective reactivity of PEI with the attractive adsorption properties and thermal stability intrinsic to clay minerals. The presented work details the successful modification of a natural clay platform (*i.e.* kaolinite) that yielded a considerably less expensive yet highly effective material for VOC capture.

### *5.2. Results and Discussion*

#### *5.2.1. Preparation and Characterization of Kao-PEI*

In order to investigate the comparatively inexpensive clays as a platform for polyamine functionalization, we first sought to successfully prepare and characterize polyethylenimine (PEI) functionalized kaolinite clay (*i.e.* Kao-PEI). The kaolinite clay was easily functionalized with PEI following a well-established wet impregnation technique, wherein the PEI is immobilized onto the porous clay substrate.[53] Briefly, the clay substrate was suspended in a solution of PEI and methanol and allowed to stir for 3 h. The wet

poly(amine)-functionalized clay was then dried *in vacuo* at 75 ˚C for 12 h. For evidence of successful modification, FT-IR spectroscopy, thermogravimetric analysis (TGA) and energy-dispersive X-ray spectroscopy (EDX) analyses were performed.

FTIR spectroscopy was used to qualitatively confirm PEI-functionalization of the kaolinite clay. Figure 5.2 depicts the overlay FT-IR spectra of unmodified Kao, Kao-PEI, and PEI. At approximately 3650 $cm^{-1}$, the three intense bands are attributed to the kaolinite hydroxyl stretching vibrations and are present in both the kaolinite and Kao-PEI spectra. Strong overlapping bands around 1000 $cm^{-1}$ include vibrations arising from the silicon-oxygen bonds and the bending vibration of the hydroxyl groups present in kaolinite. The appearance of new bands in the Kao-PEI spectra corresponding to the immobilized PEI are diagnostic of successful modification. Specifically, the bending vibrations of $NH_2$ resulting in bands at 1600 $cm^{-1}$ and at 1470 $cm^{-1}$ are evident. The broad N-H stretching bands at 3280 $cm^{-1}$ and bending bands at 1650 $cm^{-1}$, the stretching vibrations for $CH_2$ at 2871 $cm^{-1}$ and

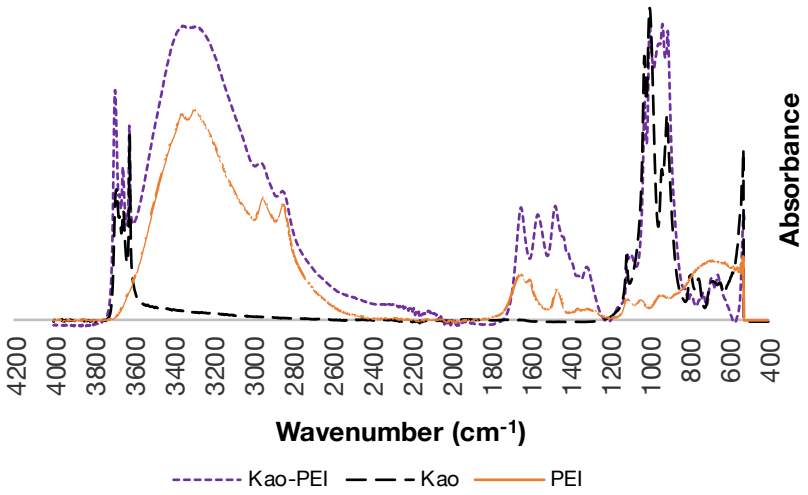


**Figure 5.2.** FTIR spectrum of PEI-functionalized kaolinite clay (Kao-PEI, dotted purple line, unmodified Kao (dashed black line), and PEI (solid orange line).

2943 $cm^{-1}$ and the bending mode of the carbon-nitrogen bond at 1330 $cm^{-1}$ are all qualitative matches for PEI's experimental vibrational bands.

TGA profiles for the Kao-PEI also support the effective modification of the substrate (Figure 5.3). Unmodified Kao shows little thermal degradation (*i.e.* < 20%) up to 1000 ˚C. Kao-PEI presents an altered temperature degradation profile. The thermal degradation of Kao-PEI is observed at approximately 300 ˚C showing a 25% mass loss until the poly(amine) is fully desorbed from the clay surface by around 400 ˚C, which ultimately results in a total mass loss of 63% over the temperature gradient. Kao-PEI clay materials were also characterized by energy-dispersive X-ray spectroscopy (EDX), and transmission electron microscopy TEM analyses. EDX analysis of Kao-PEI revealed the presence of nitrogen as compared to unmodified kaolinite.

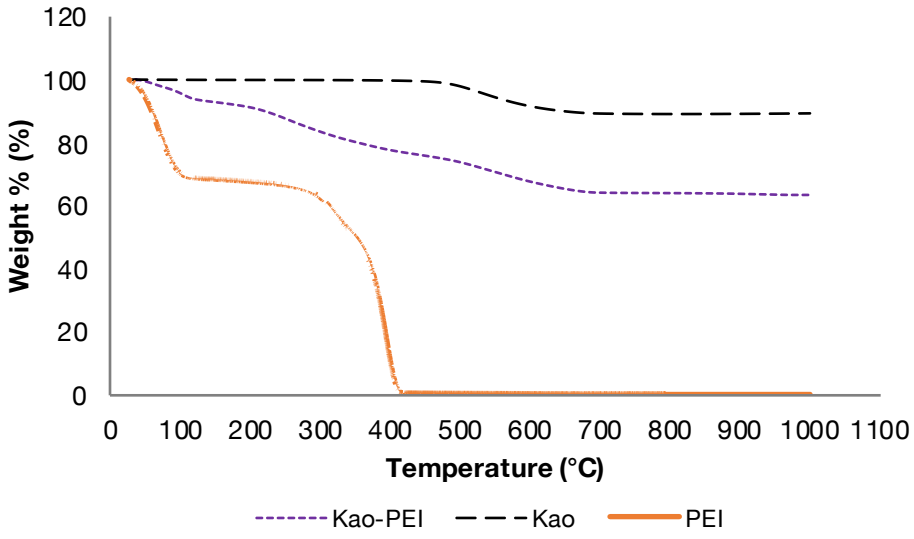


**Figure 5.3.** TGA analysis of PEI-functionalized kaolinite clay (Kao-PEI, dotted purple line, unmodified Kao (dashed black line), and PEI (solid orange line).

*5.2.2. VOC Capture Assay with Kaolinite and Kao-PEI*

Next, initial investigations into the application of Kao-PEI for the remediation VOCs were conducted. A representative compound from three functional group classes (*i.e.* aldehydes, carboxylic acids, and organodisulfides) were employed: butyraldehyde/hexanal, butyric acid, and dimethyl disulfide, respectively (Figure 5.4). Treatment of each VOC with Kao-PEI was completed in sextuplicate, and vapor reduction percentages were calculated by means of a previously established GC headspace analysis protocol (See section 5.7.2 for details).[41-43] Briefly, untreated sample vials were prepared by creating a small sample well using a glass stir rod and a small swatch of tissue paper. The vial was then capped and a 1 μL injection of the volatile liquid substrate was introduced into the vial by passing the needle through the tissue paper barrier. After a 30-minute vaporization equilibrium time, the vial was subjected to GC analysis to collect baseline vapor levels. A similar assay was also conducted in the presence of unmodified Kao and Kao-PEI. Thus, 10 mg of kaolinite or Kao-PEI was added into the tissue paper sample well and then secured with a vial cap. Once again, a 1 μL injection of the designated volatile substrate was introduced into the vial by passing the needle through the tissue paper barrier and allowed to vaporize and subsequently react with the kaolinite or Kao-PEI sorbent for 30 min. Upon completion of

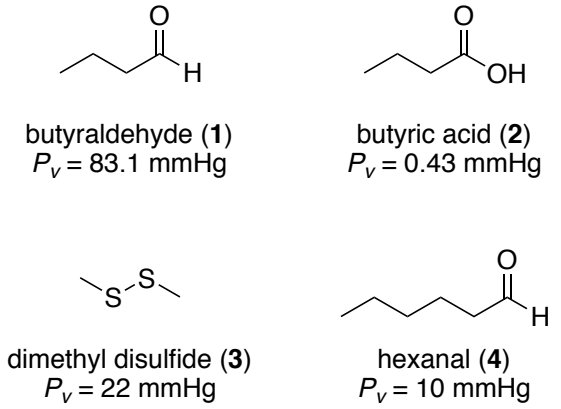


**Figure 5.4.** Representative VOCs of interest and their respective vapor pressures (20 °C) used in GC vapor capture assays.

the 30 min treatment period, the vial was subjected to GC analysis. Unmodified kaolinite was employed as control.

Figure 5.5 highlights the percent reduction for each VOC after a 30 minute exposure to either kaolinite or Kao-PEI. Butyraldehyde vapors were partially remediated in the presence of kaolinite with 33% ($P < 0.0005$) vapor reduction observed (Figure 5.5A). When treated with the Kao-PEI, butyraldehyde was completely reduced with 100% ($P < 0.0005$) vapor capture (Figure 5.5A). We surmise that the highly effective capture of aldehydes with PEI-Kao is driven by the rapid condensation of the aldehyde analyte with the poly(amine) to form imines, an observation that we confirmed spectroscopically with our 1st generation polymeric nanoparticles (Scheme 5.1A).[41-43]

Unmodified kaolinite in the presence of butyric acid vapors was somewhat effective at sequestering the carboxylic acid (18% capture ($P < 0.0005$), Figure 5.5B). We attribute this minor VOC reduction to vapor diffusion into the clay pores. Favorably, the Kao-PEI was successful in reducing 90% ($P < 0.0005$) of the butyric acid vapors (Figure 5.5B), presumably through the formation of ammonium carboxylates via acid-base reaction between the carboxylic acid vapor and the poly(amine) resident on the modified clay (Scheme 5.1B).[41-43]

Lastly, we probed the potential capture of dimethyl disulfide (DMDS). Sulfur compounds are exceptionally pungent to the human olfactory senses and thus are often targeted for remediation. DMDS vapor was treated with kaolinite and Kao-PEI, with both

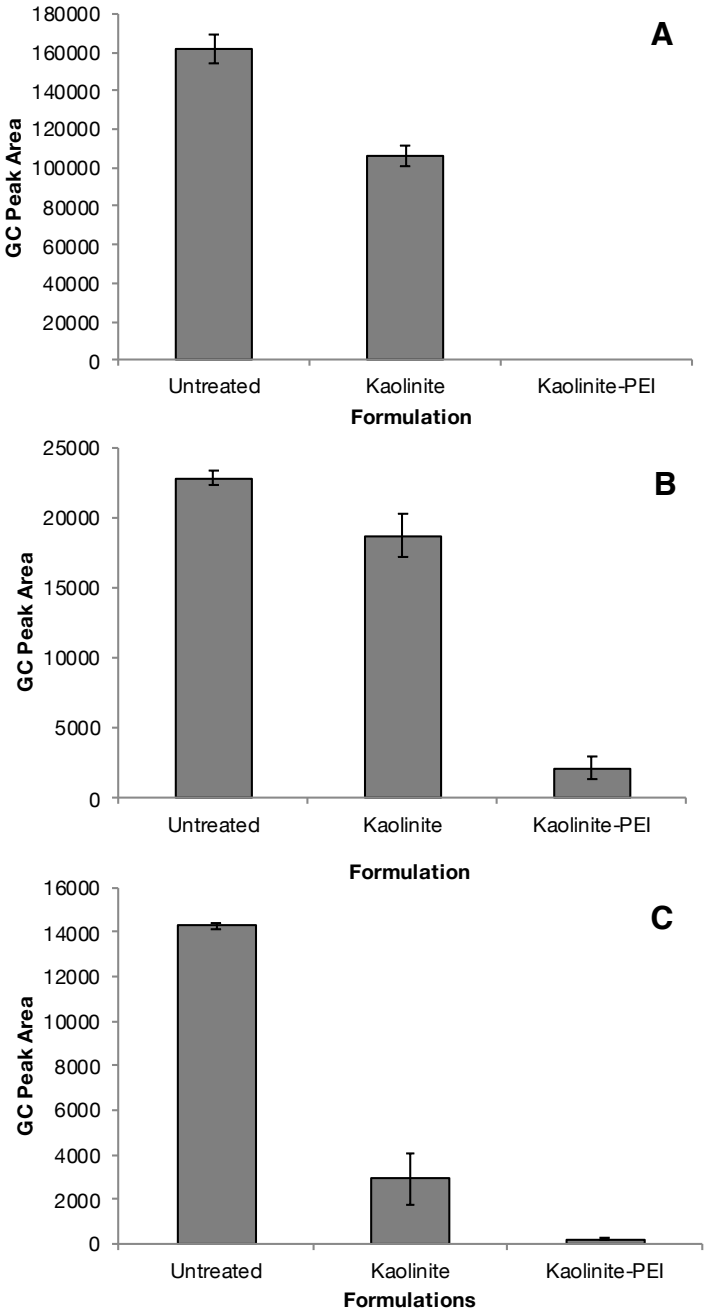


**Figure 5.5.** Vapor capture assays with Kao-PEI and Kao. **A**. butyraldehyde, **B**. butyric acid, **C**. dimethyl disulfide.

materials performing as promising adsorbents. Treatment of DMDS with kaolinite resulted in 79% ($P < 0.0005$) reduction of DMDS vapors while Kao-PEI was 99% ($P < 0.0005$) effective (Figure 5.5C). Since we have no evidence for the covalent capture of disulfides with amine nucleophiles, it was concluded that possible electrostatic or ionic capture is feasible due to the large surface area and pores available within the clay materials for capture.[43] While the unmodified kaolinite clay was poorly/moderately effective at remediating VOCs, the amine functionalized kaolinite was especially successful at capturing organics in the vapor phase. These data clearly indicate that Kao-PEI can serve as an effective sorbent for the mitigation of a selection of representative VOCs.

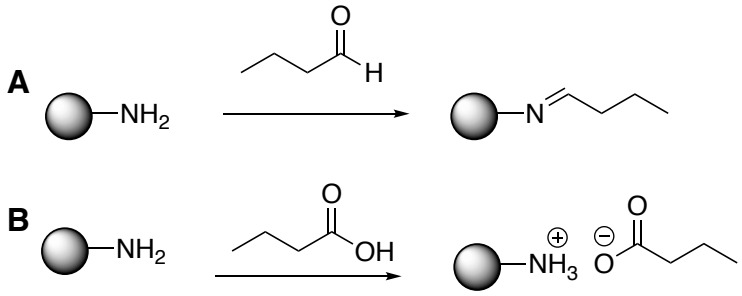


**Scheme 5.1.** Proposed Kao-PEI capture mechanism of **A**. butyraldehyde and **B**. butyric acid.

*5.2.3. Kao-PEI Hexanal Capture Time Study*

Upon successful remediation of butyraldehyde, butyric acid, and dimethyl disulfide VOCs, we sought to glean further information pertaining to the sorption kinetics as well as the ability of Kao-PEI to retain the captured VOCs following the initial 30 min analysis period. Thus, the vapor capture efficiency of Kao-PEI was followed over a period of 6 h. Hexanal was chosen as a representative aldehyde for GC vapor capture analysis at 10 min, 20 min, 30 min, 1 h, 2 h, 3 h, 4 h, and 6 h time points. At 10 min a 49% reduction is seen,

followed by a 65% reduction at 20 min, with complete hexanal vapor capture noted at 30 min (Figure 5.6).

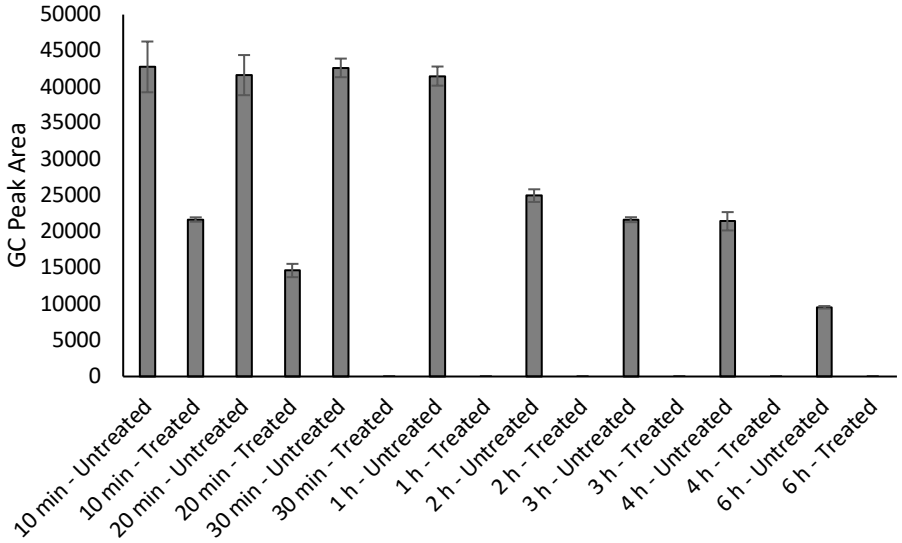


**Figure 5.6.** Hexanal vapor capture assays untreated and treated with Kao-PEI overtime.

Furthermore, there is no evidence of hexanal vapor release from the modified clay at 1 h, as no hexanal vapor is detected via GC analysis. The Kao-PEI is able to retain the captured VOCs for at least 6 h with no hexanal vapor being detected at the remaining time points. However, we do note a decrease in hexanal vapor in the untreated controls, with a significant loss of detectable VOC starting at 2 h. This is likely due to vapor leakage through the lid of the GC chamber.

### *5.3. On-Site Rendering Plant Pilot Study*

VOC emissions stem from a myriad of sources with global industries representing one of the leading producers of high VOC loads. Rendering is one such industry that involves the processing and recycling of major by-products, such as, skins, hides, feet, hooves, bones, toenails, whole carcasses and other muscle and fat tissues resulting from

meat-packing and butchering operations. This widespread industry serves a vital role in processing tremendous amounts of by-product material that must be sterilized and preferably repurposed into new products such as meat and bone meal, poultry meal, and rendered animal fats. This becomes more significant when considering that humans consume only one-third to one-half of animals produced for meat, milk, eggs, and fiber. This results in an annual processing load of over 22.7 million metric tons of animal by-products in the United States annually. Ultimately, rendering operations play a vital role in the sustainability of animal agriculture and food industries by handling massive quantities of material in a safe, environmentally responsible, and efficient manner facilitating the recovery of value-added resources.[54,55] However, it is not without undesirable side-effects. As a global industry, rendering operations handles and processes substantial quantities of raw material. The process of cooking, processing, and recycling this material emits a significant amount of VOCs, many of which are malodorous compounds. Rendering operations represent a reasonable case-study to assess the performance of PEI-Kao materials for the remediation of industrial VOC emissions and nuisance odors.

When considering viable control and remediation technologies for VOCs one must first consider the necessity for a comprehensive emission inventory or VOC load assessment. This inventory can provide the basis for planning and identifying applicable regulations, the selection of practical control options, and the industry's overall contribution to global VOC emissions. A limited number of VOC load emission studies for rendering operations have been reported. The groups of Van Langenhove *et al*. Defour *et al*., and Bhatti *et al*. have conducted assessments of rendering operations VOC emissions

only pertaining to odor nuisance compounds.[56-59] Furthermore, only one other study, reported in 2014 by Bhatti *et al*. took on the task of completing a complete VOC load emission inventory of an enclosed rendering plant.[59] Therefore, we previously pursued an all-encompassing assessment of VOC emissions at two open-air rendering plants located in the Central Valley of California, USA.[60] Via this study, a detailed analysis of the emission inventory resulting from said rendering plants was compiled resulting in 43 detectable compounds whose presence and concentration seasonally vary. Volatile organic compounds including ammonia, fatty acids such as acetic acid, aldehyde/ketones such as acetone, and ethanol constitute the bulk of these emissions. They also significantly contribute to the malodorous atmosphere surrounding rendering operations. These data along with previous results from aforementioned groups emphasize the need for appropriate techniques and technologies for VOC abatement and control.

In order to probe the usefulness of the Kao-PEI for rendering operation VOC emission capture, we sought to conduct on-site sampling experiments. Sample cartridge tubes packed with Kao-PEI clay were prepared in the hopes of screening their ability to reduce the VOC load at an open-air rendering facility in California. While at the rendering facility, ambient air was passed through the Kao-PEI packed tubes and into a sampling cartridge that assayed for volatile fatty acids (VFAs). We were interested in volatile fatty acids because they are major constituents of nuisance rendering odors. Untreated air samples, that is air that was not passed through a Kao-PEI clay packed tube, was also sampled in order to assess the percent reduction of the detectable VFAs after exposure to the Kao-PEI clay (see Figure 5.7 for sampling set-up). Air samples were collected as

follows: plant air was pumped through a commercially available sodium hydroxide-coated silica gel cartridge (700 mL $min^{-1}$ flow rate) for an allotted time of 100 min. All field air samples, untreated and treated, were collected in triplicate and analyzed via GC/MS following standardized methods by a contracted environmental analysis laboratory in California, USA.

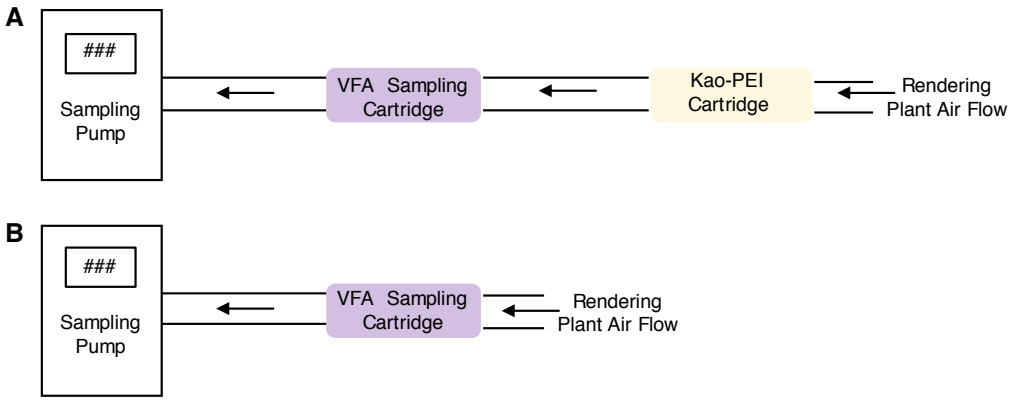


**Figure 5.7.** Rendering plant air VFA sampling experimental set-up for A) Kao-PEI treated air and B) untreated air.

The results of this analysis show that the Kao-PEI material significantly reduces the VOC load of all detectable volatile fatty acids in comparison to the untreated plant air samples. Heptanoic acid, octanoic acid, and nonanoic acid were all reduced by at least 60% (Table 5.1, Entries 10-12). Most notably, the three constituents that make up the bulk of this VOC load, acetic acid, propanoic acid, and butanoic acid, were all reduced by greater than 97% (Table 5.1, Entries 1, 2, and 4). The remaining constituents such as 2-methylpropanoic acid, 2-methylbutanoic acid, pentanoic acid *etc.* all experienced a reduction of at least 90% (Table 5.1). Ultimately, this study represents an important step in

demonstrating the applicability of PEI-modified kaolinite clay and other functionalized naturally-occurring clays in VOC mitigation in an industrial setting.

**Table 5.1**. Pilot-scale study for the Kao-PEI capture of detectable volatile fatty acids from a rendering facility.

| Entry | Volatile Fatty Acids | Unreated (ppb) | Treated (ppb) | % Reduction |
|---|---|---|---|---|
| 1 | acetic acid | 233.3 ± 5.8 | < 8 | > 97% |
| 2 | propanoic acid | 163.3 ± 5.8 | 1.9 ± 1.1 | 99% |
| 3 | 2-methylpropanoic acid | 17.0 ± 1.0 | 0.9 ± 0.4 | 95% |
| 4 | butanoic acid | 180.0 ± 10.0 | 2.0 ± 1.7 | 99% |
| 5 | 2-methylbutanoic acid | 11.7 ± 0.6 | < 0.6 | > 95% |
| 6 | 3-methylbutanoic acid | 11.3 ± 0.6 | < 0.6 | > 95% |
| 7 | pentanoic acid | 19.7 ± 1.2 | < 0.6 | > 97% |
| 8 | 4-methylpentanoic acid | 6.9 ± 0.5 | < 0.5 | > 93% |
| 9 | hexanoic acid | 10.0 ± 0.9 | < 0.5 | > 95% |
| 10 | heptanoic acid | 1.6 ± 0.2 | < 0.5 | > 69% |
| 11 | octanoic acid | 1.7 ± 0.2 | < 0.5 | > 71% |
| 12 | nonanoic acid | 1.0 ± 0.1 | < 0.4 | > 60% |

### *5.4. Conclusions*

This work highlights the ability of PEI-functionalized kaolinite to serve as an abatement material for several small molecule VOCs. The remediation of these small molecules was first explored in a laboratory setting via a gas chromatography (GC) headspace technique that assesses the removal of target VOCs from the gas phase. Specifically, this functionalized clay has shown a significant effect in capturing aldehydes, carboxylic acids, and alkyl disulfides with most of these assays showing 100% reduction of these vapors. Furthermore, upon successful scale-up of the Kao-PEI, this material was

prepped into cartridges used for on-site small-scale VOC abatement study at an open-air rendering plant in order to probe their ability to reduce volatile fatty acid emissions directly produced by rendering operations, demonstrating removal efficiencies between 60 and 99%.[61]

### *5.5. Future Directions*

Ultimately, the ability to recycle or reuse the Kao-PEI clay would greatly improve its function and utility in an industrial setting. We have attempted to drive-off captured VOCs by heating previously used Kao-PEI clay at 65, 75, 85, and 100 ˚C for 24 h. This proved ineffective upon retreatment of the Kao-PEI with hexanal; no additional capture of vapor was observed. VOC capture was observed, however, when previously used Kao-PEI clay was subsequently reused in the hexanal vapor capture GC assay. As expected, when hexanal vapor was treated with fresh Kao-PEI a 100% reduction was noted. Upon reuse of the Kao-PEI to treat a second aliquot of hexanal vapor 82% reduction was still seen (Figure 5.8). Further experiments are necessary in order to determine the regeneration potential of

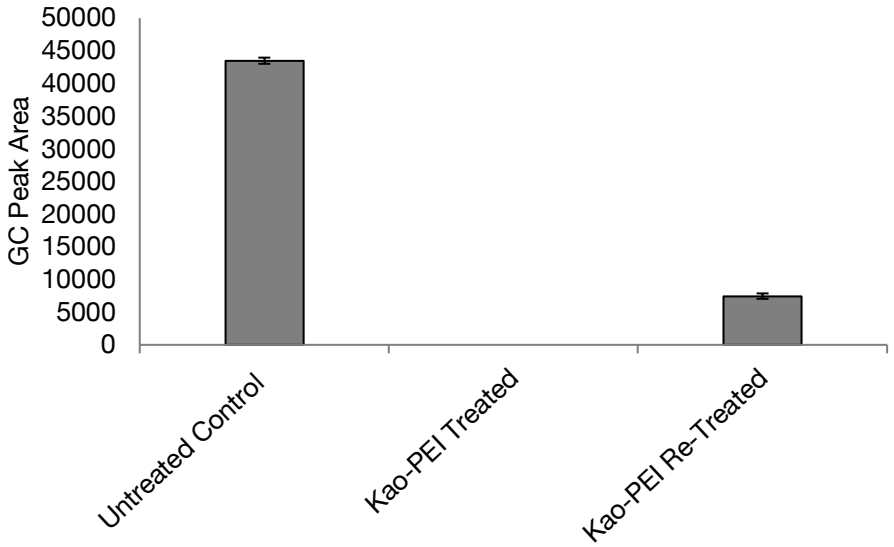


**Figure 5.8.** Hexanal re-use vapor capture assays with Kao-PEI.

this material. Thermal regeneration of the materials may still be possible at higher temperatures and longer treatment periods. Solvent regeneration, in this case, is not viable due to the non-covalent PEI-modification of the Kao clay. Attempts to wash the clay with EtOH or $H_2O$ result in loss of PEI functionalization and VOC capture efficiency as confirmed by TGA analyses of washed samples..

In order to apply our poly(amine)-functionalized clay material to other environmental remediation applications a covalent modification must be realized. Covalent grafting represents one potential functionalization route for Kao and other similar aluminum silicate clay minerals. Rubino and co-workers utilized this method to prepare an ampicillin (AMP) grafted montmorillonite (MMT) clay.[62] Upon successful functionalization, the MMT-AMP clay was embedded into a UV curable acrylate coating and applied onto a polypropylene film for the preparation of antimicrobial materials. Presumably, modifications to their reported method would yield a PEI covalently grafted

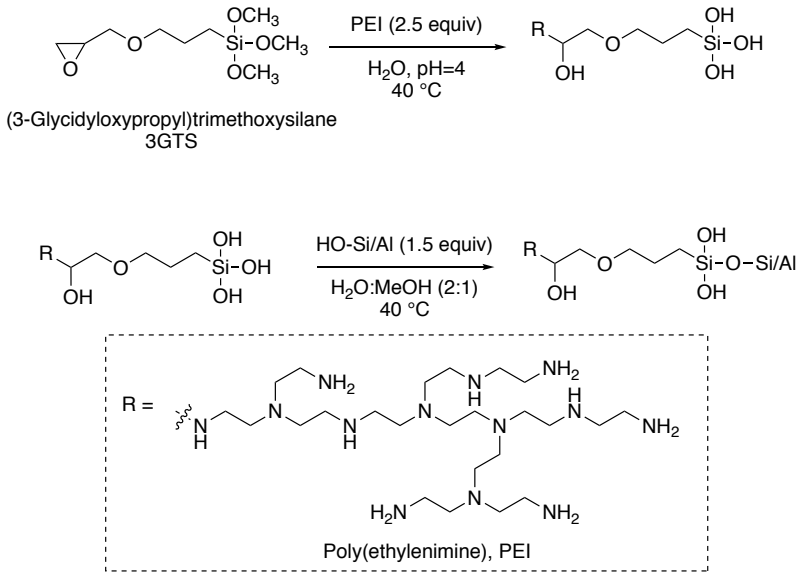


**Scheme 5.2.** Proposed two-step synthetic route for PEI covalent grafting of an aluminum silicate clay such as Kao.

clay that could be used in aqueous applications such as wastewater treatment as well as withstand solvent regeneration protocols.

In order to covalently graft PEI onto a clay mineral, a tether moiety such as 3-glycidyloxypropyl trimethoxysilane (3GTS) must be used, wherein PEI would be linked to the epoxy-terminated side chain under slightly acidic conditions. Subsequently, the silanol groups on the clay surface would be linked to the 3GTS-amine resulting in the desired functionalized clay (Scheme 5.2).

## *5.6. Acknowledgements*

Funding for this work was provided by the Fats & Proteins Research Foundation, Inc., the Poultry Protein and Fat Council, the Clemson University Animal Co-Products Research and Education Center, and the Clemson University Research. Additional thanks and appreciation to Dr. Fernanda D. Guerra, Dr. McKenzie L. Campbell and Dr. Mohamed F. Attia for their collaborative efforts on this work as well as Ms. Kim Ivey for technical assistance throughout the clay material characterization.

## *5.7. Experimental Methods*

### *5.7.1. Preparation and Characterization of Kaolinite-poly(amine) Clay*

A solution of polyethylenimine (3 g equiv. per 1 g Kao clay) and 40 mL of methanol (MeOH) were allowed to stir in a 100 mL round bottom flask at room temperature for 30 min. Kaolinite clay is then added and the suspension is stirred for an additional 3 h. Upon removal of the stir bar, the clay was allowed to settle to the bottom of the flask. The top layer of MeOH was then decanted and the wet clay was dried *in vacuo* in a vacuum oven

at 75 ˚C for 12 h. Larger scale batches (>1 gram clay) required a drying period of up to 48 h.

*5.7.2. Gas Chromatographic Vapor Capture Assay Methods*

GC analyses were carried out on a Shimadzu GC-2014 Gas Chromatograph, equipped with a Shimadzu AOC-20i Auto-Injector and a Flame Ionization Detector (FID), within the following parameters: inlet temperature: 250.0 ˚C; splitless injection at 30.9 mL $min^{-1}$; injector sampling depth: 10 mm; column flow: 1.33 mL $min^{-1}$, constant pressure; carrier gas: helium; FID temperature: 225 ˚C; temperature program: 40 ˚C for 5 min, 50 ˚C $min^{-1}$ ramp to 200 ˚C, hold for 5 min. The GC was equipped with a 30 m x 0.25 mm x 0.25 μm Zebron ZB-WAX Plus capillary GC column. Agilent Technologies Gas Chromatography 1.5 mL volume vials with septum screw-caps were used in the analysis assays.

Our previously disclosed method for vapor capture assay was used to determine the standard vapor areas for each substrate of interest followed by their percent reduction upon interaction with kaolinite and Kao-PEI. Briefly, the opening of a 1.5 mL GC vial was covered with a 5 x 5 cm piece of Kimwipe tissue paper. Using a glass stir rod, a small sample well was made with the Kimwipe by gently applying pressure with the tip of the glass stir rod. A vial cap was secured on the vial and a 1 μL injection of the volatile liquid substrate was introduced into the vial by passing the needle through the Kimwipe barrier. After a 30 min vaporization equilibrium time, the vial was subjected to GC analysis as described above to collect baseline vapor levels. A similar assay is also conducted in order to probe the effectiveness of the kaolinite and Kao-PEI material. Using the previously

described process for formation of a well within the GC vial, 10 mg of the kaolinite or Kao-PEI was added into the Kimwipe sample well and then secured with a vial cap. A 1 μL injection of the designated volatile substrate was introduced into the vial by passing the needle carefully through the Kimwipe barrier and allowed to vaporize and subsequently react with the kaolinite or Kao-PEI sorbent for 30 min. Upon completion of the 30 min reaction time, the vial was subjected to GC analysis.

*5.7.3. Kao-PEI Hexanal Capture Time Study*

Screw-top GC vials were prepared following the above described protocol for the GC vapor capture assay. Each vial was then charged with 10 mg of Kao-PEI sorbent material followed by a 1 μL injection of hexanal that was allowed to vaporize and subsequently react with the Kao-PEI sorbent. Upon completion of the prescribed reaction time, the vial was subjected to GC analysis.

Experiments were conducted in triplicate for analysis at 10 min, 20 min, 30 min, 1 h, 2 h, 3 h, 4 h, and 6 h. Hexanal analyte standards were also prepared in the same manner, *i.e.* pre-prepared vials were charged with only 1 μL of hexanal and no sorbent material. The standards were allowed to vaporize for the same amount of time as their respective treated counterparts *i.e.* 10 min, 20 min, 30 min, etc. prior to GC analysis.

*5.7.4. Kaolinite-poly(amine) Cartridge Preparation for In-Plant Sampling Experiment*

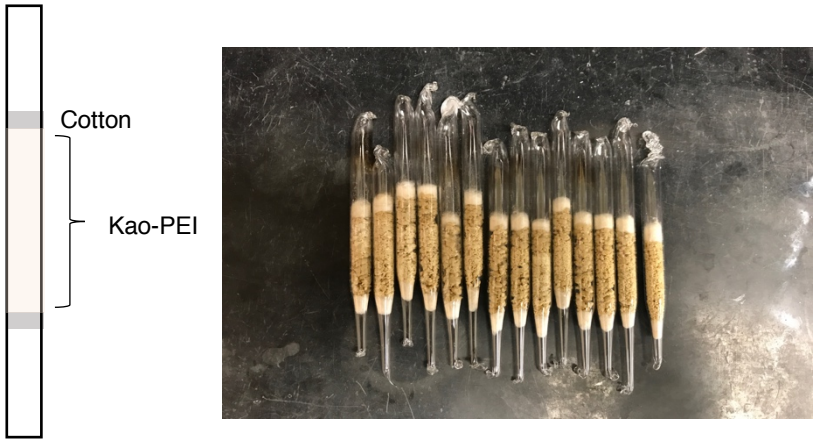


**Figure 5.9.** Kao-PEI packed cartridges for pilot-scale VOC capture test at a rendering facility**.**

Sample cartridges were prepared by packing 0.75 grams of Kao-PEI clay into a glass tube (7mm inner diameter) between two cotton plugs, consistently achieving a clay path length of *ca.* 3 cm. The cartridges were then sealed by heating the tips of the glass over a Bunsen burner until the glass became malleable enough to seal off each end of the cartridge with gentle twisting (Figure 5.9).

The Kao-PEI packed cartridges were assessed for volatile fatty acid (VFA) abatement in an open-air rendering facility in the Central Valley region of California, USA. The sampling equipment was positioned in plant near the raw material pile and the cookers. Untreated plant air was sampled in triplicate using an SKC universal air sampling pump that was plumbed to a commercially available KOH-impregnated silica gel VFA sampling cartridge by a short length of Tygon tubing. The VFA samples were collected at a 700 mL/min flow rate for 100 min. Plant air treated with Kao-PEI cartridges for VFA

abatement was sampled in triplicate using an SKC universal air sampling pump that was plumbed in sequence to a commercially available KOH-impregnated silica gel VFA sampling cartridge followed by a Kao-PEI packed cartridge using short lengths of Tygon tubing. Treated VFA samples were collect at a 700 mL/min flow rate for 100 min. After the 100 min sampling period, the VFA sampling cartridges were sealed with plastic caps and stored in zip-top bags at 0 ˚C during transport to a commercial atmospheric sampling laboratory, where they were processed using GC/MS analysis following the laboratory's standard operation procedures.

*5.7.5. Kao-PEI Reuse Experiments*

Screw-top GC vials were prepared following the GC vapor capture assay described above. Hexanal analyte standards were first prepared, in triplicate, in order to establish a baseline for untreated hexanal vapor, *i.e.* pre-prepared vials were charged with only 1 μL of hexanal and no sorbent material. The standards were allowed to vaporize for 30 min prior to GC analysis. Next, the treated vials were prepped in triplicate; each treated vial was charged with 10 mg of Kao-PEI followed by a 1 μL addition of hexanal. The hexanal was also allowed to vaporize and react with the Kao-PEI sorbent for 30 min. Following the 30 min time period, the vial was subjected to GC analysis. These same treated vials were immediately reused by injecting an additional 1 μL of hexanal into the chamber. The hexanal was once again allowed to vaporize for 30 min prior to GC analysis.

### *5.8. Supplementary Information*

*Kao and Kao-PEI SEM and EDX Imaging*

The surface morphologies of kaolinite and kaolinite-PEI samples were imaged by scanning electron microscopy (Hitachi SU-6600, SEM-EDX analysis) with an accelerating voltage of approximate 0.5 ~ 30kV with advanced variable pressure 10 ~300 Pa. For imaging, two different excitation voltages (7 and 10 kV) and a small sample detector distance (10.5 mm) were used. Under these experimental conditions, charging effects were minimal, and hence, it was not necessary to metalize the samples and no special grounding techniques were needed, so that true sample features were not masked.

The SEM images in Figure 5.S1 are of the pristine Kaolinite with different scale bars (A and B) and PEI-modified Kaolinite (C and D). These images indicate that there is no real change in crystallinity, homogeneity, and size distribution of the substrate upon PEI modification aside from some observable particle agglomeration after modification.

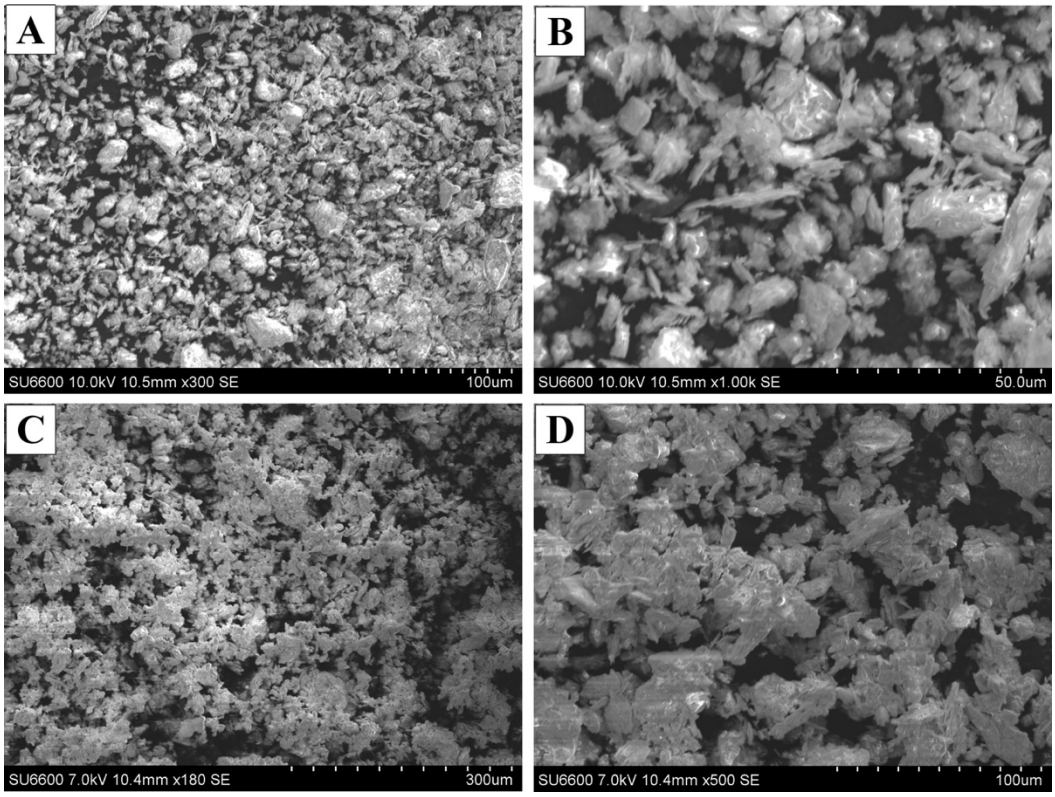


**Figure 5.S1.** SEM Images A. Kaolinite (100 μm) B. Kaolinite (50 μm) C. Kao-PEI (300 μm) D. Kao-PEI (100μm)

EDX analysis, depicted in Figure 5.S2, was also used to provide elemental identification and quantitative compositional information. It has been found that kaolinite constituted of 100 wt% of oxygen, silicon, and aluminum as expect, and no EDX signal for nitrogen was noted. In contrast, after its modification by PEI, Figure 5.S2 revealed a decrease in O, Si, Al metals to 98 wt% at expense of the nitrogen (2 wt%). Overall, EDX proves the absence of nitrogen in parent kaolinite and showed a 2 wt% nitrogen content on kaolinite surface.

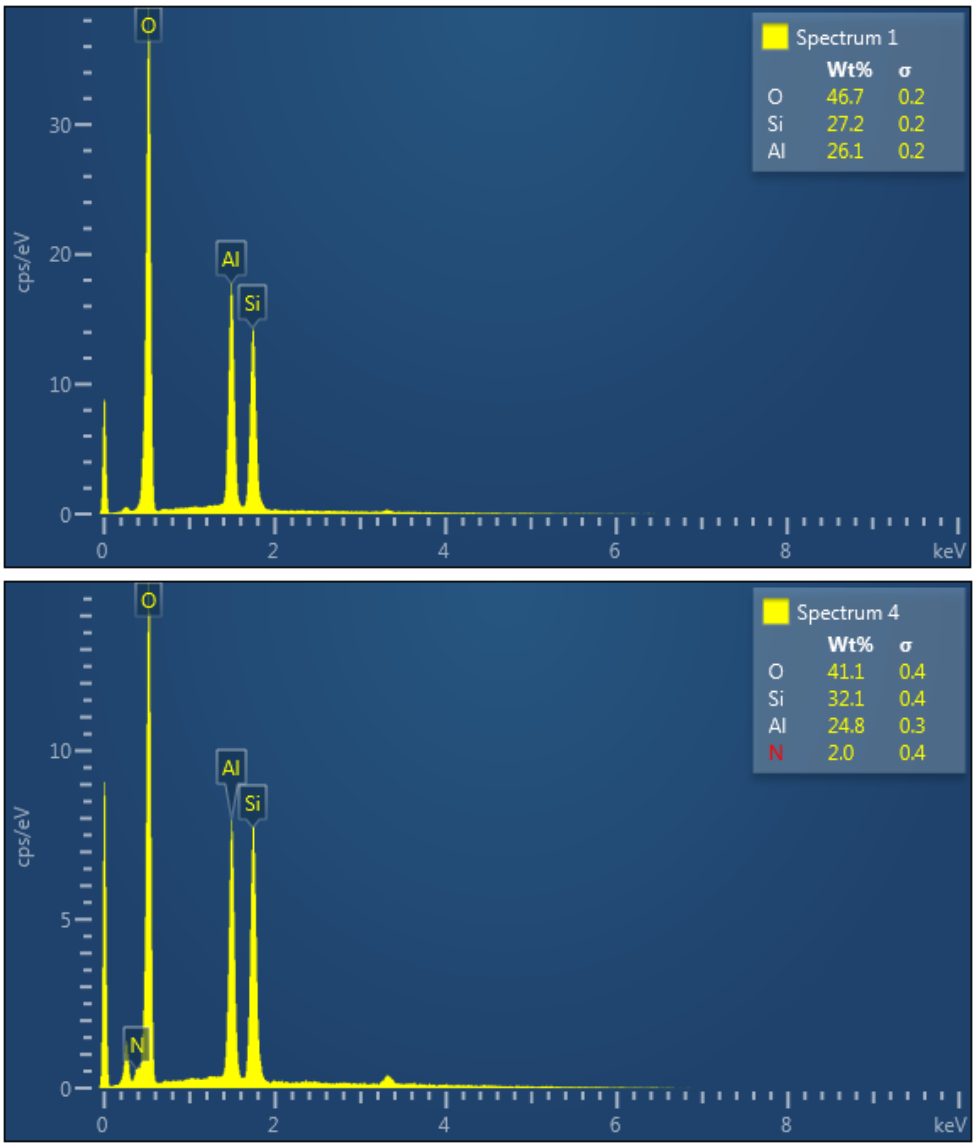


**Figure 5.S2.** EDX Images A. Kaolinite B. Kao-PEI

### *5.9. References*


1. Haagen-Smit, A. J.; Bradley, C. E.; Fox, M. M. Ozone Formation in Photochemical Oxidation of Organic Substances. *Ind. Eng. Chem.* **1953**, *45* (9), 2086-2089.

2. Hester, R.E.; Harrison, R. M.; Derwent, R. G. Sources, distributions, and fates of VOCs in the atmosphere. *Volatile Organic Compounds in the Atmosphere*. Hester, R. E., Harrison, R. M., Eds.; The Royal Society of Chemistry, 1995; 4, 1-16.

3. Goldstein, A. H.; Galbally, I. E. Known and Unexplored Organic Constituents in the Earth's Atmosphere. *Environ. Sci. Technol.* **2007**, *41* (5), 1514–1521.

4. Kesselmeier, J.; Staudt, M. Biogenic Volatile Organic Compounds (VOC): An Overview on Emission, Physiology and Ecology. *J. Atmos. Chem.* 1999, *33* (1), 23-88.

5. Atkinson, R.; Arey, J. Atmospheric Degradation of Volatile Organic Compounds. *Chem. Rev.* **2003**, *103* (12), 4605-4638.

6. Vaseashta, A.; Vaclavikova, M.; Vaseashta, S.; Gallios, G.; Roy, P.; Pummakarnchana, O. Nanostructures in environmental pollution detection, monitoring, and remediation. *Sci. Technol. Adv. Mater.* **2007**, *8*, 47-59.

7. Marnett, L. J. Health effects of aldehydes and alcohols in mobile source emissions. *Air Pollution, the Automobile, and Public Health*. Watson, A. Y., Bates, R. R., Kennedy, D. Eds.; National Academy Press: Washington, D. C., 1988.

8. Hoshika, Y. Gas chromatographic determination of lower fatty acids in air at parts-per-trillion levels. *Anal. Chem.* **1982**, *54* (14), 2433-2437.

9. Back, K. C. Formaldehyde and Other Aldehydes. *J. Occup. Environ. Med.* **1983**, *25* (7), 507.

10. Zhang, J.; Smith, K. R. Emissions of Carbonyl Compounds from Various Cookstoves in China. *Environ. Sci. Technol.* **1999**, *33* (14), 2311-2320.

11. Ranciere, F.; Dassonville, C.; Roda, C.; Laurent, A.-M.; Le Moullec, Y.; Momas, I. Contribution of ozone to airborne aldehyde formation in Paris homes. *Sci. Total Environ.* **2011**, *409* (20), 4480-4483.

12. Altshuller, A. P. Production of aldehydes as primary emissions and from secondary atmospheric reactions of alkenes and alkanes during the night and early morning hours. *Atmos. Environ. Part A. General Topics.* **1993**, *27* (1), 21-32).

13. Padhi, S. K.; Gokhale, S. Biological oxidation of gaseous VOCs – rotating biological contactor a promising and eco-friendly technique. *J. Environ. Chem. Eng.* **2014,** *2* (4), 2085-2102.

14. Raiamanickam, R.; Baskaran, D. Biodegradation of gaseous toluene with mixed microbial consortium in a biofilter: steady state and transient operation. *Bioprocess Biosyst. Eng.* **2017** *40* (12) 1801-1812.

15. Singh, R. S.; Rai, B. N.; Upadhyay, S. N. Removal of toluene vapour from air stream using a biofilter packed with polyurethane foam. *Process Safe. Environ.* **2010**, *88* (5), 366-371.

16. Mohseni, M.; Allen, D.G. Biofiltration of mixtures of hydrophilic and hydrophobic volatile organic compounds. *Chem. Eng. Sci.* **2002**, *55*, 1545–1558.

17. Huang, H.; Ying, X.; Fenga, O.; Leung, D. Y. C. Low temperature catalytic oxidation of volatile organic compounds: a review. *Catal. Sci. Technol.* **2015**, *5* (5), 2649.

18. Papaefthimiou, P.; Ioannides, T.; Verykios, X. E. Catalytic incineration of volatile organic compounds present in industrial waste streams. *Appl. Therm. Eng.* **1998**, *18* (11), 1005-1012.

19. Velu, S.; Ma, X.; Song, C. Selective Adsorption for Removing Sulfur from Jet Fuel over Zeolite-Based Adsorbents. *Ind. Eng. Chem. Res.* **2003**, *42* (21), 5293–5304.

20. Yang, R. T.; Hern´andez-Maldonado, A. J.; Yang, F. H. Desulfurization of Transportation Fuels with Zeolites Under Ambient Conditions. *Science* **2003**, 301(5629), 79–81.

21. Hern´andez-Maldonado, A. J.; Yang, F. H.; Qi, G.; Yang, R. T. Desulfurization of transportation fuels by p-complexation sorbents: Cu(I)-, Ni(II)-, and Zn(II)-zeolites. *Appl. Catal., B.* **2005**, *56* (1–2), 111–126.

22. Kwon, J. M.; Moon, J. H.; Bae, Y. S.; Lee, D. G.; Sohn, H. C.; Lee, C. H. Adsorptive Desulfurization and Denitrogenation of Refinery Fuels Using Mesoporous Silica Adsorbents. *ChemSusChem*, **2008**, *1*(4), 307–309.

23. McKinley, S. G.; Angelici, R. J. Deep desulfurization by selective adsorption of dibenzothiophenes on Ag+/SBA-15 and Ag+/SiO2. *Chem. Commun.* **2003**, *20*, 2620–2621.

24. Wang, Y.; Yang, R. T.; Heinzel, J. M. Desulfurization of jet fuel by p-complexation adsorption with metal halides supported on MCM-41 and SBA-15 mesoporous materials. *Chem. Eng. Sci.* **2008**, *63*(2), 356–365.

25. Wang, Y.; Yang, R. T.; Heinzel, J. M. Desulfurization of Jet Fuel JP-5 Light Fraction by MCM-41 and SBA-15 Supported Cuprous Oxide for Fuel Cell Applications. *Ind. Eng. Chem. Res.* **2008**, *48*(1), 142–147.

26. Chen, H.; Wang, Y.; Yang, F. H.; Yang, R. T. Desulfurization of high-sulfur jet fuel by mesoporous p-complexation adsorbents. *Chem. Eng. Sci.* **2009**, *64*(24), 5240–5246.

27. Coudert, F. O. X.; Boutin, A.; Fuchs, A. H.; Neimark, A. V. Adsorption Deformation and Structural Transitions in Metal–Organic Frameworks: From the Unit Cell to the Crystal. *J. Phys. Chem. Lett.* **2013**, *4*, 3198.

28. Keskin, S.; van Heest, T. M.; Sholl, D. S. Can metal-organic framework materials play a useful role in large-scale carbon dioxide separations? *ChemSusChem*, **2010**, *3*, 879.

29. Seoane, B.; Coronas, J.; Gascon, I.; Benavides, M. E.; Karvan, O.; Caro, J.; Kapteijn, F.; Gascon, J. Metal–organic framework based mixed matrix membranes: a solution for highly efficient $CO_2$ capture? *Chem. Soc. Rev.* **2015**, *44*, 2421.

30. D'Alessandro, D. M.; Smit, B.; Long, J. R. Carbon dioxide capture: prospects for new materials. *Angew. Chem. Int.* **2010**, *49*, 6058.

31. Demessence, A.; D'Alessandro, D. M.; Foo, M. L.; Long, J. R. Strong $CO_2$ Binding in a Water-Stable, Triazolate-Bridged Metal–Organic Framework Functionalized with Ethylenediamine. *J. Am. Chem. Soc.* **2009**, *131*, 8784.

32. Britt, D.; Furukawa, H.; Wang, B.; Glover, T. G.; Yaghi, O. M. Highly efficient separation of carbon dioxide by a metal-organic framework replete with open metal sites. *Proc. Natl. Acad. Sci. U. S. A.* **2009**, *106*, 20637.

33. Rao, A. B.; Rubin, E. S. A technical, economic, and environmental assessment of amine-based $CO_2$ capture technology for power plant greenhouse gas control. *Environ. Sci. Technol.* **2002**, *36* (20), 4467-447.

34. *Choosing an adsorption system for VOC: Carbon, zeolite, or polymers?*; EPA Technical Bulletin for Clean Air Technology Center, EPA-456/F-99-004: Research Triangle Park, NC, May 1999.

35. Khan, F. I.; Ghoshal, A. K. Removal of Volatile Organic Compounds from polluted air. *J. Loss Prevent. Proc. Ind.* **2000**, *13* (6), 527-545.

36. Sofian, I.; Harwin, Y.; Kurniawan, A.; Adityawarman, D.; Indarto, A. Nanotechnologies in water and air pollution treatment. *Environmental Technology Reviews* **2012,** *1* (1), 136–148.

37. Guerra, F. D.; Attia, M. F.; Whitehead, D. C.; Alexia, F. Nanotechnology for environmental remediation: materials and applications. *Molecules* **2018**, *23*, 1760.

38. Khin, M. M.; Nair, A. S.; Babu, V. J.; Murugan, R.; Ramakrishna, S. A review on nanomaterials for environmental remediation. *Energy Environ. Sci.* **2012**, *5* (8), 8075-8109.

39. Long, R. Q. and Yang, R. T., Carbon Nanotubes as Superior Sorbent for Dioxin Removal. *J. Am. Chem. Soc.* **2001**, *123* (9), 2058.

40. Sinha, A. K.; Suzuki, K.; Takahara, M.; Azuma, H.; Nonaka, T.; Fukumoto, K. Mesostructured Manganese Oxide/Gold Nanoparticle Composites for Extensive Air Purification. *Angew. Chem.*, **2007**, *119*(16), 2949–2952.

41. Campbell, M. L.; Guerra, F. D.; Dhulekar, J.; Alexis, F.; Whitehead, D. C. Target-Specific Capture of Environmentally Relevant Gaseous Aldehydes and Carboxylic Acids with Functional Nanoparticles. *Chem. Eur. J.* **2015**, *21* (42), 14834-14842.

42. Guerra, F. D.; Campbell, M. L.; Whitehead, D. C., Alexis, F. Tunable properties of functional nanoparticles for efficient capture of VOCs. *ChemistrySelect* **2017**, *2*, 9889-9894.

43. Guerra, F. D.; Campbell, M. L.; Attia, M. F.; Whitehead, D. C.; Alexis, F. Capture of aldehyde VOCs using a series of amine-functionalized cellulose nanocrystals. *ChemistrySelect* **2018**, *3*, 1-8.

44. Ismadji, S.; Soetaredjo, F. E.; Ayucitra, A. *Clay materials for environmental remediation*; Vol. 25; Springer, 2015.

45. Pires, J.; Pinto, M. Pillared Interlayered Clays as Adsorbents of Gases and Vaprs. In *Pillared Clays and Related Catalysts*; Gil, A.; Korili, S.A.; Trujillano, R.; Vicente M. A. Eds.; Springer, 2010, 23-28.

46. Molina-Sabio, M.; González, J.; Rodrı´guez-Reinoso, F. Adsorption of NH3 and H2S on activated carbon and activated carbon–sepiolite pellets. *Carbon* **2004**, *42* (2), 448-450.

47. Stepova, K. V.; Maquarrie, D. J.; Krip, I. M. Modified bentonites as adsorbents of hydrogen sulfide gases. *Appl. Clay Sci.* **2009**, *42 (30)*, 625-628.

48. Batista, L. C.; de S. Dantas, D.; de Farias, R. F. Dye Adsorption on Inorganic Matrices as a New Strategy to Gas Capture: Hydrogen Sulfide Adsorption on Rodhamine B Modified Kaolinite. *Synth. React. Inorg. Metal*-Org. *nano-Met. Chem.* **2014**, *44* (10), 1398-1400.

49. Zhang, Q.; Yang, C.; Huang, W.; Dang, Z.; Shu, X. Sorption of tylosin on clay minerals. *Chemosphere* **2013**, *93* (9), 2180-2186.

50. Nguyen-Thanh, D.; Block, K.; Bandosz, T. J. Adsorption of hydrogen sulfide on montmorillonites modified with iron. *Chemosphere* **2005**, *59* (3), 343-353.

52. Dandy, A. Zeolitic water content and adsorptive capacity for ammonia of microporous sepiolite. *J. Chem. Soc. A.* **1971**, *0*, 2383.

53. Wang, W.; Xiao, J.; Wei, X.; Ding, J.; Wang, X.; Song, C. Development of a new clay supported polyethylenimine composite for CO2 capture. *Appl. Energy* **2014**, *113*, 334-341.

54. Meeker, D.L. and Hamilton, C.R. An Overview of the Rendering Industry. In *Essential Rendering: All About the Animal By-Products Industry*; Meeker, D.L., Eds.; Kirby Lithographic Company, Inc.: Arlington, VA, 2006, 1–16.

55. Swisher, K. Market Report: Prices are Down but Demand Remains Strong. *Render: The International Magazine of Rendering*, April 2016, pp10–15.

56. Van Langenhove, H.R.; Van Wassenhove, F.A.; Coppin, J.K.; Van Acker, M.R.; Schamp, N.M. Gas chromatography/mass spectrometry identification of organic

volatiles contributing to rendering odors. *Environ. Sci. Technol.*, **1982**, *16*, 883–886.

57. Van Langenhove, H.R.; Van Acker, M.; Schamp, N.M. Quantitative determination of carbonyl compounds in rendering emissions by reversed-phase high performance liquid chromatography of the 2,4- dinitrophenylhydrazones. *Analyst* **1983**, *108*, 329–334.

58. Defoer, N.; De Bo, I.; Van Langenhove, H.; Dewulf, J.; Van Elst, T. Gas-chromatography-mass spectrometry as a tool for estimating odour concentrations of biofilter effluents at aerobic composting and rendering plants. *J. Chromatogr. A.* **2002**, *970*, 259–273.

59. Bhatti, Z.A.; Maqbool, F.; Langenhove, H.V. Rendering plant emissions of volatile organic compounds during sterilization and cooking processes. *Environ. Technol.* **2014**, *11*, 1321–1327.

60. Guerra, F. D.; Smith, G. D.; Alexis, F.; Whitehead, D. C. A Survey of VOC emissions from rendering plants. *Aerosol Air Qual. Res.* **2017**, *17*, 209-217.

61. Swasy, M. I.; Campbell, M. L.; Brummel, B. R.; Guerra, F. D.; Attia, M. F.; Smith, G. D.; Alexis, F.; Whitehead, D. C. Poly(amine) modified kaolinite clay for VOC capture. *Chemosphere*, **2018,** *213*, 19-24.

62. Xia, Y.; Ghasemlou, M.; Rubino, M.; Auras, R.; Baghdachi, Novel Active Surface Prepared by Embedded Functionalized Clays in an Acrylate Coating. *J. ACS Appl. Mater. Interfaces* **2015**, 7, 24944–24949.

CHAPTER SIX

# AMINE-GRAFTED CELLULOSE NANOCRYSTALS FOR PESTICIDE REMEDIATION

## *6.1. Introduction*

### *6.1.1. Pesticides*

The use of pesticides in agriculture has undeniably played a significant role in improving crop yields as well as protecting against aggressive pests and invasive weeds. The application of synthetic pesticides has become an integral component of modern agriculture, so much so, that upwards of 2.4 million metric tons of pesticide active ingredients are applied globally every year. The rapidly increasing world population and subsequent food demands have considerably increased the global use of pesticides. Further, pesticides are often applied to maintain urban plantations, to control weed and forage growth below and around infrastructure such as power lines and railways, and for mosquito control. The pervasive application of pesticides has led to universal contamination, detectable in all aspects of the ecosystem.[1,2] This contamination poses several health hazards toward the public and non-target ecological species due to their potentially toxic, stable, and less soluble active ingredients of pesticide formulations.[3,4] These active ingredients have aptly been classified based on their $LD_{50}$ values as extremely hazardous class 1A, highly hazardous class 1B, moderately hazardous class 2, and slightly hazardous class 3 active ingredients by the World Health Organization.[5]

Due to the amplified use of pesticides and the subsequent resistance developed in insects and invasive plants, the required dosage to counteract the target organism has

increased. Unsurprisingly, this increased pesticide application along with the sometimes slow environmental degradation of residual pesticides has resulted in an accumulation of active ingredients and their degradants in the environment, resulting in many instances of water source contamination, soil quality degradation, biomagnification, and reduced biodiversity. Many reports concerning the negative effects on humans and ecosystems underscore the necessity to remediate pesticides and their residues, especially from aqueous sources.[6,7]

*6.1.2. Pesticides of Interest*

Pesticides are either classified based on their target (fungicide, insecticide, herbicide, bactericides, *etc.*) or, more commonly, on their chemical composition.[3, 5] The most commonly used pesticides belong to one of four compound classes: organochlorines (OC), organophosphates, substituted ureas, or carbamates. Figure 6.1 depicts common pesticide structures from each class.

For over three decades, OC pesticides were the most widely utilized pesticides in the agricultural industry. It was eventually realized that they are very stable in the environment, displayed significant toxicity to plants and animals, and were easily absorbed by organisms and food.[8] Classified, as persistent organic pollutants, OC pesticides such as aldrin and dichlorodiphenyltrichloroethane (*i.e.* DDT) were eventually phased out of production and subsequently banned.[9-11]

Organophosphate (OP) pesticides eventually took over as the slightly safer, yet still effective, alternative. They function by inhibiting the enzyme cholinesterase (AChe) following phosphorylation of serine amino acid residues.[11] One of the first OP pesticides

to be widely used, malathion, (*i.e.* diethyl 2-[(dimethoxyphosphorothioyl)sufanyl]butanediolate), is described as a nonsystemic insecticide with highly selective toxicity.[7] Other examples include chlorpyrifos, diazinon, glyphosate, and parathion.[11] There are several reports detailing the negative effects that OPs have on aquatic fauna as well as over 200,000 deaths reported annually from OP poisoning.[12, 13]

Many developing countries are limited to the use of cheaper broad-spectrum carbamate pesticides, such as, carbofuran, carbaryl, thiram, and mancozeb. First introduced in 1956, carbamates are typically applied as insecticides and display the same mechanism of toxicity as OP pesticides by inhibiting the AChE enzyme.[14] Reports detailing the negative effects of carbaryl and carbofuran on the reproductive systems of non-target species have been reported, as well, as significant toxicological concerns for the metabolites of carbamates.[15, 16]

The least-toxic alternatives arise from the substituted urea class of pesticides. Commonly used as herbicides, they exhibit lower environmental persistence and high selectivity via a free imino hydrogen which forms hydrogen bonds to inhibit the acetolactate synthase enzyme.[17] For example, diuron has been reported to decease photosynthesis efficiency in target plants at concentrations as low as 1.5 $\mu$g $L^{-1}$. The major health concern surrounding this class involves the formation of pesticide residues that are more stable and toxic in comparison to their parent pesticide.[19]

Organochlorine Pesticides

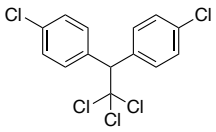

**DDT**

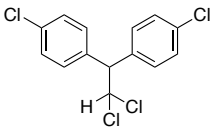

**DDD**

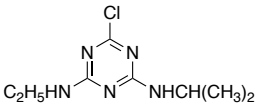

**Atrzine**

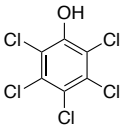

**Pentachlorophenol**

Organophosphorus Pesticides

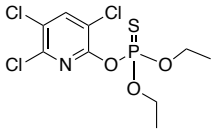

**Chlorpyrifos**

**Diazinon**

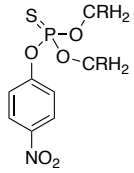

**R = $CH_3$; Parathion**
**R = H; Methyl-Parathion**

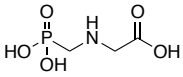

**Glyphosate**

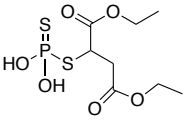

**Malathion**

Carbamate Pesticides

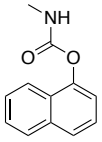

**Carbaryl**

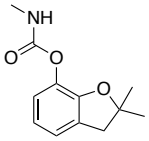

**Carbofuran**

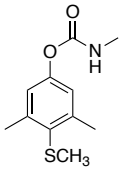

**Methiocarb**

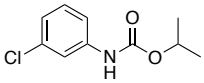

**Chlropropham**

Substituted Urea Pesticides

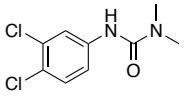

**Diuron**

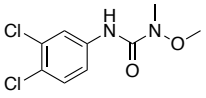

**Linuron**

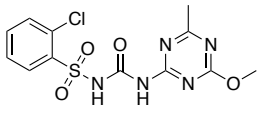

**Chlorsulfuron**

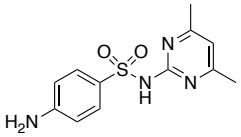

**Sulfamethazine**

**Figure 6.1.** Examples of organochlorine, organophosphorus, carbamate, and substituted urea pesticides.

*6.1.3. Traditional Remediation Techniques*

One of the biggest hurdles surrounding pesticide remediation is that it is particularly difficult to develop a single, universal method for pesticide effluent remediation.[20-22] This is highlighted by the plethora of physical, chemical, and biological methods that have been explored to mitigate pesticide pollution such as, coagulation/flocculation, photocatalytic degradation, electrochemical or aerobic degradation, oxidation, membrane filtration, nanofiltration, and adsorption.[1,2, 20-23] In terms of detectable pesticides in surface waters, microbial, photochemical, and/or chemical treatments are the primary degradative decontamination processes. There are numerous examples of microorganism-assisted methodologies, *i. e.* the application of fungi, bacteria, and viruses for pesticide remediation.[24, 25] Initially, bacteria already present in the ecosystem were studied for their ability to degrade pesticide residues. Theoretically, the use of naturally abundant bacteria would serve as a cost-effective and environmentally friendly technique, since the method would not cause any secondary pollution. It was quickly realized, however, that the time frame required for native bacteria to degrade pesticide contaminants was impractically long, and many uncontrollable environmental influences, such as temperature and pH, drastically affected the course of the microbial degradation. This prompted studies to closely evaluate naturally occurring bacteria from soil and water sources in order to understand their mechanism for organic pesticide degradation. From these findings, bacteria capable of degrading pesticides to lower molecular weight products have been isolated and their degradation pathways have been described.[26-33] Table 6.1 details a number of microorganisms that can effect the biodegradation of pesticides.

**Table 6.1.** Overview of microorganisms successfully applied to the biodegradation of pesticides.

| Pesticide | Microorganisms Involved in Biodegradation |
|---|---|
| DDT in soil | *Escherichia coli, Enterobacter aerogenes, Enterobacter cloacae, Klebsiella pneumonia, Pseudomonas putida, Bacillus species* and *Hydrogenomonas* |
| Endosulfan | *Pseudomonas spp., Bacillus spp.,* and *Flavobacterium spp.* |
| Iprodione | *Pseudomonas spp.* |
| Lindane | *Bacillus thiooxidans and Basea thiooxidans, Sphingomonas paucimobilis, Streptomyces spp.,* and *Pleurotus ostreatus* |
| Nitrobenzene | *Pseudomonas pseudoalcaligenes* and *Pseudomonas putida HS12, Comamonas spp. Pseudomonas mendocina KR-1, Pseudomonas pickettii PKO1, Cyanobacterium spp., Microcystis aeruginosa, Arthrobacter spp., Serratia spp., ,* and *Stenotrophomonas spp. Comamonadaceae* and *Clostridium spp.,* and *Rhodotorula mucilaginosa* |
| Cypermethrin | *E. coli, S. aureus, P. aeruginosa, B. subtilis, Enterobacter asuburiae* and *Pseudomonas stutzeri* |
| Carbofuran | *Pseudomonas spp., Flavobacterium spp., Achromobacterium spp., Sphingomonas spp.* and *Arthrobacter spp.* |
| Carbendazin | *Pseudomonas* |
| Aldrin | *Trichoderma viridae, Pseudomonas spp., Micrococcus spp.,* and *Bacillus spp.* |
| Endrin | *Trichoderma viridae, Pseudomonas spp., Micrococcus spp., Arthrobacter spp.,* and *Bacillus spp.* |
| Dieldrin | *Pseudomonas spp.* |

Further studies have focused on the identification of microbial enzymes, such as, oxidoreductases, dioxygenases, and hydrolases that have the potential to activate pesticides *in situ* and potentially serve as an additional tool for bioremediation.[34] While effective, biodegradation approaches are time consuming, often requiring days to months for complete metabolism to occur, leading to increased expenses that are incompatible with industrial-scale applications.[35]

Various photochemical methods, such as direct photolysis and photocatalysis, have also emerged as viable pesticide degradation strategies. Photolysis can occur either directly or indirectly, with the former occurring when the pesticide of interest adsorbs light energy, enters an excited state, and undergoes a chemical transformation, contingent on there being enough energy to overcome the activation barrier.[36] The latter occurs when pesticides react with other photochemically produced species such as hydroxyl radicals and ions.[36-39] Direct photochemical degradation is limited to gas phase interactions in the atmosphere, shallow layers of soil, and in surface water due the need for direct contact of the appropriate wavelength of light with the pesticide matrix.[40] Light sources with greater intensities than sunlight have also been employed. For example, xenon or krypton lamps are able to produce light pulses over a range of wavelengths (*i.e.* 200–1000 nm) in very short and intense intervals (50–3000 μs). This approach has been applied effectively to pesticide contaminated water, degrading atrazine, simazine, chlorpyrifos-methyl, pirimiphos-methyl, phosmet, and azinphos-ethyl.[41]

Alternatively, photocatalysis relies on the use of a semiconductor metal oxide catalyst such as, $TiO_2$, $WO_3$, or ZnO to accelerate the photoreaction.[42-44] Briefly, the semiconductor catalyst (C) absorbs an energy quantum to produce energetic species ($e^-$ and $h^+$) followed by subsequent transfer of excited electrons to the oxidant ($Ox_1$). Simultaneously, the catalyst accepts electrons from the reductant ($Red_2$) to fill the holes left in the semiconductor valance band (Equation 6.1). Further, in the presence of $H_2O$ and/or hydroxyl ions, hydroxyl radicals (·OH) are formed

$$C \xrightarrow{h\nu} C\,(e^- + h^+)$$

$$h^+ + Red_2 \longrightarrow Ox_2$$

$$e^- + Ox_1 \longrightarrow Red_1$$

**Equation 6.1.** Photocatalysis with a semiconductor

and may form other reactive radicals such as superoxide radical anion ($O_2 \cdot^-$) that can react with pesticides. When the solid conductor is used in aqueous sources, a colloidal suspension is formed that is stable upon irradiation. This method has been successfully applied to the degradation of a carbamic, chlorinate, triazine, and urea pesticides.[43-45] For instance, Higarashi and Jardim studied the remediation of diuron in contaminated soil using a $TiO_2$ photocatalyst. When irradiated with sunlight, they observed that the pesticide and its intermediates were completely degraded in the topsoil, up to a depth of 4 cm.[43] Photocatalysts are an attractive method because they are generally cost-effective, chemically inert, non-toxic, and easily attainable.[45] The disadvantages of this method is the difficulty associated with identifying an appropriate light source to facilitate practical remediation efforts. Often, a compatible light source that was identified in the laboratory becomes unsuitable when applied in the field, due to either undesired photon absorption by the pesticide formulating agents or the increased opaqueness of environmentally relevant solutions.[46-48]

In aqueous systems, such as wastewater, the most common pathways applied to promote chemical degradation are hydrolysis and oxidation. Hydrolysis is an attractive method because it has been proven to be economical and effective. Hydrolysis occurs via a water substitution or elimination reaction pathway. Whether the degradation occurs more rapidly at a high pH (alkaline hydrolysis) or a low pH (acid hydrolysis) varies among pesticides. The rate of hydrolysis also depends on the temperature, where increased temperatures (~100 ˚C) are typically required for degradation to occur within 24 h.[49] Oxidation processes, specifically advanced oxidation processes (AOPs), require the

addition of oxidants such as hydrogen peroxide/ferrous salts, $TiO_2$ photocatalysts, and ozone, as well as formulating agents and surfactants to quench and remove the oxidative species.[50-52] Currently, the limiting factor surrounding AOPs is the high cost of many of the necessary oxidants.[20]

*6.1.4. Nanomaterials for Pesticide Remediation*

A variety of nanomaterials and nanocomposites have also been established as useful technologies for water pollutant remediation. Numerous reports can be found in the literature detailing the adsorption of pollutants, mitigation of pathogens, and degradation of toxins into less-toxic derivatives.[35, 54-61] Some examples include the use of $TiO_2$, ZnO, metal oxide and sulfide nanomaterial photocatalysts that possess attractive characteristics, such as optimal morphology, size, and higher adsorption capacity. Additionally, they do not require mass transfer allowing the process to be applicable with atmospheric oxygen under ambient conditions. On exposure to the appropriate light source, these materials generate electron–hole pairs which migrate to the surface of the semiconductor material, promoting pesticide degradation via photooxidation or photoreduction.[62-64] Degradation efficiency can be amplified by decreasing the particle size or by doping the photocatalyst, with both manipulations leading to changes in the band gap, making photooxidation or photoreduction more facile.[63, 64]

Metal oxide nanomaterials can also function as reactive sorbents, promoting hydrolytic reactions in aqueous solutions. Sastny *et al.* reported the reactive adsorption of parathion methyl upon treatment with mesoporous $MnO_2$ via the nucleophilic attack on the phosphorus atom, followed by release of 4-nitrophenol.[65] OC pesticides are also

susceptible to degradative nanoadsorbants such as $TiO_2$ (via photocatalysis) and $Fe^0$ nanoparticles (via redox reaction). Bandala and coworkers reported that the treatment of pesticide contaminated water with $TiO_2$ NPs and UV lamps resulted in oxidation of aldrin into dieldrin, chlordane, and 1,2-hydroxy-dieldrin.[66] Further, doping of the $TiO_2$ photocatalyst with species such as nitrogen, $IO_3$, or other metal ions has been reported to increase degradation efficieny. For instance, malathion degradation increased by over 170% when treated with an Au and Pd doped $TiO_2$ nanotube film in comparison to the undoped version.[67] It is suggested that increased adsorption is a result of the metal ions present in the semiconductor lattice promoting the formation of $Ti^{3+}$ ions, causing more surface defects and increasing adsorption of oxygen onto the titania surface. Moreover, the quantum yield of the photoreaction is bolstered as a result of the metal ions increasing the charge separation of the electrons and holes in the conduction and valance bands.[67]

Zero valent iron based NP catalysts, such as nZVI, have been very effective at degrading nearly all halogenated hydrocarbons, in under 24 h, to their less toxic hydrocarbon derivatives by means of a dichlorination mechanism.[68-73] Thus numerous studies have been conducted to determine the optimized nanoparticle formulations. Elliot *et al*. disclosed the significance of nZVI particle size on degradation efficiency. More specifically, a greater percent degradation of lindane was observed for 60 nm nZVI in comparison to 10 $\mu$m commercial iron, 95 and 60% degradation, respectively.[74]

Cellulose nanocrystal (CNC) represents one class of nanomaterial that is an ideal platform for further functionalization due to the large surface area of the substrate as well as the presence of the C6 carbinol functionality that can serve as a handle for covalent bond

formation. Cellulose-based materials are also abundant in nature, renewable, biodegradable, and biocompatible. Our group has explored poly(ethylenimine) (*i.e.* PEI) functionalized nanoparticles, microparticles, cellulose nanocrystals, and kaolinite clay materials for VOC remediation.[75-78] We have also explored the use of PEI-modified cellulose microcrystals for the removal of poly- and perfluorinated surfactants from water.[79] In continuation of our efforts in this area, we sought to evaluate the preparation of a series amine-functionalized cellulose nanocrystals (CNCs) to serve as a new material for the remediation of pesticide residues from water.

## *6.2. Results and Discussion*

### *6.2.1. Preparation and Characterization of Amine-Modified CNC*

Samples of cellulose nanocrystals grafted with ethylenediamine (EDA), tris(2-aminoethyl)amine (TRIS), and poly(ethylenimine) (PEI) were prepared following a protocol previously described by our group.[77] Briefly, commercially available CNC was oxidized via an aqueous TEMPO-mediated process wherein the primary, C6-alcohols of

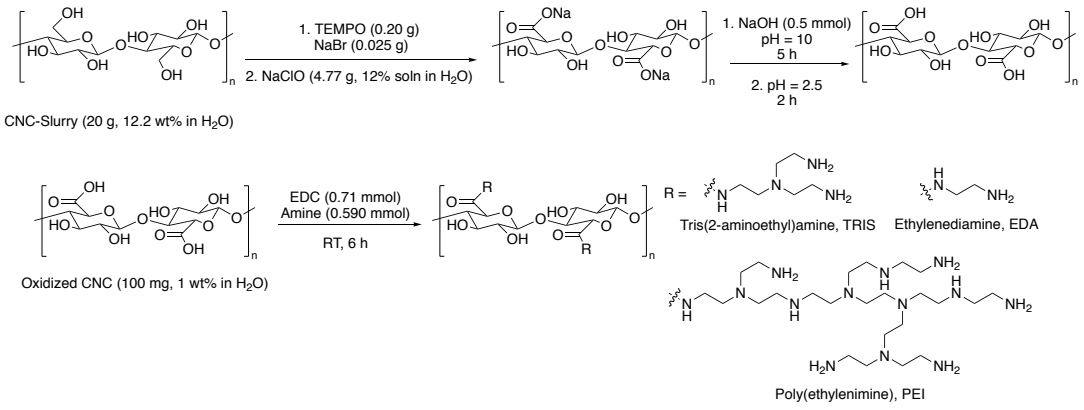


**Scheme 6.1.** TEMPO-mediated oxidation of CNC followed by ion exchange to effect the neutralization of the C-6 sodium carboxylates. EDC assisted amine-functionalization of oxidized CNC with TRIS, EDA, or PEI.

the CNC material were selectively oxidized to their corresponding sodium carboxylates. Following successful oxidation, the material was treated with an ion-exchange solution in order to convert the C6 sodium carboxylates to their neutral counterparts. Finally, CNC-EDA, CNC-TRIS, and CNC-PEI were obtained after carbodiimide coupling with EDA, TRIS, or PEI, respectively (Scheme 6.1).

The amine-modified CNC materials were characterized by Fourier-transform infrared spectroscopy (FTIR) and thermogravimetric analysis (TGA). Changes to a diagnostic carbonyl stretching frequency were easily followed throughout the chemical modification process by FTIR (Figure 6.2 A). Following TEMPO oxidation, the new C-6 carbonyl produces an identifiable C=O stretch at 1712 $cm^{-1}$ that is not present in the unmodified CNC starting material. Furthermore, upon amine (EDA, TRIS, or PEI) functionalization this carbonyl stretch experiences a shift to smaller wavenumbers, around 1585 $cm^{-1}$, suggesting successful amide bond formation following EDC coupling of the C6 carbonyl of the oxidized CNC and the prescribed amine. This shift is likely due to the larger electron donation of the more electropositive amide bond into the carbonyl as compared to its carboxylic acid predecessor. It is important to note the absence of characteristic amine N-H $sp^3$ stretches in the oxidized CNC materials which are coincident with the OH stretches from the CNC core of the material. Thermogravimetric analysis of the amine-modified materials resulted in similar degradation profiles that each differ in comparison to the oxidized CNC precursor prior to amine coupling, lending further support of successful amine-modification (Figure 6.2 B).

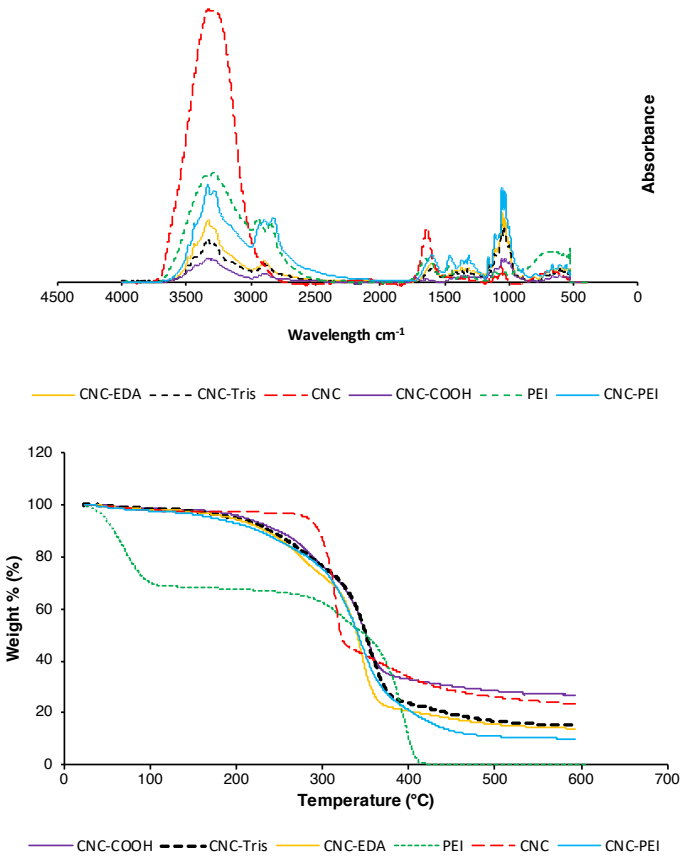


**Figure 6.2.** A) Infrared spectra of amine-modified CNC. CNC-COOH (purple line), CNC-TRIS (black line), CNC-EDA (yellow line) and CNC-PEI (blue line). B) TGA analysis of CNC (red line), CNC-COOH (purple line), CNC-TRIS (black line), CNC-EDA (yellow line) and CNC-PEI (blue line).

*6.2.2. Pesticide Remediation in Organic Solvent*

As previously discussed, organophosphorus pesticides are currently the most commonly utilized pesticide class of agrochemicals. Malathion is one such OP pesticide that is primarily used as an insecticide to control mosquito and fruit fly populations. Malathion also serves as a viable alternative to the traditionally-used organochlorine (OC) compounds, such as DDT, lindane, and endosulfan.[80] These OC pesticides are notorious for their persistent and biocumulative nature, which resulted in the release of highly toxic pesticide residues into natural water supplies. While OP pesticides do serve as a less harmful alternative to chlorinated pesticides they still represent a major environmental concern, especially in the context of water source contamination.[7, 81-83]

In the context of pesticide remediation from aqueous environments, we sought to implement amine-modified CNCs as a material to facilitate pesticide degradation. In order to easily assess and compare the remediation efficiency of each amine-CNC material, a GC analysis protocol was first optimized using solutions of DCM spiked with malathion. OP pesticides tend to be

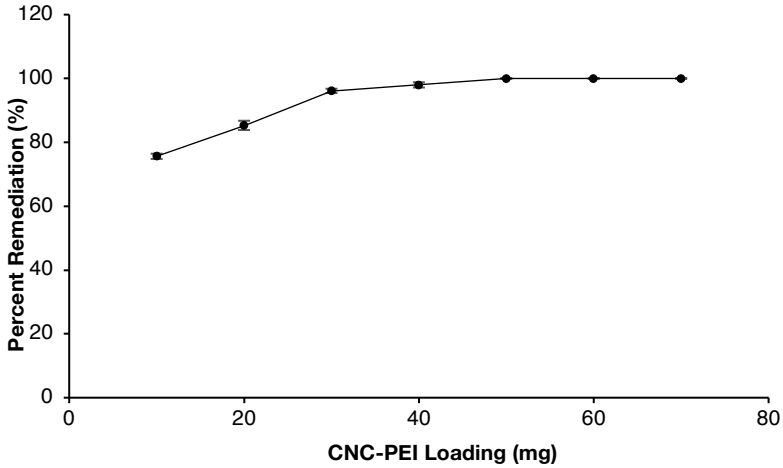


**Figure 6.3.** CNC-PEI loading experiment: Malathion pesticide samples treated with increasing amounts of CNC-PEI.

poorly water soluble, therefore, these initial analyses allowed for a higher degree of OP pesticide solubility as well as clean chromatograms for analysis. The loading of CNC-PEI was first optimized. Briefly, 1.5 mL glass screw top GC vials were charged with 10, 20, 30, 40, 50, 60, and 70 mg of the CNC-PEI material followed by a 1 mL aliquot of a solution of 165 ppm malathion in DCM. The vials were then capped and sealed with Teflon tape followed by Parafilm to avoid evaporation of the DCM solvent. Control vials were also prepared consisting only of the 1 mL 165 ppm solution of pesticide in DCM and analyzed at time 0 h as well as 24 h. The vials were then placed on an orbital shaker for 24 h. Following treatment with amine modified CNCs for 24 h, the vials were subjected to GC analysis. All experiments were conducted in triplicate and pesticide degradation percentages were calculated. Following the CNC-PEI loading experiments, it was determined that 50 mg of the material was sufficient to completely degrade a 165 ppm solution of malathion in DCM. An increase in remediation apparent when increasing the CNC-PEI loading from 10 mg to 50 mg with 75.6 ± 0.8% and 100% remediation of malathion, respectively (Figure 6.3). Using the optimized 50 mg CNC-PEI loading, it was also concluded that agitation was necessary for

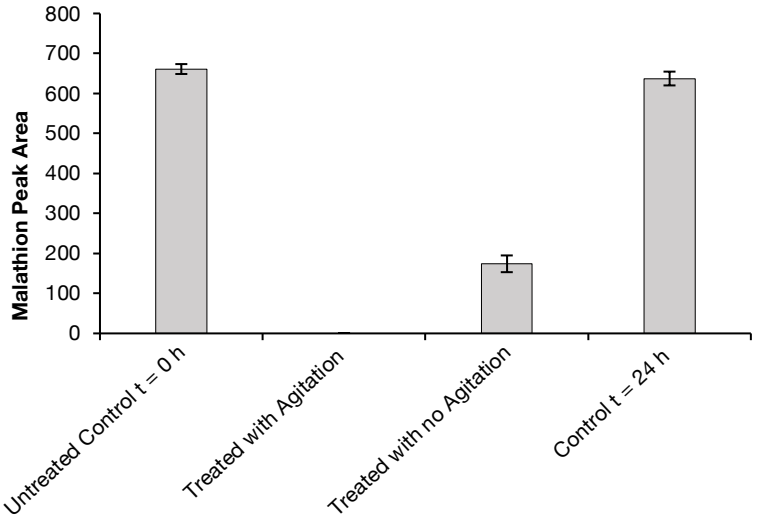


**Figure 6.4.** Agitation experiment that demonstrates the necessity of agitation of the amine-modified material and the

complete degradation to occur with only 74% reduction reported with no agitation compared to 100% with agitation of the CNC-PEI and malathion solution (Figure 6.4).

Lastly, all three amine-modified materials were assessed for their pesticide degradation effectiveness. A 50 mg loading of EDA-, TRIS-, and PEI-modified CNC resulted in 59 ± 2%, 50 ± 5%, and 100% remediation of malathion, respectively (Figure 6.5). The superior performance of the CNC-PEI material is likely due to the additional reactive sites available as compared to the mono- and di-functional EDA and TRIS caps, respectively. Lastly, a sample of unmodified CNC was tested as a control in order to demonstrate the necessity of the amine functionalization step for effective remediation. Upon subjecting a DCM solution of malathion to unmodified CNCs, the chromatogram revealed only malathion, suggesting no appreciable degradation by the unmodified CNC.

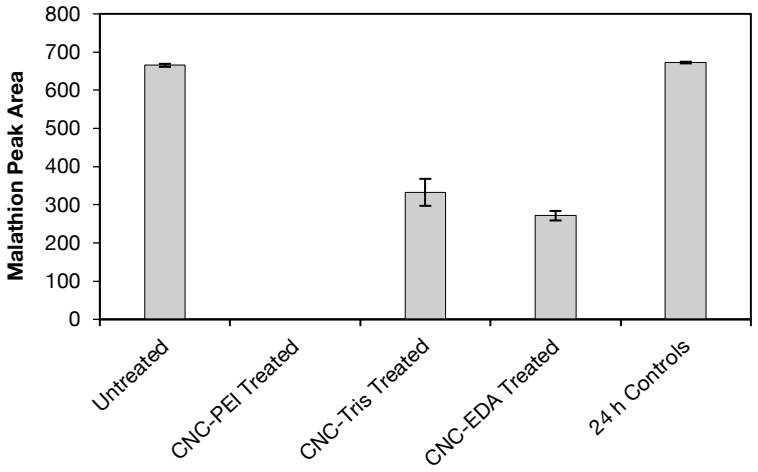


**Figure 6.5.** Pesticide remediation assays with PEI-, TRIS-, and EDA-functionalized CNC. Untreated samples contain only pesticide solution and serve as controls at t = 0 h.

*6.2.3. Pesticide Remediation in Aqueous Systems*

Following the successful remediation of malathion in organic solvent, we sought to investigate the efficiency of the CNC-PEI material in an aqueous environment. Many insecticides are typically utilized as a liquid or spray that employ water as the carrier.[84] Therefore, commercially available pesticide formulations of malathion, permethrin, and

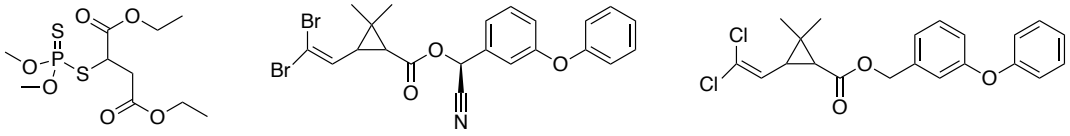

**VI.1; Malathion** **VI.2; Deltamethrin** **VI.3; Permethrin**

**Figure 6.6.** Commercially available pesticides treated with treatment with CNC-PEI.

deltamethrin were employed (Figure 6.6). These commercial formulations are widely available at local hardware stores or from internet vendors. It is important to note that many commercial pesticide solutions are formulated as a mixture of the active ingredient and other components. The active ingredient is the pesticide, therefore, pure standards of each pesticide were used to identify the peaks of interest in the GC chromatograms of the

complex commercially available solutions. Each commercially available pesticide solution was prepared as instructed on the packaging prior to treatment with the amine-CNC materials and analysis. As previously described, control GC vials containing only pesticide solution as well as treated vials containing the prescribed pesticide and 50 mg CNC-PEI were prepared. All experiments were conducted in triplicate with agitation for 24 h. Treatment of the commercially available malathion solution with 50 mg CNC-PEI, resulted in 100 % degradation of the OP pesticide at ambient temperature (Figure 6.7 A). Similarly, treatment of the deltamethrin solution with CNC-PEI resulted in a 95 ± 0.9 % reduction at ambient temperature (Figure 6.7 B). The analysis of the commercial permethrin preparation was complicated by the fact that the active

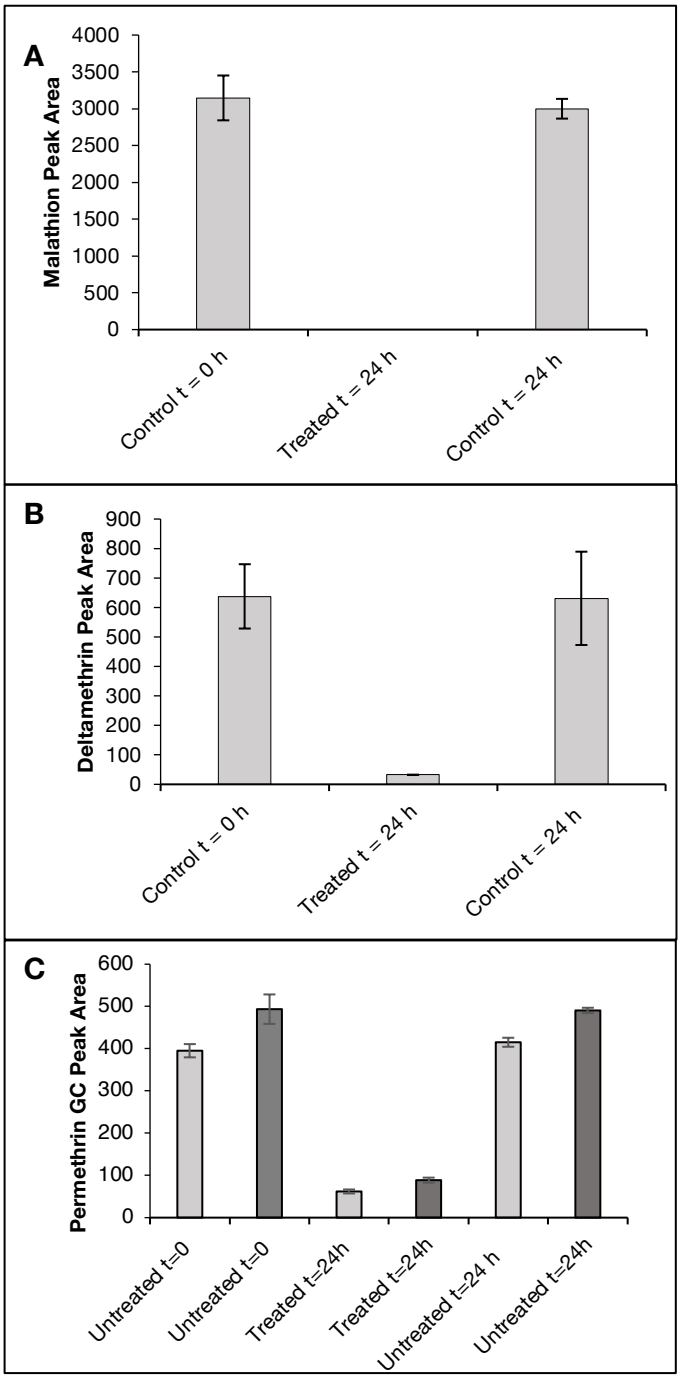


**Figure 6.7.** Degradation of malathion (**A**), deltamethrin (**B**), and permethrin (**C**) with CNC-PEI. Untreated samples contain only pesticide solution and serve as controls at t = 0 h and t = 24 h. Malathion (**A**) and deltamethrin (**B**) were conducted at RT while permethrin (**C**) was conducted to 35 °C.

ingredient is present as a pair of detectable *cis*/*trans* stereoisomers about the central cyclopropane ring. Nevertheless, upon treatment with CNC-PEI samples at a slightly elevated temperature of 35 ˚C, the two peaks exhibited an average of 84.3 ± 0.7% and 78 ± 2% reduction, respectively (Figure 6.7 C).

*6.2.4. Pesticide Degradation Mechanism*

Next, in order to probe the mechanism of degradation, we sought to identify the by-products resulting from the interaction of malathion and CNC-PEI. Thus, a 165 ppm solution of malathion was prepared in deionized water, and treated with 50 mg of CNC-PEI followed by agitation for 24 h. The CNC-PEI material was then removed from the reaction mixture by filtration, and the filtrate was then analyzed via GC-MS in order to identify the degradation products resulting from CNC-PEI treatment. Two main degradation products, *O*,*O*-dimethyl phosphorodithioic acid (**VI-4'**, DMTP) and diethyl fumarate (**VI-5**), were identified by GC-MS analysis. These compounds have previously been reported as commonly observed hydrolysis degradation by-products of malathion.[85-87] We believe that, in our system, these products arise from a facile CNC-PEI induced elimination of one of the ester α-protons from malathion to generate DMTP and diethyl fumarate (Scheme 6.2). The diethyl fumarate degradation product returned a mass

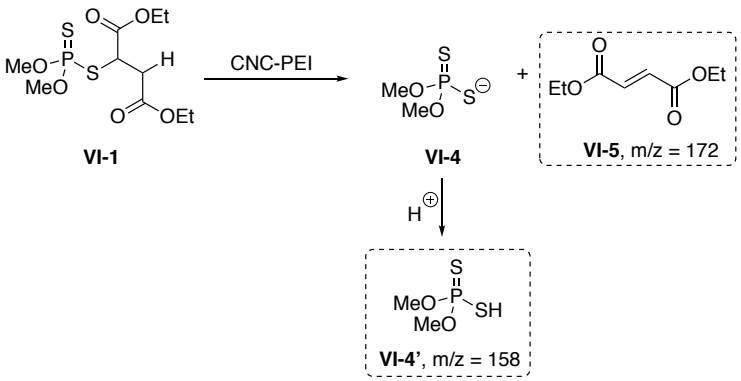


**Scheme 6.2.** Suggested malathion degradation by-products.

spectrum that was consistent with data published in the National Institute of Standards and Technology (NIST) library; while the DMTP (m/z = 158) mass spectrum exhibits a fragmentation pattern that is easily assigned to by-product **VI-4'**.[88] In a previous study, Bavcon *et. al.* monitored the degradation of malathion in untreated water, where only 30% of an initial 10.3 ppm malathion concentration was degraded over 14 days.[89] Consistent with this previous observation of slow degradation of malathion in untreated water, control GC-MS experiments with untreated aqueous malathion samples revealed no detectable degradation over 24 h. Additionally, maloxon, a commonly observed toxic oxidation by-product which is the P=O congener of malathion, was not detected via GC-MS.[89, 90]

Next, we also investigated the degradation products of deltamethrin after treatment with CNC-PEI. Upon GC-MS analysis, three lower molecular weight by-products were identified (Scheme 6.3). Deltamethrin by-product **VI-6** (m/z = 429) is presumably the result of cleavage of the diaryl ether moiety, while compounds **VI-7'** (m/z = 281) and **VI-8'** (m/z = 209) are likely by-products of ester cleavage. More

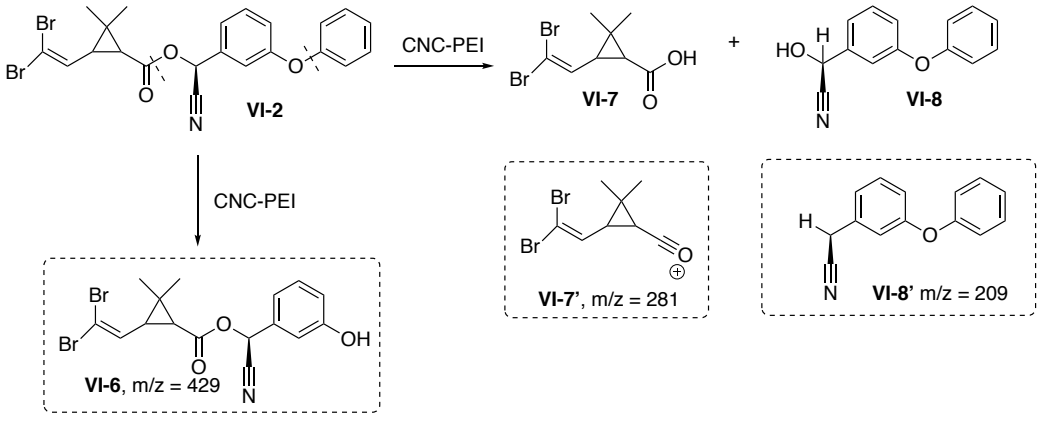


**Scheme 6.3.** Proposed deltamethrin degradation by-products.

specifically, compound **VI-7'** is the acylium ion of deltamethrinic acid (**VI-7**) while **VI-8'** is the counterpart to α-hydroxy-3-phenoxy-benzeneacetonitrile (**VI-8**). Deltamethrinic acid, **VI-7**, and α-hydroxy-3-phenoxy-benzeneacetonitrile, **VI-8,** have previously been reported in the literature as a major hydrolysis degradation by-products in aquatic environments.[91-93] Further, the mass spectrum of **VI-8** aligns well with that of the neutral 3-phenoxyphenylacetonitrile on the NIST database.[94] An additional by-product was detected via GC-MS; however, its identity is as yet unclear; further investigations are being conducted in order to elucidate the structure and clarify the degradation pathway of deltamethrin in the presence of CNC-PEI.

*6.2.5. CNC-PEI Reuse Experiment*

Next, we explored the reusability of the material for pesticide remediation by re-subjecting used CNC-PEI samples to further treatment with additional aliquots of pesticide-contaminated water (Figure 6.9). Thus, spent CNC-PEI samples were filtered from the pesticide solution and washed with 10 mL aliquots of deionized water until no pesticide contaminants or degradation products were detected upon GC analysis. The washed material was then

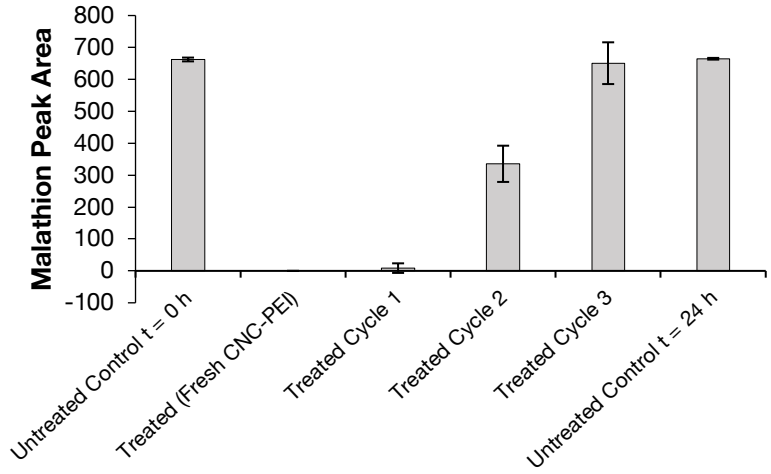


**Figure 6.9.** CNC-PEI reuse experiments. Complete loss of function is observed at reuse cycle 3.

allowed to air dry for 24 h. The dried CNC-PEI was then subjected to FTIR and TGA analyses to monitor any potential changes to the used material. No signs of drastic PEI loss were detected following the first wash cycle (Figure 6.10). The CNC-PEI was then re-subjected to fresh samples of malathion contaminated water and the degree of malathion degradation was analyzed by GC. A previously used and washed sample of CNC-PEI resulted in 98 ± 4% degradation following the first reuse cycle (Figure 6.9). Following a subsequent reuse cycle, however, only 50 ± 13% malathion degradation was achieved. It is clear that the effectiveness of the CNC-PEI material does decrease as the number of wash and reuse cycles increases. For example, the 3rd reuse experiment resulted in no detectable malathion degradation.

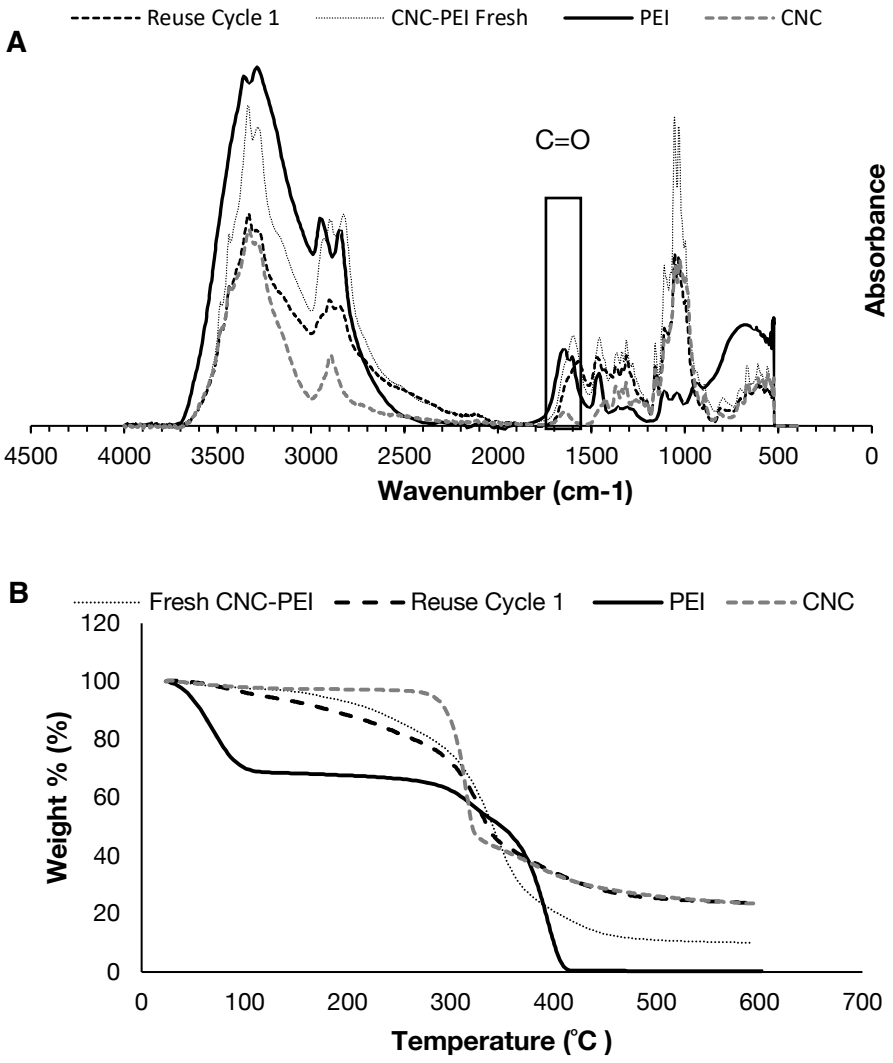


**Figure 6.10.** A) Infrared spectra of fresh CNC-PEI, CNC-PEI after Reuse Cycle 1, PEI and unmodified CNC. B) TGA analysis of fresh CNC-PEI, CNC-PEI after reuse cycle 1, PEI, and unmodified CNC.

### *6.3. Conclusions and Future Directions*

This research has demonstrated the successful preparation and characterization of amine-functionalized CNC-materials. Further, these nanomaterials were successfully applied as effective tools for the degradation of various pesticides into their respective lower molecular weight by-products in both organic and aqueous media. Namely, ethylenediamine (EDA), tris(2-aminoethyl)amine (TRIS), or poly(ethylenimine) (PEI) grafted CNC materials were evaluated for their ability to remediate pesticide solutions. These formulations represent an economical, non-toxic, and viable new nanocellulose functionalized material for pesticide remediation.

Self-decontaminating materials (SDM) are the product of a surface modification that renders the material resistant or reactive to various threats such as pesticides, hazardous chemicals, and chemical warfare agents.[95] Polymeric coatings, heterogeneous catalysts, metal-organic frameworks, quaternary ammonium salts, peroxide solutions, and nucleophiles all represent possible options for incorporation into a SDM.[95-97] There are examples in the literature detailing the successful application of SDM materials for the degradation of organophosphate esters via a hydrolysis mechanism.[98, 99] It can be imagined that our CNC-PEI materials could potentially serve as inspiration for new SDMs targeted toward the hydrolysis of organophosphate ester pesticides and chemical warfare agents. For example, cellulose nanofibers, presumably, would possess the desired adsorbent properties as well the ability to be functionalized with the PEI reactive functionality.

Cellulose nanofibers (CNFs) can be liberated from wood biomass following a commonly utilized pretreatment and mechanical disintegration protocol.[100] Typically, TEMPO-assisted catalytic oxidation serves as an effective pretreatment strategy. The prescribed method, closely resembles the TEMPO-mediated oxidation that is applied to our CNC slurries prior to amine coupling. Briefly, the wood biomass is subjected to a TEMPO/NaBr/NaClO oxidation in basified water, wherein the primary hydroxyl groups are converted to their sodium carboxylate derivatives. This is followed by gentle mechanical disintegration of the solution to obtain individual cellulose nanofibers. These fibers could then be functionalized with PEI using an EDC coupling protocol. The amine-functionalized CNFs could then be prepared into films by casting and drying the aqueous solution or into a non-woven fabric via electrospinning. A practical SDM should be non-toxic, have a rapid response to the threat, produce by-products of a lower toxicity compared to the parent threat, and function in all weather conditions. Therefore, these materials would be characterized and then tested for their response to organophosphate pesticides and other OP containing pollutants.

## *6. 4. Acknowledgements*

Funding for this work was provided by the Fats & Proteins Research Foundation, Inc., the Poultry Protein and Fat Council, the Clemson University Animal Co-Products Research and Education Center, and the Clemson University Research Foundation. I also would like to gratefully acknowledge Dr. Mohamed F. Attia for his efforts toward the synthesis and characterization of these materials as well as Ms. Kim Ivey for technical assistance throughout the CNC-material characterization.

## *6. 5. Experimental Methods*

### *6. 5. 1. General Materials and Methods*

Cellulose nanocrystal (CNC) slurry (12.2 wt.% in $H_2O$) was purchased from Cellulose Lab. Ethylendiamine (EDA), tris(2-aminoethyl)amine (Tris), Poly(ethyleneimine) solution (PEI) (1200-1300 Da, 50 wt.% in $H_2O$), 10-15% sodium hypochlorite solution (NaClO), sodium hydroxide, 2,2,6,6-Tetramethylpiperidine 1-oxyl free radical (TEMPO), *N*-(3-Dimethylaminopropyl)-*N'*-ethylcarbodiimide hydrochloride (EDC), and sodium bromide were purchased from Sigma-Aldrich and used without any further purification. Gas Chromatography (GC) analyses were conducted using an Agilent 7890A Gas Chromatograph equipped with an Agilent G4513A and a Flame Ionization Detector (FID). A Zebron ZB-MultiResidue-1 capillary GC column (30 m x 0.25 mm x 0.25 μm) was installed for pesticide detection. Agilent Technologies Gas Chromatography 1.5 mL volume vials with septum screw-caps were used in the analysis assays. Thermal gravimetric analysis (TGA) was performed on a TA Instrument Hi-Res TGA 2950 analyzer. Analysis was conducted under nitrogen from 25 to 1000 ˚C using a 10 ˚C $min^{-1}$

gradient. Fourier Transform Infrared (FTIR) analysis was performed with a Nicolet Magna 500 with NicPlan FT-IR Microscope and Mapping Stage.

### *6. 5. 2. Synthesis and Characterization of Polyamine-Grafted Cellulose Nanocrystals*

**TEMPO-mediated Oxidation and Ion Exchange**

A 20 g sample of a CNC slurry (12.2 wt.% in $H_2O$) was suspended in a water solution containing 0.20 g of TEMPO and 0.025 g of sodium bromide. A 4.77 g portion of a 12% aq. NaClO solution was added to the cellulose suspension in order to initiate the TEMPO-mediated oxidation. The reaction was performed at room temperature and stirred for 5 h. Additionally, a pH of 10 was maintained by adding of a 0.5M NaOH solution. After 5 h, the solution was thoroughly washed with water by means of dialysis to remove any unreacted reagents. The pH of this purified suspension was then adjusted to a pH of 2.5 in order to neutralize the C-6 sodium carboxylates that resulted from the oxidation. The aqueous suspension was then washed thoroughly via dialysis, freeze-dried, and stored at –20 ˚C.

**Amine-Functionalization**

In order to achieve successful amine-functionalization, a 100 mg sample of the oxidized CNC was re-suspended in water (1% cellulose/water) in a 50 mL beaker. Next, 110 mg of EDC and the prescribed amine was added to the suspension. Specifically, ethylenediamine (40 $\mu$L, 0.590 mmol), tris(2-aminoethyl)amine (89 $\mu$L, 0.590 mmol), or poly(ethylenimine) (40 $\mu$L, 0.590 mmol) were added and allowed to stir for 6 h at room temperature. The modified cellulose nanocrystals were thoroughly washed with water by

dialysis followed by freeze-drying and storage at –20 ˚C prior to full characterization and testing for pesticide remediation.

*6. 5. 3. Gas Chromatographic Pesticide Remediation Assay Methods*

GC analyses were carried out within the following parameters: inlet temperature: 170.0 ˚C; splitless injection at 15 mL $min^{-1}$; column flow: 2.0143 mL $min^{-1}$, constant pressure; carrier gas: helium; FID temperature: 340 ˚C; temperature program: 100 ˚C for 0.5 min, ramp to 180 ˚C at 20 ˚C $min^{-1}$, hold for 4.5 min., final ramp to 240 ˚C at 6 ˚C $min^{-1}$, hold for 14.5 min.

In order to assess the effectiveness of the amine-modified CNC materials we opted to determine the standard pesticide area followed by the percent reduction of that area upon interaction with the material. In other words, the area of an untreated pesticide sample was compared to the area of treated pesticide samples. Control experiments were also necessary in order to ensure that pesticide remediation was not a result of solvent, agitation, or time. In order to determine the standard pesticide area, before treatment with CNC-material, a 165 ppm solution of malathion pesticide in DCM was prepared. This solution was then added in 1 mL aliquots to 1.5 mL glass screw top GC vials. The vials were immediately subjected to GC analysis to determine the untreated pesticide peak area at t = 0 h. An additional set of vials were prepared, this time with 50 mg of the prescribed amine-functionalized CNC and the 165 ppm malathion pesticide solution. The vials were then capped and sealed with Teflon tape followed by Parafilm to avoid evaporation of the DCM solvent. These treated vials were then placed on an agitator plate for 24 h prior to GC analysis. A final set of control vials were also analyzed that contained only a 165 ppm

pesticide solution aged for 24 h. All experiments were conducted in triplicate. Pesticide remediation percentages could then be calculated by comparing the untreated pesticide peak area to the treated pesticide peak area.

*6. 5. 4. CNC-PEI Material Loading Experiment*

To determine the optimal material loading for effective pesticide remediation, a series of GC vials were prepared containing a 165 ppm malathion solution in DCM as well as increasing amounts of CNC-PEI material. Thus, 1.5 mL glass screw-top GC vials were prepped with 10, 20, 30, 40, 50 ,60, and 70 mg of the CNC-PEI material followed by 1 mL of a 165 ppm malathion solution in DCM. The vials were then capped and sealed with Teflon tape followed by Parafilm to avoid evaporation of the DCM solvent. Control vials were also prepared consisting only of the 1 mL 165 ppm solution of pesticide in DCM and analyzed at time 0 h as well as 24 h. Vials were then placed on an agitator plate for 24 h. Upon completion of the 24 h reaction time, the vial was subjected to GC analysis. All experiments were conducted in triplicate and pesticide degradation percentages were calculated.

*6. 5. 5. Agitation Experiment*

In order to determine whether or not agitation was required for pesticide remediation to occur, two experiments were conducted under otherwise identical conditions where one sample set was set on the agitator plate for the treatment period while the other sample set was allowed to stand on the benchtop. Untreated control samples were also prepared for analysis at time 0 h and 24 h. All trials were completed in triplicate. Upon

GC analysis, it was concluded that agitation was necessary for optimal pesticide degradation to occur.

*6. 5. 6. Evaluation of CNC-PEI in Aqueous Systems*

All commercially available pesticides were purchased from a local hardware store or over the internet. Pesticide solutions were prepared following the directions indicated on the respective packaging or used directly from the bottle as directed. More specifically, the Southern AG® malathion commercial pesticide was purchased over the internet in its 50% emulsifiable concentrate formulation. Therefore, this pesticide was prepared as a 2 tsp/gal aqueous solution as described on the label. While, the deltamethrin (Eliminator® Ant, Flea, and Tick Killer) and permethrin (Eliminator® Home Insect Killer) were both purchased from a local hardware store as their ready-to-use formulations, with 2.5% and 0.02% active pesticide ingredient, respectively.

Pure samples of each pesticide sample were so prepared by making a solution of 10 mg of pesticide per 1 mL of water. Due to the poor aqueous solubility of most pesticides, these solutions were allowed to sonicate for approximately 20 min and then analyzed by means of GC. These analytical pesticide standards were prepared to facilitate comparison to the commercial pesticide formulation that contain a number of additives along with the active pesticide ingredient. Once the retention times of each pesticide was determined, the remediation experiments could be completed. GC vials were prepared following the previously described method: control untreated vials (t =0 h and t = 24 h) contained only 1 mL of the pesticide solution while treated samples contained 1 mL of the pesticide solution and 50 mg CNC-PEI. All experiments were conducted in triplicate.

*6. 5. 7. GC-MS Methods for Pesticide Degradation By-Product Detection*

Pesticide samples containing degradation by-products were evaluated using a Shimadzu GC-2010 Plus, equipped with a AOC-20i auto injector, coupled to a QP2010 SE mass spectrometer. A Shimadzu GC SH-Rxi-5ms capillary column (15 m x 0.25 mm x 0.25 μm) and a Shimadzu SH-RXI-5SIL MS column (30 m x 0.25 mm x 0.25 μm) were installed for product detection. GC analyses were carried out within the following parameters: inlet temperature: 50.0 ˚C; split injection (4 μL) at 14.1 mL $min^{-1}$; column flow: 1.0 mL $min^{-1}$, constant pressure; carrier gas: helium; temperature program: 40 ˚C for 3 min.; ramp to 320 ˚C at 20 ˚C $min^{-1}$, hold for 10 min. MS analyses were conducted as follows: ion source temperature: 200 ˚C; interface temperature: 100 ˚C; solvent cut time: 3 min.

*6. 5. 8. Malathion and Deltamethrin Degradation Studies*

A 165 ppm solution of malathion was prepared in deionized water, 50 mg of CNC-PEI was added and the suspension was allowed to stir for 24 h at room temperature. Next, the solvent and any soluble compounds were filtered from the solid CNC-PEI materials and washed with deionized $H_2O$. The filtrate was then analyzed via GC-MS in order to identify the mass of all present compounds.

Similarly, a 165 ppm solution of deltamethrin was prepared in deionized water, 50 mg of CNC-PEI was added and the suspension was allowed to stir for 24 h at room temperature. Next, the water and any soluble compounds were filtered from the solid CNC-PEI materials, and the collected nanocrystals were washed with deionized $H_2O$. The aqueous filtrates were then analyzed via GC-MS in order to identify the mass of all

detectable by-products of deltamethrin degradation. Upon GC-MS analysis, three lower molecular weight by-products were identified.

### *6.6. Supplementary Information*

#### *6.6.1. GC-MS Data for Malathion Degradation*

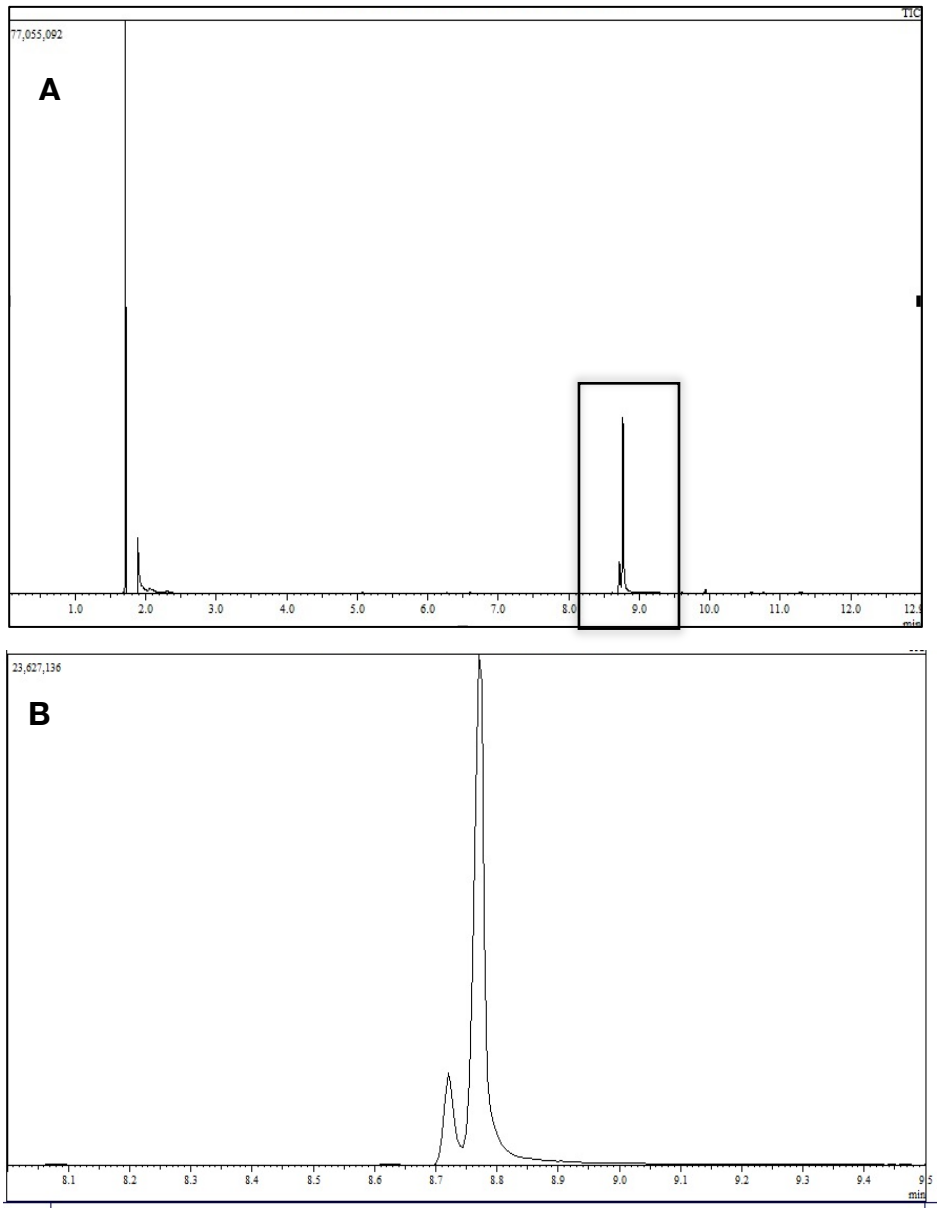


**Figure 6. 11.** GC trace of malathion solution following 24 h treatment with CNC-PEI. A) Full GC analysis chromatogram B) Zoomed in to highlight peaks at RT = 8.70 and 8.75 min. Note: Peaks seen before RT = 3 min can be attributed to solvent oversaturation and impurities.

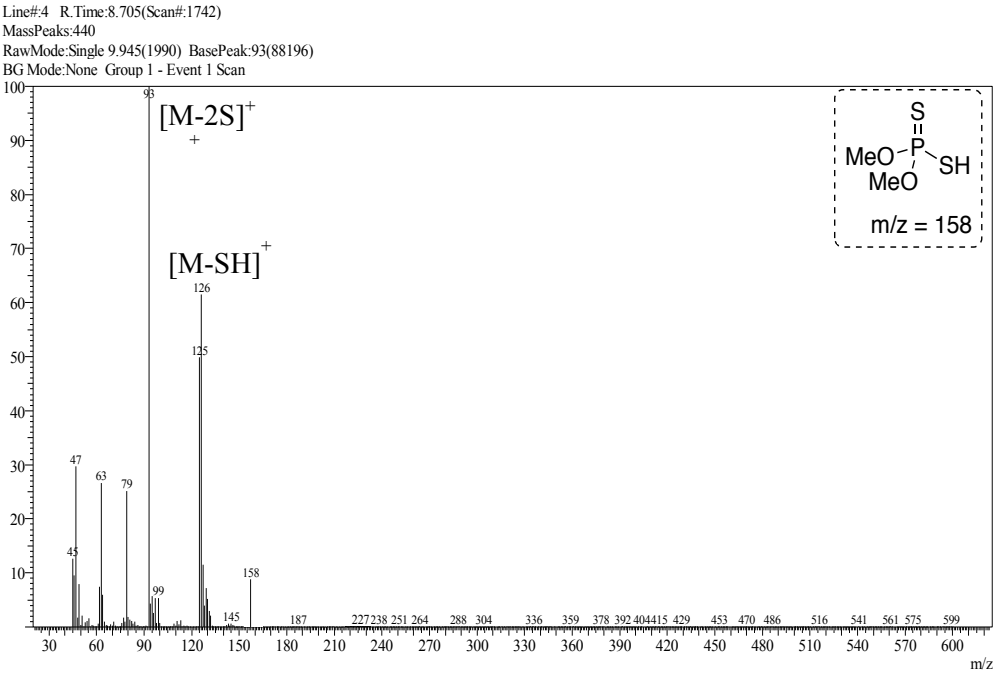


**Figure 6.12.** Identification of malathion hydrolysis by-products by GC-MS. Mass spectrum of *O*,*O*-dimethyl phosphorodithioic acid (DMTP) (m/z=158), RT = 8.70 min.

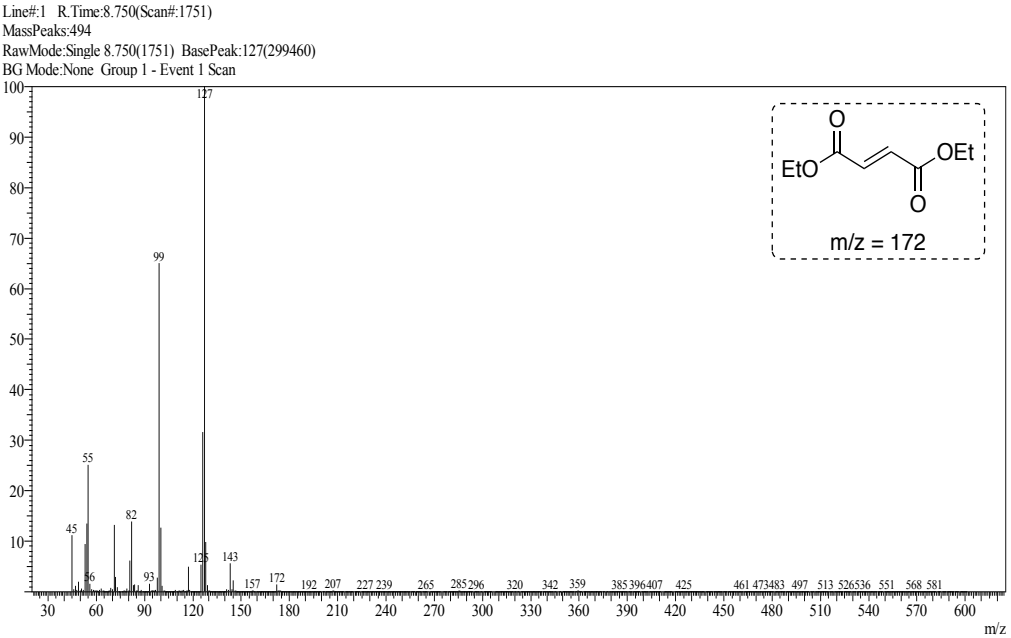


**Figure 6.13.** Identification of malathion hydrolysis by-products by GC-MS. Mass spectrum of diethyl fumarate (m/z=172), RT = 8.75 min.

*6.6.2. GC-MS Data for Deltamethrin Degradation*

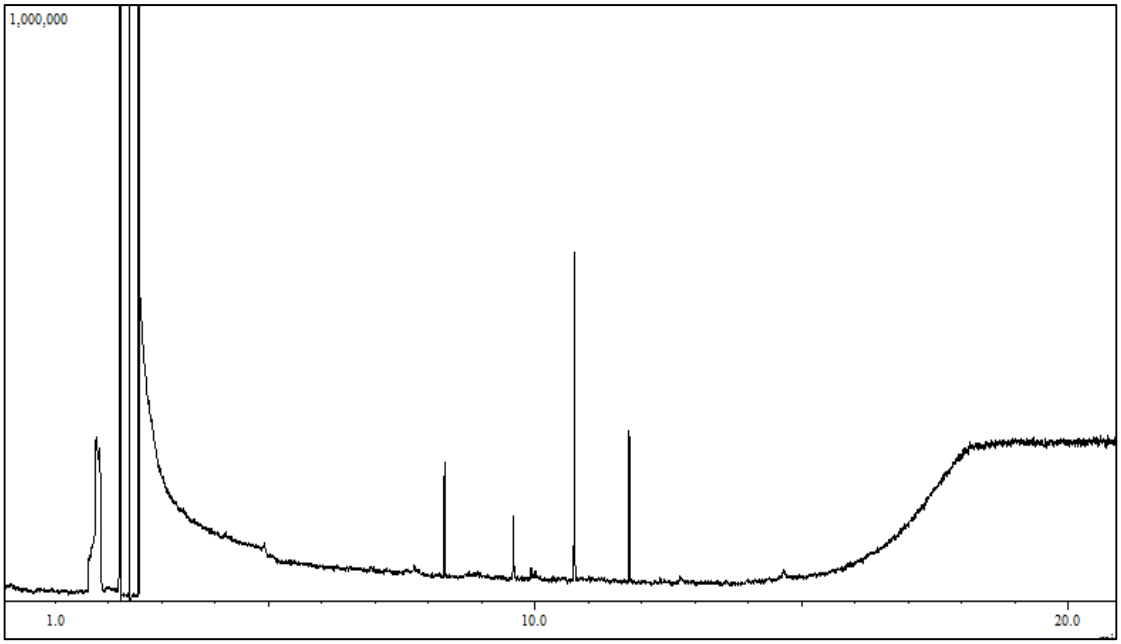


**Figure 6.14.** GC trace of deltamethrin solution following 24 h treatment with CNC-PEI. GC analysis chromatogram. Peaks attributed to degradation by-products were found at RT = 8.3, 9.6, 10.73, and 11.77 min.

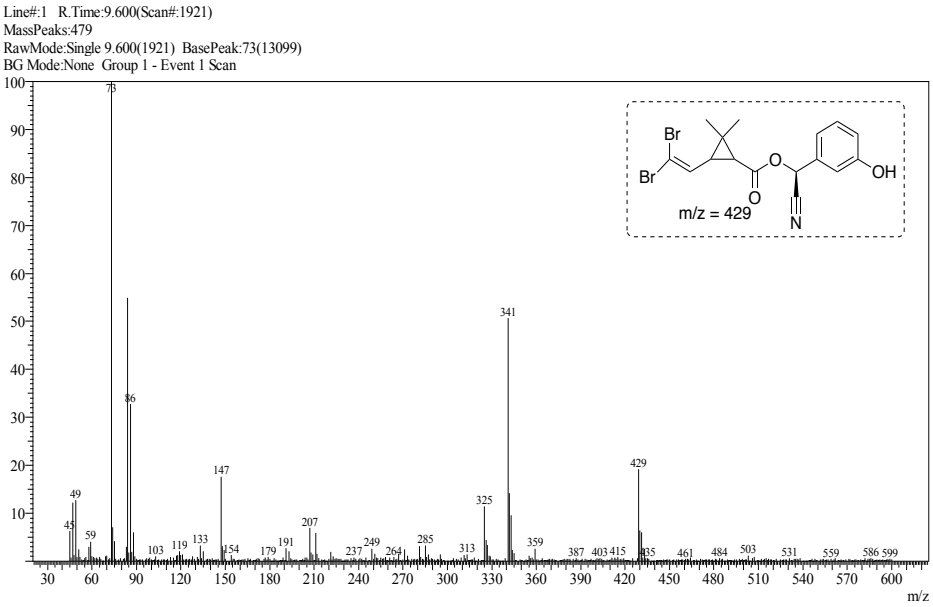


**Figure 6.15.** Identification of deltamethrin by-product by GC-MS. Mass spectrum of suggested compound (m/z=429), RT = 9.6 min.

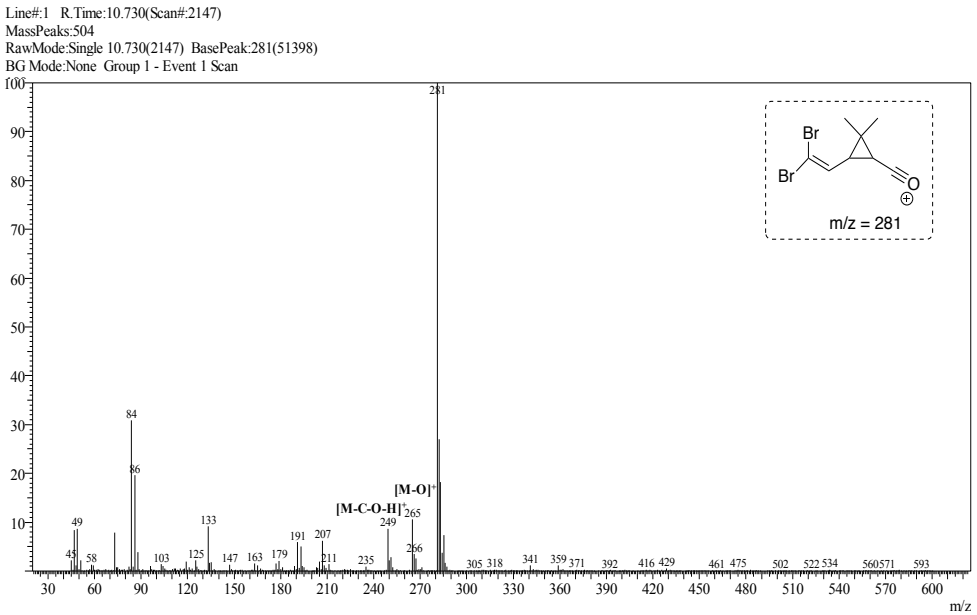


**Figure 6.16.** Identification of deltamethrin degradation by-products by GC-MS. Mass spectrum of (m/z=281) the acylium ion of deltamethrinic acid, RT = 10.73 min.

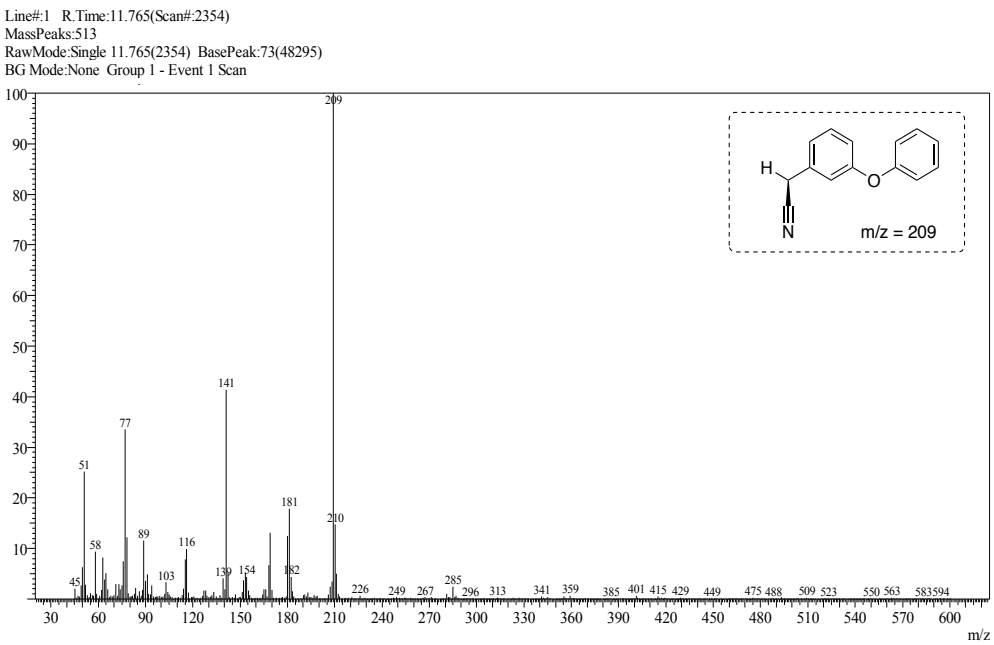


**Figure 6.17.** Identification of deltamethrin degradation by-products by GC-MS. Mass spectrum of 3-phenoxyphenyl-acetonitrile (m/z=209), RT = 11.765 min.

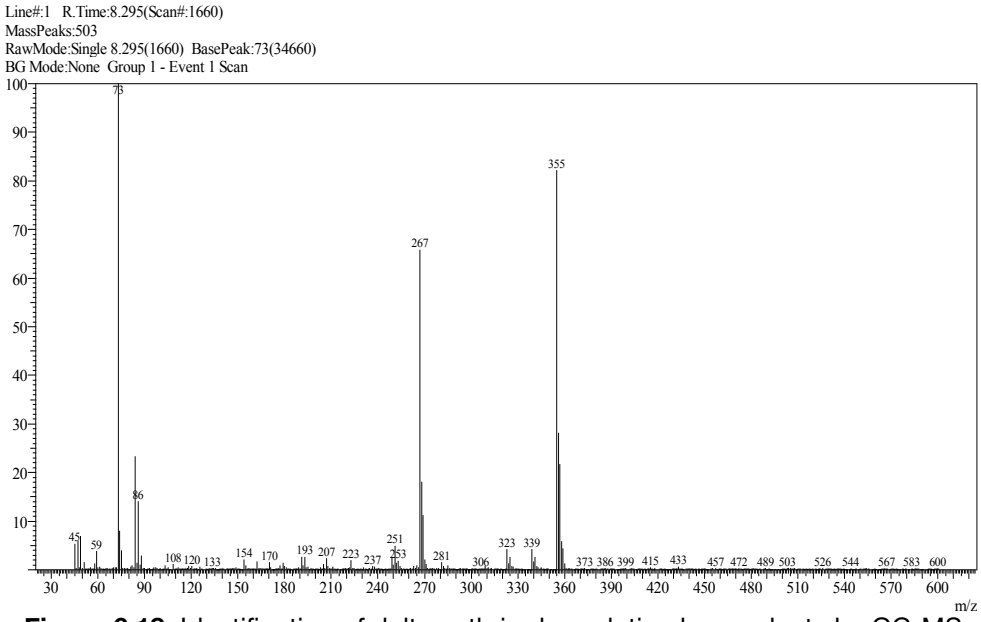


**Figure 6.18.** Identification of deltamethrin degradation by-products by GC-MS. Mass spectrum of unidentified compound (m/z=355), RT = 8.3 min.

### *6.7. References*


1. Malato, S.; Blanco, J.; Maldonado, M. I.; Oller, I.; Gernjak, W.; Perez-Estrada, L. Coupling solar photo-Fenton and biotreatment at industrial scale: main results of a demonstration plant. *J. Hazard. Mater.* **2007**, *146*, 440–446.

2. Zapata, A.; Malato, S.; Sanchez-Perez, J. A.; Oller, I.; Maldonado, M. I. Scale-up strategy for a combined solar photo-Fenton/biological system for remediation of pesticide-contaminated water. *Catal. Today* **2010**, *151*, 100– 106.

3. Rhind, S. M. Endocrine disrupting compounds and farm animals: their properties, actions and routes of exposure. *Domest. Anim. Endocrinol.* **2002**, *23*, 179–187.

4. Cerillo, I.; Olea-Serrano, M. F.; Ibarluzea, J.; Exposito, J.; Torne, P., Laguna, J.; Pedraza, V.; Olea, N. Environmental and lifestyle factors for organochlorine exposure among women living in Southern Spain. *Chemosphere* **2006**, *62*, 1917– 1924.

5. The WHO Recommended Classification of Pesticides by Hazard and Guidelines to Classification Citation: International Program on Chemical Safety. World Health Organization, 2009. WHO Press, World Health Organization, Geneva, Switzerland.

6. Kolpin, D. W.; Thurman, E. M.; Goolsby, D. A. Occurrence of selected pesticides and their metabolites in near-surface aquifers of the mid-Western United States. *Environ. Sci. Technol.* **1996**, *30*, 335–340.

7. Aker, W. G.; Hu, X.; Wang, P.; Hwang, H. M. Comparing the relative toxicity of malathion and malaoxon in blue catfish *Ictalurus furcatus*. *Environ. Toxicol.* **2008**, *23*, 548–554.

8. Sudaryanto, A.; Kunisue, T.; Kajiwara, N.; Iwata, H.; Adibroto, T. A.; Hartono, P.; Tanabe, S. Specific accumulation of organochlorines in human breast milk from Indonesia: levels, distribution, accumulation kinetics and infant health risk. *Environ Pollut*. **2006**, *139*, 107–117,

9. Zhenwu, T.; Huang, Q.; Yang, Y.; Zhu, X.; Haihui, F. Organochlorine pesticides in the lower reaches of Yangtze River: occurrence, ecological risk and temporal trends. *Ecotoxicol. Environ. Saf*. **2013**, *87*, 89–97.

10. Kafilzadeh, F. Assessment of organochlorine pesticide residues in water, sediments and fish from Lake Tashk. *Iran Achiev. Life Sci*. **2015**, *9*, 107–111.

11. Ecobichon, DJ. Pesticides. In: Amdur MO, Doull J, Klaassen CD (eds) Casarett and Doull's toxicology: the basic science of poisons, 4th edn. Pergamon Press, New York, **1991**, p 580.

12. Fernandez-Casalderrey, A.; Ferrando, M. D.; Andreu-Moliner, E. Endosulfan and diazinon toxicity to the freshwater rotifer *Brachionus calyciflorus*. *J. Environ. Sci. Health Part B* **1992**, *27*, 155–164.

13. Ray, A. K.; Ghosh, M. C. Aquatic toxicity of carbamates and organophosphates. In: Gupta RC (ed) Toxicology of organophosphate & carbamate compounds. Elsevier, Burlington, **2006**, pp 657–672.

14. Lin, J. H.; Kao, W. C.; Tsai, K.P.; Chen, C. Y. A novel algal toxicity testing technique for assessing the toxicity of both metallic and organic toxicants. *Water Res*. **2005**, *39*, 1869–1877.

15. Baligar, P. N.; Kaliwal, B. B. Induction of gonadal toxicity to female rats after chronic exposure to mancozeb. *Ind. Health* **2001**, *39*, 235.

16. Baligar, P. N.; Kaliwal, B. B. Reproductive toxicity of carbofuran to the female mice: effects on estrous cycle and follicles. *Ind. Health* **2002**, *40*, 345.

17. Wang, Y. S.; Chen, W. C.; Lin, L. C.; Yen, J. H. Dissipation of herbicides chlorsulfuron and imazosulfuron in the soil and the effects on the soil bacterial community. *J. Environ. Sci. Health Part B* **2010**, *45*, 449–455.

18. Ricart, M.; Guasch, H.; Barcelo, D.; Brix, R.; Conceicao, M. H.; Geiszinger, A.; de Alda, M. J. L.; Lopez-Doval, J. C.; Munoz, I.; Postigo, C.; Romani, A. M.; Villagrasa, M.; Sabater, S. Primary and complex stressors in polluted mediterranean rivers: pesticide effects on biological communities. *J. Hydrol.* **2010**, *383*, 52–61.

19. Bottaro, M.; Frascarolo, P. Gosetti, F.; Mazzucco, E.; Giatiotti, V.; Polati, S.; Pollici, E.; Piacentini, L.; Pavese, G.; Gennaro, M. C. Hydrolytic and photoinduced degradation of tribenuron methyl studied by HPLC-DADMS/ MS. *J. Am. Soc. Mass Spectrom.* **2008**, *19*, 1221–1229.

20. Herrmann, J. M.; Guillard, C. Photocatalytic degradation of pesticides in agricultural used waters. *C. R. Acad. Sci. Paris, Series IIC, Chimie*. **2000**, *3*, 417–422.

21. Benitez, F. J.; Acero, J. L.; Gonzalez, T.; Garcia, J. Organic matter removal from wastewaters with manure, household waste or sewage sludge. *Process Biochem.* **2001**, *37*, 257–265.

22. Miltner, R.J.; Baker, D. B.; Speth, T. F.; Fronk, C. A. Treatment of Seasonal Pesticides in Surface Waters. *J. Am. Water Works Assoc*. **1989**, *81*, 43-52.

23. Firozjaei, S. A. A.; Latifi, A. M.; Khodi, S.; Abolmaali, S.; Choopani, A. A Review on Biodegradation of Toxic Organophosphate Compounds. *J. Appl. Biotechnol. Rep*. **2015**, *2*, 215–224.

24. Nwankwegu, A. S.; Onwosi, C. O. Bioremediation of gasoline contaminated agricultural soil by bioaugmentation. *Environ. Technol. Innov*. **2017**, *7*, 1–11.

25. Rajiv, K.; Sinha, D. V.; Shanu, S.; Shweta, S.; Sunil, H. Bioremediation of contaminated sites: allow cost nature's biotechnology for environmental cleanup by versatile microbes, plants & earthworms. Solid Waste Management and Environmental Remediation. Nova Science Publishers, Incoparate, Hauppauge, **2009**, pp 1–69.

26. Ferreira, L.; Rosales, E.; Danko, A. S.; Sanromán, M. A.; Pazos, M. M. Bacillus thuringiensis a promising bacterium for degrading emerging pollutants. *Process Saf. Environ*. **2016**, *101*, 19–26.

27. Karpouzas, D.; Fotopoulou, A.; Menkissoglu-Spiroudi, U.; Singh, B. Non-specific biodegradation of the organophosphorus pesticides, cadusafos and ethoprophos, by two bacterial isolates. *FEMS Microbiol. Ecol*. **2005**, *53*, 369-378.

28. Thatheyus, A. J.; Selvam, A. D. G. Synthetic pyrethroids: Toxicity and biodegradation. *Appl. Ecol. Environ. Sci*. **2013**, *1*, 33-36.

29. Porto, A. L. M.; Melgar, G. Z.; Kasemodel, M. C.; Nitschke, M. Biodegradation of Pesticides, Pesticides in the Modern World-Pesticides Use and Management, Dr. Margarita Stoytcheva (Ed.) 2011.

30. Kato, T.; Haruki, M.; Imanaka, T. Isolation and characterization of long-chain-alkane degrading Bacillus thermoleovorans from deep subterranean petroleum reservoirs. *J. Biosci. Bioeng.* **2001**, *91*, 64-70.

31. Walker, A.; Perekh, N. R.; Roberts, S. J.; Welch, S. J. Evidence of the enhanced biodegradation of napropamide in soil. *Pesticide. Sci.* **1993**, *39*, 55-60.

32. Grant, R. J.; Daniell, T. J.; Betts, W. B. Isolation and identification of synthetic pyrethroid degrading bacteria. *J. Appl. Microbiol.* **2002**, *92*, 534-540.

33. Nawab, A.; Alimand, A.; Malik, A. Determination of organochlorine pesticides in Agricultural soil with special reference to alpha-HCH degradation by Pseudomonas Strains. *Bioresor. Technol.* **2003**, *88*, 41-46.

34. Scott, C.; Pandey, G.; Hartley, C. J.; Jackson, C. J.; Cheesman, M. J.; Taylor, M. C.; Pandey, R.; Khurana, J.L.; Teese, M.; Coppin, C. W.; Weir, K. M.; Russell, R. J.; Oakeshott, J. G. The enzymatic basis for pesticide bioremediation. *Indian J. Microbiol.* **2008**, *48*, 65-79.

35. Rani, M.; Shanker, U.; Jassal, V. Recent strategies for removal and degradation of persistent & toxic organochlorine pesticides using nanoparticles: a review. *J. Environ. Manageme.* **2017**, *190*, 208-222.

36. Wayne, R. P. *Principles and Applications of Photochemistry* Oxford University Press, Oxford, **1988**.

37. Zika, R. G.; Cooper, W. J. (Eds.), Photochemistry of Environmental Aquatic Systems, ACS Symposium Series 327, American Chemical Soc. Washington, DC, **1987**.

38. Hwang, H. M.; Hodson, R. E.; Lee, R. F. Degradation of phenol and chlorophenols by sunlight and microbes in estuarine water. *Environ. Sci. Technol.*, **1986**, *20*, 1002-1007.

39. Haag, W. R.; Hoigné, J. Photo-sensitized oxidation in natural water via ·OH radical *Chemosphere* **1985**, *14*, 1659-1671.

40. Rani, S.; Sud, D. Role of enhanced solar radiation for degradation of triazophos pesticide in soil matrix. *Sol. Energy* **2015**, *120*, 494–504.

41. Baranda, A. B.; Fundazuri, O.; de Marañón, I. M. Photodegradation of several triazidic and organophosphorus pesticides in water by pulsed light technology. *J. Photochem. Photobiol. A Chem.* **2014**, *286*, 29–39.

42. Pelizzetti, E.; Minero, C.; Carlin, V.; Borgarello, E. Photocatalytic soil decontamination. *Chemosphere* **1992**, *25*, 343–351.

43. Higarashi, M. M.; Jardim, W. F. Remediation of pesticide contaminated soil using $TiO_2$ mediated by solar light. *Catal. Today* **2002**, *76*, 201–207.

44. Morales-Pérez, A. A.; Arias, C.; Ramírez-Zamora, R. M. Removal of atrazine from water using an iron photo catalyst supported on activated carbon. *Adsorption* **2016**, *22*, 49–58.

45. Ibhadon, A. O.; Fitzpatrick, P. Heterogeneous photocatalysis: recent advances and applications. *Catalysts* **2013**, *3*, 189–218.

46. Durand, G.; Abad, J. L.; Sanchez-Baeza, F.; Messeguer, A.; Barcelo, D. Unequivocal identification of compounds formed in the photodegradation of fenitrothion in water/ methanol and proposal of selected transformation pathways. *J. Agric. Food Chem.* **1994**, *42*, 814–821.

47. Mengyue, Z.; Shifu, C.; Yaowu, T. Photocatalytic degradation of organophosphorus pesticides using thin film of TiO2. *J. Chem. Tech. Biotechnol.* **1995**, *64*, 339–344.

48. Doong, R.; Chang, W. Photoassisted titanium dioxide mediated degradation of organophosphorus pesticides by hydrogen peroxide. *J. Photochem. Photobiol. A: Chem.* **1997**, *107*, 239–244.

49. Beyke, G. L. Thermally enhanced hydrolysis for treatment of pesticides and explosives. *Remediation* **2018**, *28*,17–22.

50. Chiron, S.; Fernandez-Alba, A.; Rodriguez, A.; Garcia-Calvo, E. Pesticide chemical oxidation: state of the art. *Water Res.* **2000**, *34*, 366–377.

51. Pérez-Estrada, L. A.; Malato, S.; Gernjak, W.; Aguëra, A.; Thurman, E. M.; Ferrer, I.; Fernández-Alba, A. R. Photo-Fenton degradation of diclofenac: identification of main intermediates and degradation pathway. *Environ. Sci. Technol.* **2005**, *39*, 8300–8306.

52. Lucas, M. S.; Peres, J. A. Decolorization of the azo dye Reactive Black 5 by Fenton and photo-Fenton oxidation. *Dyes Pigm.* **2006**, *71*, 236–244.

53. Comninellis, C.; Kapalka, A.; Malato, S.; Parsons, S. A.; Poulios, I.; Mantzavinos, D. Advanced oxidation processes for water treatment: advances and trends for R&D. *J. Chem. Technol. Biotechnol.* **2008**, *83*, 769–776.

54. Mangun, C. L.; Yue, Z.; Economy, J.; Maloney, S.; Kemme, P.; Cropek, D. Adsorption of organic contaminants from water using tailored ACFs. *Chem. Mater.* **2001**, *13*, 2356– 2360.

55. Lowry, G. V.; Johnson, K. M. Congener-specific dechlorination of dissolved PCBs by microscale and nanoscale zerovalent iron in a water/methanol solution. *Environ. Sci. Technol.* **2004**, *38*, 5208–5216.

56. Acevedo, A.; Carpio, E. A.; Rodriguez, J.; Manzano, M. A. Disinfection of natural water by solar photocatalysis using immobilized TiO2 devices: efficiency in eliminating indicator bacteria and operating life of the system. *J. Sol. Energy Eng.* **2012**, *134*, 011008-1-10.

57. Ghasemzadeh, G.; Momenpour, M.; Omidi, F.; Hosseini, M. R.; Ahani, M.; Barzegari, A. Applications of nanomaterials in water treatment and environmental remediation. *Front. Environ. Sci. Eng.* **2014**, *8*, 471-482.

58. Wayland, H. A.; Boury, S. N.; Chhetri, B. P.; Brandt, A.; Proskurnin, M. A.; Filichkina, V. A.; Zharov, V. P.; Biris, A. S.; Ghosh, A. Advanced Cellulosic Materials for Treatment and Detection of Industrial Contaminants in Wastewater. *ChemistrySelect*, 2016, *1*, 4472-4488.

59. Guerra, F. D.; Attia, M. F.; Whitehead, D. C.; Alexis, F. Nanotechnology for environmental remediation: materials and applications. *Molecules* **2018**, *23*, 1760.

60. Yang, Y. C.; Baker, J. A.; Ward, J. R. Decontamination of chemical warfare agents. *Chem. Rev.* **1992**, *92*, 1729–1743.

61. Tiwari, D. K.; Behari, J.; Sen, P. Application of nanoparticles in waste water treatment. *World Appl. Sci. J.* **2008**, *3*, 417–433.

62. Ahmed, S.; Rasul, M. G.; Martens, W. N.; Brown, R.; Hashib, M. A. Heterogenous photocatalytic degradation of phenols in wastewater: a review on current status and developments. *Desalination* **2010**, *261*, 3–18.

63. Yasmina, M.; Mourad, K.; Mohammed, S. H.; Khaoula, C. Treatment heterogenous photocatalysis: factors influencing the photocatalytic degradation by $TiO_2$. *Energy Proc.* **2014**, *50*, 559–566.

64. Lavand, A. B.; Malghe, Y. S. Visible light photocatalytic degradation of 4-chlorophenol using C/ZnO/CdS nanocomposites. *J. Saudi. Chem. Soc.* **2015**, *19*, 471–478.

65. Sastny, M.; Štengl, V.; Henych, J.; Tolasz, J.; Voma, P. C.; Ederer, J. Mesoporous manganese oxide for the degradation of organophosphates pesticides. *J. Mater. Sci.* **2016**, *51*, 2634– 2642.

66. Bandala, E. R.; Gelover, S.; Leal, M. T.; Arancibia-Bulnes, C.; Jimenez, A.; Estrada, C. A. Solar photocatalytic degradation of Aldrin. *Catal. Today* **2002**, *76*, 189–199.

67. Yu, H.; Wang, X.; Sun, H.; Huo, M. Photocatalytic degradation of malathion in aqueous solution using an Au–Pd–$TiO_2$ nanotube film. *J. Hazard. Mater.* **2010**, *184*, 753–758.

68. Zhang, W. X.; Wang, C. B.; Lien, H. L. Treatment of chlorinated organic contaminants with nanoscale bimetallic particles. *Catal. Today* **1998**, *404*, 387–395.

69. Lien, H. L.; Zhang, W. X. Transformation of chlorinated methanes by nanoscale iron particles. *J. Environ. Eng.* **1999**, *125*, 1042–1047.

70. Lien, H. L.; Zhang, W. X. Nanoscale iron particles for complete reduction of chlorinated ethenes. *Colloids Surf. A* **2001**, *191*, 97–105.

71. Lien, H. L.; Zhang, W. X. Hydrodechlorination of chlorinated ethanes by nanoscale Pd/Fe bimetallic particles. *J. Environ. Eng.* **2005**, *131*, 4–10.

72. Wang, Z.; Peng, P.; Huang, W. Dechlorination of γ-hexachlorocyclohexane by zero-valent metallic iron. *J. Hazard. Mater.* **2009**, *166*, 992–997.

73. Shih, Y.; Hsu, C.; Su, Y. Reduction of hexachlorobenzene by nanoscale zero-valent iron: kinetics, pH effect, and degradation mechanism. *Sep. Purif. Technol.* **2011**, *76*, 268–274.

74. Elliott, D. W.; Lien, H. L.; Zhang, W. X. Degradation of lindane by zero-valent iron nanoparticles. *J. Environ. Eng.* **2009**, *135*, 317–324.

75. Campbell, M. L.; Guerra, F. D.; Dhulekar, J., Alexis, F.; Whitehead, D. C. Target-Specific Capture of Environmentally Relevant Gaseous Aldehydes and Carboxylic Acids with Functional Nanoparticles. *Chem. Eur. J.* **2015**, *21*, 14834-14842.

76. Guerra, F. D.; Campbell, M. L.; Whitehead, D. C., Alexis, F. Tunable properties of functional nanoparticles for efficient capture of VOCs. *ChemistrySelect* **2017**, *2*, 9889- 9894.

77. Guerra, F. D.; Campbell, M. L.; Attia, M. F.; Whitehead, D. C.; Alexis, F. Capture of aldehyde VOCs using a series of amine-functionalized cellulose nanocrystals. *ChemistrySelect* **2018**, *3*, 1-8.

78. Swasy, M. I.; Campbell, M. L.; Brummel, B. R.; Guerra, F. D.; Attia, M. F.; Smith, G. D.' Alexis, F.; Whitehead, D. C. Poly(amine) modified kaolinite clay for VOC capture. *Chemosphere* **2018**, *213*, 19-24.

79. Ateia, M.; Attia, M. F.; Maroli, A.; Tharayil, N.; Alexis, F.; Whitehead, D. C.; Karanfil, T. Rapid Removal of Poly- and Perfluorinated Alkyl Substances by Polyethylenimine-functionalized Cellulose Microcrystals at Environmentally Relevant Conditions. *Environ. Sci. Technol. Lett.* **2018**, *5*, 764-769.

80. Chambers, W. H. Organophosphorous compounds: an overview. In *Oranophosphates, Chemistry, Fate, and Effects*. Chambers J. E., Levi, P. E., Eds.; Academic Press, San Diego, 1992; pp 3-17.

81. Karalliedde, L.; Senanayake, N. Organophosphorus insecticide poisoning. *J. Int. Fed. Clin. Chem.* **1999**, *11*, 4-9.

82. LaGrega, M. D. *Hazardous waste management*. Buckingham P. L, Evans J. C Hazardous waste management, 2nd edn. McGraw-Hill, New York, 2001.

83. Raushel, F. M. Chemical biology: Catalytic detoxification. *Nature* 2011, *469*, 310–311.

84. Sarwar, M. Commonly Available Commercial Insecticide Formulations and Their Applications in the Field. *International Journal of Materials Chemistry and Physics* **2015**, *1*, 116-123.

85. Racke, K. D. Degradation of organophosphorus insecticides in environmental matrices. In *Organophosphates, Chemistry, Fate, and Effects*; Chambers, J. E.; Levi, P. E., Ed.; Academic Press, San Diego, 1992; pp 47-73.

86. Pehkonen, S. O.; Zhang, Q. The degradation of organophosphorus pesticides in natural waters: A critical review. *Crit. Rev. Environ. Sci. Technol.* **2002**, *32*, 17-72.

87. Zhao, X.; Hwang, H. M. A study of the degradation of organophosphorus pesticides in river waters and the identification of their degradation products by chromatography coupled with mass spectrometry. *Arch. Environ. Contam. Toxicol.* **2009**, *56*, 646-653.

88. NIST Chemistry Web Book. https://webbook.nist.gov/cgi/cbook.cgi?ID=C623916&Mask=200#Mass-Spec (accessed Jan. 10, 2019)

89. Bavcon, M.; Trebše, P.; Zupančič-Kralj, L. Investigations of the determination and transformations of diazinon and malathion under environmental conditions using gas chromatography coupled with a flame ionisation detector. *Chemosphere* **2003**, *50*, 595–601.

90. Borwn, M. A.; Petreas, M. X.; Okamoto, H. S.; Mischeke, T.; Stephens, R. D. Monitoring of malathion and its impurities and environmental transformation products on surfaces and in air following an aerial application. *Envir. Sci. Tech.* **1993**, *27*, 388–397.

91. Muir, D. C. G.; Rawn, G. P. Grift, N. P. Fate of the pyrethroid insecticide deltamethrin in small ponds: a mass balance study. *J. Agric. Food Chem.* **1985**, *33*, 603-609.

92. Erstfeld, K. M. Environmental fate of synthetic pyrethroids during spray drift and field runoff treatments in aquatic microcosms. *Chemosphere* **1999**, *39*, 1737-1769.

93. Chen, S.; Lai, K.; Li, Y.; Hu, M.; Zhang, Y.; Zeng, Y. Biodegradation of deltamethrin and its hydrolysis product 3-phenoxybenzaldehyde by a newly isolated Streptomyces aureus strain HP-S-01. *Appl. Microbiol. Biotechnol.* **2011**, *90*, 1471–1483.

94. NIST Chemistry Web Book. https://webbook.nist.gov/cgi/cbook.cgi?Name=3-Phenoxyphenylacetonitrile+&Units=SI&cMS=on#Mass-Spec (accessed March. 15, 2019).

95. Wynne, J. H.; Fulmer, P. A.; McCluskey, D. M.; Mackey, N. M.; Buchanan, J. P. Synthesis and Development of a Multifunctional Self- Decontaminating Polyurethane Coating. *ACS Appl. Mater. Interfaces* **2011**, *3*, 2005–2011.

96. Obendorf, S. K. Improving Personal Protection Through Novel Materials. *AATCC Review* **2010**, *10*, 44–50.

97. Zhu, J.; Bahramian, Q.; Gibson, P.; Schreuder-Gibson, H.; Sun, G. Chemical and Biological Decontamination Functions of Nano- fibrous Membranes. *J. Mater. Chem.* **2012**, *22*, 8532–8540.

98. Salter, B.; Owens, J.; Hayn, R.; McDonald, R.; Shannon, E. N- chloramide Modified Nomex® as a Regenerable Self-Decontaminating Material for Protection Against Chemical Warfare Agents. *J. Mater. Sci.* **2009**, *44*, 2069–2078.

99. Bromberg, L.; Creasy, W. R.; McGarvey, D. J.; Wilusz, E.; Hatton, T. A. Nucleophilic Polymers and Gels in Hydrolytic Degradation of Chemical Warfare Agents. *ACS Appl. Mater. Interfaces* **2015**, *7*, 22001–22011.

100. Isogai, A.; Bergström, L. Preparation of cellulose nanofibers using green and sustainable chemistry. *Curr. Opin. Green Sustain. Chem.* **2018**, *12*, 15–21.

Appendix A

Supplementary Information for Chapter 2

FUNCTIONAL PEPTIDES FOR ENANTIOSELECTIVE HYPERVALENT IODINE(III)-MEDIATED CHEMISTRY

$^{1}$H NMR Spectra of Racemic **II-2**, 1-oxo-1-phenylpropan-2-yl-4-methylbenzenesulfonate

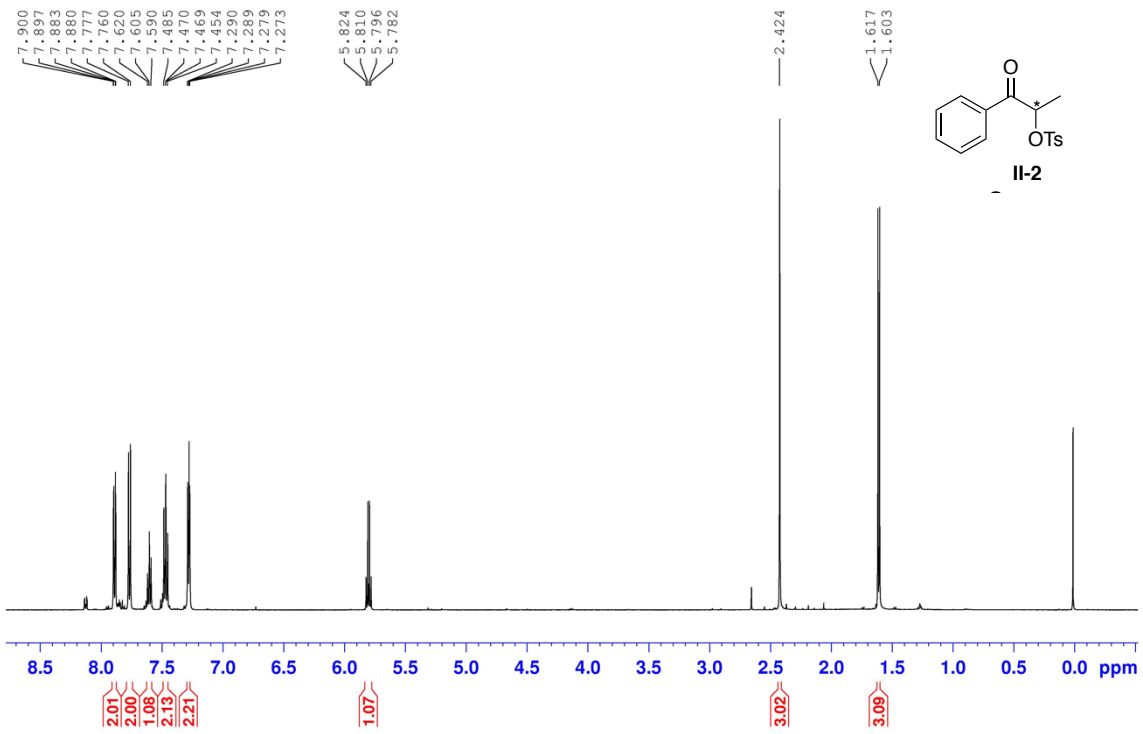

$^{13}$C NMR Spectra of Racemic **II-2**, 1-oxo-1-phenylpropan-2-yl-4-methylbenzenesulfonate

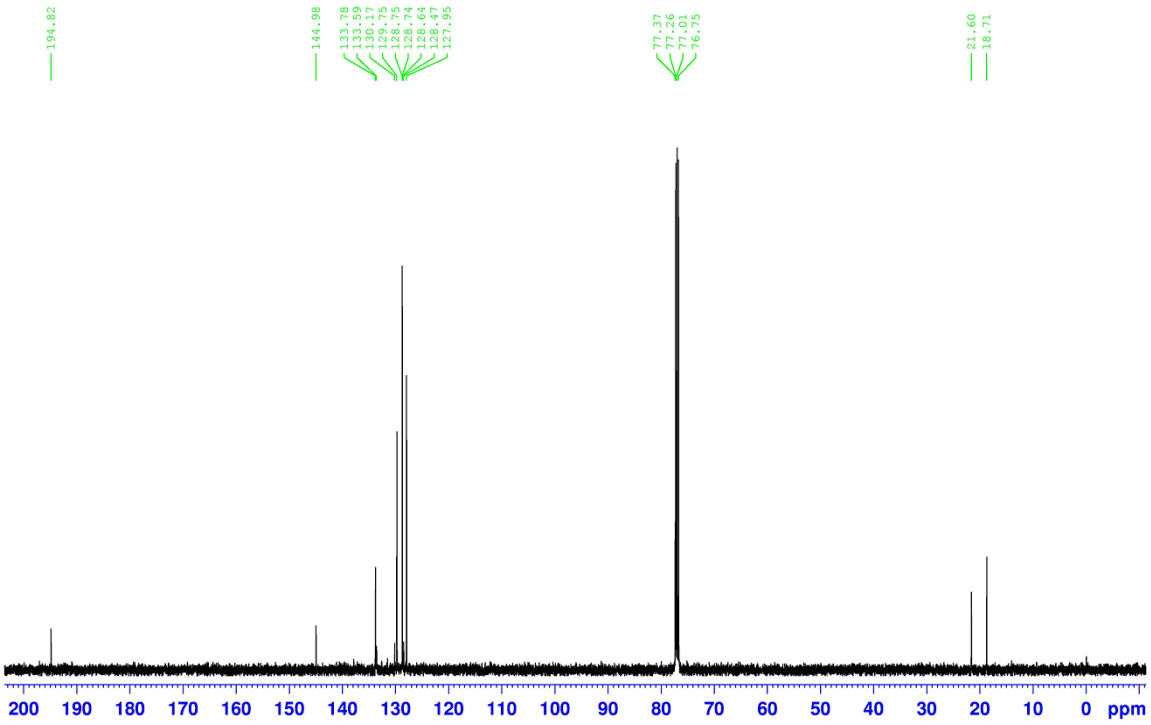

HPLC Chromatogram of Racemic **II-2**, 1-oxo-1-phenylpropan-2-yl-4-methylbenzenesulfonate

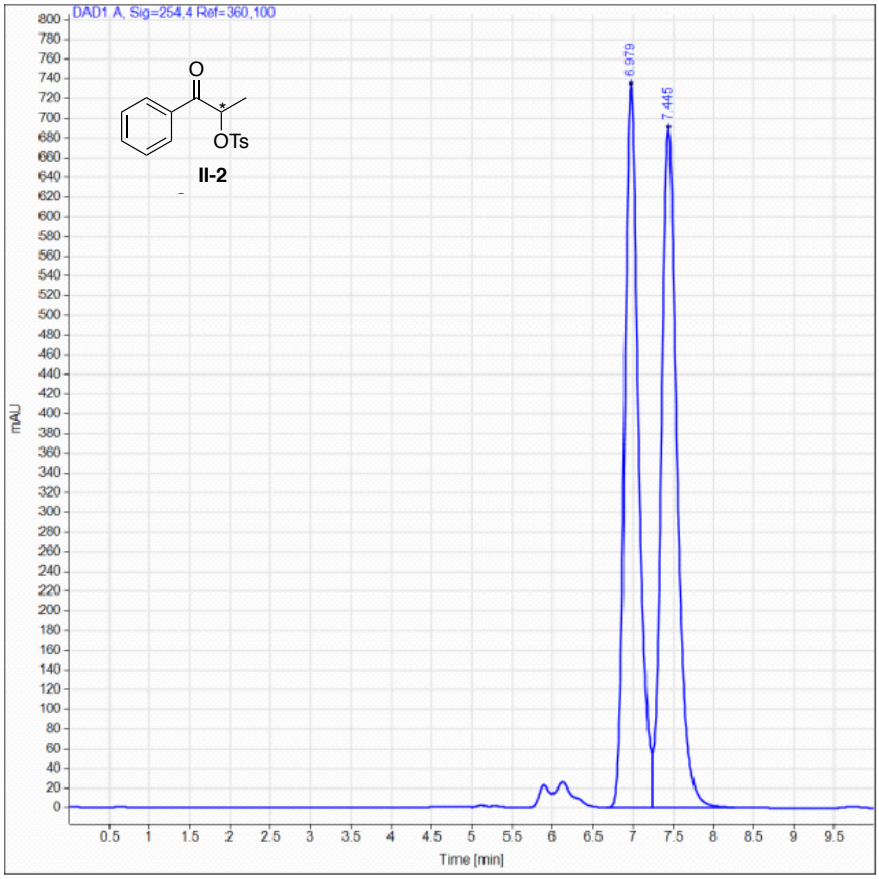


**Signal:** DAD1 A, Sig=254,4 Ref=360,100

| RT [min] | Type | Width [min] | Area | Height | Area% | Name |
|---|---|---|---|---|---|---|
| 6.979 | BV | 0.1832 | 8862.8965 | 732.5300 | 48.9902 | |
| 7.445 | VB | 0.2025 | 9228.2725 | 687.8895 | 51.0098 | |
| | | Sum | 18091.1689 | | | |

"Hit" Peptides and the corresponding HPLC Chromatograms for the α-Oxytosylation of Propiophenone Product **II-2**, Enantiomer RT = ~7.1 and ~7.6.

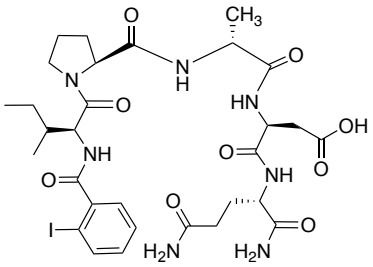

**II-13**
2-IBA-Ile-Pro-D-Ala-Asp-Gln
48% *ee*

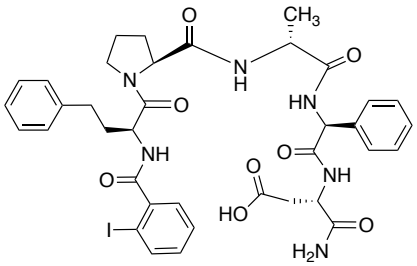

**II-14**
2-IBA-hPhe-Pro-D-Ala-Phg-Asp
23% *ee*

HPLC Trace for Peptide **II-13**, 48% ee

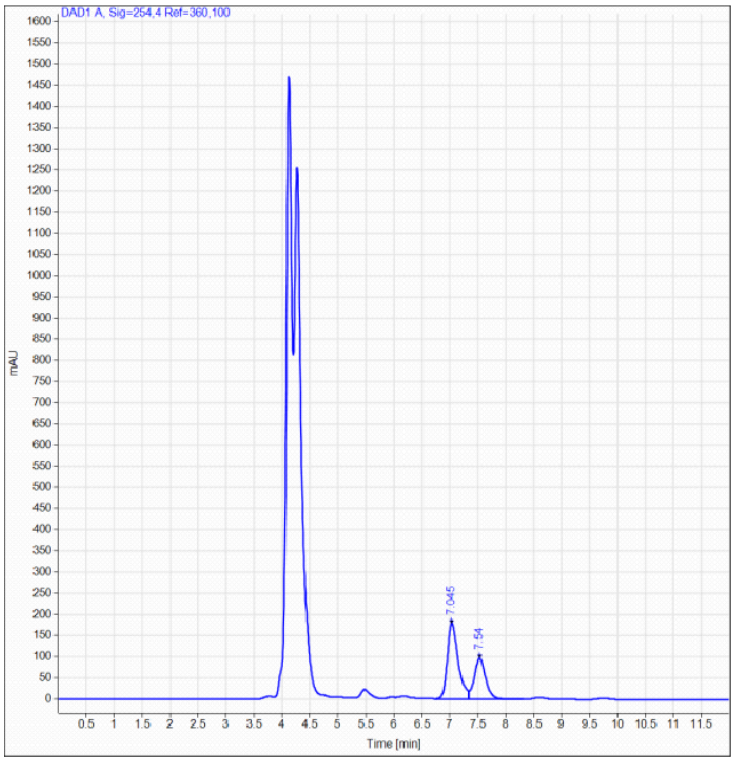


**Signal:** DAD1 A, Sig=254,4 Ref=360,100

| RT [min] | Type | Width [min] | Area | Height | Area% | Name |
|---|---|---|---|---|---|---|
| 7.045 | BV | 0.2072 | 2431.0994 | 178.1330 | 64.0814 | |
| 7.540 | VB | 0.2130 | 1362.6653 | 96.3601 | 35.9186 | |
| | | Sum | 3793.7646 | | | |

HPLC Trace for Peptide **II-14**, 23% ee

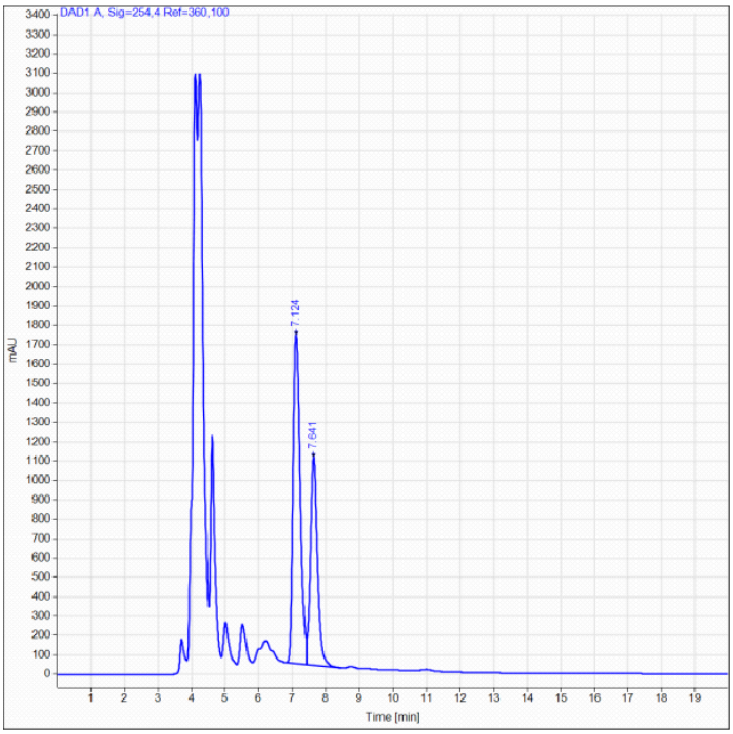


**Signal:** DAD1 A, Sig=254,4 Ref=360,100

| RT [min] | Type | Width [min] | Area | Height | Area% | Name |
|---|---|---|---|---|---|---|
| 7.124 | BV | 0.2374 | 25547.2715 | 1698.9398 | 61.7190 | |
| 7.641 | VB | 0.2217 | 15845.5850 | 1076.6442 | 38.2810 | |
| | | Sum | 41392.8564 | | | |

[1]H NMR Spectra of Racemic **II-4**, 5-benzoyldihydrofuran-2(3H)-one

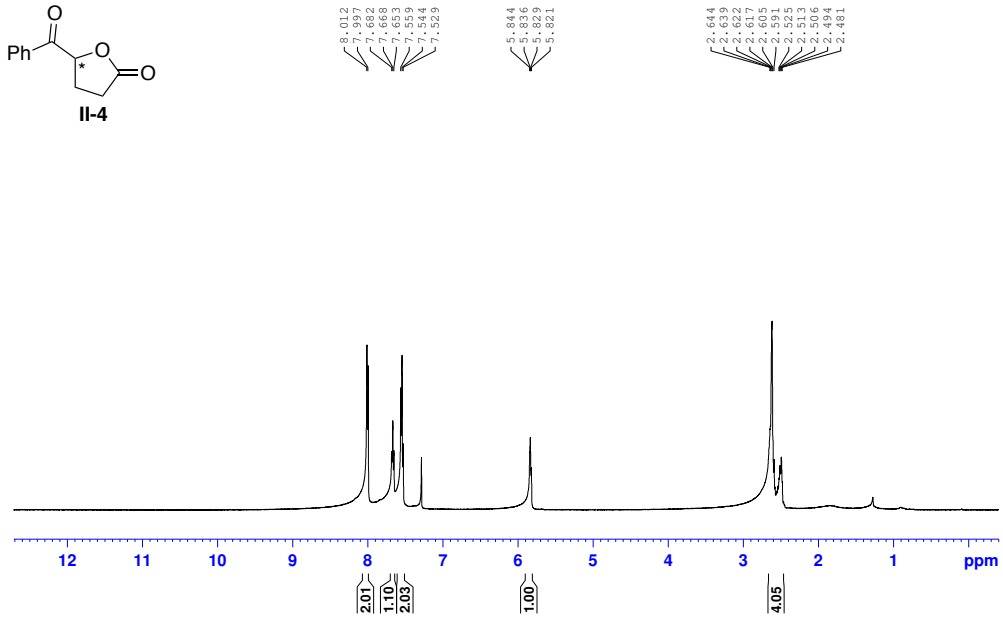

$^{13}$C NMR Spectra of Racemic **II-4**, 5-benzoyldihydrofuran-2(3H)-one

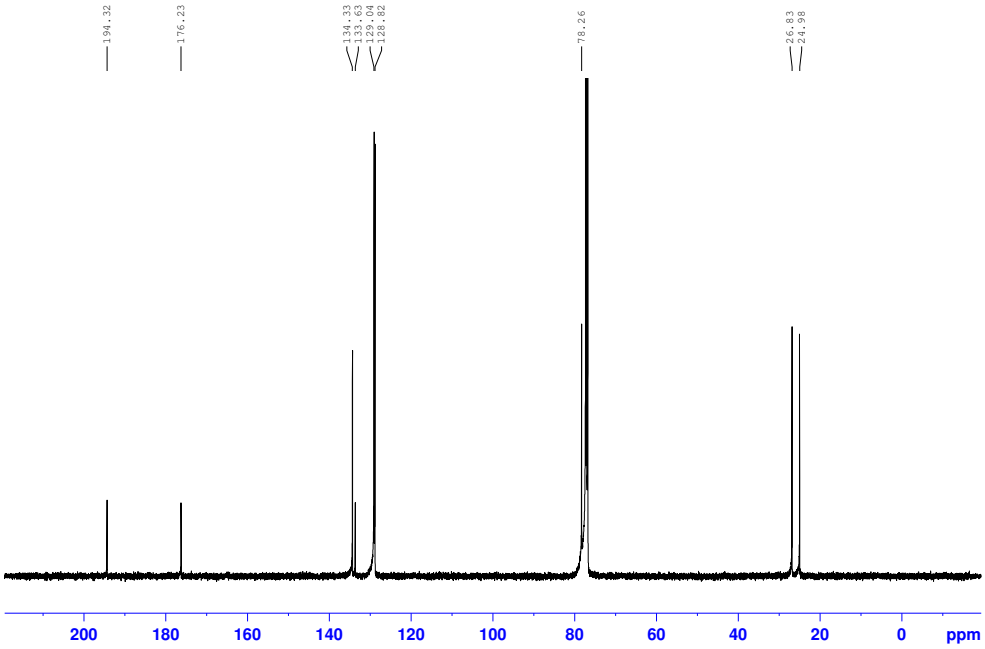

Chiral HPLC Spectra of Racemic **II-4**, 5-benzoyldihydrofuran-2(3H)-one

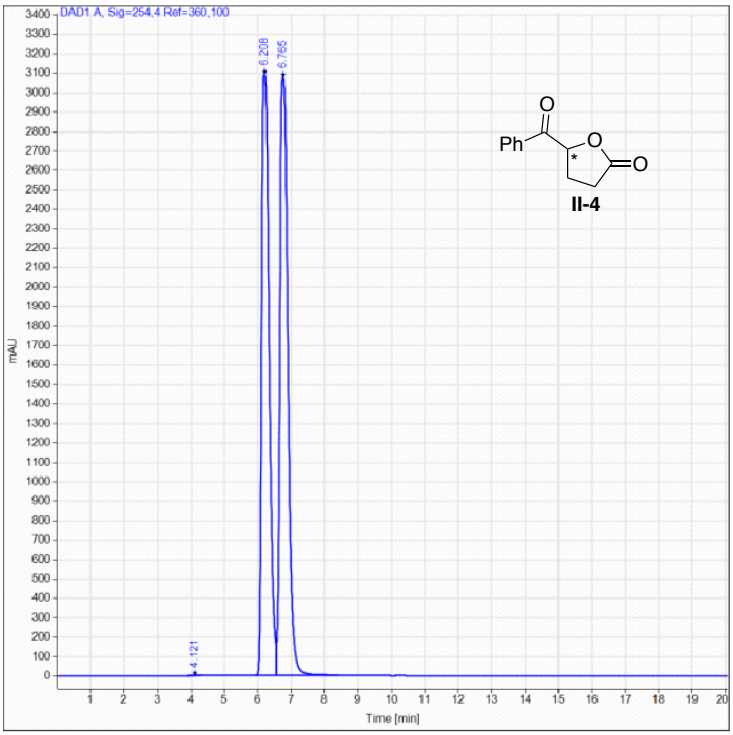


**Signal:** DAD1 A, Sig=254,4 Ref=360,100

| RT [min] | Type | Width [min] | Area | Height | Area% | Name |
|---|---|---|---|---|---|---|
| 4.121 | BB | 0.1337 | 9.6778 | 1.0479 | 0.0097 | |
| 6.208 | BV | 0.2416 | 48204.7266 | 3096.3640 | 48.4590 | |
| 6.765 | VB | 0.2581 | 51260.8086 | 3080.5359 | 51.5312 | |
| | | Sum | 99475.2130 | | | |

“Hit” Peptides for the Oxidative Cyclization of 5-oxo-5-Phenylvaleric Acid

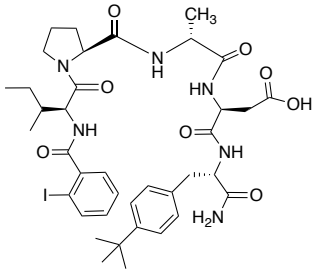

**II-15**
2-IBA-Ile-Pro-D-Ala-Asp-tPhe
10% *ee*

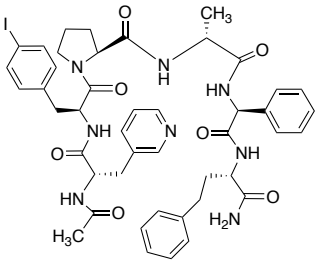

**II-16**
3-Pya-4-I-Phe-Pro-D-Ala-Phg-hPhe
-18% *ee*

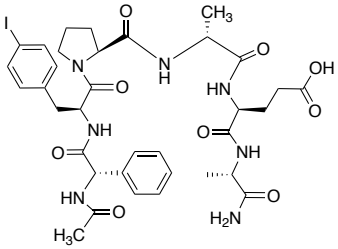

**II-17**
Phg-4-I-Phe-Pro-D-Ala-Glu-Ala
-16% *ee*

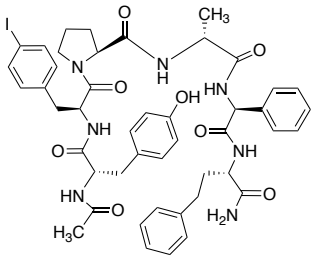

**II-18**
Tyr—4-I-Phe-Pro-D-Ala-Phg-hPhe
-22% *ee*

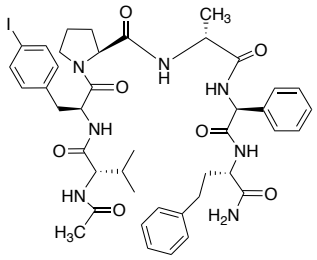

**II-19**
Val-4-I-Phe-Pro-D-Ala-Phg-hPhe
-20% *ee*

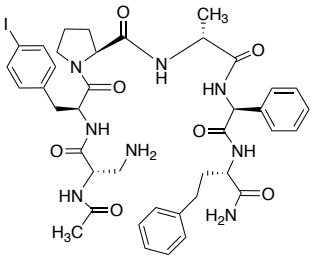

**II-20**
Dap-4-I-Phe-Pro-D-Ala-Glu-Ala
-24% *ee*

HPLC Trace for Peptide **II-15**, 10% *ee*

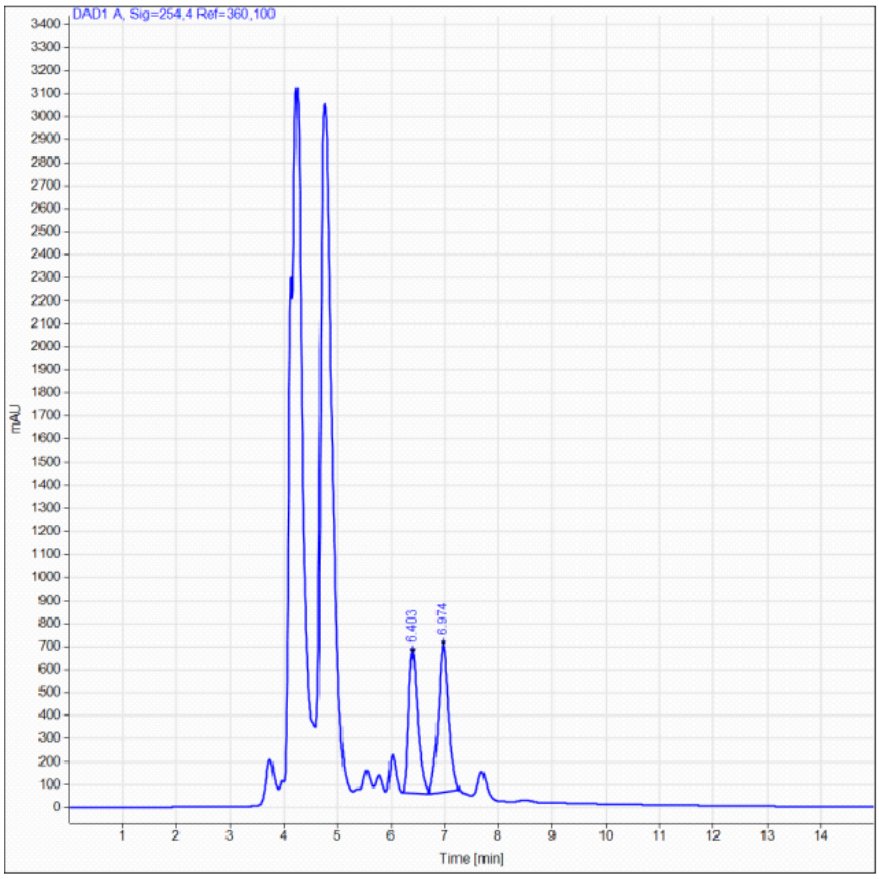


**Signal:** DAD1 A, Sig=254,4 Ref=360,100

| RT [min] | Type | Width [min] | Area | Height | Area% | Name |
|---|---|---|---|---|---|---|
| 6.403 | BV | 0.1762 | 7136.9219 | 611.2090 | 44.7990 | |
| 6.974 | MM | 0.2302 | 8794.0771 | 636.7302 | 55.2010 | |
| | | Sum | 15930.9990 | | | |

HPLC Trace for Peptide **II-16**, 18% *ee*

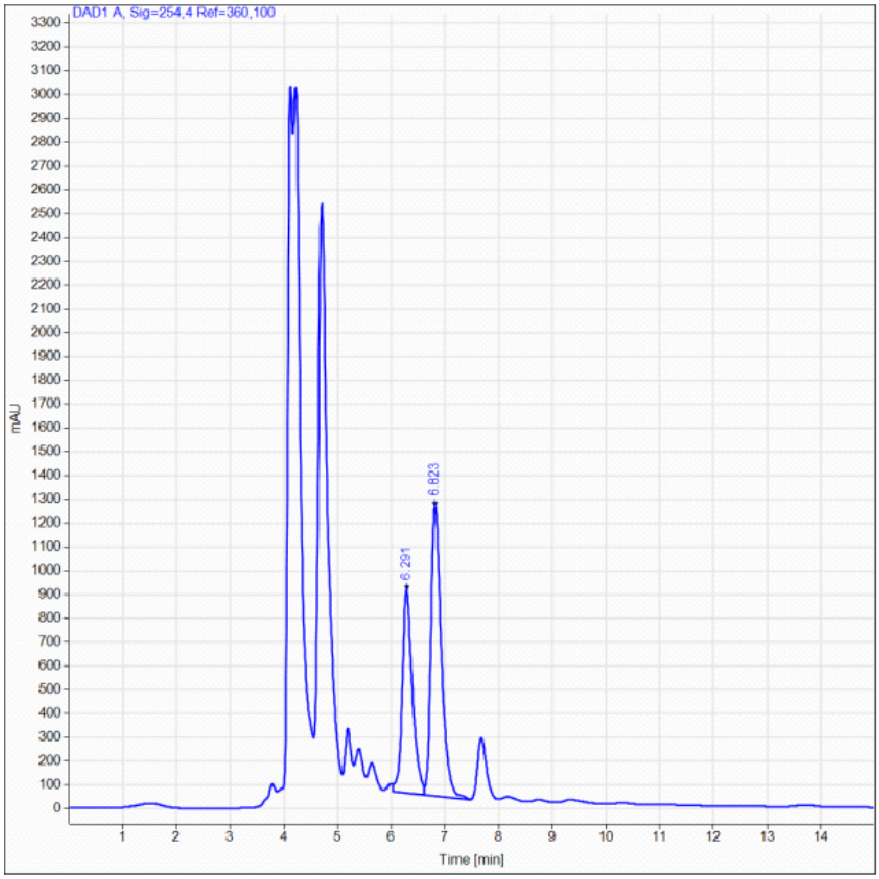


**Signal:** DAD1 A, Sig=254,4 Ref=360,100

| RT [min] | Type | Width [min] | Area | Height | Area% | Name |
|---|---|---|---|---|---|---|
| 6.291 | VV | 0.1935 | 11084.7988 | 853.7969 | 40.6650 | |
| 6.823 | VB | 0.2009 | 16174.0029 | 1218.1382 | 59.3350 | |
| | | Sum | 27258.8018 | | | |

HPLC Trace for Peptide **II-17**, 16% *ee*

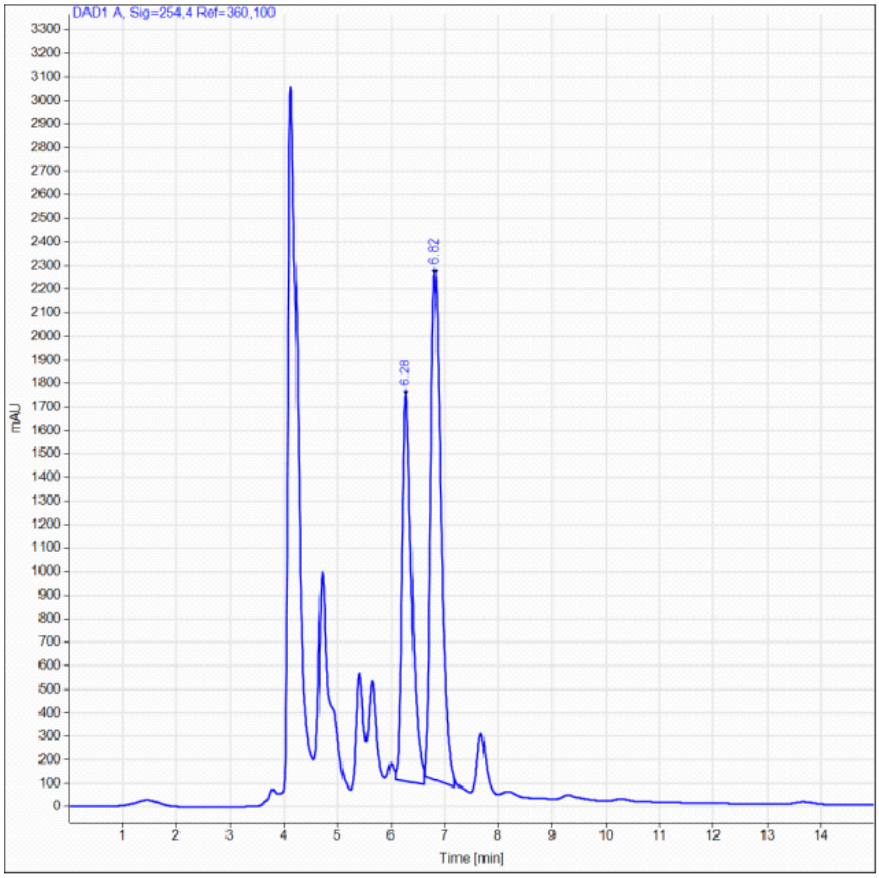


**Signal:** DAD1 A, Sig=254,4 Ref=360,100

| RT [min] | Type | Width [min] | Area | Height | Area% | Name |
|---|---|---|---|---|---|---|
| 6.280 | VV | 0.1887 | 20614.3730 | 1638.9723 | 42.1122 | |
| 6.820 | MM | 0.2199 | 28336.6992 | 2147.8640 | 57.8878 | |
| | | Sum | 48951.0723 | | | |

HPLC Trace for Peptide **II-18**, 22% *ee*

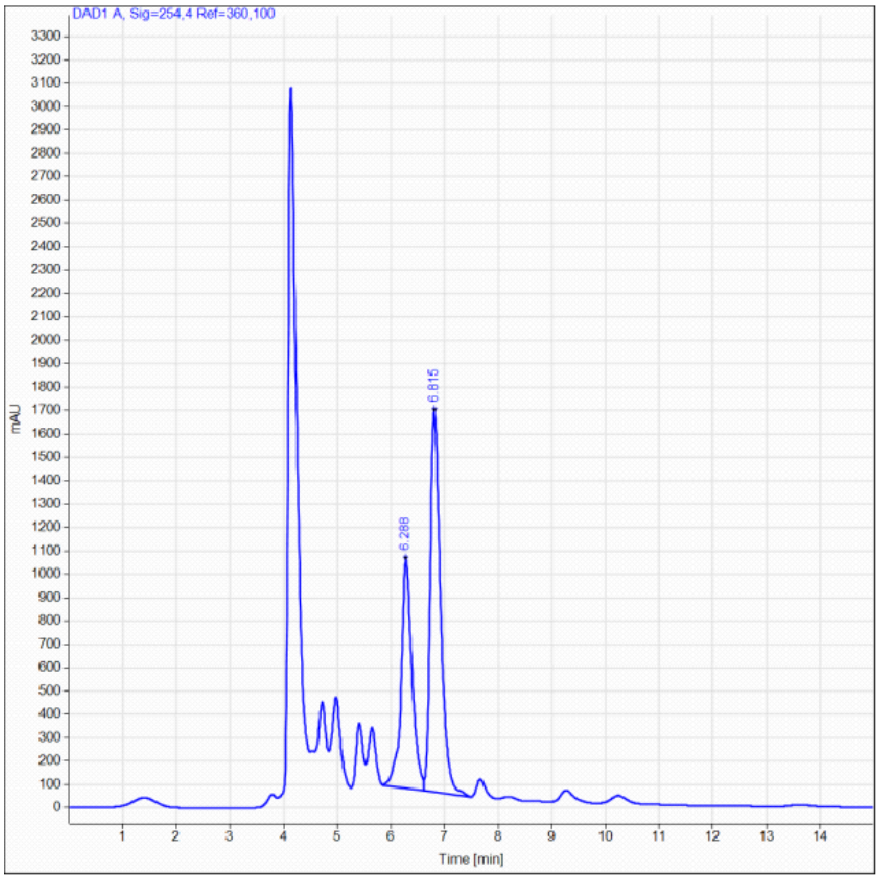


**Signal:** DAD1 A, Sig=254,4 Ref=360,100

| RT [min] | Type | Width [min] | Area | Height | Area% | Name |
|---|---|---|---|---|---|---|
| 6.288 | BV | 0.2065 | 13794.9414 | 978.3549 | 39.0368 | |
| 6.815 | VB | 0.2005 | 21543.3418 | 1626.4016 | 60.9632 | |
| | | Sum | 35338.2832 | | | |

HPLC Trace for Peptide **II-19**, 20% *ee*

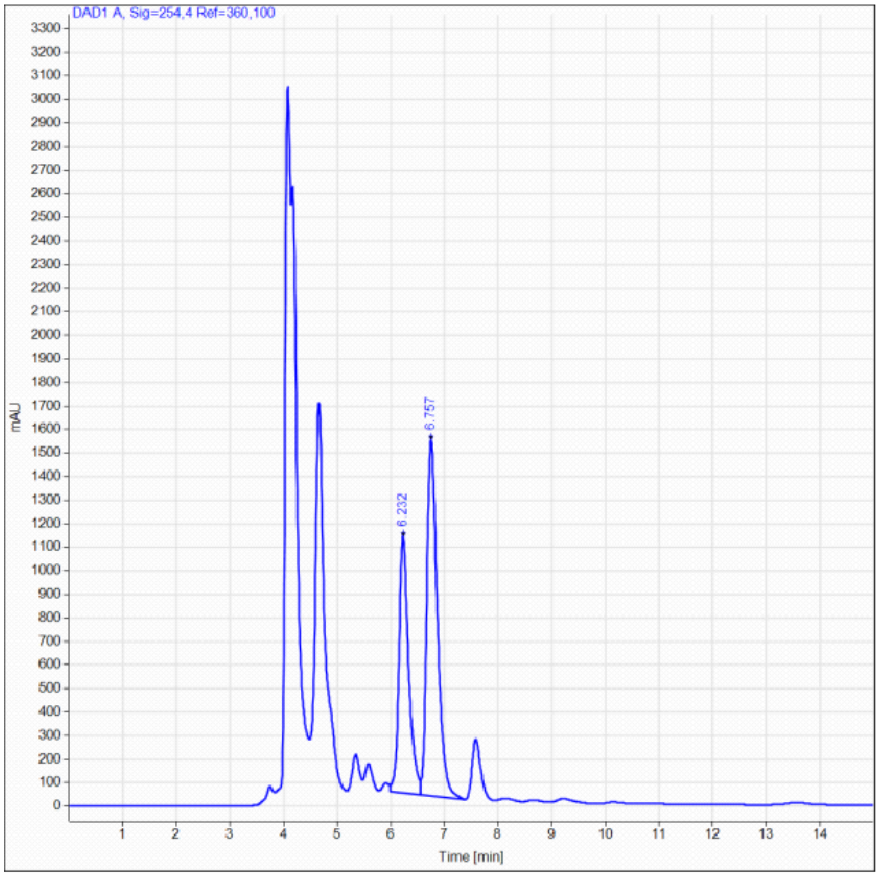


**Signal:** DAD1 A, Sig=254,4 Ref=360,100

| RT [min] | Type | Width [min] | Area | Height | Area% | Name |
|---|---|---|---|---|---|---|
| 6.232 | VV | 0.1878 | 13837.4365 | 1092.0048 | 40.1872 | |
| 6.757 | VB | 0.2069 | 20595.0137 | 1512.5914 | 59.8128 | |
| | | Sum | 34432.4502 | | | |

HPLC Trace for Peptide **II-20**, 24% *ee*

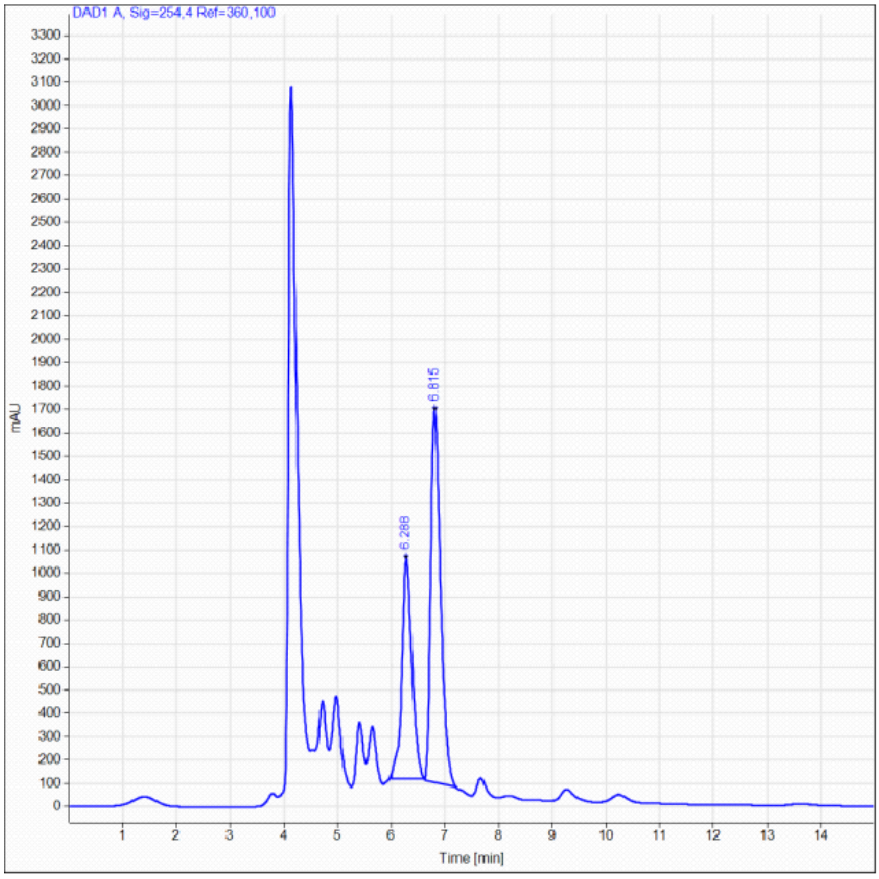


**Signal:** DAD1 A, Sig=254,4 Ref=360,100

| RT [min] | Type | Width [min] | Area | Height | Area% | Name |
|---|---|---|---|---|---|---|
| 6.288 | MM | 0.2169 | 12255.1992 | 941.9001 | 37.9082 | |
| 6.815 | MM | 0.2103 | 20073.3848 | 1590.5735 | 62.0918 | |
| | | Sum | 32328.5840 | | | |

1st Generation Aryl-Iodo Peptides Screened in the α-Oxytosylation of Propiophenone

Table A1: Scaffold A Peptides

| Sequence | Exact Mass | Calc. [M+H]+ | Calc. [M+Na]+ | Observed [M+H]+ or [M+Na]+ | % *ee* of II-2 |
|---|---|---|---|---|---|
| Ac-Asn-4-I-Phe-Pro-D-Ala-Trp-Glu | 929.2569 | 930.2649 | 952.2461 | 930.10 | 9.7 |
| Ac-Ile-4-I-Phe-Pro-D-Ala-Ala-Ala | 755.2503 | 756.2583 | 778.2395 | 756.10 | 0 |
| Ac-Nva-4-I-Phe-Pro-D-Ala-Asp-Tyr | 877.2507 | 878.2587 | 900.2399 | 878.10 | 8.6 |
| Ac-Phe-4-I-Phe-Pro-D-Ala-hPhe-Dap | 894.2925 | 895.3005 | 917.2817 | 895.14 | 14.3 |
| Ac-Nle-4-I-Phe-Pro-D-Ala-Thr-Ala | 785.2609 | 786.2689 | 808.2501 | 808.40 | 0 |
| Ac-Leu-4-I-Phe-Pro-D-Ala-Lys-Val | 840.3395 | 841.3475 | 863.3287 | 841.19 | NP |
| Ac-Tle-4-I-Phe-Pro-D-Ala-Ile-Dap | 812.3082 | 813.3162 | 835.2974 | 813.16 | 12.4 |
| Ac-Trp-4-I-Phe-Pro-D-Ala-Ala-Glu | 886.2511 | 887.2591 | 909.2403 | 887.10 | 4.6 |
| Ac-Nle-4-I-Phe-Pro-D-Ala-Ile-Tle | 839.3442 | 840.3522 | 862.3334 | 862.48 | 8.8 |
| Ac-Tyr-4-I-Phe-Pro-D-Ala-Ile-hPhe | 937.3235 | 938.3315 | 960.3127 | 960.46 | NP |
| Ac-Tle-4-I-Phe-Pro-D-Ala-Bip-Leu | 949.3599 | 950.3679 | 972.3491 | 972.59 | 0 |
| Ac-Tyr-4-I-Phe-Pro-D-Ala-Thr-Ser | 851.2351 | 852.2431 | 874.2243 | 852.08 | 3.6 |
| Ac-Asp-4-I-Phe-Pro-D-Ala-Ala-Gln | 814.2147 | 815.2227 | 837.2039 | 837.46 | 8.6 |
| Ac-Dap-4-I-Phe-Pro-D-Ala-Ile-dPhe | 922.3238 | 923.3318 | 945.313 | 923.17 | 3.6 |
| Ac-Nva-4-I-Phe-Pro-D-Ala-Thr-hPhe | 861.2922 | 862.3002 | 884.2814 | 862.14 | 7.3 |
| Ac-Bip-4-I-Phe-Pro-D-Ala-Tle-Ile | 949.3599 | 950.3679 | 972.3491 | 950.21 | 8.6 |
| Ac-Asn-4-I-Phe-Pro-D-Ala-Ser-Dap | 787.215 | 788.223 | 810.2042 | 788.06 | 6.6 |
| Ac-Nva-4-I-Phe-Pro-D-Ala-Nle-His | 849.3034 | 850.3114 | 872.2926 | 850.15 | 3.8 |
| Ac-Ile-4-I-Phe-Pro-D-Ala-Phe-Lys | 888.3395 | 889.3475 | 911.3287 | 889.51 | 16 |
| Ac-Lys-4-I-Phe-Pro-D-Ala-Tyr-Nva | 890.3188 | 891.3268 | 913.308 | 891.17 | 12.4 |
| Ac-Tle-4-I-Phe-Pro-D-Ala-hPhe-Val | 873.8345 | 874.8425 | 896.8237 | 896.97 | 9.6 |
| Ac-Phg-4-I-Phe-Pro-D-Ala-hPhe-Leu | 907.3129 | 908.3209 | 930.3021 | 930.54 | NP |
| Ac-Ser-4-I-Phe-Pro-D-Ala-Nle-Abu | 785.2609 | 786.2689 | 808.2501 | 808.49 | 0 |
| Ac-Leu-4-I-Phe-Pro-D-Ala-Lys-Val | 840.3395 | 841.3475 | 863.3287 | 863.57 | 4.6 |
| Ac-Ala-4-I-Phe-Pro-D-Ala-Ile-Glu | 813.2558 | 814.2638 | 836.245 | 836.49 | 8.7 |
| Ac-Nva-4-I-Phe-Pro-D-Ala-4-Pya-2-Nap | 895.2878 | 896.2958 | 918.277 | 918.52 | NP |
| Ac-Phe-4-I-Phe-Pro-D-Ala-dPhe-Nle | 983.3442 | 984.3522 | 1006.3334 | 984.19 | 3.8 |
| Ac-dPhe-4-I-Phe-Pro-D-Ala-Tle-Thr | 937.3235 | 938.3315 | 960.3127 | 938.17 | 9.4 |
| Ac-Thr-4-I-Phe-Pro-D-Ala-Bip-1-Nap | 1021.3235 | 1022.3315 | 1044.3127 | 1022.17 | 1.2 |
| Ac-Phg-4-I-Phe-Pro-D-Ala-Nva-Phe | 879.2816 | 880.2896 | 902.2708 | 880.13 | 7.6 |
| Ac-2-Pya-4-I-Phe-Pro-D-Ala-Glu-Phe | 924.2667 | 925.2747 | 947.2559 | 925.11 | NP |
| Ac-1-Nap-4-I-Phe-Pro-D-Ala-Orn-Tle | 924.3395 | 925.3475 | 947.3287 | 925.20 | 2.3 |

| | | | | | |
|---|---|---|---|---|---|
| Ac-1-Nap-4-I-Phe-Pro-D-Ala-Asp-Ile | 925.2871 | 926.2951 | 948.2763 | 926.14 | 13.2 |
| Ac-Leu-4-I-Phe-Pro-D-Ala-hPhe-Leu | 887.3442 | 888.3522 | 910.3334 | 888.19 | 6.5 |
| Ac-1-Nap-4-I-Phe-Pro-D-Ala-Nle-Phg | 943.3129 | 944.3209 | 966.3021 | 944.16 | 3.4 |
| Ac-Nva-4-I-Phe-Pro-D-Ala-Ser-Tyr | 849.2558 | 850.2638 | 872.245 | 850.10 | 2.7 |
| Ac-Bip-4-I-Phe-Pro-D-Ala-Nva-Ala | 893.2973 | 894.3053 | 916.2865 | 916.55 | NP |
| Ac-Ile-4-I-Phe-Pro-D-Ala-dPhe-Ser | 923.3079 | 924.3159 | 946.2971 | 946.56 | 6.5 |
| Ac-Ile-4-I-Phe-Pro-D-Ala-Asn-Ser | 814.2511 | 815.2591 | 837.2403 | 837.50 | 10 |
| Ac-Glu-4-I-Phe-Pro-D-Ala-Abu-Glu | 843.23 | 844.238 | 866.2192 | 866.48 | 3.4 |
| Ac-Trp-4-I-Phe-Pro-D-Ala-Orn-Thr | 901.2984 | 902.3064 | 924.2876 | 924.55 | 5.4 |
| Ac-Asn-4-I-Phe-Pro-D-Ala-hPhe-Val | 874.2875 | 875.2955 | 897.2767 | 897.54 | 3.7 |
| Ac-Gln-4-I-Phe-Pro-D-Ala-2-Nap-dPhe | 1048.9805 | 1049.9885 | 1071.9697 | 1072.23 | 11.6 |
| Ac-Dap-4-I-Phe-Pro-D-Ala-Glu-Ser | 802.2147 | 803.2227 | 825.2039 | 825.46 | 9.6 |
| Ac-dPhe-4-I-Phe-Pro-D-Ala-Orn-3-Pya | 985.3347 | 986.3427 | 1008.3239 | 1008.58 | 14.8 |
| Ac-Gln-4-I-Phe-Pro-D-Ala-Nle-tPhe | 873.3286 | 874.3366 | 896.3178 | 896.58 | 2.8 |
| Ac-4-Pya-4-I-Phe-Pro-D-Ala-Ala-3-Pya | 867.2565 | 868.2645 | 890.2457 | 890.51 | 17.3 |
| Ac-Val-4-I-Phe-Pro-D-Ala-hPhe-Trp | 946.3238 | 947.3318 | 969.313 | 969.57 | 12.2 |
| Ac-Dap-4-I-Phe-Pro-D-Ala-Nva-Phe | 818.2612 | 819.2692 | 841.2504 | 841.09 | 6.8 |
| Ac-Gln-4-I-Phe-Pro-D-Ala-Ser-Ala | 786.2198 | 787.2278 | 809.209 | 809.05 | 2.9 |
| Ac-Orn-4-I-Phe-Pro-D-Ala-Tyr-tPhe | 980.3657 | 981.3737 | 1003.3549 | 1003.19 | 7.4 |
| Ac-Leu-4-I-Phe-Pro-D-Ala-Dap-Orn | 813.3034 | 814.3114 | 836.2926 | 836.13 | 4.6 |
| Ac-Val-4-I-Phe-Pro-D-Ala-Phg-hPhe | 893.2973 | 894.3053 | 916.2865 | 894.15 | 12.4 |
| Ac-Phe-4-I-Phe-Pro-D-Ala-Phg-hPhe | 941.2973 | 942.3053 | 964.2865 | 942.15 | 2.6 |
| Ac-Dap-4-I-Phe-Pro-D-Ala-Phg-hPhe | 880.2769 | 881.2849 | 903.2661 | 881.12 | 3.8 |
| Ac-Asp-4-I-Phe-Pro-D-Ala-Phg-hPhe | 909.2558 | 910.2638 | 932.245 | 910.10 | 11.6 |
| Ac-Abu-4-I-Phe-Pro-D-Ala-Phg-hPhe | 879.2816 | 880.2896 | 902.2708 | 880.13 | 8.9 |
| Ac-tPhe-4-I-Phe-Pro-D-Ala-Phg-hPhe | 997.3599 | 998.3679 | 1020.3491 | 998.21 | 6.4 |
| Ac-Gln-4-I-Phe-Pro-D-Ala-Phg-hPhe | 922.2875 | 923.2955 | 945.2767 | 923.14 | 6.3 |
| Ac-Ser-4-I-Phe-Pro-D-Ala-Phg-hPhe | 881.2609 | 882.2689 | 904.2501 | 882.11 | 11.2 |
| Ac-Ala-4-I-Phe-Pro-D-Ala-Phg-hPhe | 865.266 | 866.274 | 888.2552 | 888.44 | 2.5 |
| Ac-Trp-4-I-Phe-Pro-D-Ala-Phg-hPhe | 980.3082 | 981.3162 | 1003.2974 | 1003.48 | 9.4 |
| Ac-Glu-4-I-Phe-Pro-D-Ala-Phg-hPhe | 923.2715 | 924.2795 | 946.2607 | 946.44 | 3.5 |
| Ac-Nva-4-I-Phe-Pro-D-Ala-Phg-hPhe | 893.2973 | 894.3053 | 916.2865 | 916.47 | 11.3 |
| Ac-Leu-4-I-Phe-Pro-D-Ala-Phg-hPhe | 907.3129 | 908.3209 | 930.3021 | 930.48 | 7.4 |
| Ac-Bip-4-I-Phe-Pro-D-Ala-Phg-hPhe | 1017.3286 | 1018.3366 | 1040.3178 | 1040.50 | 0 |
| Ac-Tle-4-I-Phe-Pro-D-Ala-Phg-hPhe | 907.3129 | 908.3209 | 930.3021 | 930.48 | 9.2 |
| Ac-His-4-I-Phe-Pro-D-Ala-Phg-hPhe | 931.2878 | 932.2958 | 954.277 | 954.46 | 5.4 |
| Ac-Asn-4-I-Phe-Pro-D-Ala-Phg-hPhe | 908.2718 | 909.2798 | 931.261 | 931.44 | 7.1 |
| Ac-Tyr-4-I-Phe-Pro-D-Ala-Phg-hPhe | 957.2922 | 958.3002 | 980.2814 | 980.46 | 10.5 |

| | | | | | |
|---|---|---|---|---|---|
| Ac-Phg-4-I-Phe-Pro-D-Ala-Phg-hPhe | 927.2816 | 928.2896 | 950.2708 | 950.45 | NP |
| Ac-Thr-4-I-Phe-Pro-D-Ala-Phg-hPhe | 895.2766 | 896.2846 | 918.2658 | 918.45 | 2.6 |
| Ac-Lys-4-I-Phe-Pro-D-Ala-Phg-hPhe | 922.3238 | 923.3318 | 945.313 | 945.49 | 14.7 |
| Ac-Nle-4-I-Phe-Pro-D-Ala-Phg-hPhe | 907.3129 | 908.3209 | 930.3021 | 930.48 | 3.8 |
| Ac-Orn-4-I-Phe-Pro-D-Ala-Phg-hPhe | 908.3082 | 909.3162 | 931.2974 | 931.48 | 4.3 |
| Ac-hPhe-4-I-Phe-Pro-D-Ala-Phg-hPhe | 955.3129 | 956.3209 | 978.3021 | 978.48 | 0 |
| Ac-dPhe-4-I-Phe-Pro-D-Ala-Phg-hPhe | 1017.3286 | 1018.3366 | 1040.3178 | 1040.50 | 12.9 |
| Ac-1-Nap-4-I-Phe-Pro-D-Ala-Phg-hPhe | 991.3129 | 992.3209 | 1014.3021 | 1014.12 | 6.7 |
| Ac-4-Pya-4-I-Phe-Pro-D-Ala-Phg-hPhe | 942.2925 | 943.3005 | 965.2817 | 965.10 | 0 |
| Ac-2-Nap-4-I-Phe-Pro-D-Ala-Phg-hPhe | 991.3129 | 992.3209 | 1014.3021 | 1014.12 | NP |
| Ac-3-Pya-4-I-Phe-Pro-D-Ala-Phg-hPhe | 942.2925 | 943.3005 | 965.2817 | 965.10 | 8.6 |
| Ac-2-Pya-4-I-Phe-Pro-D-Ala-Phg-hPhe | 942.2925 | 943.3005 | 965.2817 | 943.14 | 4.8 |
| Ac-Bip-4-I-Phe-Pro-D-Ala-Tle-hPhe | 949.3599 | 950.3679 | 972.3491 | 950.21 | 12.4 |
| Ac-Nle-4-I-Phe-Pro-D-Ala-Bip-Asp | 951.3028 | 952.3108 | 974.292 | 952.15 | 8.4 |
| Ac-Thr-4-I-Phe-Pro-D-Ala-Ser-Asp | 803.1987 | 804.2067 | 826.1879 | 804.05 | 2.4 |
| Ac-Thr-4-I-Phe-Pro-D-Ala-Ala-Nle | 785.2609 | 786.2689 | 808.2501 | 786.11 | 0 |
| Ac-Ala-4-I-Phe-Pro-D-Ala-Ser-Ile | 771.2453 | 772.2533 | 794.2345 | 772.09 | 2.8 |
| Ac-hPhe-4-I-Phe-Pro-D-Ala-Bip-Tle | 997.3599 | 998.3679 | 1020.3491 | 998.21 | 5.4 |
| Ac-hPhe-4-I-Phe-Pro-D-Ala-Bip-Ala | 955.3129 | 956.3209 | 978.3021 | 956.16 | 7.8 |

Table A2: Scaffold B Peptides

| Sequence | Exact Mass | Calc. [M+H]+ | Calc. [M+Na]+ | Observed [M+H]+ or [M+Na]+ | % *ee* of II-2 |
|---|---|---|---|---|---|
| 2-IBA-tPhe-Pro-D-Ala-Phg-Phg | 884.2758 | 885.2838 | 907.265 | 885.05 | 8.4 |
| 2-IBA-Tyr-Pro-D-Ala-Tle-Thr | 792.2344 | 793.2424 | 815.2236 | 815.04 | 7.5 |
| 2-IBA-Val-Pro-D-Ala-Orn-Bip | 865.3024 | 866.3104 | 888.2916 | 888.11 | NP |
| 2-IBA-tPhe-Pro-D-Ala-Phg-Nle | 864.3071 | 865.3151 | 887.2963 | 887.12 | 9.4 |
| 2-IBA-Trp-Pro-D-Ala-tPhe-Nle | 917.3337 | 918.3417 | 940.3229 | 918.11 | NP |
| 2-IBA-3-Pya-Pro-D-Ala-1-Nap-Abu | 845.2398 | 846.2478 | 868.229 | 846.41 | 2.4 |
| 2-IBA-2-Nap-Pro-D-Ala-1-Nap-Val | 908.2758 | 909.2838 | 931.265 | 909.44 | 6.4 |
| 2-IBA-Orn-Pro-D-Ala-Bip-Thr | 839.2503 | 840.2583 | 862.2395 | 840.42 | 7.9 |
| 2-IBA-Gln-Pro-D-Ala-Lys-Val | 770.2612 | 771.2692 | 793.2504 | 792.45 | 1.2 |
| 2-IBA-Thr-Pro-D-Ala-Tle-Leu | 742.2551 | 743.2631 | 765.2443 | 765.62 | 2.2 |
| 2-IBA-dPhe-Pro-D-Ala-Lys-2-Pya | 914.2976 | 915.3056 | 937.2868 | 915.07 | 0 |
| 2-IBA-Val-Pro-D-Ala-Orn-Bip | 865.3024 | 866.3104 | 888.2916 | 888.45 | 17.1 |
| 2-IBA-Nle-Pro-D-Ala-Nle-Ile | 754.2915 | 755.2995 | 777.2807 | 777.10 | 12.8 |
| 2-IBA-Val-Pro-D-Ala-Abu-Dap | 699.2241 | 700.2321 | 722.2133 | 722.03 | 4.7 |
| 2-IBA-Ile-Pro-D-Ala-Tle-Ile | 788.2758 | 789.2838 | 811.265 | 811.09 | 7.8 |
| 2-IBA-Ile-Pro-D-Ala-Phg-Asp | 776.2031 | 777.2111 | 799.1923 | 799.01 | 3.2 |
| 2-IBA-2-Nap-Pro-D-Ala-2-Nap-Leu | 922.2915 | 923.2995 | 945.2807 | 945.44 | 9.6 |
| 2-IBA-Gln-Pro-D-Ala-Bip-Bip | 975.2816 | 976.2896 | 998.2708 | 997.47 | 4.8 |
| 2-IBA-Tle-Pro-D-Ala-Nva-Ser | 714.2238 | 715.2318 | 737.213 | 737.37 | 6.7 |
| 2-IBA-tPhe-Pro-D-Ala-Asp-Ser | 820.2293 | 821.2373 | 843.2185 | 821.78 | NP |
| 2-IBA-Thr-Pro-D-Ala-Asp-3-Pya | 779.1776 | 780.1856 | 802.1668 | 802.51 | 7.5 |
| 2-IBA-Glu-Pro-D-Ala-His-Phe | 828.2092 | 829.2172 | 851.1984 | 829.38 | 11.3 |
| 2-IBA-Phe-Pro-D-Ala-2-Pya-Leu | 823.2554 | 824.2634 | 846.2446 | 824.42 | 6.8 |
| 2-IBA-Lys-Pro-D-Ala-Lys-Gln | 799.2878 | 800.2958 | 822.277 | 822.66 | 9.4 |
| 2-IBA-Thr-Pro-D-Ala-hPhe-2-Pya | 825.2347 | 826.2427 | 848.2239 | 847.42 | 14.2 |
| 2-IBA-Trp-Pro-D-Ala-2-Pya-1-Nap | 946.2663 | 947.2743 | 969.2555 | 968.46 | NP |
| 2-IBA-1-Nap-Pro-D-Ala-2-Pya-Trp | 946.2663 | 947.2743 | 969.2555 | 969.42 | 8.6 |
| 2-IBA-Phe-Pro-D-Ala-2-Nap-Glu | 888.2344 | 889.2424 | 911.2236 | 911.56 | 4.6 |
| 2-IBA-Val-Pro-D-Ala-Phg-hPhe | 822.2602 | 823.2682 | 845.2494 | 823.03 | 8.6 |
| 2-IBA-Val-Pro-D-Ala-hPhe-Phg | 822.2602 | 823.2682 | 845.2494 | 845.41 | 3.4 |
| 2-IBA-hPhe-Pro-D-Ala-Lys-Leu | 817.3024 | 818.3104 | 840.2916 | 818.47 | 12.2 |
| 2-IBA-Leu-Pro-D-Ala-Nva-Glu | 756.2344 | 757.2424 | 779.2236 | 757.40 | 5.9 |
| 2-IBA-Tyr-Pro-D-Ala-Asn-Nva | 791.214 | 792.222 | 814.2032 | 792.38 | 4.7 |

| | | | | | |
|---|---|---|---|---|---|
| 2-IBA-Nva-Pro-D-Ala-Tyr-Asn | 791.214 | 792.222 | 814.2032 | 792.38 | 8.7 |
| 2-IBA-Phg-Pro-D-Ala-Tyr-Asn | 825.1983 | 826.2063 | 848.1875 | 848.35 | 5.0 |
| 2-IBA-Tyr-Pro-D-Ala-Asn-Phg | 825.1983 | 826.2063 | 848.1875 | 847.39 | 2.0 |
| 2-IBA-Trp-Pro-D-Ala-Ile-hPhe | 875.2867 | 876.2947 | 898.2759 | 898.62 | 12.4 |
| 2-IBA-Trp-Pro-D-Ala-hPhe-Trp | 875.2867 | 876.2947 | 898.2759 | 898.66 | 14.2 |
| 2-IBA-Tyr-Pro-D-Ala-Tyr-Asn | 855.2089 | 856.2169 | 878.1981 | 878.58 | 7.6 |
| 2-IBA-Tyr-Pro-D-Ala-Asn-Phg | 825.1983 | 826.2063 | 848.1875 | 848.53 | 4.3 |
| 2-IBA-Ile-Pro-D-Ala-Tle-Orn | 755.2867 | 756.2947 | 778.2759 | 778.62 | 5.8 |
| 2-IBA-hPhe-Pro-D-Ala-Phg-Asp | 824.2031 | 825.2111 | 847.1923 | 847.35 | 23 |
| 2-IBA-Asp-Pro-D-Ala-Phg-hPhe | 824.2031 | 825.2111 | 847.1923 | 825.75 | 3.6 |
| 2-IBA-Ile-Pro-D-Ala-Asp-Gln | 771.2089 | 772.2169 | 794.1981 | 794.54 | 48 |
| 2-IBA-Asp-Pro-D-Ala-Gln-Ile | 771.2089 | 772.2169 | 794.1981 | 771.98 | 14.5 |
| 2-IBA-Dap-Pro-D-Ala-Ile-2-Nap | 811.2554 | 812.2634 | 834.2446 | 834.58 | 14.6 |
| 2-IBA-2-Nap-Pro-D-Ala-1-Nap-Dap | 811.2554 | 812.2634 | 834.2446 | 812.18 | 12.6 |
| 2-IBA-Phg-Pro-D-Ala-hPhe-Val | 808.2445 | 809.2525 | 831.2337 | 809.17 | 4.8 |
| 2-IBA-Val-Pro-D-Ala-hPhe-Phg | 808.2445 | 809.2525 | 831.2337 | 831.39 | 5.8 |
| 2-IBA-Abu-Pro-D-Ala-Abu-Nva | 684.2132 | 685.2212 | 707.2024 | 706.40 | 8.4 |
| 2-IBA-Abu-Pro-D-AlaNva-Abu | 684.2132 | 685.2212 | 707.2024 | 707.54 | 16.2 |
| 2-IBA-Lys-Pro-D-Ala-Ser-Dap | 716.2143 | 717.2223 | 739.2035 | 739.02 | 12.6 |
| 2-IBA-hPhe-Pro-D-Ala-Phg-hPhe | 856.2445 | 857.2525 | 879.2337 | 879.05 | 13.7 |
| 2-IBA-Phe-Pro-D-Ala-Phg-hPhe | 856.2445 | 857.2525 | 879.2337 | 879.05 | 12.3 |
| 2-IBA-Phe-Pro-D-Ala-Phg-Dap | 781.2085 | 782.2165 | 804.1977 | 804.02 | 8.7 |
| 2-IBA-Phe-Pro-D-Ala-Asn-hPhe | 837.2347 | 838.2427 | 860.2239 | 860.04 | NP |
| 2-IBA-Gln-Pro-D-Ala-Lys-2-Nap | 868.2769 | 869.2849 | 891.2661 | 891.09 | 12.6 |
| 2-IBA-Ala-Pro-D-Ala-1-Nap-Orn | 797.2398 | 798.2478 | 820.229 | 820.05 | 6.7 |
| 2-IBA-1-Nap-Pro-D-Ala-Orn-Ala | 797.2398 | 798.2478 | 820.229 | 798.17 | 4.3 |
| 2-IBA-Orn-Pro-D-Ala-Phg-Ile | 761.2398 | 762.2478 | 784.229 | 762.17 | 7.8 |
| 2-IBA-Thr-Pro-D-Ala-tPhe-Abu | 804.2707 | 805.2787 | 827.2599 | 805.20 | 5.6 |
| 3-IBA-His-Pro-D-Ala-Tyr-Leu | 828.2456 | 829.2536 | 851.2348 | 829.79 | 16.2 |
| 2-IBA-tPhe-Pro-D-Ala-Phg-Phg | 791.3964419 | 792.4044419 | 814.3856419 | 792.17 | 6.6 |
| 2-IBA-Tyr-Pro-D-Ala-Tle-Thr | 790.4917993 | 791.4997993 | 813.4809993 | 813.30 | 5.7 |
| 2-IBA-Val-Pro-D-Ala-Orn-Bip | 789.5871567 | 790.5951567 | 812.5763567 | 812.40 | NP |
| 2-IBA-tPhe-Pro-D-Ala-Phg-Nle | 788.6825141 | 789.6905141 | 811.6717141 | 811.49 | 10.4 |
| 2-IBA-Trp-Pro-D-Ala-tPhe-Nle | 787.7778715 | 788.7858715 | 810.7670715 | 788.55 | NP |
| 2-IBA-3-Pya-Pro-D-Ala-1-Nap-Abu | 786.8732289 | 787.8812289 | 809.8624289 | 788.04 | 12.4 |
| 2-IBA-2-Nap-Pro-D-Ala-1-Nap-Val | 785.9685863 | 786.9765863 | 808.9577863 | 787.14 | 8.2 |
| 2-IBA-Orn-Pro-D-Ala-Bip-Thr | 785.0639437 | 786.0719437 | 808.0531437 | 786.23 | 2.4 |
| 2-IBA-Gln-Pro-D-Ala-Lys-Val | 784.1593011 | 785.1673011 | 807.1485011 | 806.35 | 9.5 |

| | | | | | |
|---|---|---|---|---|---|
| 2-IBA-Thr-Pro-D-Ala-Tle-Leu | 783.2546585 | 784.2626585 | 806.2438585 | 806.62 | 0 |
| 2-IBA-dPhe-Pro-D-Ala-Lys-2-Pya | 782.3500159 | 783.3580159 | 805.3392159 | 783.12 | 3.8 |
| 2-IBA-Val-Pro-D-Ala-Orn-Bip | 781.4453733 | 782.4533733 | 804.4345733 | 804.59 | 5.4 |
| 2-IBA-Nle-Pro-D-Ala-Nle-Ile | 780.5407306 | 781.5487306 | 803.5299306 | 803.35 | 9.2 |
| 2-IBA-Val-Pro-D-Ala-Abu-Dap | 779.636088 | 780.644088 | 802.625288 | 802.45 | 0 |
| 2-IBA-Ile-Pro-D-Ala-Tle-Ile | 778.7314454 | 779.7394454 | 801.7206454 | 801.54 | 8.7 |
| 2-IBA-Ile-Pro-D-Ala-Phg-Asp | 777.8268028 | 778.8348028 | 800.8160028 | 800.64 | 6.4 |
| 2-IBA-2-Nap-Pro-D-Ala-2-Nap-Leu | 776.9221602 | 777.9301602 | 799.9113602 | 800.07 | 4.7 |
| 2-IBA-Gln-Pro-D-Ala-Bip-Bip | 776.0175176 | 777.0255176 | 799.0067176 | 798.21 | 5.8 |
| 2-IBA-Tle-Pro-D-Ala-Nva-Ser | 775.112875 | 776.120875 | 798.102075 | 798.26 | 8.7 |
| 2-IBA-tPhe-Pro-D-Ala-Asp-Ser | 774.2082324 | 775.2162324 | 797.1974324 | 775.76 | 3.2 |
| 2-IBA-Thr-Pro-D-Ala-Asp-3-Pya | 773.3035898 | 774.3115898 | 796.2927898 | 796.63 | 0 |
| 2-IBA-Glu-Pro-D-Ala-His-Phe | 772.3989472 | 773.4069472 | 795.3881472 | 773.57 | 3.2 |
| 2-IBA-Phe-Pro-D-Ala-2-Pya-Leu | 771.4943046 | 772.5023046 | 794.4835046 | 772.66 | 5.4 |
| 2-IBA-Lys-Pro-D-Ala-Lys-Gln | 770.589662 | 771.597662 | 793.578862 | 793.96 | 7.6 |
| 2-IBA-Thr-Pro-D-Ala-hPhe-2-Pya | 769.6850194 | 770.6930194 | 792.6742194 | 791.87 | 8.2 |
| 2-IBA-Trp-Pro-D-Ala-2-Pya-1-Nap | 768.7803768 | 769.7883768 | 791.7695768 | 790.97 | 1.5 |
| 2-IBA-1-Nap-Pro-D-Ala-2-Pya-Trp | 767.8757342 | 768.8837342 | 790.8649342 | 791.02 | 8.2 |
| 2-IBA-Phe-Pro-D-Ala-2-Nap-Glu | 766.9710916 | 767.9790916 | 789.9602916 | 790.30 | 5.2 |
| 2-IBA-Val-Pro-D-Ala-Phg-hPhe | 766.066449 | 767.074449 | 789.055649 | 766.84 | 7.6 |
| 2-IBA-Val-Pro-D-Ala-hPhe-Phg | 765.1618064 | 766.1698064 | 788.1510064 | 788.31 | 4.3 |
| 2-IBA-hPhe-Pro-D-Ala-Lys-Leu | 764.2571638 | 765.2651638 | 787.2463638 | 765.43 | 8.7 |
| 2-IBA-Leu-Pro-D-Ala-Nva-Glu | 763.3525212 | 764.3605212 | 786.3417212 | 764.52 | 9.6 |
| 2-IBA-Tyr-Pro-D-Ala-Asn-Nva | 762.4478786 | 763.4558786 | 785.4370786 | 763.62 | 3.6 |
| 2-IBA-Nva-Pro-D-Ala-Tyr-Asn | 761.543236 | 762.551236 | 784.532436 | 762.71 | 3.7 |
| 2-IBA-Phg-Pro-D-Ala-Tyr-Asn | 760.6385934 | 761.6465934 | 783.6277934 | 783.79 | 5.5 |
| 2-IBA-Tyr-Pro-D-Ala-Asn-Phg | 759.7339508 | 760.7419508 | 782.7231508 | 781.92 | 1,4 |
| 2-IBA-Trp-Pro-D-Ala-Ile-hPhe | 758.8293082 | 759.8373082 | 781.8185082 | 782.16 | 4.8 |
| 2-IBA-Trp-Pro-D-Ala-hPhe-Trp | 757.9246656 | 758.9326656 | 780.9138656 | 781.29 | 16.2 |
| 2-IBA-Tyr-Pro-D-Ala-Tyr-Asn | 757.020023 | 758.028023 | 780.009223 | 780.39 | 6.9 |
| 2-IBA-Tyr-Pro-D-Ala-Asn-Phg | 756.1153804 | 757.1233804 | 779.1045804 | 779.44 | 4.8 |
| 2-IBA-Ile-Pro-D-Ala-Tle-Orn | 755.2107378 | 756.2187378 | 778.1999378 | 778.54 | 1.3 |
| 2-IBA-hPhe-Pro-D-Ala-Phg-Asp | 754.3060952 | 755.3140952 | 777.2952952 | 777.46 | 7.2 |
| 2-IBA-Asp-Pro-D-Ala-Phg-hPhe | 753.4014526 | 754.4094526 | 776.3906526 | 754.95 | NP |
| 2-IBA-Ile-Pro-D-Ala-Asp-Gln | 752.49681 | 753.50481 | 775.48601 | 775.83 | 5.8 |
| 2-IBA-Asp-Pro-D-Ala-Gln-Ile | 751.5921674 | 752.6001674 | 774.5813674 | 752.37 | 1.6 |
| 2-IBA-Dap-Pro-D-Ala-Ile-2-Nap | 750.6875248 | 751.6955248 | 773.6767248 | 774.02 | 4.7 |
| 2-IBA-2-Nap-Pro-D-Ala-1-Nap-Dap | 749.7828822 | 750.7908822 | 772.7720822 | 750.71 | 0 |

| | | | | | |
|---|---|---|---|---|---|
| 2-IBA-Phg-Pro-D-Ala-hPhe-Val | 748.8782396 | 749.8862396 | 771.8674396 | 749.81 | 8.3 |
| 2-IBA-Val-Pro-D-Ala-hPhe-Phg | 747.9735969 | 748.9815969 | 770.9627969 | 771.12 | 1.9 |
| 2-IBA-Abu-Pro-D-Ala-Abu-Nva | 747.0689543 | 748.0769543 | 770.0581543 | 769.26 | NP |
| 2-IBA-Abu-Pro-D-AlaNva-Abu | 746.1643117 | 747.1723117 | 769.1535117 | 769.49 | 2.5 |
| 2-IBA-Lys-Pro-D-Ala-Ser-Dap | 745.2596691 | 746.2676691 | 768.2488691 | 768.07 | 2.5 |
| 2-IBA-hPhe-Pro-D-Ala-Phg-hPhe | 744.3550265 | 745.3630265 | 767.3442265 | 767.16 | 0 |
| 2-IBA-Phe-Pro-D-Ala-Phg-hPhe | 743.4503839 | 744.4583839 | 766.4395839 | 766.26 | 2.6 |
| 2-IBA-tPhe-Pro-D-Ala-Phg-Phg | 742.5457413 | 743.5537413 | 765.5349413 | 743.32 | 1.5 |
| 2-IBA-Tyr-Pro-D-Ala-Tle-Thr | 741.6410987 | 742.6490987 | 764.6302987 | 764.45 | 6 |
| 2-IBA-Val-Pro-D-Ala-Orn-Bip | 740.7364561 | 741.7444561 | 763.7256561 | 763.55 | 0 |
| 2-IBA-tPhe-Pro-D-Ala-Phg-Nle | 739.8318135 | 740.8398135 | 762.8210135 | 762.64 | 0 |
| 2-IBA-Trp-Pro-D-Ala-tPhe-Nle | 738.9271709 | 739.9351709 | 761.9163709 | 739.70 | 2.1 |
| 2-IBA-3-Pya-Pro-D-Ala-1-Nap-Abu | 738.0225283 | 739.0305283 | 761.0117283 | 739.19 | 7 |
| 2-IBA-2-Nap-Pro-D-Ala-1-Nap-Val | 737.1178857 | 738.1258857 | 760.1070857 | 738.29 | 3.6 |
| 2-IBA-Orn-Pro-D-Ala-Bip-Thr | 736.2132431 | 737.2212431 | 759.2024431 | 737.38 | 2.7 |
| 2-IBA-Gln-Pro-D-Ala-Lys-Val | 735.3086005 | 736.3166005 | 758.2978005 | 757.50 | 2.2 |
| 2-IBA-Thr-Pro-D-Ala-Tle-Leu | 734.4039579 | 735.4119579 | 757.3931579 | 757.77 | 4.7 |
| 2-IBA-dPhe-Pro-D-Ala-Lys-2-Pya | 733.4993153 | 734.5073153 | 756.4885153 | 734.27 | 0 |
| 2-IBA-Val-Pro-D-Ala-Orn-Bip | 732.5946727 | 733.6026727 | 755.5838727 | 755.74 | 14.1 |
| 2-IBA-Nle-Pro-D-Ala-Nle-Ile | 731.6900301 | 732.6980301 | 754.6792301 | 754.50 | 2.1 |
| 2-IBA-Val-Pro-D-Ala-Abu-Dap | 730.7853875 | 731.7933875 | 753.7745875 | 753.59 | 8.6 |
| 2-IBA-Ile-Pro-D-Ala-Tle-Ile | 729.8807449 | 730.8887449 | 752.8699449 | 752.69 | 3.4 |
| 2-IBA-Ile-Pro-D-Ala-Phg-Asp | 728.9761023 | 729.9841023 | 751.9653023 | 751.79 | NP |
| 2-IBA-2-Nap-Pro-D-Ala-2-Nap-Leu | 728.0714597 | 729.0794597 | 751.0606597 | 751.22 | 3.9 |
| 2-IBA-Gln-Pro-D-Ala-Bip-Bip | 727.1668171 | 728.1748171 | 750.1560171 | 749.36 | 7 |
| 2-IBA-Tle-Pro-D-Ala-Nva-Ser | 726.2621745 | 727.2701745 | 749.2513745 | 749.41 | 0 |
| 2-IBA-tPhe-Pro-D-Ala-Asp-Ser | 725.3575319 | 726.3655319 | 748.3467319 | 726.91 | 0 |
| 2-IBA-Thr-Pro-D-Ala-Asp-3-Pya | 724.4528893 | 725.4608893 | 747.4420893 | 747.78 | 14.8 |
| 2-IBA-Glu-Pro-D-Ala-His-Phe | 723.5482467 | 724.5562467 | 746.5374467 | 724.72 | 10.4 |
| 2-IBA-Phe-Pro-D-Ala-2-Pya-Leu | 722.6436041 | 723.6516041 | 745.6328041 | 723.81 | 12.4 |
| 2-IBA-Lys-Pro-D-Ala-Lys-Gln | 721.7389615 | 722.7469615 | 744.7281615 | 745.11 | 5.1 |
| 2-IBA-Thr-Pro-D-Ala-hPhe-2-Pya | 720.8343189 | 721.8423189 | 743.8235189 | 743.02 | 3.1 |
| 2-IBA-Trp-Pro-D-Ala-2-Pya-1-Nap | 719.9296763 | 720.9376763 | 742.9188763 | 742.12 | 4.6 |
| 2-IBA-1-Nap-Pro-D-Ala-2-Pya-Trp | 719.0250337 | 720.0330337 | 742.0142337 | 742.17 | 7.1 |
| 2-IBA-Phe-Pro-D-Ala-2-Nap-Glu | 718.1203911 | 719.1283911 | 741.1095911 | 741.45 | 1.3 |
| 2-IBA-Val-Pro-D-Ala-Phg-hPhe | 717.2157485 | 718.2237485 | 740.2049485 | 717.99 | 3.9 |
| 2-IBA-Val-Pro-D-Ala-hPhe-Phg | 716.3111058 | 717.3191058 | 739.3003058 | 739.46 | 1 |
| 2-IBA-hPhe-Pro-D-Ala-Lys-Leu | 715.4064632 | 716.4144632 | 738.3956632 | 716.57 | NP |

| | | | | | |
|---|---|---|---|---|---|
| 2-IBA-Leu-Pro-D-Ala-Nva-Glu | 714.5018206 | 715.5098206 | 737.4910206 | 715.67 | 4.5 |
| 2-IBA-Tyr-Pro-D-Ala-Asn-Nva | 713.597178 | 714.605178 | 736.586378 | 714.77 | 8.6 |
| 2-IBA-Nva-Pro-D-Ala-Tyr-Asn | 712.6925354 | 713.7005354 | 735.6817354 | 713.86 | 0 |
| 2-IBA-Phg-Pro-D-Ala-Tyr-Asn | 711.7878928 | 712.7958928 | 734.7770928 | 734.94 | 2.7 |
| 2-IBA-Tyr-Pro-D-Ala-Asn-Phg | 710.8832502 | 711.8912502 | 733.8724502 | 733.07 | 2.1 |
| 2-IBA-Trp-Pro-D-Ala-Ile-hPhe | 709.9786076 | 710.9866076 | 732.9678076 | 733.31 | 2.9 |
| 2-IBA-tPhe-Pro-D-Ala-Phg-Phg | 709.073965 | 710.081965 | 732.063165 | 709.85 | 3.7 |
| 2-IBA-Tyr-Pro-D-Ala-Tle-Thr | 708.1693224 | 709.1773224 | 731.1585224 | 730.98 | 2.4 |
| 2-IBA-Val-Pro-D-Ala-Orn-Bip | 707.2646798 | 708.2726798 | 730.2538798 | 730.07 | 0 |
| 2-IBA-tPhe-Pro-D-Ala-Phg-Nle | 706.3600372 | 707.3680372 | 729.3492372 | 729.17 | 6.3 |
| 2-IBA-Trp-Pro-D-Ala-tPhe-Nle | 705.4553946 | 706.4633946 | 728.4445946 | 706.23 | 7.7 |
| 2-IBA-3-Pya-Pro-D-Ala-1-Nap-Abu | 704.550752 | 705.558752 | 727.539952 | 705.72 | 5.1 |
| 2-IBA-2-Nap-Pro-D-Ala-1-Nap-Val | 703.6461094 | 704.6541094 | 726.6353094 | 704.81 | 0.0 |
| 2-IBA-Orn-Pro-D-Ala-Bip-Thr | 702.7414668 | 703.7494668 | 725.7306668 | 703.91 | 0.0 |
| 2-IBA-Gln-Pro-D-Ala-Lys-Val | 701.8368242 | 702.8448242 | 724.8260242 | 724.03 | NP |
| 2-IBA-Thr-Pro-D-Ala-Tle-Leu | 700.9321816 | 701.9401816 | 723.9213816 | 724.30 | 11.1 |
| 2-IBA-dPhe-Pro-D-Ala-Lys-2-Pya | 700.027539 | 701.035539 | 723.016739 | 700.80 | 5.3 |
| 2-IBA-Val-Pro-D-Ala-Orn-Bip | 699.1228964 | 700.1308964 | 722.1120964 | 722.27 | 15.0 |
| 2-IBA-Nle-Pro-D-Ala-Nle-Ile | 698.2182538 | 699.2262538 | 721.2074538 | 721.03 | 3.7 |
| 2-IBA-Val-Pro-D-Ala-Abu-Dap | 697.3136112 | 698.3216112 | 720.3028112 | 720.12 | 14.0 |
| 2-IBA-Ile-Pro-D-Ala-Tle-Ile | 696.4089686 | 697.4169686 | 719.3981686 | 719.22 | 17 |
| 2-IBA-Ile-Pro-D-Ala-Phg-Asp | 695.504326 | 696.512326 | 718.493526 | 718.31 | 5 |
| 2-IBA-2-Nap-Pro-D-Ala-2-Nap-Leu | 694.5996834 | 695.6076834 | 717.5888834 | 717.75 | 9 |
| 2-IBA-Gln-Pro-D-Ala-Bip-Bip | 693.6950408 | 694.7030408 | 716.6842408 | 715.88 | NP |
| 2-IBA-Tle-Pro-D-Ala-Nva-Ser | 692.7903982 | 693.7983982 | 715.7795982 | 715.94 | NP |
| 2-IBA-tPhe-Pro-D-Ala-Asp-Ser | 691.8857556 | 692.8937556 | 714.8749556 | 693.43 | 0 |
| 2-IBA-Thr-Pro-D-Ala-Asp-3-Pya | 690.981113 | 691.989113 | 713.970313 | 714.31 | 0 |
| 2-IBA-Glu-Pro-D-Ala-His-Phe | 690.0764704 | 691.0844704 | 713.0656704 | 691.24 | 9.1 |
| 2-IBA-Phe-Pro-D-Ala-2-Pya-Leu | 689.1718278 | 690.1798278 | 712.1610278 | 690.34 | 20.0 |
| 2-IBA-Lys-Pro-D-Ala-Lys-Gln | 688.2671852 | 689.2751852 | 711.2563852 | 711.64 | 6.1 |
| 2-IBA-Thr-Pro-D-Ala-hPhe-2-Pya | 687.3625426 | 688.3705426 | 710.3517426 | 709.55 | 13.2 |
| 2-IBA-Trp-Pro-D-Ala-2-Pya-1-Nap | 686.4579 | 687.4659 | 709.4471 | 708.65 | 19.4 |
| 2-IBA-1-Nap-Pro-D-Ala-2-Pya-Trp | 685.5532574 | 686.5612574 | 708.5424574 | 708.70 | NP |
| 2-IBA-Phe-Pro-D-Ala-2-Nap-Glu | 684.6486148 | 685.6566148 | 707.6378148 | 707.98 | 8.4 |
| 2-IBA-Val-Pro-D-Ala-Phg-hPhe | 683.7439721 | 684.7519721 | 706.7331721 | 684.52 | 8.0 |
| 2-IBA-Val-Pro-D-Ala-hPhe-Phg | 682.8393295 | 683.8473295 | 705.8285295 | 705.99 | 4.4 |
| 2-IBA-hPhe-Pro-D-Ala-Lys-Leu | 681.9346869 | 682.9426869 | 704.9238869 | 683.10 | 2.3 |
| 2-IBA-Leu-Pro-D-Ala-Nva-Glu | 681.0300443 | 682.0380443 | 704.0192443 | 682.20 | 2.8 |

| | | | | | |
|---|---|---|---|---|---|
| 2-IBA-Tyr-Pro-D-Ala-Asn-Nva | 680.1254017 | 681.1334017 | 703.1146017 | 681.29 | 6.7 |
| 2-IBA-Nva-Pro-D-Ala-Tyr-Asn | 679.2207591 | 680.2287591 | 702.2099591 | 680.39 | 0.0 |
| 2-IBA-Phg-Pro-D-Ala-Tyr-Asn | 678.3161165 | 679.3241165 | 701.3053165 | 701.47 | 4.2 |
| 2-IBA-Tyr-Pro-D-Ala-Asn-Phg | 677.4114739 | 678.4194739 | 700.4006739 | 699.60 | 17 |
| 2-IBA-tPhe-Pro-D-Ala-Phg-Phg | 676.5068313 | 677.5148313 | 699.4960313 | 677.28 | 6.6 |
| 2-IBA-Tyr-Pro-D-Ala-Tle-Thr | 675.6021887 | 676.6101887 | 698.5913887 | 698.41 | 5.7 |
| 2-IBA-Val-Pro-D-Ala-Orn-Bip | 674.6975461 | 675.7055461 | 697.6867461 | 697.51 | NP |
| 2-IBA-tPhe-Pro-D-Ala-Phg-Nle | 673.7929035 | 674.8009035 | 696.7821035 | 696.60 | 10.4 |
| 2-IBA-Trp-Pro-D-Ala-tPhe-Nle | 672.8882609 | 673.8962609 | 695.8774609 | 673.66 | NP |
| 2-IBA-3-Pya-Pro-D-Ala-1-Nap-Abu | 671.9836183 | 672.9916183 | 694.9728183 | 673.15 | 2.4 |
| 2-IBA-2-Nap-Pro-D-Ala-1-Nap-Val | 671.0789757 | 672.0869757 | 694.0681757 | 672.25 | 6.8 |
| 2-IBA-Orn-Pro-D-Ala-Bip-Thr | 670.1743331 | 671.1823331 | 693.1635331 | 671.34 | 3.6 |
| 2-IBA-Gln-Pro-D-Ala-Lys-Val | 669.2696905 | 670.2776905 | 692.2588905 | 691.46 | 2.8 |
| 2-IBA-Thr-Pro-D-Ala-Tle-Leu | 668.3650479 | 669.3730479 | 691.3542479 | 691.73 | 5.4 |
| 2-IBA-dPhe-Pro-D-Ala-Lys-2-Pya | 667.4604053 | 668.4684053 | 690.4496053 | 668.23 | 0 |
| 2-IBA-Val-Pro-D-Ala-Orn-Bip | 666.5557627 | 667.5637627 | 689.5449627 | 689.70 | 2.7 |
| 2-IBA-Nle-Pro-D-Ala-Nle-Ile | 665.6511201 | 666.6591201 | 688.6403201 | 688.46 | 6.4 |
| 2-IBA-Val-Pro-D-Ala-Abu-Dap | 664.7464775 | 665.7544775 | 687.7356775 | 687.56 | 8.3 |
| 2-IBA-Ile-Pro-D-Ala-Tle-Ile | 663.8418349 | 664.8498349 | 686.8310349 | 686.65 | 4.9 |
| 2-IBA-Ile-Pro-D-Ala-Phg-Asp | 662.9371923 | 663.9451923 | 685.9263923 | 685.75 | 3.2 |
| 2-IBA-2-Nap-Pro-D-Ala-2-Nap-Leu | 662.0325497 | 663.0405497 | 685.0217497 | 685.18 | 0 |
| 2-IBA-Gln-Pro-D-Ala-Bip-Bip | 661.1279071 | 662.1359071 | 684.1171071 | 683.32 | 8.4 |
| 2-IBA-Tle-Pro-D-Ala-Nva-Ser | 660.2232645 | 661.2312645 | 683.2124645 | 683.37 | 3.6 |
| 2-IBA-tPhe-Pro-D-Ala-Asp-Ser | 659.3186219 | 660.3266219 | 682.3078219 | 660.87 | NP |
| 2-IBA-Thr-Pro-D-Ala-Asp-3-Pya | 658.4139793 | 659.4219793 | 681.4031793 | 681.74 | 13.3 |
| 2-IBA-Glu-Pro-D-Ala-His-Phe | 657.5093367 | 658.5173367 | 680.4985367 | 658.68 | 14.4 |
| 2-IBA-Phe-Pro-D-Ala-2-Pya-Leu | 656.6046941 | 657.6126941 | 679.5938941 | 657.77 | 15.6 |
| 2-IBA-Lys-Pro-D-Ala-Lys-Gln | 655.7000515 | 656.7080515 | 678.6892515 | 679.07 | 16.7 |
| 2-IBA-Thr-Pro-D-Ala-hPhe-2-Pya | 654.7954089 | 655.8034089 | 677.7846089 | 676.98 | 17.9 |
| 2-IBA-Trp-Pro-D-Ala-2-Pya-1-Nap | 653.8907663 | 654.8987663 | 676.8799663 | 676.08 | NP |
| 2-IBA-1-Nap-Pro-D-Ala-2-Pya-Trp | 652.9861237 | 653.9941237 | 675.9753237 | 676.14 | 8.8 |
| 2-IBA-Phe-Pro-D-Ala-2-Nap-Glu | 652.0814811 | 653.0894811 | 675.0706811 | 675.41 | 3.2 |
| 2-IBA-Val-Pro-D-Ala-Phg-hPhe | 651.1768384 | 652.1848384 | 674.1660384 | 651.95 | 7.6 |
| 2-IBA-Val-Pro-D-Ala-hPhe-Phg | 650.2721958 | 651.2801958 | 673.2613958 | 673.42 | 4.5 |
| 2-IBA-hPhe-Pro-D-Ala-Lys-Leu | 649.3675532 | 650.3755532 | 672.3567532 | 650.54 | 8.6 |
| 2-IBA-Leu-Pro-D-Ala-Nva-Glu | 648.4629106 | 649.4709106 | 671.4521106 | 649.63 | 2.1 |
| 2-IBA-Tyr-Pro-D-Ala-Asn-Nva | 647.558268 | 648.566268 | 670.547468 | 648.73 | 0 |
| 2-IBA-Nva-Pro-D-Ala-Tyr-Asn | 646.6536254 | 647.6616254 | 669.6428254 | 647.82 | 8.6 |

| | | | | | |
|---|---|---|---|---|---|
| 2-IBA-Phg-Pro-D-Ala-Tyr-Asn | 645.7489828 | 646.7569828 | 668.7381828 | 668.90 | 4.3 |
| 2-IBA-Tyr-Pro-D-Ala-Asn-Phg | 644.8443402 | 645.8523402 | 667.8335402 | 667.03 | 9.2 |
| 2-IBA-tPhe-Pro-D-Ala-Phg-Phg | 643.9396976 | 644.9476976 | 666.9288976 | 644.71 | 6.6 |
| 2-IBA-Tyr-Pro-D-Ala-Tle-Thr | 643.035055 | 644.043055 | 666.024255 | 665.84 | 5.7 |
| 2-IBA-Val-Pro-D-Ala-Orn-Bip | 642.1304124 | 643.1384124 | 665.1196124 | 664.94 | NP |
| 2-IBA-tPhe-Pro-D-Ala-Phg-Nle | 641.2257698 | 642.2337698 | 664.2149698 | 664.03 | 10.4 |
| 2-IBA-Trp-Pro-D-Ala-tPhe-Nle | 640.3211272 | 641.3291272 | 663.3103272 | 641.10 | NP |
| 2-IBA-3-Pya-Pro-D-Ala-1-Nap-Abu | 639.4164846 | 640.4244846 | 662.4056846 | 640.58 | 2.0 |
| 2-IBA-2-Nap-Pro-D-Ala-1-Nap-Val | 638.511842 | 639.519842 | 661.501042 | 639.68 | 4.0 |
| 2-IBA-Orn-Pro-D-Ala-Bip-Thr | 637.6071994 | 638.6151994 | 660.5963994 | 638.78 | 7.4 |
| 2-IBA-Gln-Pro-D-Ala-Lys-Val | 636.7025568 | 637.7105568 | 659.6917568 | 658.89 | 1.2 |
| 2-IBA-Thr-Pro-D-Ala-Tle-Leu | 635.7979142 | 636.8059142 | 658.7871142 | 659.17 | 6.5 |
| 2-IBA-dPhe-Pro-D-Ala-Lys-2-Pya | 634.8932716 | 635.9012716 | 657.8824716 | 635.67 | 3.7 |
| 2-IBA-Val-Pro-D-Ala-Orn-Bip | 633.988629 | 634.996629 | 656.977829 | 657.14 | 4.5 |
| 2-IBA-Nle-Pro-D-Ala-Nle-Ile | 633.0839864 | 634.0919864 | 656.0731864 | 655.89 | 2.4 |
| 2-IBA-Val-Pro-D-Ala-Abu-Dap | 632.1793438 | 633.1873438 | 655.1685438 | 654.99 | 0.0 |
| 2-IBA-Ile-Pro-D-Ala-Tle-Ile | 631.2747012 | 632.2827012 | 654.2639012 | 654.08 | 6.8 |
| 2-IBA-Ile-Pro-D-Ala-Phg-Asp | 630.3700586 | 631.3780586 | 653.3592586 | 653.18 | 3.2 |
| 2-IBA-2-Nap-Pro-D-Ala-2-Nap-Leu | 629.465416 | 630.473416 | 652.454616 | 652.61 | 4.6 |
| 2-IBA-Gln-Pro-D-Ala-Bip-Bip | 628.5607734 | 629.5687734 | 651.5499734 | 650.75 | 3.6 |
| 2-IBA-Tle-Pro-D-Ala-Nva-Ser | 627.6561308 | 628.6641308 | 650.6453308 | 650.81 | 7.6 |
| 2-IBA-tPhe-Pro-D-Ala-Asp-Ser | 626.7514882 | 627.7594882 | 649.7406882 | 628.30 | NP |
| 2-IBA-Thr-Pro-D-Ala-Asp-3-Pya | 625.8468456 | 626.8548456 | 648.8360456 | 649.18 | 13.3 |
| 2-IBA-Glu-Pro-D-Ala-His-Phe | 624.942203 | 625.950203 | 647.931403 | 626.11 | 14.4 |
| 2-IBA-Phe-Pro-D-Ala-2-Pya-Leu | 624.0375604 | 625.0455604 | 647.0267604 | 625.21 | 15.6 |
| 2-IBA-Lys-Pro-D-Ala-Lys-Gln | 623.1329178 | 624.1409178 | 646.1221178 | 646.50 | 16.7 |
| 2-IBA-Thr-Pro-D-Ala-hPhe-2-Pya | 622.2282752 | 623.2362752 | 645.2174752 | 644.42 | 17.9 |
| 2-IBA-Trp-Pro-D-Ala-2-Pya-1-Nap | 621.3236326 | 622.3316326 | 644.3128326 | 643.51 | NP |
| 2-IBA-1-Nap-Pro-D-Ala-2-Pya-Trp | 620.41899 | 621.42699 | 643.40819 | 643.57 | 8.3 |
| 2-IBA-Phe-Pro-D-Ala-2-Nap-Glu | 619.5143473 | 620.5223473 | 642.5035473 | 642.84 | 5.4 |
| 2-IBA-Val-Pro-D-Ala-Phg-hPhe | 618.6097047 | 619.6177047 | 641.5989047 | 619.38 | 2.3 |
| 2-IBA-Val-Pro-D-Ala-hPhe-Phg | 617.7050621 | 618.7130621 | 640.6942621 | 640.85 | 1.5 |
| 2-IBA-hPhe-Pro-D-Ala-Lys-Leu | 616.8004195 | 617.8084195 | 639.7896195 | 617.97 | 6.8 |
| 2-IBA-Leu-Pro-D-Ala-Nva-Glu | 615.8957769 | 616.9037769 | 638.8849769 | 617.06 | 4.3 |
| 2-IBA-Tyr-Pro-D-Ala-Asn-Nva | 614.9911343 | 615.9991343 | 637.9803343 | 616.16 | 2.5 |
| 2-IBA-Nva-Pro-D-Ala-Tyr-Asn | 614.0864917 | 615.0944917 | 637.0756917 | 615.25 | 5.6 |
| 2-IBA-Phg-Pro-D-Ala-Tyr-Asn | 613.1818491 | 614.1898491 | 636.1710491 | 636.33 | 0 |
| 2-IBA-Tyr-Pro-D-Ala-Asn-Phg | 612.2772065 | 613.2852065 | 635.2664065 | 634.47 | 1.3 |

| | | | | | |
|---|---|---|---|---|---|
| 2-IBA-Trp-Pro-D-Ala-Ile-hPhe | 611.3725639 | 612.3805639 | 634.3617639 | 634.70 | 2.8 |
| 2-IBA-Trp-Pro-D-Ala-hPhe-Trp | 610.4679213 | 611.4759213 | 633.4571213 | 633.84 | 3.2 |
| 2-IBA-Tyr-Pro-D-Ala-Tyr-Asn | 609.5632787 | 610.5712787 | 632.5524787 | 632.93 | 6 |
| 2-IBA-Tyr-Pro-D-Ala-Asn-Phg | 608.6586361 | 609.6666361 | 631.6478361 | 631.99 | 0 |
| 2-IBA-Ile-Pro-D-Ala-Tle-Orn | 607.7539935 | 608.7619935 | 630.7431935 | 631.08 | 3.4 |
| 2-IBA-hPhe-Pro-D-Ala-Phg-Asp | 606.8493509 | 607.8573509 | 629.8385509 | 630.00 | 1.3 |
| 2-IBA-tPhe-Pro-D-Ala-Phg-Phg | 605.9447083 | 606.9527083 | 628.9339083 | 606.72 | 6.6 |
| 2-IBA-Tyr-Pro-D-Ala-Tle-Thr | 605.0400657 | 606.0480657 | 628.0292657 | 627.85 | 5.7 |
| 2-IBA-Val-Pro-D-Ala-Orn-Bip | 604.1354231 | 605.1434231 | 627.1246231 | 626.94 | NP |
| 2-IBA-tPhe-Pro-D-Ala-Phg-Nle | 603.2307805 | 604.2387805 | 626.2199805 | 626.04 | 10 |
| 2-IBA-Trp-Pro-D-Ala-tPhe-Nle | 602.3261379 | 603.3341379 | 625.3153379 | 603.10 | NP |
| 2-IBA-3-Pya-Pro-D-Ala-1-Nap-Abu | 601.4214953 | 602.4294953 | 624.4106953 | 602.59 | 7.9 |
| 2-IBA-2-Nap-Pro-D-Ala-1-Nap-Val | 600.5168527 | 601.5248527 | 623.5060527 | 601.68 | 8.2 |
| 2-IBA-Orn-Pro-D-Ala-Bip-Thr | 599.6122101 | 600.6202101 | 622.6014101 | 600.78 | 8.4 |
| 2-IBA-Gln-Pro-D-Ala-Lys-Val | 598.7075675 | 599.7155675 | 621.6967675 | 620.90 | 8.6 |
| 2-IBA-Thr-Pro-D-Ala-Tle-Leu | 597.8029249 | 598.8109249 | 620.7921249 | 621.17 | 8.9 |
| 2-IBA-dPhe-Pro-D-Ala-Lys-2-Pya | 596.8982823 | 597.9062823 | 619.8874823 | 597.67 | 9.1 |
| 2-IBA-Val-Pro-D-Ala-Orn-Bip | 595.9936397 | 597.0016397 | 618.9828397 | 619.14 | 9.3 |
| 2-IBA-Nle-Pro-D-Ala-Nle-Ile | 595.0889971 | 596.0969971 | 618.0781971 | 617.90 | 9.6 |
| 2-IBA-Val-Pro-D-Ala-Abu-Dap | 594.1843545 | 595.1923545 | 617.1735545 | 616.99 | 9.8 |

Table A3: 2nd Generation Peptides Screened in the α-Oxytosylation of Propiophenone

| Sequence | Exact Mass | Calc. [M+H]+ | Calc. [M+Na]+ | Observed [M+H]+ or [M+Na]+ | % *ee* of II-2 |
|---|---|---|---|---|---|
| 2-IBA-Ile-Pro-D-Ala-Asp-Ile | 756.2344 | 757.2424 | 779.2236 | 779.38 | 16.2 |
| 2-IBA-Ile-Pro-D-Ala-Asp-Val | 742.2187 | 743.2267 | 765.2079 | 742.99 | 17.8 |
| 2-IBA-Ile-Pro-D-Ala-Asp-Phe | 790.2187 | 791.2267 | 813.2079 | 813.33 | 18.4 |
| 2-IBA-Ile-Pro-D-Ala-Asp-Dap | 729.1983 | 730.2063 | 752.1875 | 752.57 | 21.8 |
| 2-IBA-Ile-Pro-D-Ala-Asp-Asp | 758.1772 | 759.1852 | 781.1664 | 781.33 | 6.3 |
| 2-IBA-Ile-Pro-D-Ala-Asp-Abu | 728.2031 | 729.2111 | 751.1923 | 729.47 | 8.2 |
| 2-IBA-Ile-Pro-D-Ala-Asp-tPhe | 846.2813 | 847.2893 | 869.2705 | 869.43 | 10.4 |
| 2-IBA-Ile-Pro-D-Ala-Asp-Ser | 730.1823 | 731.1903 | 753.1715 | 753.29 | 22.5 |
| 2-IBA-Ile-Pro-D-Ala-Asp-Ala | 714.1874 | 715.1954 | 737.1766 | 737.56 | 18.4 |
| 2-IBA-Ile-Pro-D-Ala-Asp-Trp | 829.2296 | 830.2376 | 852.2188 | 830.50 | 22.8 |
| 2-IBA-Ile-Pro-D-Ala-Asp-Glu | 772.1929 | 773.2009 | 795.1821 | 795.34 | 13.2 |
| 2-IBA-Ile-Pro-D-Ala-Asp-Nva | 742.2187 | 743.2267 | 765.2079 | 743.49 | 16.7 |
| 2-IBA-Ile-Pro-D-Ala-Asp-Leu | 756.2344 | 757.2424 | 779.2236 | 779.38 | 8.7 |
| 2-IBA-Ile-Pro-D-Ala-Asp-Bip | 865.2548 | 866.2628 | 888.244 | 888.40 | 4.2 |
| 2-IBA-Ile-Pro-D-Ala-Asp-Tle | 756.2344 | 757.2424 | 779.2236 | 757.50 | 9.4 |
| 2-IBA-Ile-Pro-D-Ala-Asp-His | 780.2092 | 781.2172 | 803.1984 | 780.98 | 10.2 |
| 2-IBA-Ile-Pro-D-Ala-Asp-Asn | 757.1932 | 758.2012 | 780.1824 | 780.30 | 11.6 |
| 2-IBA-Ile-Pro-D-Ala-Asp-Tyr | 806.2136 | 807.2216 | 829.2028 | 829.58 | 12.8 |
| 2-IBA-Ile-Pro-D-Ala-Asp-Phg | 776.2031 | 777.2111 | 799.1923 | 776.98 | 3.2 |
| 2-IBA-Ile-Pro-D-Ala-Asp-Thr | 744.198 | 745.206 | 767.1872 | 744.97 | 0 |
| 2-IBA-Ile-Pro-D-Ala-Asp-Lys | 771.2453 | 772.2533 | 794.2345 | 772.17 | 9.3 |
| 2-IBA-Ile-Pro-D-Ala-Asp-Nle | 756.2344 | 757.2424 | 779.2236 | 757.01 | 2.6 |
| 2-IBA-Ile-Pro-D-Ala-Asp-Orn | 757.2296 | 758.2376 | 780.2188 | 780.34 | 18.3 |
| 2-IBA-Ile-Pro-D-Ala-Asp-hPhe | 804.2344 | 805.2424 | 827.2236 | 827.60 | 18.4 |
| 2-IBA-Ile-Pro-D-Ala-Asp-dPhe | 866.25 | 867.258 | 889.2392 | 867.52 | 22.6 |
| 2-IBA-Ile-Pro-D-Ala-Asp-1-Nap | 840.2344 | 841.2424 | 863.2236 | 863.38 | 18.4 |
| 2-IBA-Ile-Pro-D-Ala-Asp-4-Pya | 791.214 | 792.222 | 814.2032 | 792.48 | 14.2 |
| 2-IBA-Ile-Pro-D-Ala-Asp-2-Nap | 840.2344 | 841.2424 | 863.2236 | 863.38 | 16.4 |
| 2-IBA-Ile-Pro-D-Ala-Asp-3-Pya | 791.214 | 792.222 | 814.2032 | 792.04 | 17.4 |
| 2-IBA-Ile-Pro-D-Ala-Asp-2-Pya | 791.214 | 792.222 | 814.2032 | 791.99 | 3.2 |
| 2-IBA-Ile-Pro-D-Ala-Asp-Abu | 769.266 | 770.274 | 792.2552 | 792.64 | 8.9 |
| 2-IBA-Ile-Pro-D-Ala-Val-Gln | 755.2503 | 756.2583 | 778.2395 | 756.18 | 10.2 |
| 2-IBA-Ile-Pro-D-Ala-Phe-Gln | 803.2503 | 804.2583 | 826.2395 | 826.40 | 12.6 |

| | | | | | |
|---|---|---|---|---|---|
| 2-IBA-Ile-Pro-D-Ala-Dap-Gln | 742.2299 | 743.2379 | 765.2191 | 743.50 | 3.4 |
| 2-IBA-Ile-Pro-D-Ala-Abu-Gln | 741.2347 | 742.2427 | 764.2239 | 764.38 | 7.8 |
| 2-IBA-Ile-Pro-D-Ala-tPhe-Gln | 859.3129 | 860.3209 | 882.3021 | 860.09 | 16.7 |
| 2-IBA-Ile-Pro-D-Ala-Gln-Gln | 784.2405 | 785.2485 | 807.2297 | 807.35 | 3.2 |
| 2-IBA-Ile-Pro-D-Ala-Ser-Gln | 743.214 | 744.222 | 766.2032 | 766.58 | 21.4 |
| 2-IBA-Ile-Pro-D-Ala-Ala-Gln | 727.219 | 728.227 | 750.2082 | 750.37 | 18.6 |
| 2-IBA-Ile-Pro-D-Ala-Trp-Gln | 842.2612 | 843.2692 | 865.2504 | 865.37 | 10.2 |
| 2-IBA-Ile-Pro-D-Ala-Glu-Gln | 785.2245 | 786.2325 | 808.2137 | 808.47 | 4.8 |
| 2-IBA-Ile-Pro-D-Ala-Nva-Gln | 755.2503 | 756.2583 | 778.2395 | 756.18 | 9.3 |
| 2-IBA-Ile-Pro-D-Ala-Leu-Gln | 769.266 | 770.274 | 792.2552 | 770.53 | NP |
| 2-IBA-Ile-Pro-D-Ala-Bip-Gln | 879.2816 | 880.2896 | 902.2708 | 902.43 | 6.8 |
| 2-IBA-Ile-Pro-D-Ala-Tle-Gln | 769.266 | 770.274 | 792.2552 | 770.04 | 9 |
| 2-IBA-Ile-Pro-D-Ala-His-Gln | 793.2408 | 794.2488 | 816.23 | 794.01 | 4.3 |
| 2-IBA-Ile-Pro-D-Ala-Asn-Gln | 770.2249 | 771.2329 | 793.2141 | 771.00 | 12.7 |
| 2-IBA-Ile-Pro-D-Ala-Tyr-Gln | 819.2453 | 820.2533 | 842.2345 | 842.35 | 18.9 |
| 2-IBA-Ile-Pro-D-Ala-Phg-Gln | 789.2347 | 790.2427 | 812.2239 | 812.60 | 6.8 |
| 2-IBA-Ile-Pro-D-Ala-Thr-Gln | 757.2296 | 758.2376 | 780.2188 | 758.50 | 3.4 |
| 2-IBA-Ile-Pro-D-Ala-Lys-Gln | 784.2769 | 785.2849 | 807.2661 | 807.43 | 0 |
| 2-IBA-Ile-Pro-D-Ala-Nle-Gln | 769.266 | 770.274 | 792.2552 | 792.52 | 2.6 |
| 2-IBA-Ile-Pro-D-Ala-Orn-Gln | 770.2612 | 771.2692 | 793.2504 | 793.73 | 8.9 |
| 2-IBA-Ile-Pro-D-Ala-hPhe-Gln | 817.266 | 818.274 | 840.2552 | 840.42 | 10.2 |
| 2-IBA-Ile-Pro-D-Ala-dPhe-Gln | 879.2816 | 880.2896 | 902.2708 | 902.75 | 8.9 |
| 2-IBA-Ile-Pro-D-Ala-1-Nap-Gln | 853.266 | 854.274 | 876.2552 | 854.19 | 3.7 |
| 2-IBA-Ile-Pro-D-Ala-4-Pya-Gln | 804.2456 | 805.2536 | 827.2348 | 827.49 | 3.2 |
| 2-IBA-Ile-Pro-D-Ala-2-Nap-Gln | 853.266 | 854.274 | 876.2552 | 876.42 | 10.2 |
| 2-IBA-Ile-Pro-D-Ala-3-Pya-Gln | 804.2456 | 805.2536 | 827.2348 | 805.02 | 4.8 |
| 2-IBA-Ile-Pro-D-Ala-2-Pya-Gln | 804.2456 | 805.2536 | 827.2348 | 805.02 | 8.7 |
| 2-IBA-Val-Pro-D-Ala-Asp-Gln | 757.1932 | 758.2012 | 780.1824 | 758.46 | 4.6 |
| 2-IBA-Phe-Pro-D-Ala-Asp-Gln | 805.1932 | 806.2012 | 828.1824 | 828.34 | 2.3 |
| 2-IBA-Dap-Pro-D-Ala-Asp-Gln | 744.1728 | 745.1808 | 767.162 | 767.32 | 16.8 |
| 2-IBA-Asp-Pro-D-Ala-Asp-Gln | 773.1517 | 774.1597 | 796.1409 | 774.08 | 14.2 |
| 2-IBA-Abu-Pro-D-Ala-Asp-Gln | 743.1776 | 744.1856 | 766.1668 | 766.43 | 6.8 |
| 2-IBA-tPhe-Pro-D-Ala-Asp-Gln | 861.2558 | 862.2638 | 884.245 | 862.03 | 5.3 |
| 2-IBA-Gln-Pro-D-Ala-Asp-Gln | 786.1834 | 787.1914 | 809.1726 | 809.29 | 2.9 |
| 2-IBA-Ser-Pro-D-Ala-Asp-Gln | 745.1568 | 746.1648 | 768.146 | 768.53 | 7.2 |
| 2-IBA-Ala-Pro-D-Ala-Asp-Gln | 729.1619 | 730.1699 | 752.1511 | 729.94 | 0 |
| 2-IBA-Trp-Pro-D-Ala-Asp-Gln | 844.2041 | 845.2121 | 867.1933 | 844.98 | 2.6 |
| 2-IBA-Glu-Pro-D-Ala-Asp-Gln | 787.1674 | 788.1754 | 810.1566 | 810.32 | 4.3 |

| | | | | | |
|---|---|---|---|---|---|
| 2-IBA-Nva-Pro-D-Ala-Asp-Gln | 757.1932 | 758.2012 | 780.1824 | 758.46 | 9.5 |
| 2-IBA-Leu-Pro-D-Ala-Asp-Gln | 777.2089 | 778.2169 | 800.1981 | 800.36 | 10.2 |
| 2-IBA-Bip-Pro-D-Ala-Asp-Gln | 881.2245 | 882.2325 | 904.2137 | 904.37 | 18.3 |
| 2-IBA-Tle-Pro-D-Ala-Asp-Gln | 771.2089 | 772.2169 | 794.1981 | 794.68 | 16.4 |
| 2-IBA-His-Pro-D-Ala-Asp-Gln | 795.1837 | 796.1917 | 818.1729 | 796.11 | 2.8 |
| 2-IBA-Asn-Pro-D-Ala-Asp-Gln | 772.1677 | 773.1757 | 795.1569 | 795.32 | 8.3 |
| 2-IBA-Tyr-Pro-D-Ala-Asp-Gln | 821.1881 | 822.1961 | 844.1773 | 822.12 | 6.5 |
| 2-IBA-Phg-Pro-D-Ala-Asp-Gln | 791.1776 | 792.1856 | 814.1668 | 791.95 | 12.7 |
| 2-IBA-Thr-Pro-D-Ala-Asp-Gln | 759.1725 | 760.1805 | 782.1617 | 782.28 | 4.2 |
| 2-IBA-Lys-Pro-D-Ala-Asp-Gln | 786.2198 | 787.2278 | 809.209 | 809.59 | 13.2 |
| 2-IBA-Nle-Pro-D-Ala-Asp-Gln | 771.2089 | 772.2169 | 794.1981 | 794.36 | 19.5 |
| 2-IBA-Orn-Pro-D-Ala-Asp-Gln | 772.2041 | 773.2121 | 795.1933 | 773.13 | 20.2 |
| 2-IBA-hPhe-Pro-D-Ala-Asp-Gln | 819.2089 | 820.2169 | 842.1981 | 842.36 | 9.3 |
| 2-IBA-dPhe-Pro-D-Ala-Asp-Gln | 881.2245 | 882.2325 | 904.2137 | 882.49 | 5.6 |
| 2-IBA-1-Nap-Pro-D-Ala-Asp-Gln | 855.2089 | 856.2169 | 878.1981 | 878.36 | 2.5 |
| 2-IBA-4-Pya-Pro-D-Ala-Asp-Gln | 806.1885 | 807.1965 | 829.1777 | 829.34 | 0 |
| 2-IBA-2-Nap-Pro-D-Ala-Asp-Gln | 855.2089 | 856.2169 | 878.1981 | 856.48 | 2.3 |
| 2-IBA-3-Pya-Pro-D-Ala-Asp-Gln | 806.1885 | 807.1965 | 829.1777 | 829.34 | 11.4 |
| 2-IBA-2-Pya-Pro-D-Ala-Asp-Gln | 806.1885 | 807.1965 | 829.1777 | 807.12 | 8.7 |
| | | | | | |
| 2-IBA-hPhe-Pro-D-Ala-Phg-Ile | 822.2602 | 823.2682 | 845.2494 | 823.03 | 13.3 |
| 2-IBA-hPhe-Pro-D-Ala-Phg-Val | 808.2445 | 809.2525 | 831.2337 | 809.02 | 2.4 |
| 2-IBA-hPhe-Pro-D-Ala-Phg-Phe | 856.2445 | 857.2525 | 879.2337 | 857.02 | 7.8 |
| 2-IBA-hPhe-Pro-D-Ala-Phg-Dap | 795.2241 | 796.2321 | 818.2133 | 796.68 | 9.6 |
| 2-IBA-hPhe-Pro-D-Ala-Phg-Abu | 794.2289 | 795.2369 | 817.2181 | 795.10 | 10.4 |
| 2-IBA-hPhe-Pro-D-Ala-Phg-tPhe | 912.3071 | 913.3151 | 935.2963 | 913.08 | 3.4 |
| 2-IBA-hPhe-Pro-D-Ala-Phg-Gln | 837.2347 | 838.2427 | 860.2239 | 838.69 | 6.4 |
| 2-IBA-hPhe-Pro-D-Ala-Phg-Ser | 796.2081 | 797.2161 | 819.1973 | 819.36 | 8.9 |
| 2-IBA-hPhe-Pro-D-Ala-Phg-Ala | 780.2132 | 781.2212 | 803.2024 | 780.99 | 2.1 |
| 2-IBA-hPhe-Pro-D-Ala-Phg-Trp | 895.2554 | 896.2634 | 918.2446 | 896.03 | 0 |
| 2-IBA-hPhe-Pro-D-Ala-Phg-Glu | 838.2187 | 839.2267 | 861.2079 | 838.99 | 3.8 |
| 2-IBA-hPhe-Pro-D-Ala-Phg-Nva | 808.2445 | 809.2525 | 831.2337 | 809.70 | 12.2 |
| 2-IBA-hPhe-Pro-D-Ala-Phg-Leu | 822.2602 | 823.2682 | 845.2494 | 823.72 | 4.6 |
| 2-IBA-hPhe-Pro-D-Ala-Phg-Bip | 932.2758 | 933.2838 | 955.265 | 955.43 | 2.6 |
| 2-IBA-hPhe-Pro-D-Ala-Phg-Tle | 822.2602 | 823.2682 | 845.2494 | 845.41 | 5.4 |
| 2-IBA-hPhe-Pro-D-Ala-Phg-His | 846.235 | 847.243 | 869.2242 | 847.69 | 13.2 |
| 2-IBA-hPhe-Pro-D-Ala-Phg-Asn | 823.219 | 824.227 | 846.2082 | 824.09 | 7.8 |
| 2-IBA-hPhe-Pro-D-Ala-Phg-Tyr | 872.2394 | 873.2474 | 895.2286 | 873.01 | 12.5 |

| | | | | | |
|---|---|---|---|---|---|
| 2-IBA-hPhe-Pro-D-Ala-Phg-Phg | 842.2289 | 843.2369 | 865.2181 | 865.38 | 0 |
| 2-IBA-hPhe-Pro-D-Ala-Phg-Thr | 810.2238 | 811.2318 | 833.213 | 811.68 | 7.6 |
| 2-IBA-hPhe-Pro-D-Ala-Phg-Lys | 837.2711 | 838.2791 | 860.2603 | 860.42 | 4.8 |
| 2-IBA-hPhe-Pro-D-Ala-Phg-Nle | 822.2602 | 823.2682 | 845.2494 | 823.03 | 3.4 |
| 2-IBA-hPhe-Pro-D-Ala-Phg-Orn | 823.2554 | 824.2634 | 846.2446 | 824.03 | 8.2 |
| 2-IBA-hPhe-Pro-D-Ala-Phg-hPhe | 870.2602 | 871.2682 | 893.2494 | 871.03 | 2.7 |
| 2-IBA-hPhe-Pro-D-Ala-Phg-dPhe | 932.2758 | 933.2838 | 955.265 | 933.73 | NP |
| 2-IBA-hPhe-Pro-D-Ala-Phg-1-Nap | 906.2602 | 907.2682 | 929.2494 | 929.41 | 11.2 |
| 2-IBA-hPhe-Pro-D-Ala-Phg-4-Pya | 857.2398 | 858.2478 | 880.229 | 880.39 | 10.7 |
| 2-IBA-hPhe-Pro-D-Ala-Phg-2-Nap | 906.2602 | 907.2682 | 929.2494 | 907.13 | 4.5 |
| 2-IBA-hPhe-Pro-D-Ala-Phg-3-Pya | 857.2398 | 858.2478 | 880.229 | 858.01 | 3.4 |
| 2-IBA-hPhe-Pro-D-Ala-Phg-2-Pya | 857.2398 | 858.2478 | 880.229 | 858.70 | 7.9 |

Appendix B

Supplementary Information for Chapter 3

HYPERVALENT IODOARENE PEPTIDES FOR THE $\alpha$-OXYTOSYLATION OF 1-INDANONE

$^1$H NMR Spectra of Racemic **III-8**, 1-oxo-2,3-dihydro-1H-inden-2-yl 4-methylbenzenesulfonate

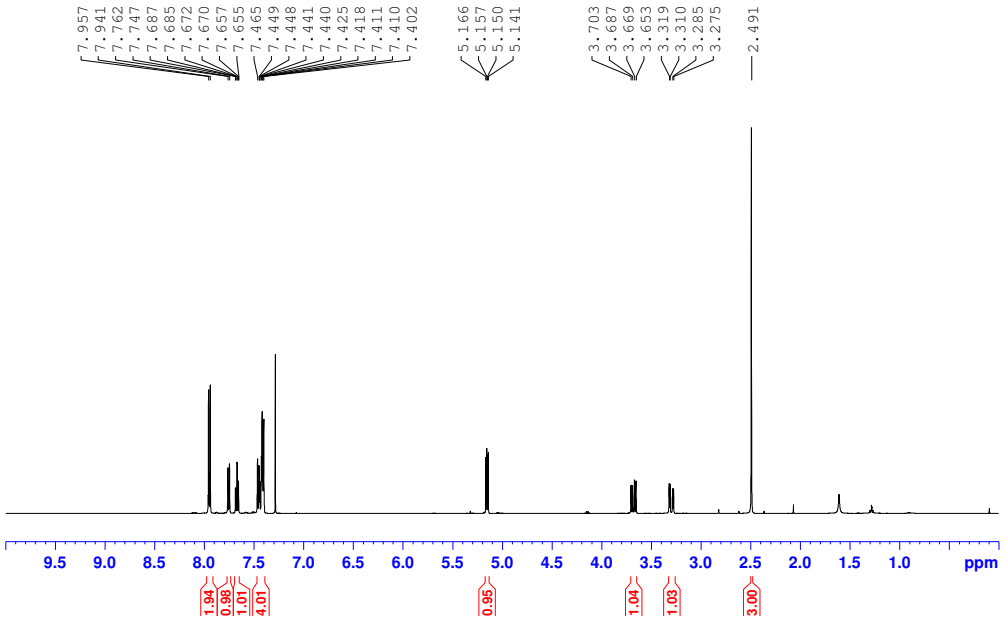

$^{13}C$ NMR Spectra of Racemic **III-8**, 1-oxo-2,3-dihydro-1H-inden-2-yl 4-methylbenzenesulfonate

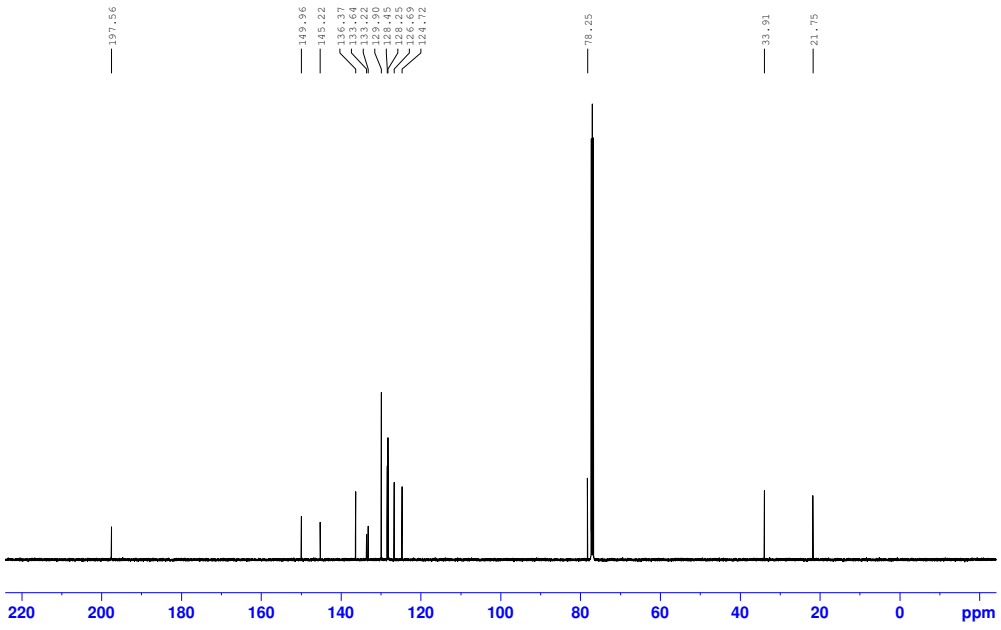

$^{1}$H NMR Spectra of Racemic **III-32**, 1-oxo-2,3-dihydro-1H-inden-2-yl naphthalene-1-sulfonate

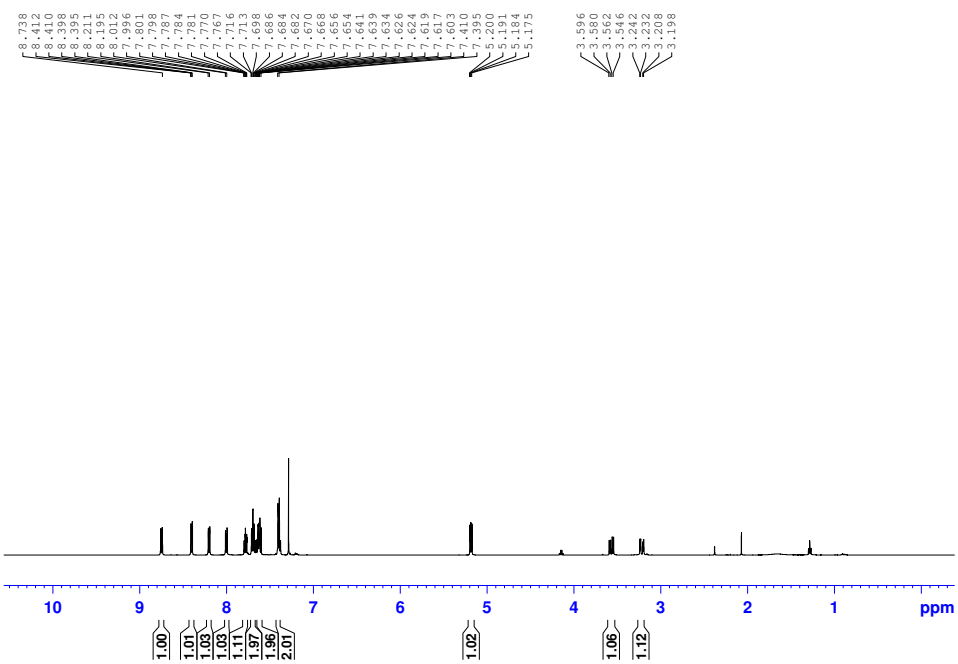

$^{13}$C NMR Spectra of Racemic **III-32,** 1-oxo-2,3-dihydro-1H-inden-2-yl naphthalene-1-sulfonate

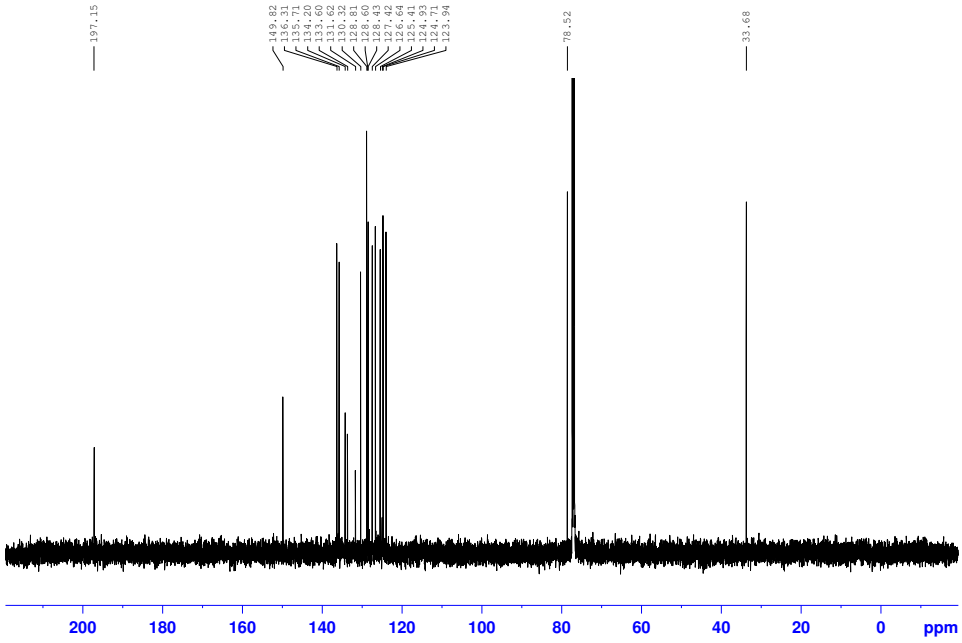

[1]H NMR Spectra of Racemic **III-33**, 1-oxo-2,3-dihydro-1H-inden-2-yl methanesulfonate

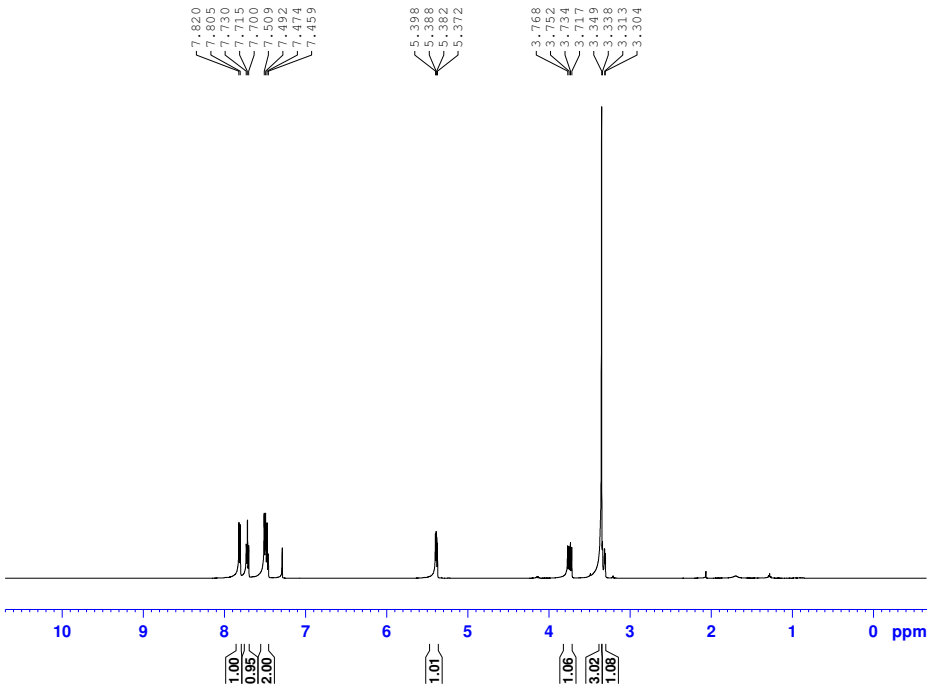

$^{13}$C NMR Spectra of Racemic **III-33**, 1-oxo-2,3-dihydro-1H-inden-2-yl methanesulfonate

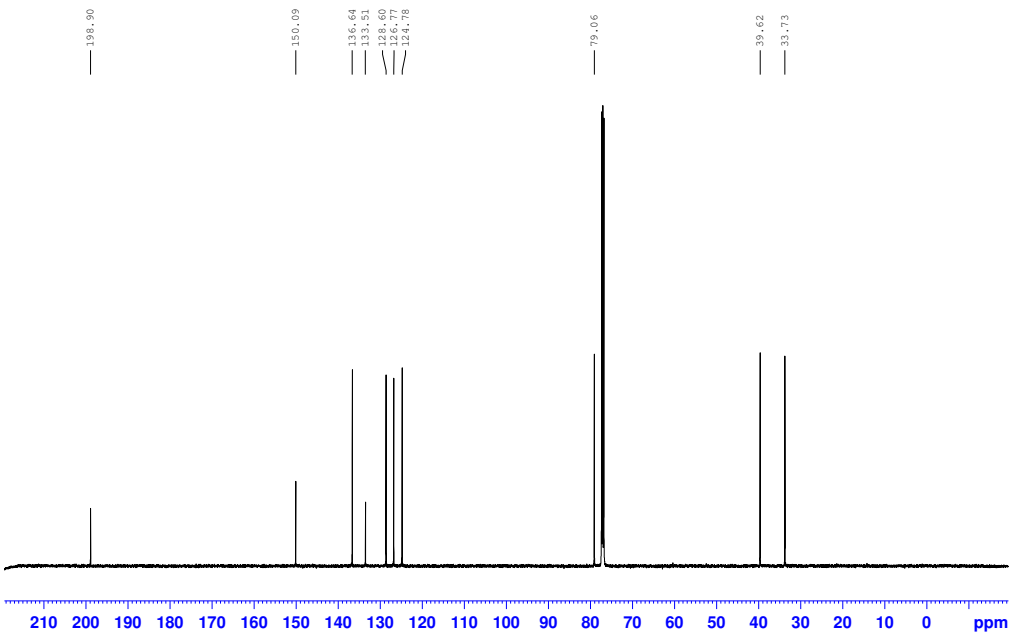

HPLC Chromatogram of Racemic **III-8**, 1-oxo-2,3-dihydro-1H-inden-2-yl 4-methylbenzenesulfonate

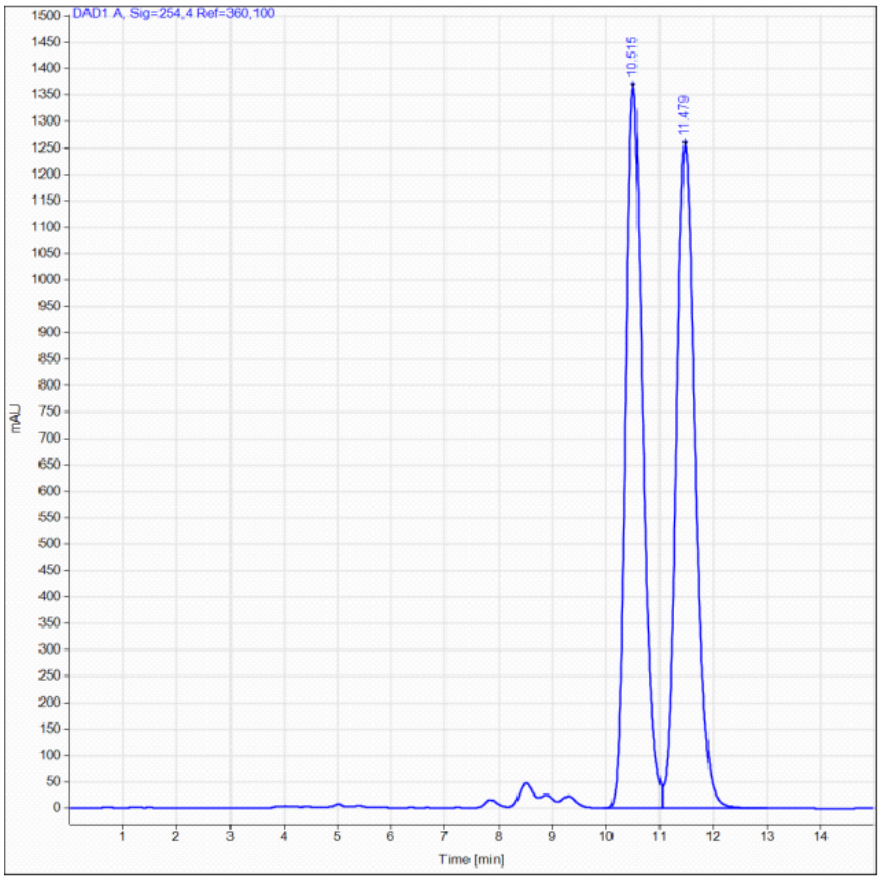


**Signal:** DAD1 A, Sig=254,4 Ref=360,100

| RT [min] | Type | Width [min] | Area | Height | Area% | Name |
|---|---|---|---|---|---|---|
| 10.515 | BV | 0.3442 | 30478.7578 | 1366.5145 | 49.6200 | |
| 11.479 | VB | 0.3794 | 30945.6250 | 1256.1721 | 50.3800 | |
| | | Sum | 61424.3828 | | | |

HPLC Chromatogram of **III-8** from "hit" peptide **III-10**, 48% *ee*

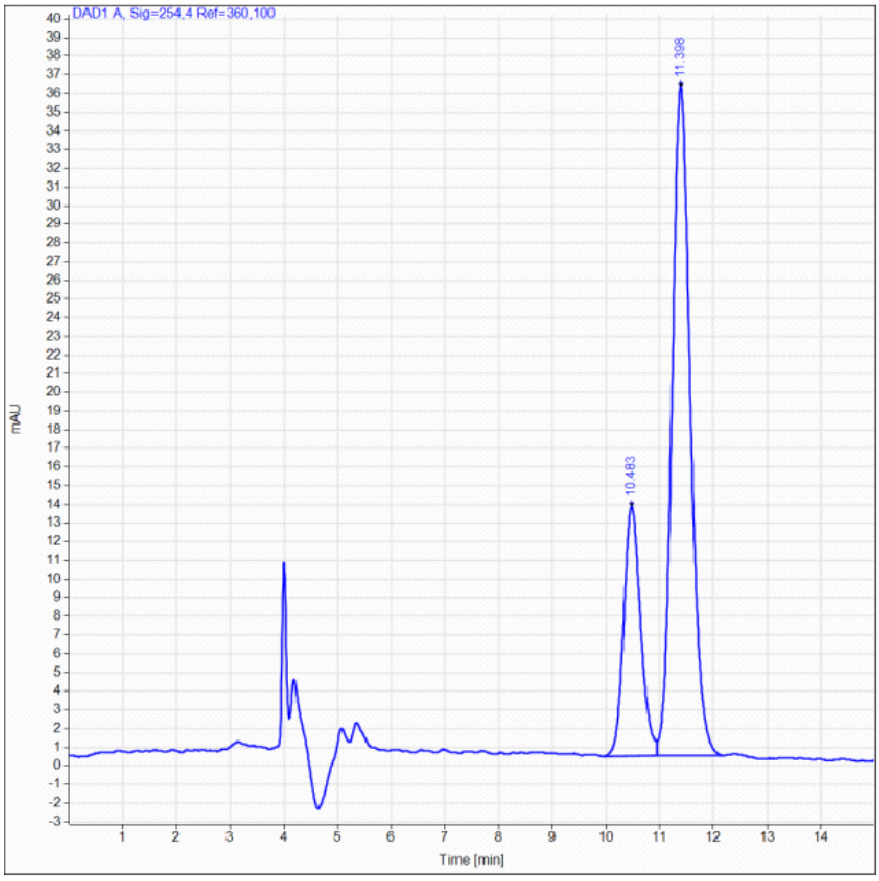


**Signal:** DAD1 A, Sig=254,4 Ref=360,100

| RT [min] | Type | Width [min] | Area | Height | Area% | Name |
|---|---|---|---|---|---|---|
| 10.483 | BV | 0.3342 | 293.6139 | 13.3698 | 25.5536 | |
| 11.398 | VB | 0.3644 | 855.3958 | 35.8491 | 74.4464 | |
| | | Sum | 1149.0096 | | | |

HPLC Chromatogram of **III-8** from "hit" peptide **III-10** under optimized reaction conditions , 65% *ee*

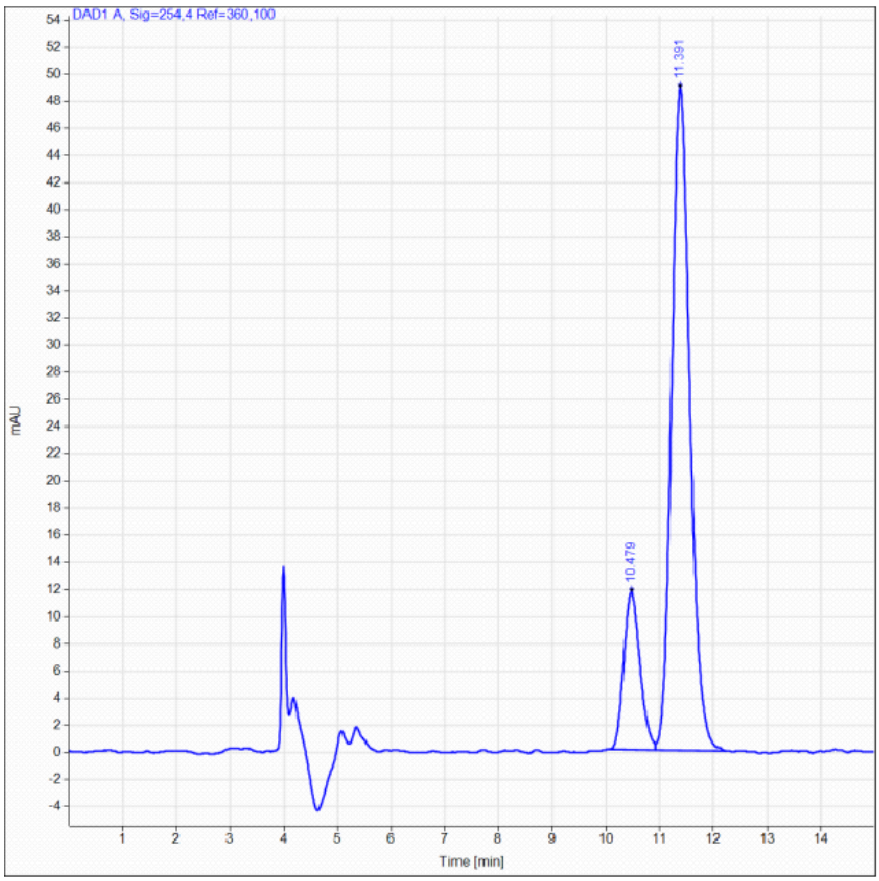


**Signal:** DAD1 A, Sig=254,4 Ref=360,100

| RT [min] | Type | Width [min] | Area | Height | Area% | Name |
|---|---|---|---|---|---|---|
| 10.479 | BV | 0.3304 | 245.6842 | 11.6345 | 17.4428 | |
| 11.391 | VB | 0.3654 | 1162.8314 | 48.9005 | 82.5572 | |
| | | Sum | 1408.5156 | | | |

Non-Polar (Hexanes and Toluene) Co-Solvent Screen

HPLC Chromatogram for Racemic Product **III-8**

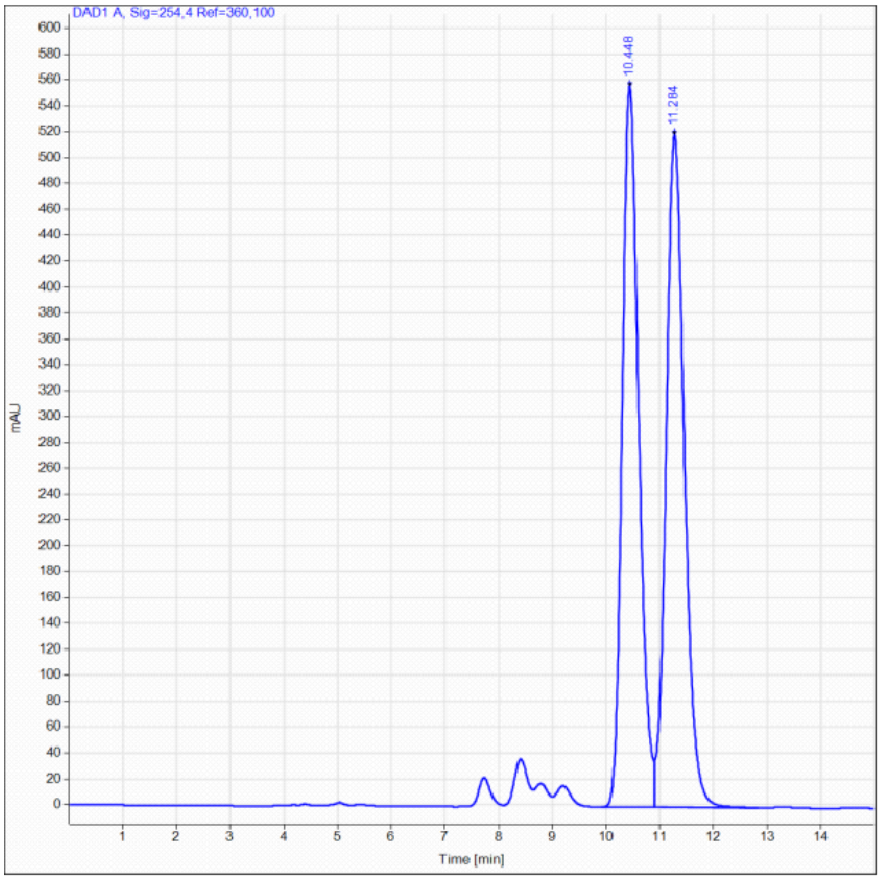


**Signal:** DAD1 A, Sig=254,4 Ref=360,100

| RT [min] | Type | Width [min] | Area | Height | Area% | Name |
|---|---|---|---|---|---|---|
| 10.448 | BV | 0.3301 | 11952.0762 | 557.5700 | 49.3081 | |
| 11.284 | VB | 0.3618 | 12287.5264 | 519.6852 | 50.6919 | |
| | | Sum | 24239.6025 | | | |

Table 3.6, Entry 1: Product **III-8**, 22% *ee*

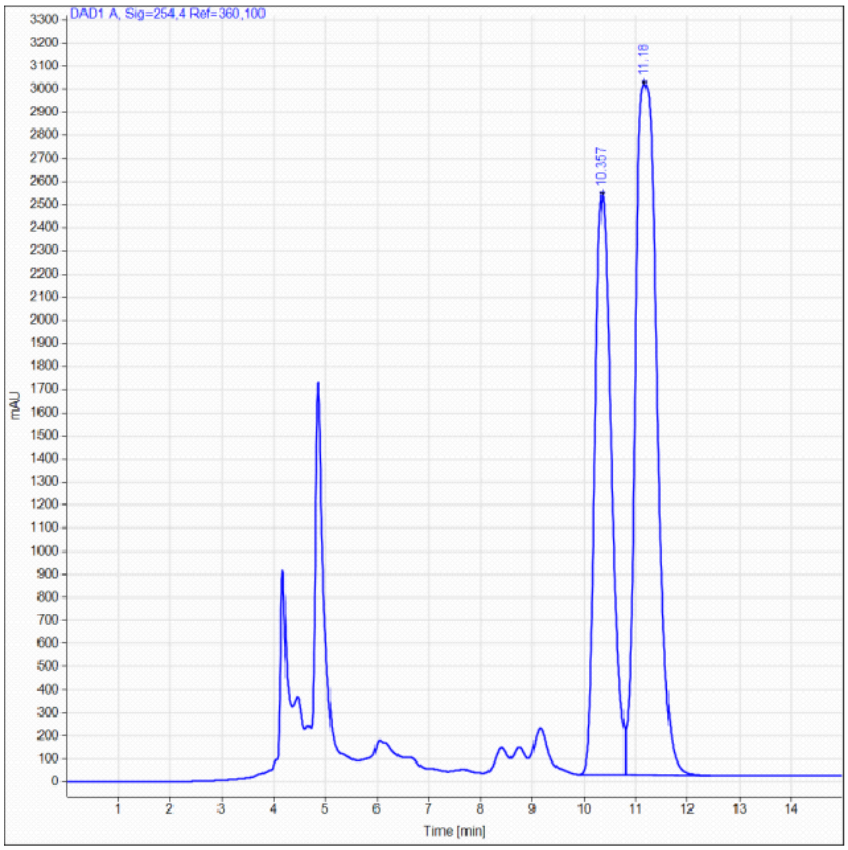


**Signal:** DAD1 A, Sig=254,4 Ref=360,100

| RT [min] | Type | Width [min] | Area | Height | Area% | Name |
|---|---|---|---|---|---|---|
| 10.357 | BV | 0.3469 | 55647.3789 | 2507.3840 | 39.0632 | |
| 11.180 | VB | 0.4548 | 86807.4141 | 2989.0322 | 60.9368 | |
| | | Sum | 142454.7930 | | | |

Table 3.6, Entry 2: Product **III-8**, 22% *ee*

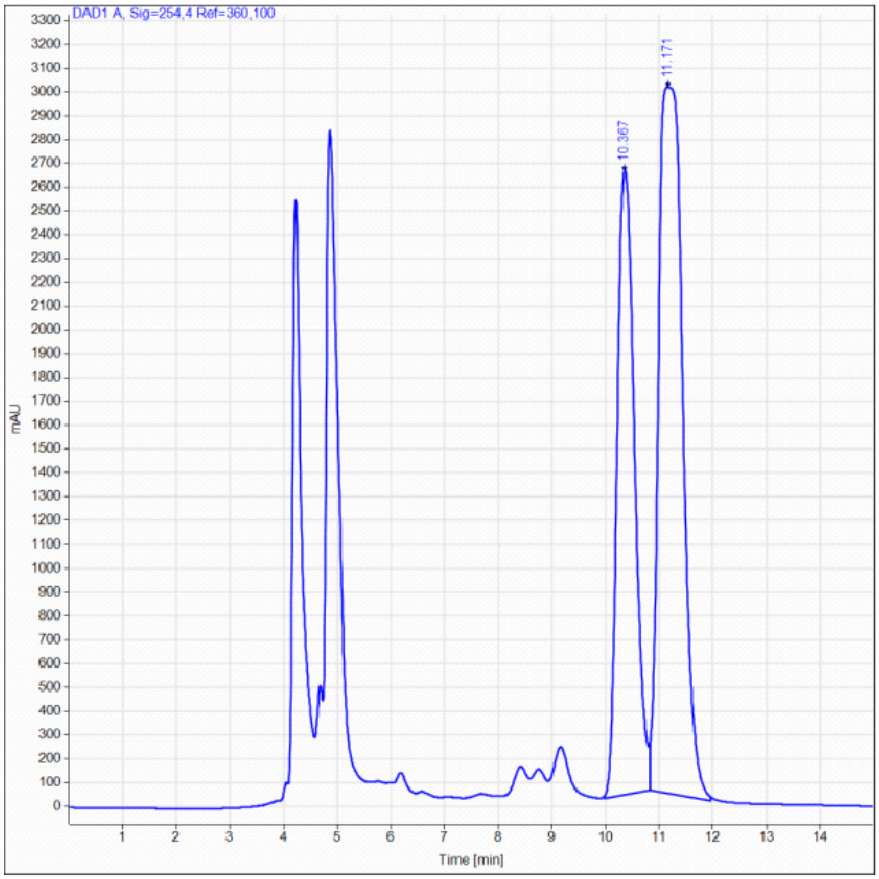


**Signal:** DAD1 A, Sig=254,4 Ref=360,100

| RT [min] | Type | Width [min] | Area | Height | Area% | Name |
|---|---|---|---|---|---|---|
| 10.367 | MM | 0.3758 | 59112.8906 | 2621.9800 | 39.0394 | |
| 11.171 | MM | 0.5186 | 92305.7031 | 2966.4111 | 60.9606 | |
| | | Sum | 151418.5938 | | | |

Table 3.6, Entry 3: Product **III-8**, 28% *ee*

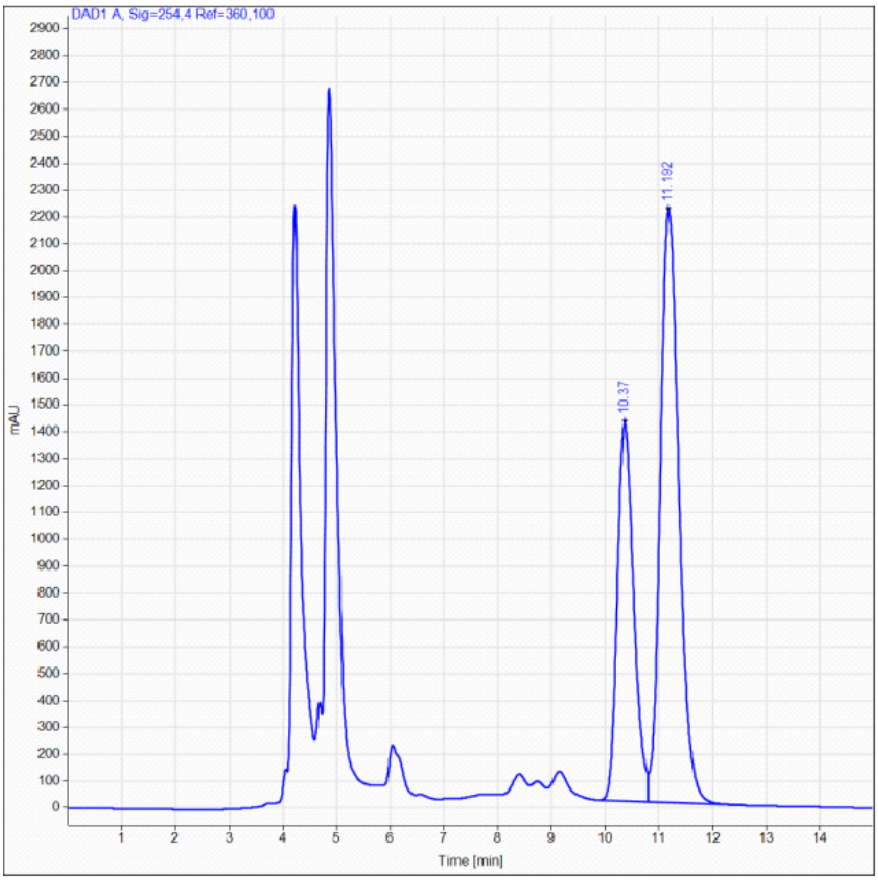


**Signal:** DAD1 A, Sig=254,4 Ref=360,100

| RT [min] | Type | Width [min] | Area | Height | Area% | Name |
|---|---|---|---|---|---|---|
| 10.370 | BV | 0.3284 | 29882.7539 | 1403.7006 | 36.0524 | |
| 11.192 | VBA | 0.3726 | 53004.2422 | 2203.4326 | 63.9476 | |
| | | Sum | 82886.9961 | | | |

Table 3.6, Entry 4: Product **III-8**, 27% *ee*

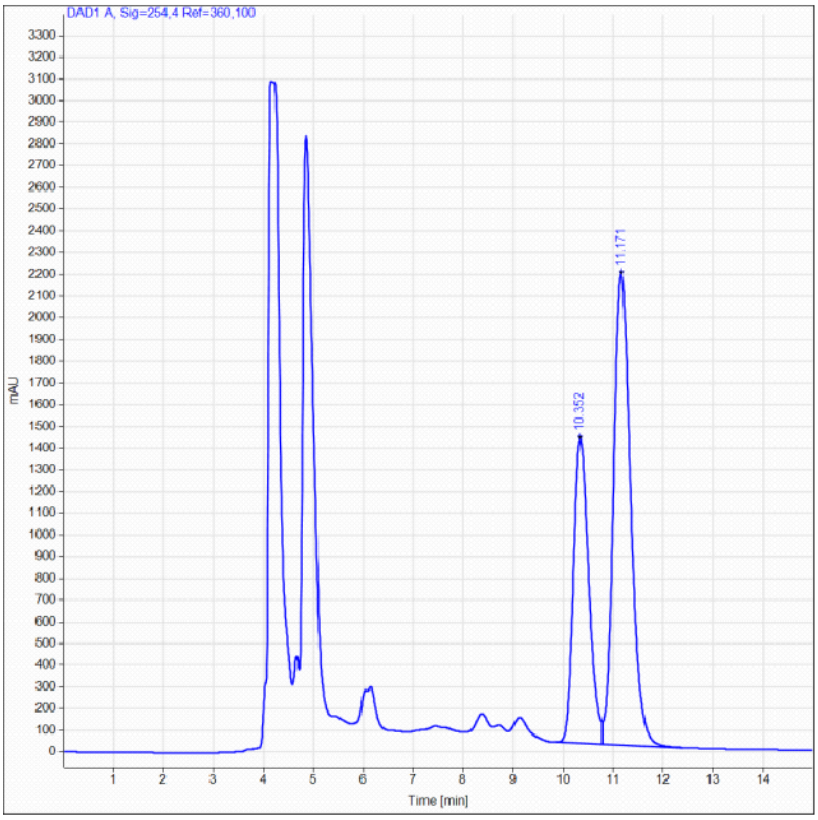


**Signal:** DAD1 A, Sig=254,4 Ref=360,100

| RT [min] | Type | Width [min] | Area | Height | Area% | Name |
|---|---|---|---|---|---|---|
| 10.352 | BV | 0.3281 | 29767.6074 | 1399.8297 | 36.4573 | |
| 11.171 | VBA | 0.3713 | 51882.9648 | 2167.2859 | 63.5427 | |
| | | Sum | 81650.5723 | | | |

Table 3.6, Entry 5: Product **III-8**, 15% *ee*

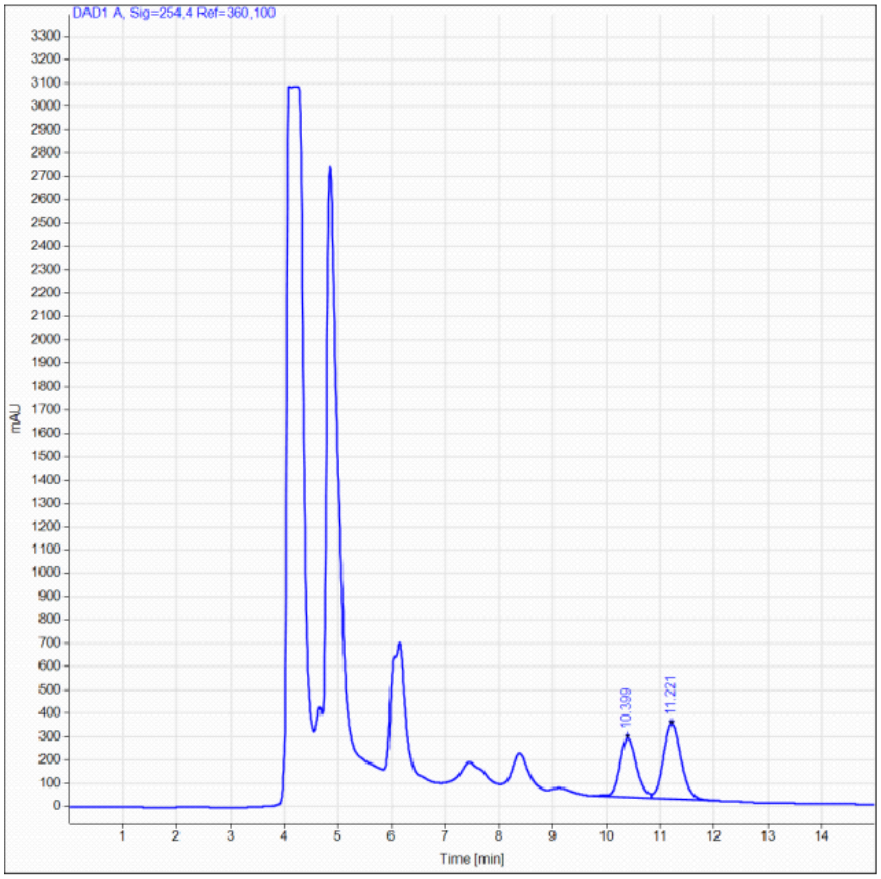


**Signal:** DAD1 A, Sig=254,4 Ref=360,100

| RT [min] | Type | Width [min] | Area | Height | Area% | Name |
|---|---|---|---|---|---|---|
| 10.399 | BV | 0.3313 | 5452.6807 | 253.1517 | 42.5415 | |
| 11.221 | VB | 0.3535 | 7364.6396 | 321.2422 | 57.4585 | |
| | | Sum | 12817.3203 | | | |

Table 3.6, Entry 6: Product **III-8**, 14% *ee*

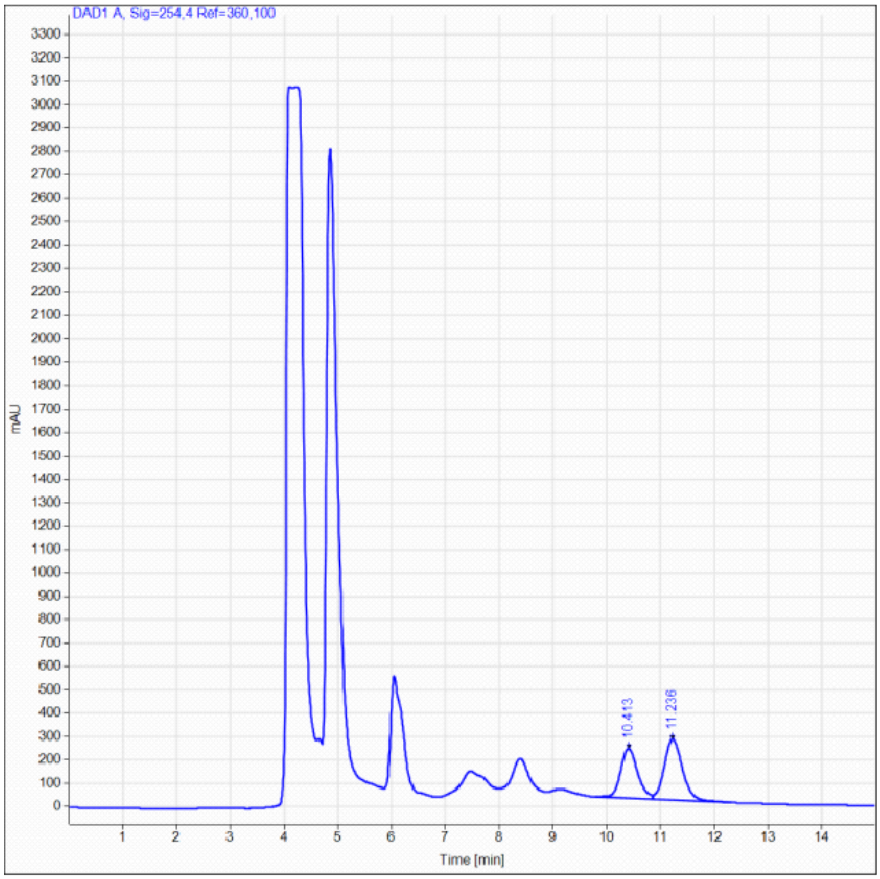


**Signal:** DAD1 A, Sig=254,4 Ref=360,100

| RT [min] | Type | Width [min] | Area | Height | Area% | Name |
|---|---|---|---|---|---|---|
| 10.413 | BV | 0.3349 | 4640.2798 | 212.4171 | 43.1119 | |
| 11.236 | VB | 0.3615 | 6123.0654 | 259.2653 | 56.8881 | |
| | | Sum | 10763.3452 | | | |

Table 3.6, Entry 7: Product **III-8**, 28% *ee*

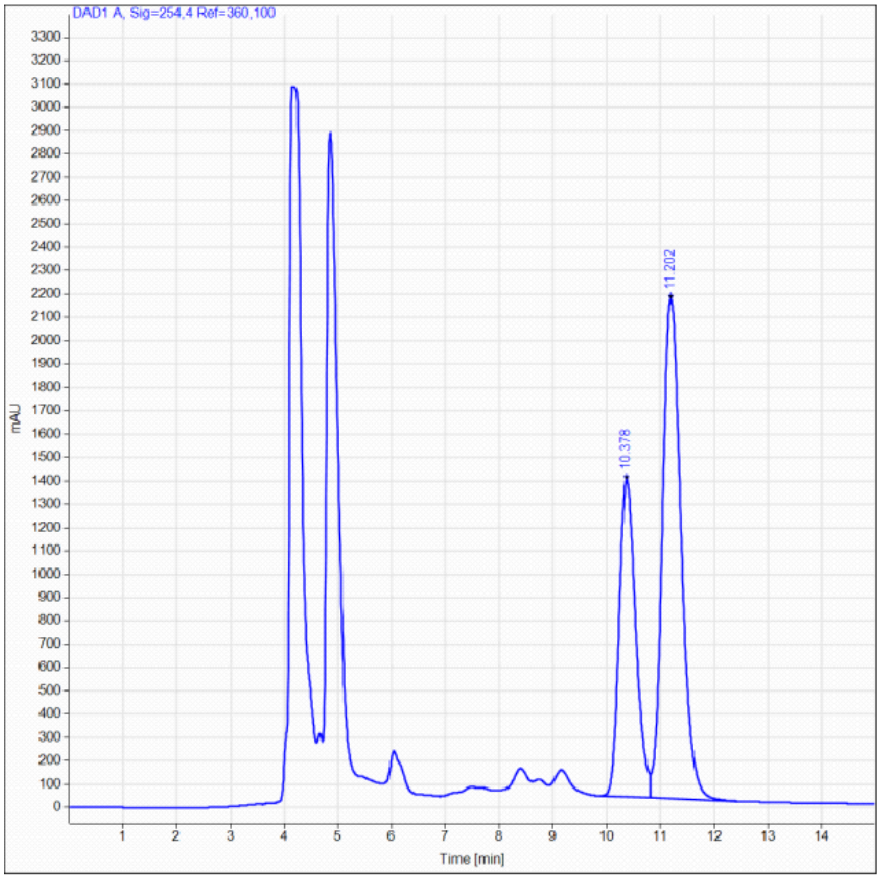


**Signal:** DAD1 A, Sig=254,4 Ref=360,100

| RT [min] | Type | Width [min] | Area | Height | Area% | Name |
|---|---|---|---|---|---|---|
| 10.378 | BV | 0.3293 | 29062.5996 | 1359.8998 | 36.0345 | |
| 11.202 | VB | 0.3731 | 51589.6406 | 2140.9775 | 63.9655 | |
| | | Sum | 80652.2402 | | | |

Table 3.6, Entry 8: Product **III-8**, 26% *ee*

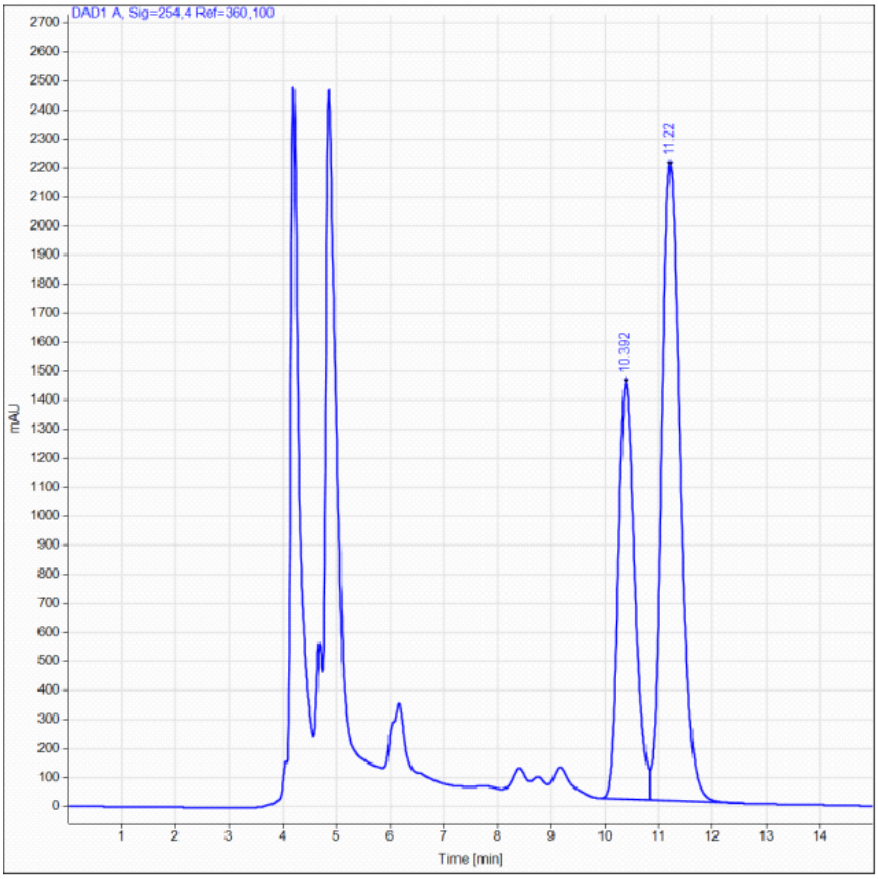


**Signal:** DAD1 A, Sig=254,4 Ref=360,100

| RT [min] | Type | Width [min] | Area | Height | Area% | Name |
|---|---|---|---|---|---|---|
| 10.392 | BV | 0.3313 | 30681.4258 | 1435.9722 | 36.7551 | |
| 11.220 | VBA | 0.3734 | 52793.7539 | 2189.1245 | 63.2449 | |
| | | Sum | 83475.1797 | | | |

Table 3.6, Entry 9: Product **III-8**, 22% *ee*

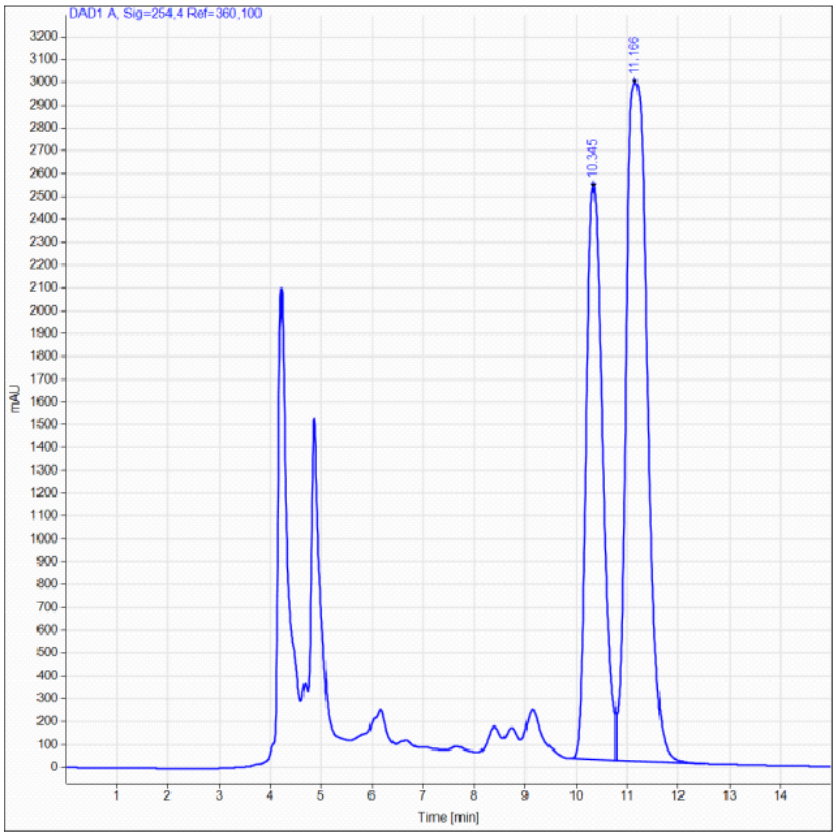


**Signal:** DAD1 A, Sig=254,4 Ref=360,100

| RT [min] | Type | Width [min] | Area | Height | Area% | Name |
|---|---|---|---|---|---|---|
| 10.345 | BV | 0.3468 | 55549.2305 | 2504.4170 | 39.1640 | |
| 11.166 | VBA | 0.4552 | 86288.3125 | 2967.8594 | 60.8360 | |
| | | Sum | 141837.5430 | | | |

Table 3.6, Entry 10: Product **III-8**, 24% *ee*

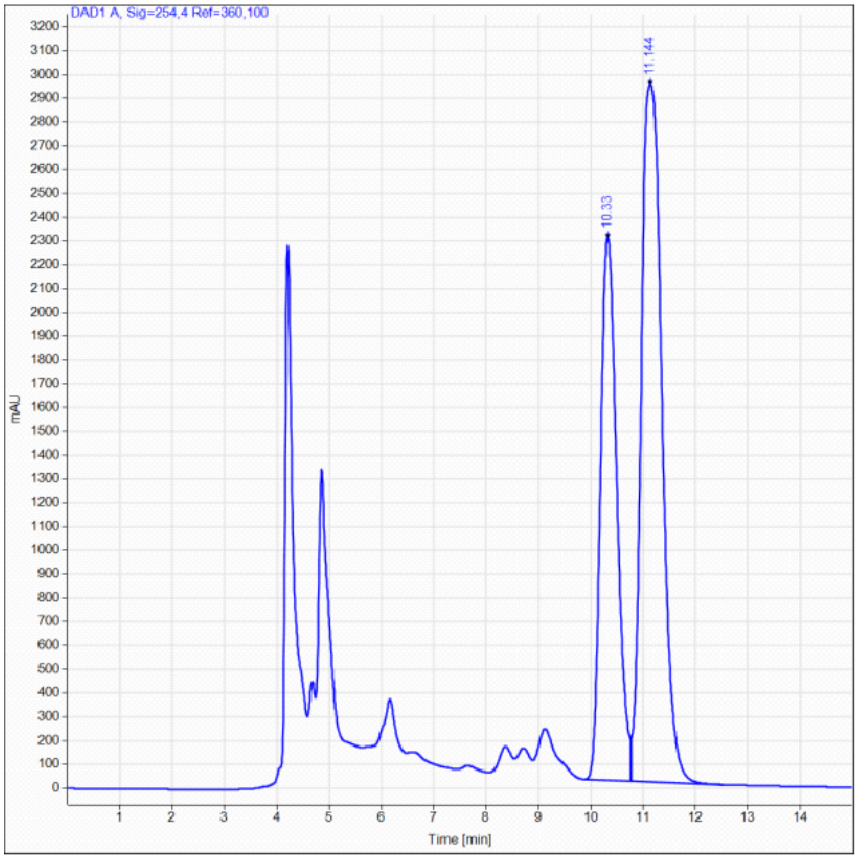


**Signal:** DAD1 A, Sig=254,4 Ref=360,100

| RT [min] | Type | Width [min] | Area | Height | Area% | Name |
|---|---|---|---|---|---|---|
| 10.330 | BV | 0.3364 | 49347.8242 | 2280.9819 | 37.9812 | |
| 11.144 | VBA | 0.4305 | 80579.0781 | 2933.5876 | 62.0188 | |
| | | Sum | 129926.9023 | | | |

Peptides Screened in the α-sulfonylation of 1-indanone reaction using alternative nucleophiles

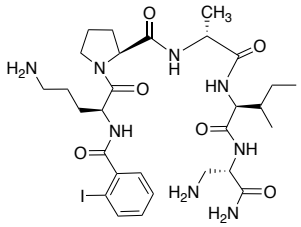

**III-32**
2-IBA-Orn-Pro-D-Ala-Ile-Dap

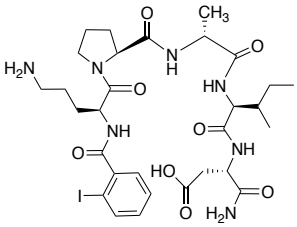

**III-33**
2-IBA-Orn-Pro-D-Ala-Ile-Asp

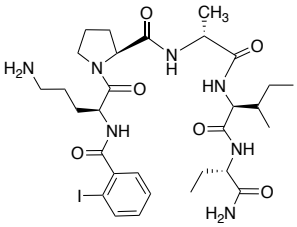

**III-34**
2-IBA-Orn-Pro-D-Ala-Ile-Abu

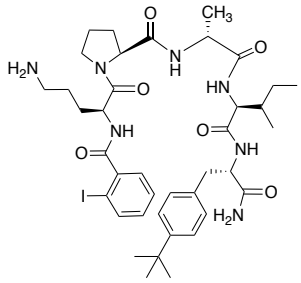

**III-35**
2-IBA-Orn-Pro-D-Ala-Ile-tPhe

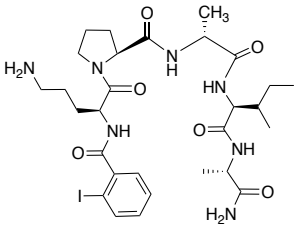

**III-36**
2-IBA-Orn-Pro-D-Ala-Ile-Ala

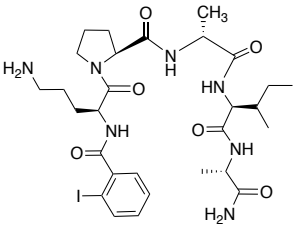

**III-37**
2-IBA-Orn-Pro-D-Ala-Ile-Phg

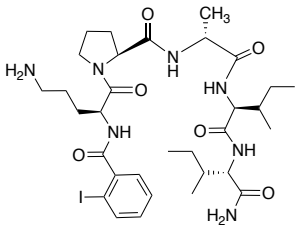

**III-38**
2-IBA-Orn-Pro-D-Ala-Ile-Ile

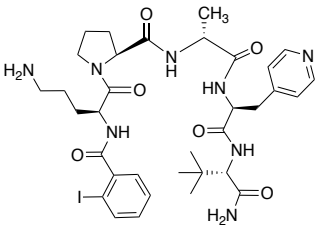

**III-39**
2-IBA-Orn-Pro-D-Ala-4-Pya-Tle

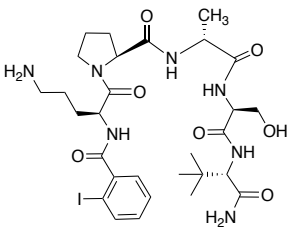

**III-40**
2-IBA-Orn-Pro-D-Ala-Ser-Tle

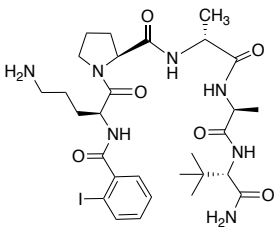

**III-41**
2-IBA-Orn-Pro-D-Ala-Ala-Tle

HPLC Chromatograms for Product **III-32**

Chiral HPLC Spectra of Racemic **III-32**, 1-oxo-2,3-dihydro-1H-inden-2-yl naphthalene-1-sulfonate

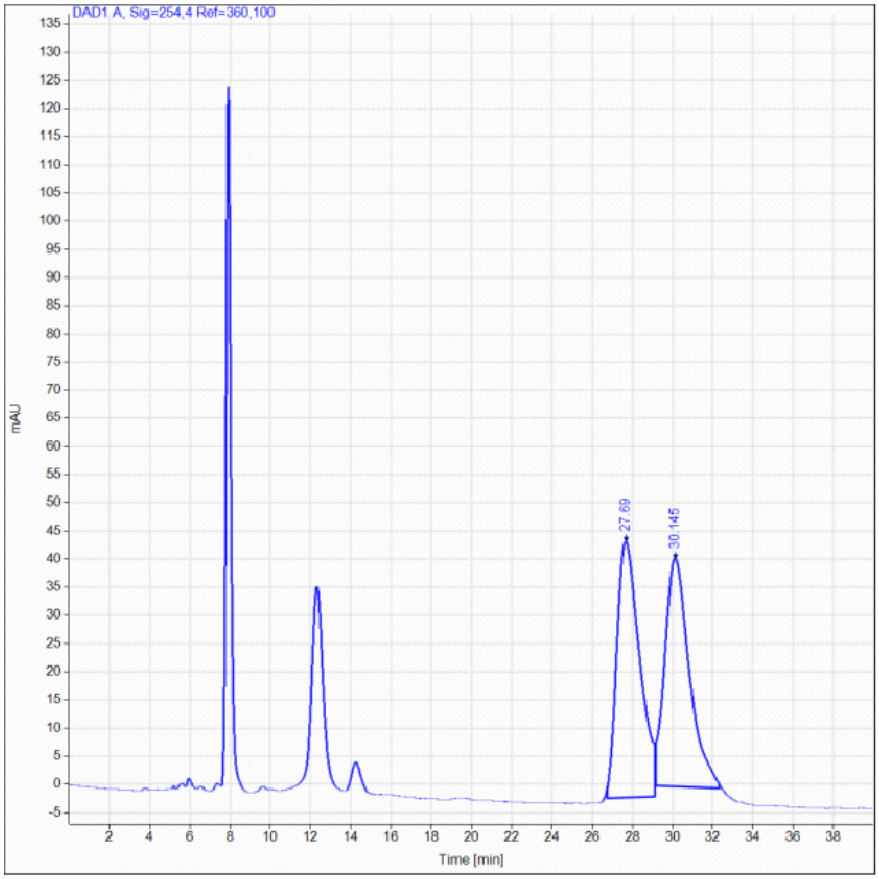


**Signal:** DAD1 A, Sig=254,4 Ref=360,100

| RT [min] | Type | Width [min] | Area | Height | Area% | Name |
|---|---|---|---|---|---|---|
| 27.690 | MM | 1.3045 | 3556.3416 | 45.4365 | 50.9323 | |
| 30.145 | MM | 1.4087 | 3426.1462 | 40.5345 | 49.0677 | |
| | | Sum | 6982.4878 | | | |

HPLC Trace for Peptide **III-8**, 11% *ee*

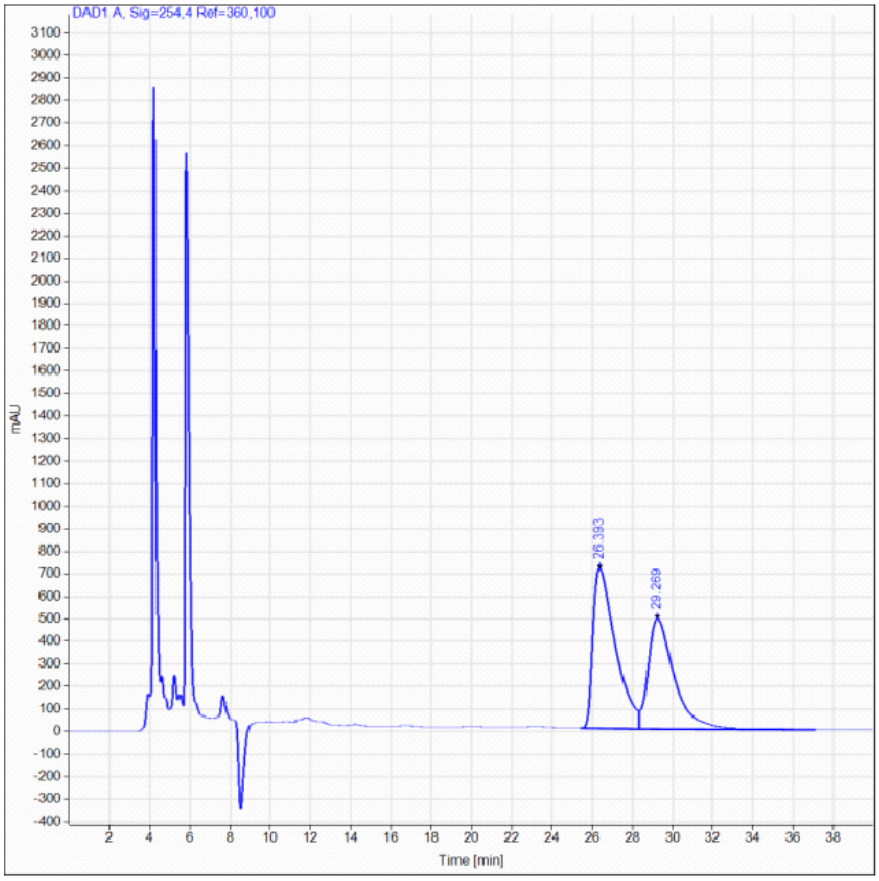


**Signal:** DAD1 A, Sig=254,4 Ref=360,100

| RT [min] | Type | Width [min] | Area | Height | Area% | Name |
|---|---|---|---|---|---|---|
| 26.393 | BV | 1.1491 | 54993.5508 | 708.9007 | 55.6783 | |
| 29.269 | VB | 1.3348 | 43776.5781 | 488.8492 | 44.3217 | |
| | | Sum | 98770.1289 | | | |

HPLC Trace for Peptide **III-26**, 17% *ee*

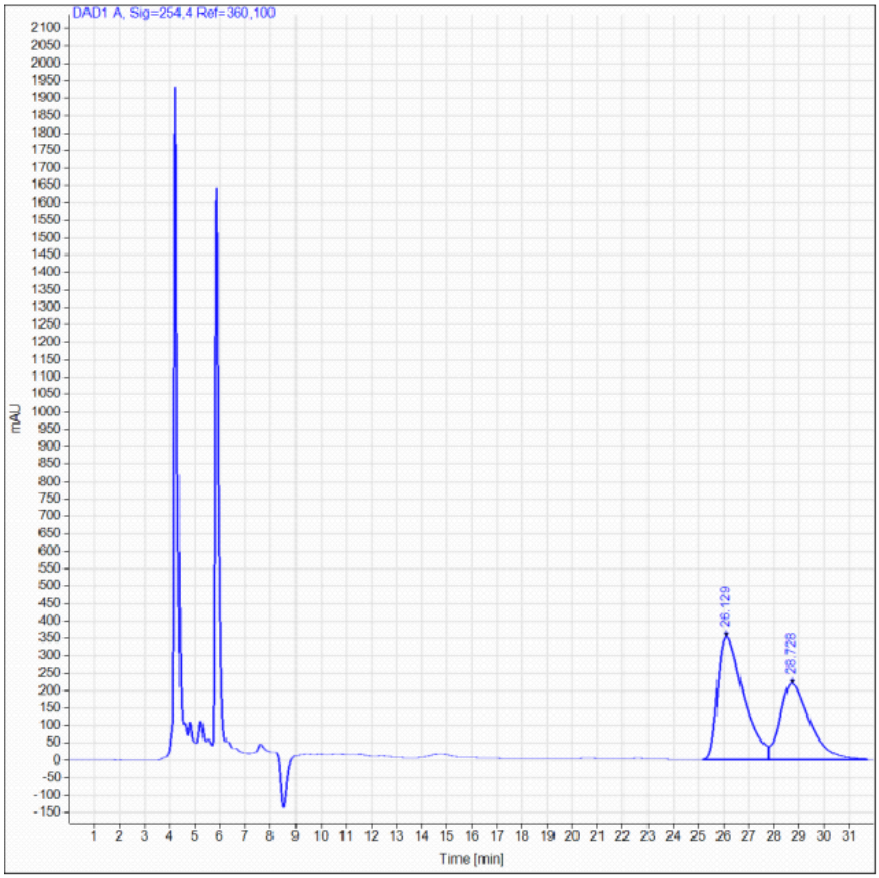


**Signal:** DAD1 A, Sig=254,4 Ref=360,100

| RT [min] | Type | Width [min] | Area | Height | Area% | Name |
|---|---|---|---|---|---|---|
| 26.129 | BV | 1.0718 | 25166.7988 | 352.1265 | 58.5252 | |
| 28.728 | VBA | 1.2345 | 17834.8359 | 218.4552 | 41.4748 | |
| | | Sum | 43001.6348 | | | |

HPLC Trace for Peptide **III-27**, 9% *ee*

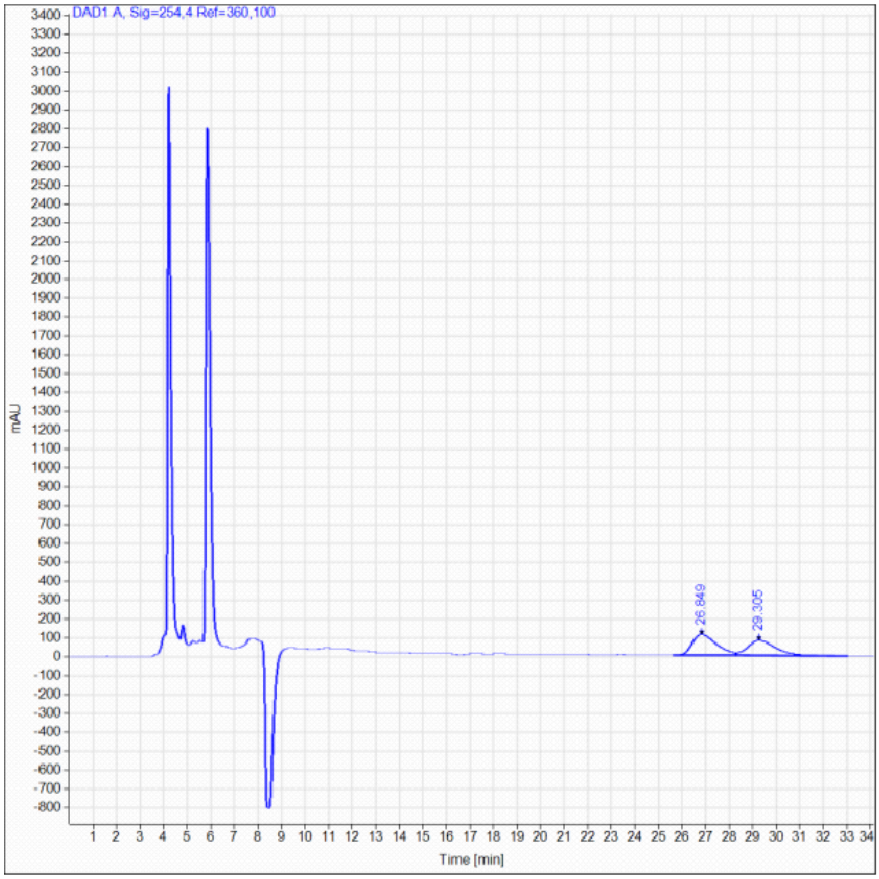


**Signal:** DAD1 A, Sig=254,4 Ref=360,100

| RT [min] | Type | Width [min] | Area | Height | Area% | Name |
|---|---|---|---|---|---|---|
| 26.849 | BV | 1.0963 | 7911.0405 | 110.3564 | 54.4106 | |
| 29.305 | VB | 1.2446 | 6628.4795 | 79.8368 | 45.5894 | |
| | | Sum | 14539.5200 | | | |

HPLC Trace for Peptide **III-28**, 22% *ee*

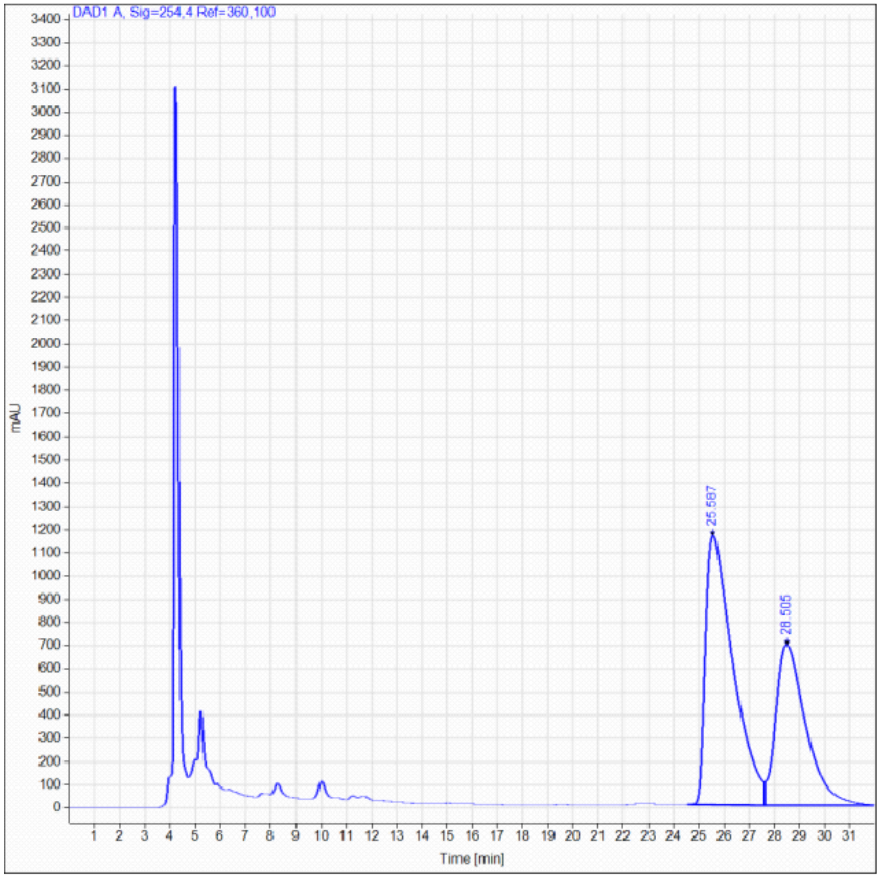


**Signal:** DAD1 A, Sig=254,4 Ref=360,100

| RT [min] | Type | Width [min] | Area | Height | Area% | Name |
|---|---|---|---|---|---|---|
| 25.587 | BV | 1.1337 | 88873.8359 | 1160.1893 | 60.7644 | |
| 28.505 | VBA | 1.2468 | 57385.7617 | 691.0809 | 39.2356 | |
| | | Sum | 146259.5977 | | | |

HPLC Trace for Peptide **III-29**, 21% *ee*

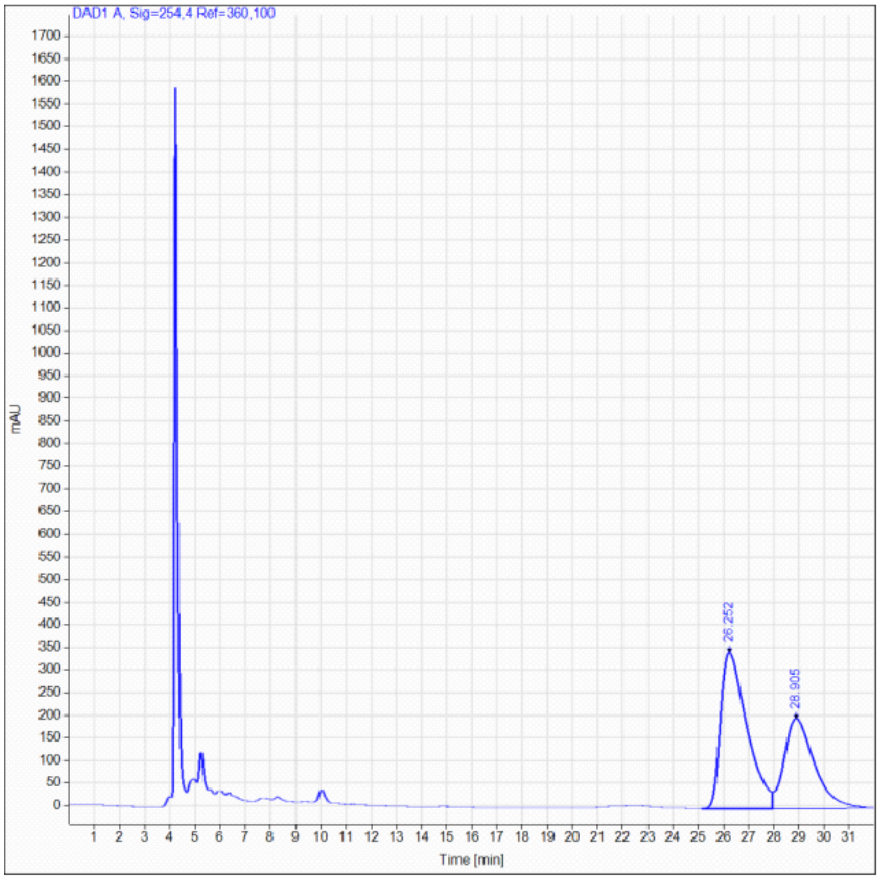


**Signal:** DAD1 A, Sig=254,4 Ref=360,100

| RT [min] | Type | Width [min] | Area | Height | Area% | Name |
|---|---|---|---|---|---|---|
| 26.252 | BV | 1.0990 | 25091.5664 | 345.6203 | 60.3177 | |
| 28.905 | VBA | 1.2479 | 16507.4297 | 198.9828 | 39.6823 | |
| | | Sum | 41598.9961 | | | |

HPLC Trace for Peptide **III-30**, 15% *ee*

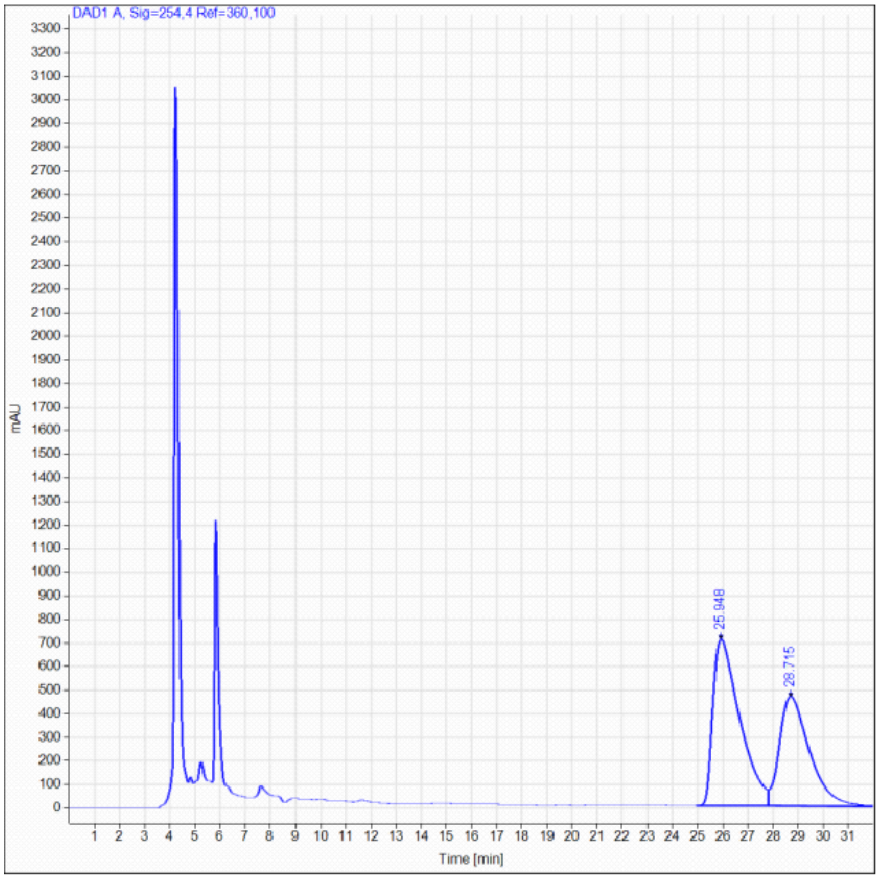


**Signal:** DAD1 A, Sig=254,4 Ref=360,100

| RT [min] | Type | Width [min] | Area | Height | Area% | Name |
|---|---|---|---|---|---|---|
| 25.948 | BV | 1.1039 | 52461.5352 | 705.1958 | 57.6696 | |
| 28.715 | VBA | 1.2496 | 38507.5781 | 464.2858 | 42.3304 | |
| | | Sum | 90969.1133 | | | |

HPLC Trace for Peptide **III-31**, 6% *ee*

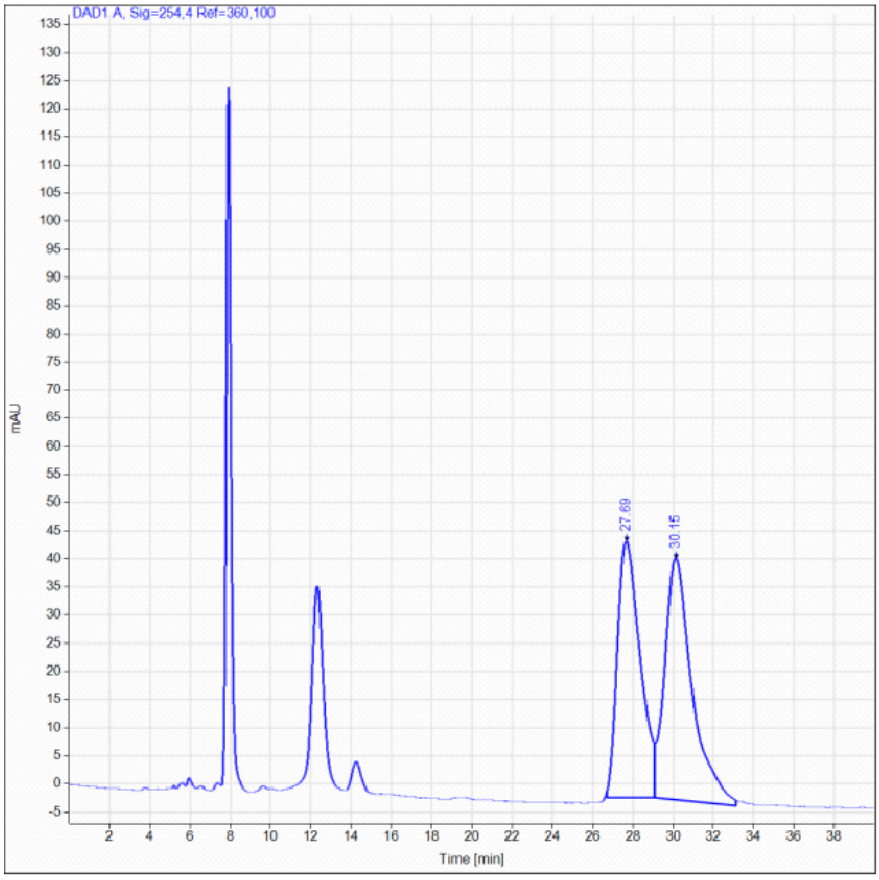


**Signal:** DAD1 A, Sig=254,4 Ref=360,100

| RT [min] | Type | Width [min] | Area | Height | Area% | Name |
|---|---|---|---|---|---|---|
| 27.690 | MM | 1.3061 | 3571.5229 | 45.5744 | 46.8418 | |
| 30.150 | MM | 1.5726 | 4053.1184 | 42.9547 | 53.1582 | |
| | | Sum | 7624.6414 | | | |

HPLC Trace for Peptide **III-32**, 17% *ee*

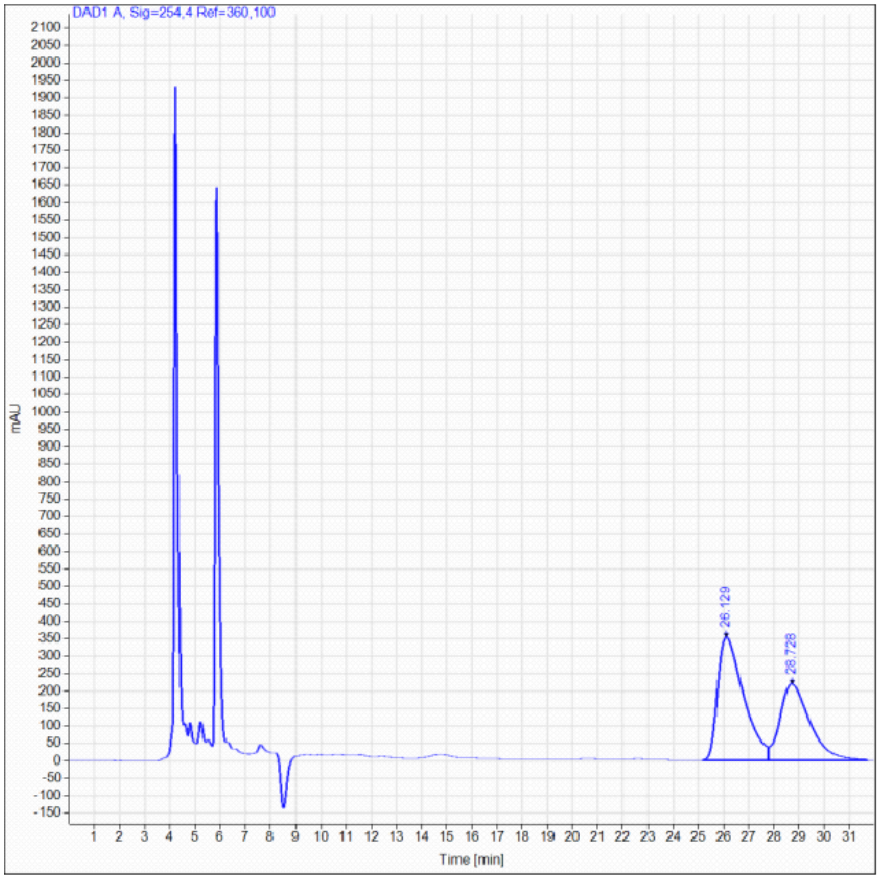


**Signal:** DAD1 A, Sig=254,4 Ref=360,100

| RT [min] | Type | Width [min] | Area | Height | Area% | Name |
|---|---|---|---|---|---|---|
| 26.129 | BV | 1.0718 | 25166.7988 | 352.1265 | 58.5252 | |
| 28.728 | VBA | 1.2345 | 17834.8359 | 218.4552 | 41.4748 | |
| | | Sum | 43001.6348 | | | |

HPLC Trace for Peptide **III-33**, 12% *ee*

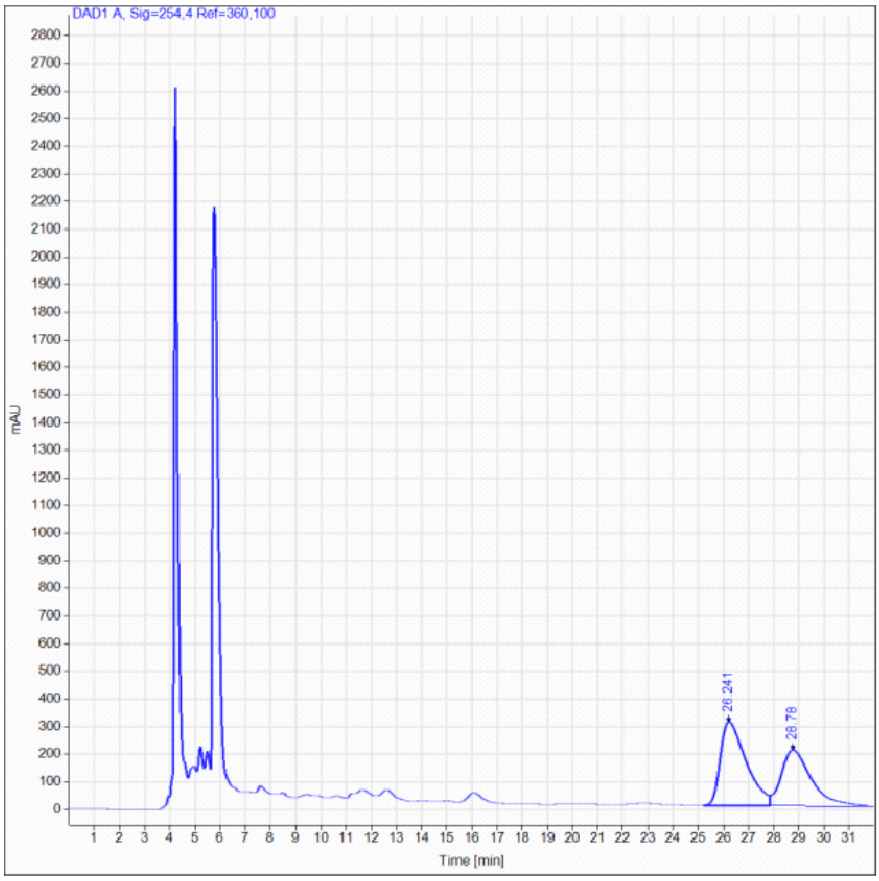


**Signal:** DAD1 A, Sig=254,4 Ref=360,100

| RT [min] | Type | Width [min] | Area | Height | Area% | Name |
|---|---|---|---|---|---|---|
| 26.241 | BV | 1.0750 | 21617.8027 | 302.7755 | 56.2033 | |
| 28.780 | VBA | 1.2450 | 16845.7852 | 202.4059 | 43.7967 | |
| | | Sum | 38463.5879 | | | |

HPLC Trace for Peptide **III-34**, NP

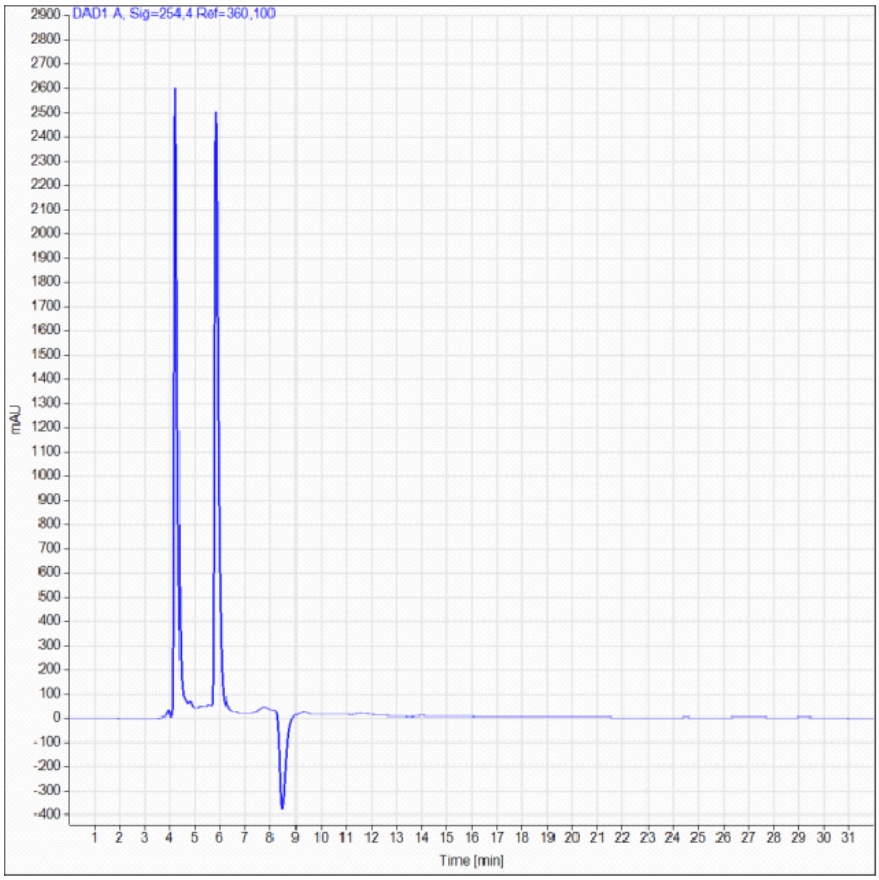

HPLC Trace for Peptide **III-35**, 19% *ee*

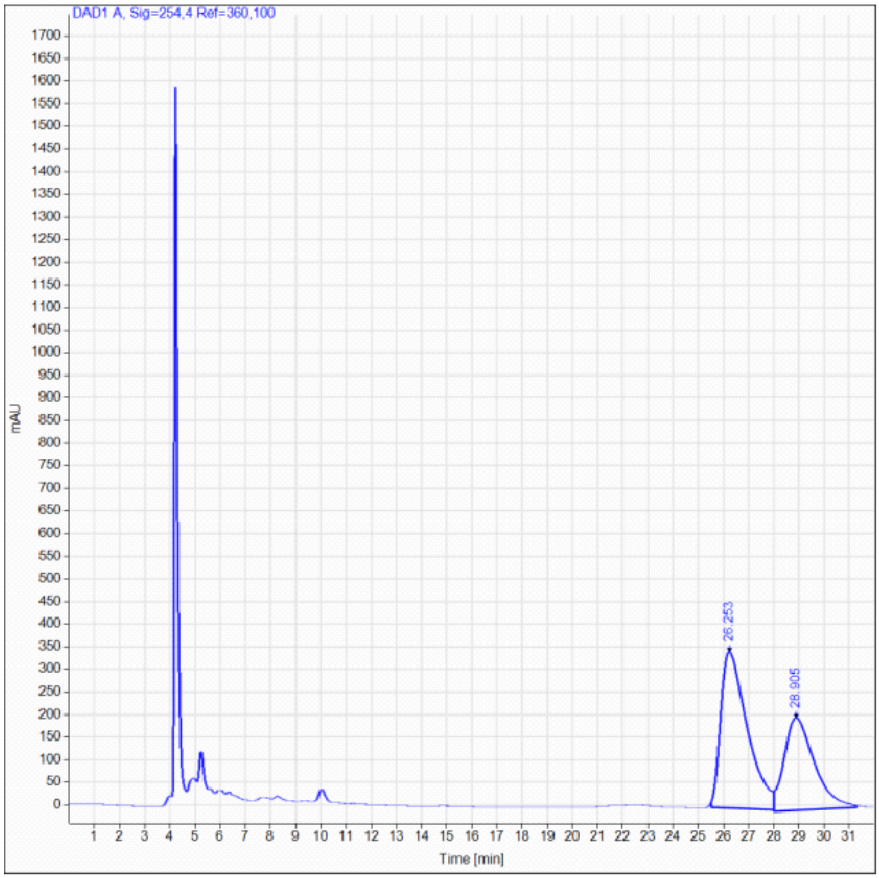


**Signal:** DAD1 A, Sig=254,4 Ref=360,100

| RT [min] | Type | Width [min] | Area | Height | Area% | Name |
|---|---|---|---|---|---|---|
| 26.253 | MM | 1.2212 | 25370.6836 | 346.2538 | 59.7018 | |
| 28.905 | MM | 1.3908 | 17125.0098 | 205.2135 | 40.2982 | |
| | | Sum | 42495.6934 | | | |

Chiral HPLC Spectra of Racemic **III-33**, 1-oxo-2,3-dihydro-1H-inden-2-yl methanesulfonate

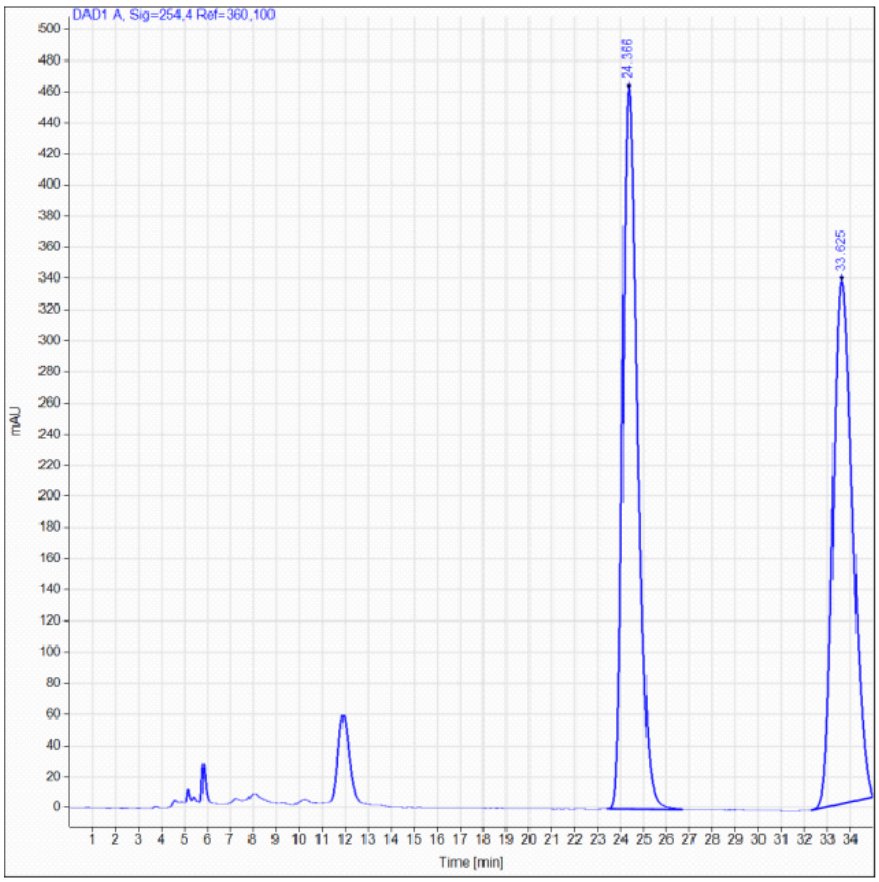


**Signal:** DAD1 A, Sig=254,4 Ref=360,100

| RT [min] | Type | Width [min] | Area | Height | Area% | Name |
|---|---|---|---|---|---|---|
| 24.366 | BB | 0.6956 | 21034.4004 | 463.3337 | 51.1602 | |
| 33.625 | BBA | 0.9298 | 20080.3984 | 335.7488 | 48.8398 | |
| | | Sum | 41114.7988 | | | |

HPLC Chromatograms for Product **III-33**

HPLC Trace for Peptide **III-8**, 28% *ee*

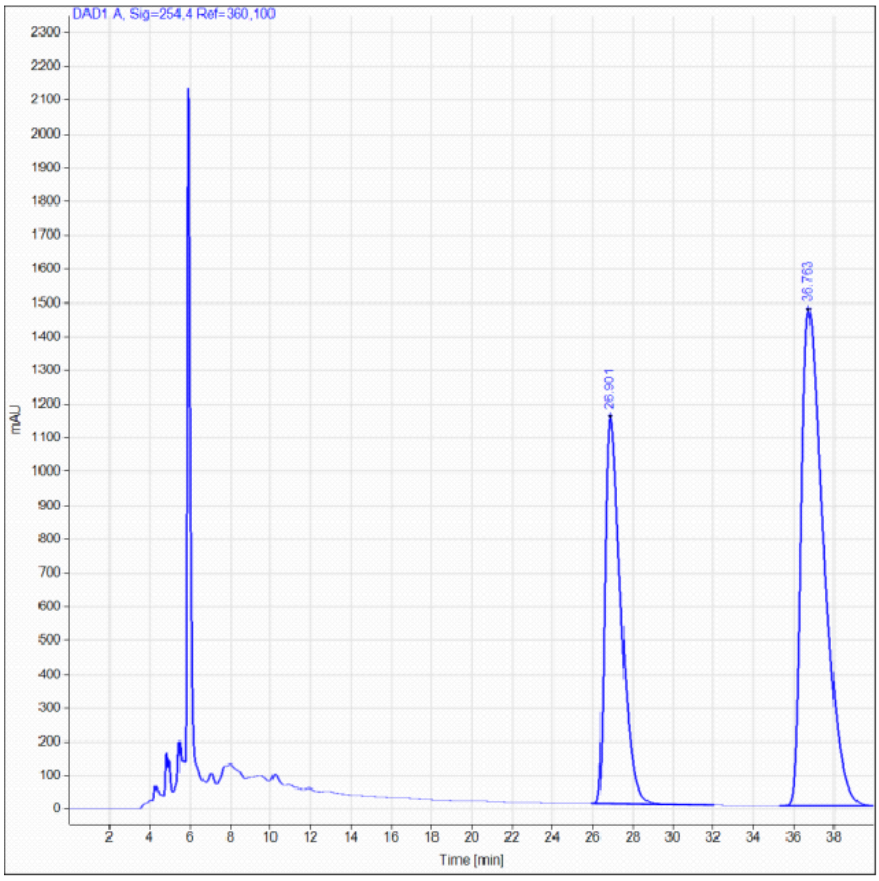


**Signal:** DAD1 A, Sig=254,4 Ref=360,100

| RT [min] | Type | Width [min] | Area | Height | Area% | Name |
|---|---|---|---|---|---|---|
| 26.901 | BB | 0.8409 | 63457.2344 | 1140.9440 | 35.8172 | |
| 36.763 | BBA | 1.1740 | 113712.5391 | 1464.3606 | 64.1828 | |
| | | Sum | 177169.7734 | | | |

HPLC Trace for Peptide **III-26**, 35% *ee*

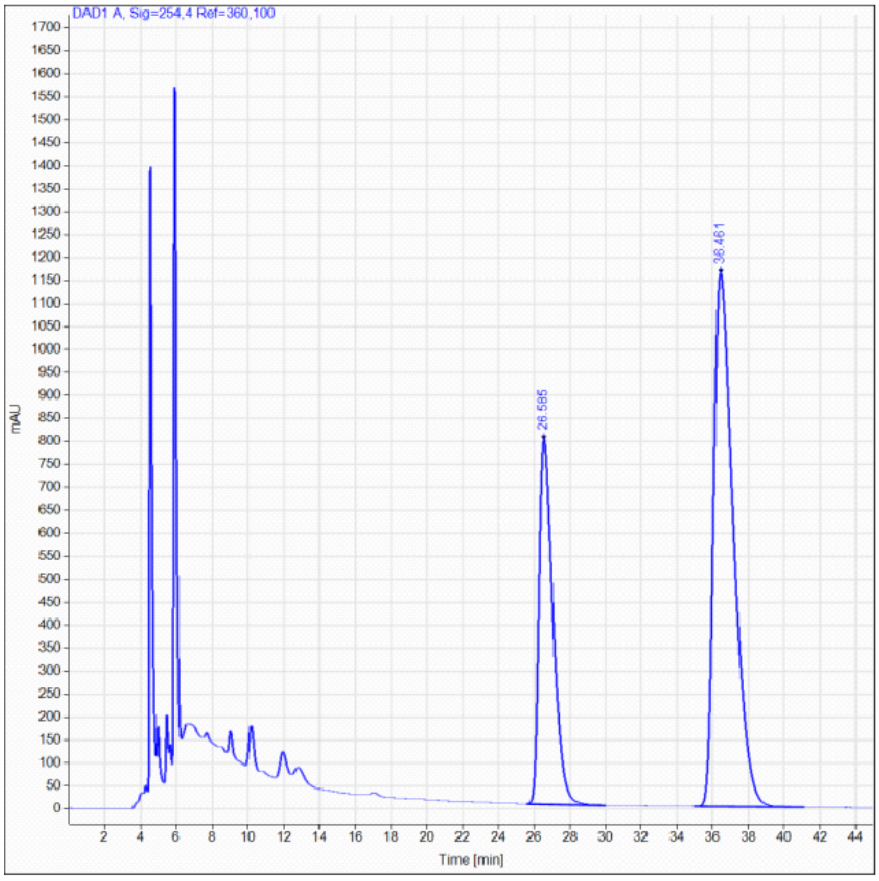


**Signal:** DAD1 A, Sig=254,4 Ref=360,100

| RT [min] | Type | Width [min] | Area | Height | Area% | Name |
|---|---|---|---|---|---|---|
| 26.585 | BB | 0.8297 | 43234.3242 | 793.4055 | 32.6587 | |
| 36.461 | BB | 1.1617 | 89148.0781 | 1161.1962 | 67.3413 | |
| | | Sum | 132382.4023 | | | |

HPLC Trace for Peptide **III-27**, 26% *ee*

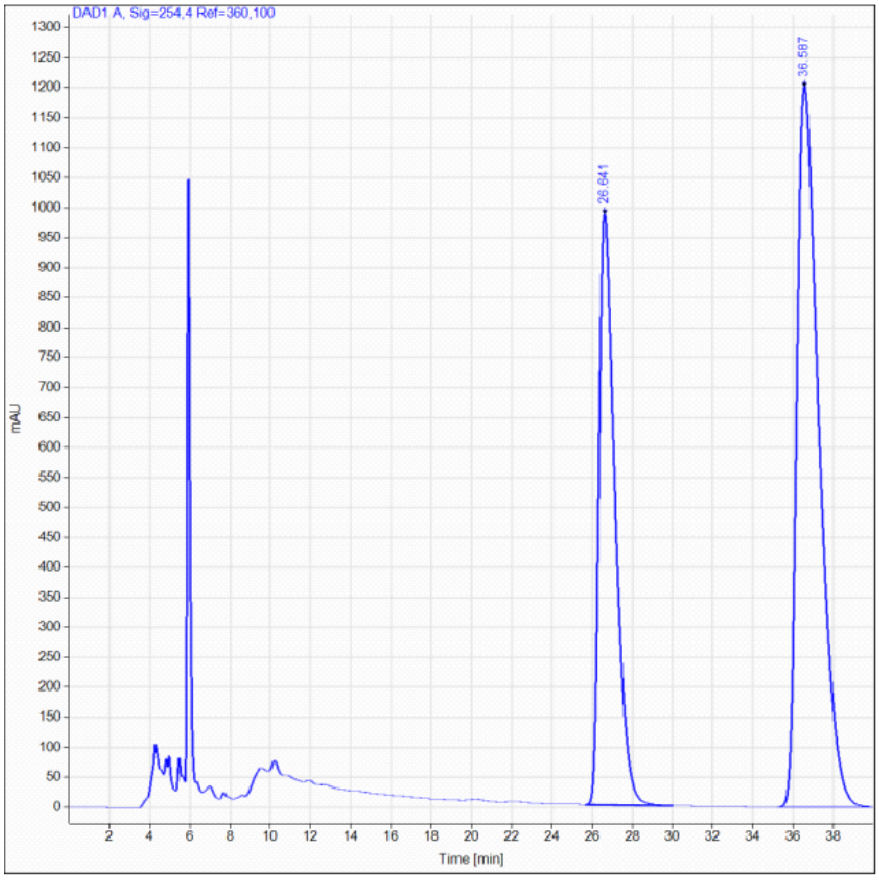


**Signal:** DAD1 A, Sig=254,4 Ref=360,100

| RT [min] | Type | Width [min] | Area | Height | Area% | Name |
|---|---|---|---|---|---|---|
| 26.641 | BB | 0.8417 | 54784.4219 | 986.8619 | 37.3192 | |
| 36.587 | BBA | 1.1565 | 92015.0938 | 1202.8762 | 62.6808 | |
| | | Sum | 146799.5156 | | | |

HPLC Trace for Peptide **III-28**, 21% *ee*

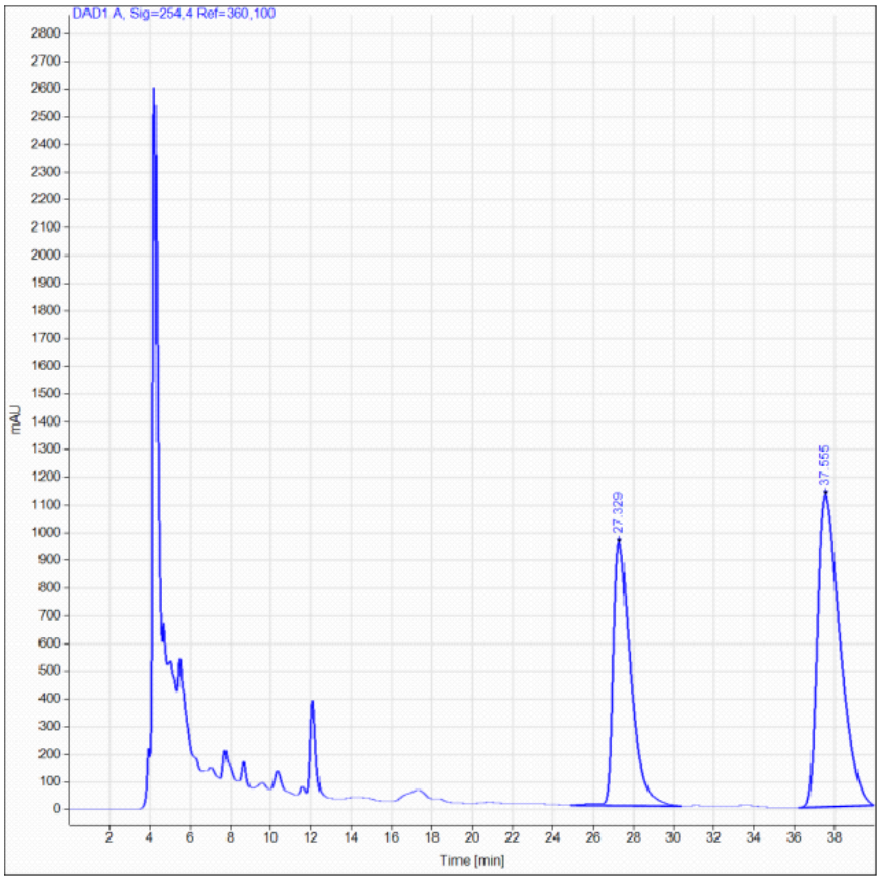


**Signal:** DAD1 A, Sig=254,4 Ref=360,100

| RT [min] | Type | Width [min] | Area | Height | Area% | Name |
|---|---|---|---|---|---|---|
| 27.329 | BB | 0.9005 | 56755.5156 | 947.9655 | 39.2822 | |
| 37.555 | BBA | 1.1798 | 87726.1016 | 1124.9202 | 60.7178 | |
| | | Sum | 144481.6172 | | | |

HPLC Trace for Peptide **III-29**, 17% *ee*

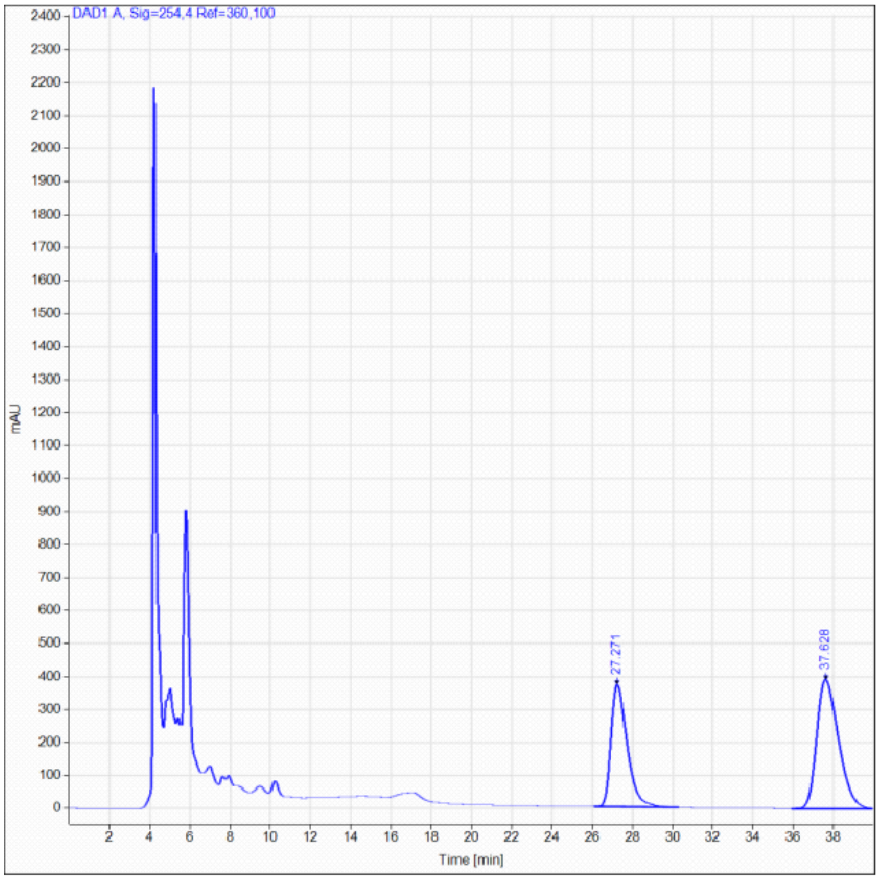


**Signal:** DAD1 A, Sig=254,4 Ref=360,100

| RT [min] | Type | Width [min] | Area | Height | Area% | Name |
|---|---|---|---|---|---|---|
| 27.271 | BB | 0.8549 | 20839.2813 | 371.2292 | 41.5120 | |
| 37.628 | BBA | 1.1594 | 29361.3652 | 391.3105 | 58.4880 | |
| | | Sum | 50200.6465 | | | |

HPLC Trace for Peptide **III-30**, 20% *ee*

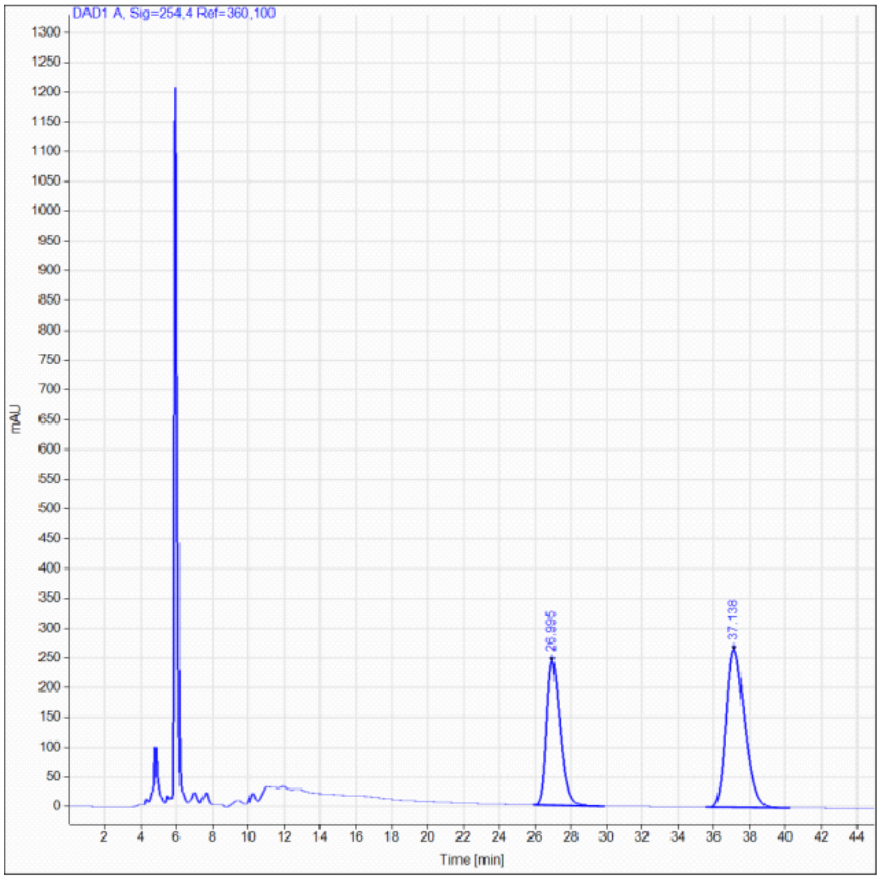


**Signal:** DAD1 A, Sig=254,4 Ref=360,100

| RT [min] | Type | Width [min] | Area | Height | Area% | Name |
|---|---|---|---|---|---|---|
| 26.995 | BB | 0.8051 | 12706.0098 | 241.7644 | 39.8678 | |
| 37.138 | BB | 1.1167 | 19164.3379 | 265.3047 | 60.1322 | |
| | | Sum | 31870.3477 | | | |

HPLC Trace for Peptide **III-31**, 23% *ee*

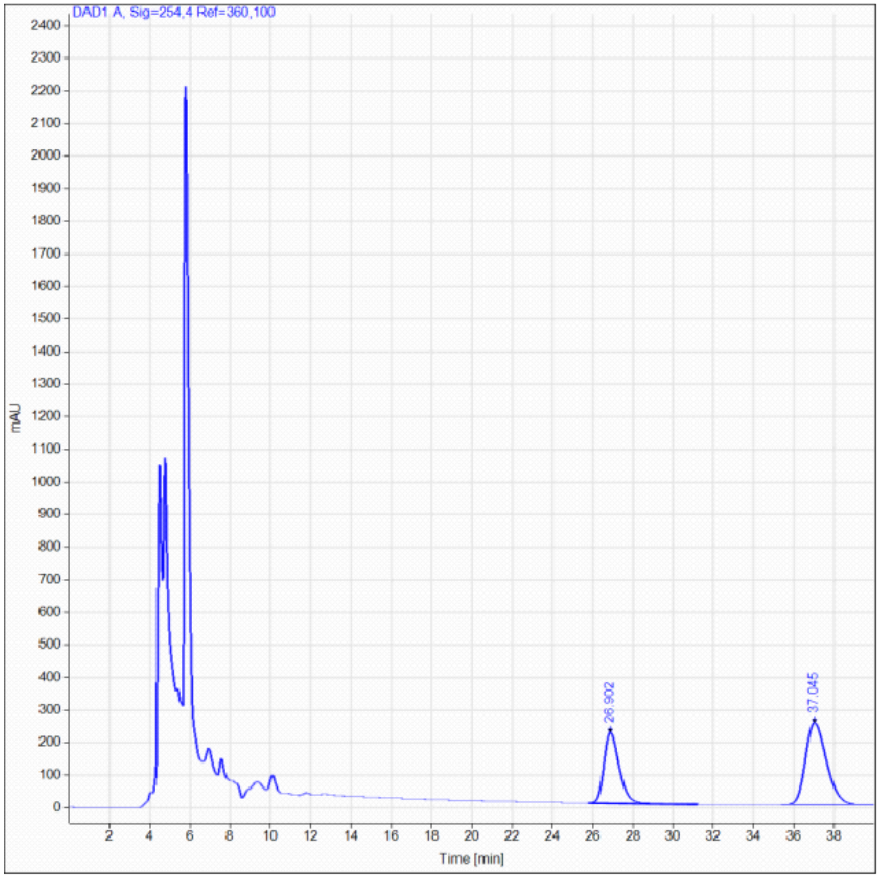


**Signal:** DAD1 A, Sig=254,4 Ref=360,100

| RT [min] | Type | Width [min] | Area | Height | Area% | Name |
|---|---|---|---|---|---|---|
| 26.902 | BB | 0.8115 | 11420.1094 | 217.1539 | 38.5498 | |
| 37.045 | BBA | 1.1261 | 18204.2285 | 252.2092 | 61.4502 | |
| | | Sum | 29624.3379 | | | |

HPLC Trace for Peptide **III-32**, 24% *ee*

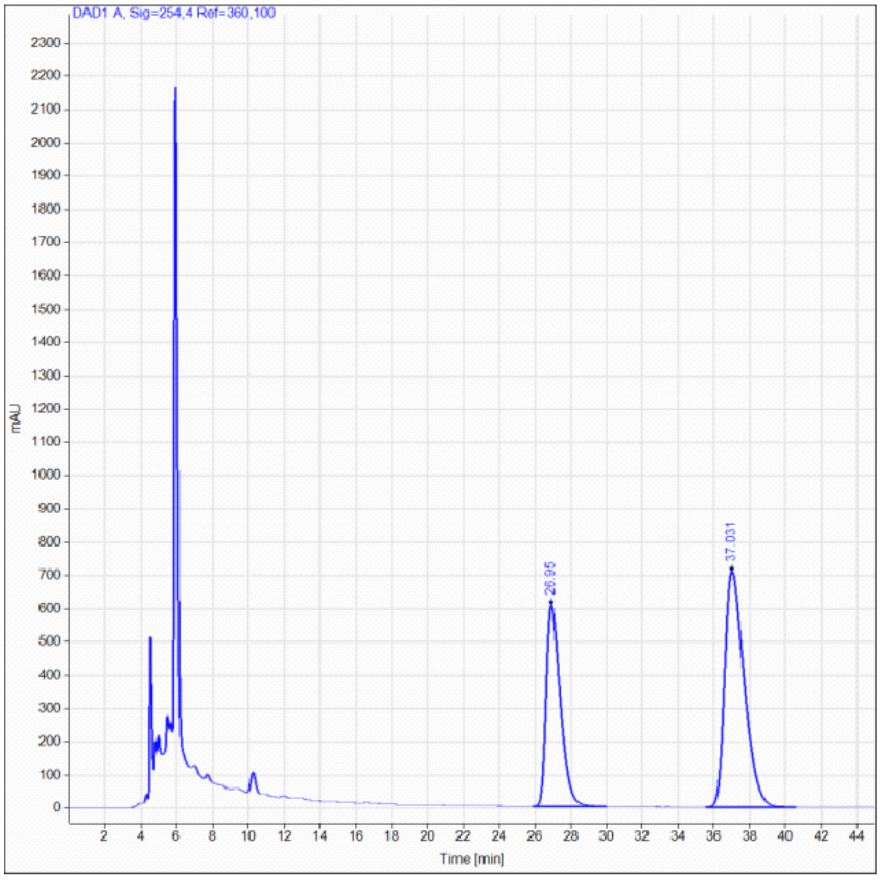


**Signal:** DAD1 A, Sig=254,4 Ref=360,100

| RT [min] | Type | Width [min] | Area | Height | Area% | Name |
|---|---|---|---|---|---|---|
| 26.950 | BB | 0.8286 | 32988.6367 | 604.5789 | 38.1500 | |
| 37.031 | BB | 1.1580 | 53482.2070 | 709.0618 | 61.8500 | |
| | | Sum | 86470.8438 | | | |

HPLC Trace for Peptide **III-33**, 20% *ee*

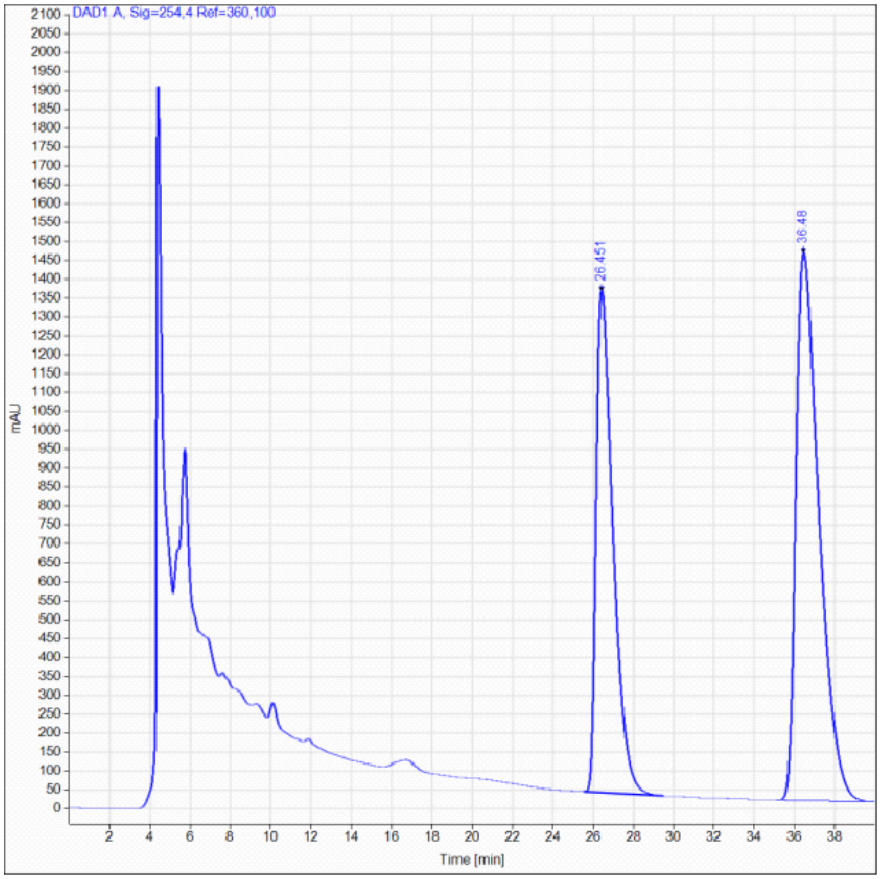


**Signal:** DAD1 A, Sig=254,4 Ref=360,100

| RT [min] | Type | Width [min] | Area | Height | Area% | Name |
|---|---|---|---|---|---|---|
| 26.451 | BB | 0.8758 | 77128.0781 | 1327.5740 | 40.1715 | |
| 36.480 | BBA | 1.1902 | 114868.8359 | 1446.9567 | 59.8285 | |
| | | Sum | 191996.9141 | | | |

HPLC Trace for Peptide **III-34**, 14% *ee*

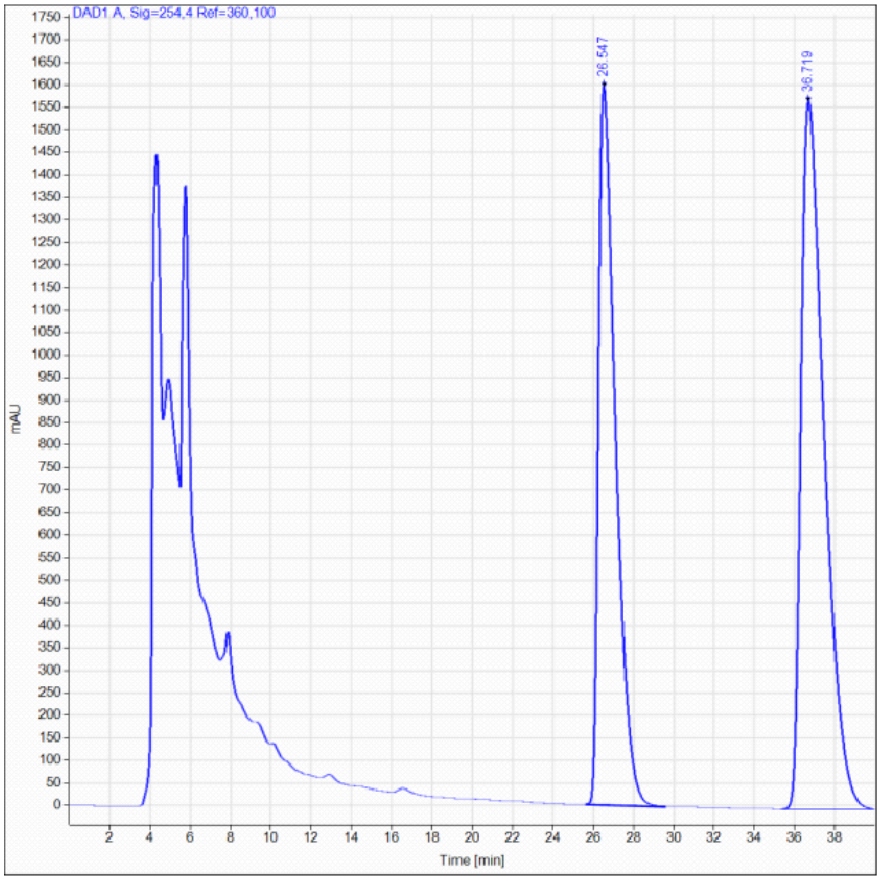


**Signal:** DAD1 A, Sig=254,4 Ref=360,100

| RT [min] | Type | Width [min] | Area | Height | Area% | Name |
|---|---|---|---|---|---|---|
| 26.547 | BB | 0.8951 | 94540.9531 | 1595.8921 | 42.8377 | |
| 36.719 | BBA | 1.2083 | 126154.7344 | 1571.9073 | 57.1623 | |
| | | Sum | 220695.6875 | | | |

HPLC Trace for Peptide **III-35**, 15% *ee*

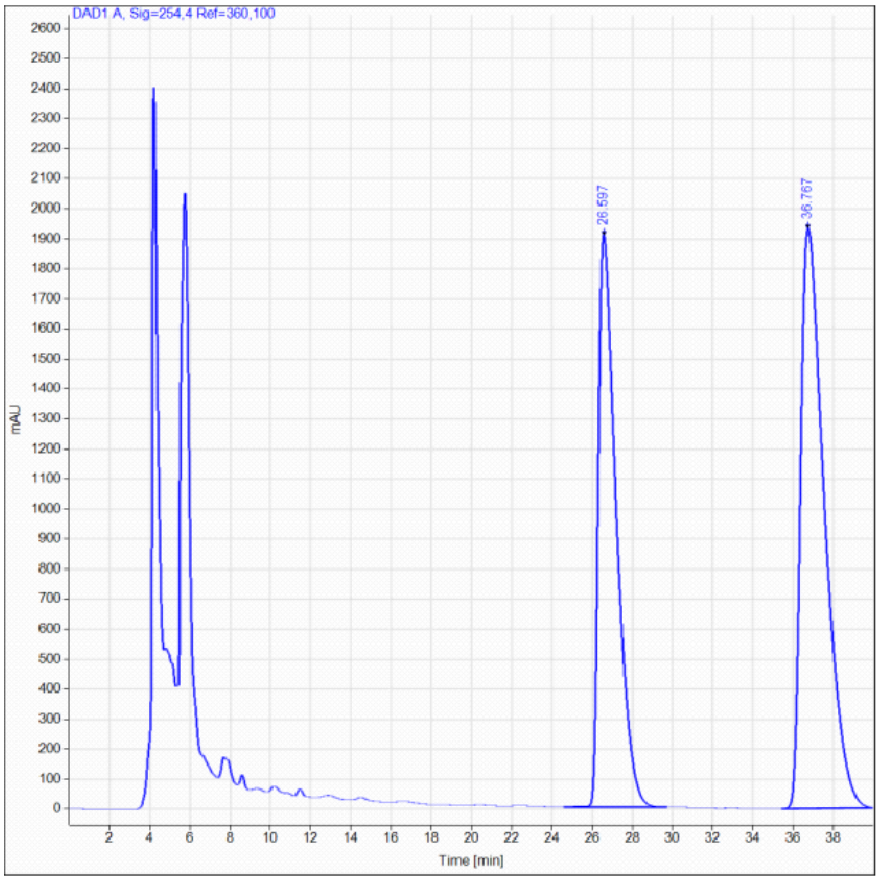


**Signal:** DAD1 A, Sig=254,4 Ref=360,100

| RT [min] | Type | Width [min] | Area | Height | Area% | Name |
|---|---|---|---|---|---|---|
| 26.597 | BB | 0.9233 | 117559.4453 | 1906.6980 | 42.5371 | |
| 36.767 | BBA | 1.2394 | 158809.5781 | 1931.1302 | 57.4629 | |
| | | Sum | 276369.0234 | | | |

Table B1: Peptides Screened in the $\alpha$-Oxytosylation of 1-Indanone

| Sequence | Exact Mass | Calc. [M+H]+ | Calc. [M+Na]+ | Observed [M+H]+ or [M+Na]+ | % *ee* of II-8 |
|---|---|---|---|---|---|
| Ac-Ser-4-I-Phe-Pro-D-Ala-Phg-hPhe | 881.2609 | 882.2689 | 904.2501 | 882.11 | 8.7 |
| Ac-Ala-4-I-Phe-Pro-D-Ala-Phg-hPhe | 865.266 | 866.274 | 888.2552 | 888.43 | 9 |
| Ac-Trp-4-I-Phe-Pro-D-Ala-Phg-hPhe | 980.3082 | 981.3162 | 1003.2974 | 1003.44 | 5.6 |
| Ac-Glu-4-I-Phe-Pro-D-Ala-Phg-hPhe | 923.2715 | 924.2795 | 946.2607 | 946.44 | 4.5 |
| Ac-Nva-4-I-Phe-Pro-D-Ala-Phg-hPhe | 893.2973 | 894.3053 | 916.2865 | 916.47 | 7 |
| Ac-Leu-4-I-Phe-Pro-D-Ala-Phg-hPhe | 907.3129 | 908.3209 | 930.3021 | 930.48 | 3.4 |
| Ac-Bip-4-I-Phe-Pro-D-Ala-Phg-hPhe | 1017.3286 | 1018.3366 | 1040.3178 | 1040.50 | 5.6 |
| Ac-Tle-4-I-Phe-Pro-D-Ala-Phg-hPhe | 907.3129 | 908.3209 | 930.3021 | 930.48 | 3.2 |
| Ac-His-4-I-Phe-Pro-D-Ala-Phg-hPhe | 931.2878 | 932.2958 | 954.277 | 954.46 | 3.5 |
| Ac-Asn-4-I-Phe-Pro-D-Ala-Phg-hPhe | 908.2718 | 909.2798 | 931.261 | 931.44 | 1.2 |
| Ac-Tyr-4-I-Phe-Pro-D-Ala-Phg-hPhe | 957.2922 | 958.3002 | 980.2814 | 980.46 | 0 |
| Ac-Phg-4-I-Phe-Pro-D-Ala-Phg-hPhe | 927.2816 | 928.2896 | 950.2708 | 950.45 | 3.4 |
| Ac-Thr-4-I-Phe-Pro-D-Ala-Phg-hPhe | 895.2766 | 896.2846 | 918.2658 | 918.45 | 9.1 |
| Ac-Lys-4-I-Phe-Pro-D-Ala-Phg-hPhe | 922.3238 | 923.3318 | 945.313 | 945.49 | 3 |
| Ac-Nle-4-I-Phe-Pro-D-Ala-Phg-hPhe | 907.3129 | 908.3209 | 930.3021 | 930.48 | 4.5 |
| Ac-Orn-4-I-Phe-Pro-D-Ala-Phg-hPhe | 908.3082 | 909.3162 | 931.2974 | 931.48 | 7.8 |
| Ac-hPhe-4-I-Phe-Pro-D-Ala-Phg-hPhe | 955.3129 | 956.3209 | 978.3021 | 978.48 | 8 |
| Ac-dPhe-4-I-Phe-Pro-D-Ala-Phg-hPhe | 1017.3286 | 1018.3366 | 1040.3178 | 1040.32 | 6 |
| Ac-1-Nap-4-I-Phe-Pro-D-Ala-Phg-hPhe | 991.3129 | 992.3209 | 1014.3021 | 1014.17 | 6.7 |
| Ac-4-Pya-4-I-Phe-Pro-D-Ala-Phg-hPhe | 942.2925 | 943.3005 | 965.2817 | 965.10 | 6.5 |
| 2-IBA-hPhe-Pro-D-Ala-Lys-Leu | 817.3024 | 818.3104 | 840.2916 | 840.11 | 12.1 |
| 2-IBA-Tyr-Pro-D-Ala-Asn-Phg | 825.1983 | 826.2063 | 848.1875 | 848.01 | 10 |
| 2-IBA-Leu-Pro-D-Ala-Nva-Glu | 756.2344 | 757.2424 | 779.2236 | 779.04 | NP |
| 2-IBA-Val-Pro-D-Ala-hPhe-Phg | 822.2602 | 823.2682 | 845.2494 | 845.07 | 19.7 |
| 2-IBA-Ala-Pro-D-Ala-Orn-hPhe | 747.2241 | 748.2321 | 770.2133 | 770.03 | 18.4 |
| 2-IBA-Tyr-Pro-D-Ala-Asn-Nva | 791.214 | 792.222 | 814.2032 | 814.02 | 0 |
| 2-IBA-Nva-Pro-D-Ala-Tyr-Asn | 791.214 | 792.222 | 814.2032 | 814.43 | 7.3 |
| 2-IBA-Phe-Pro-D-Ala-Val-Ile | 774.2602 | 775.2682 | 797.2494 | 797.07 | 10 |

| | | | | | |
|---|---|---|---|---|---|
| Ac-Val-4-I-Phe-Pro-D-Ala-Phg-hPhe | 893.2973 | 894.3053 | 916.2865 | 894.15 | 11 |
| Ac-hPhe-4-I-Phe-Pro-D-Ala-Bip-Ala | 955.3129 | 956.3209 | 978.3021 | 956.16 | 2.5 |
| 2-IBA-hPhe-Pro-D-Ala-Orn-Phg | 808.2445 | 809.2525 | 831.2337 | 809.09 | 0 |
| 2-IBA-Ile-Pro-D-Ala-Asp-tPhe | 846.2813 | 847.2893 | 869.2705 | 847.13 | 3 |
| 2-IBA-Ile-Pro-D-Ala-Asp-Asp | 758.1772 | 759.1852 | 781.1664 | 759.03 | 5 |
| 2-IBA-Ile-Pro-D-Ala-1-Nap-Gln | 853.266 | 854.274 | 876.2552 | 854.17 | 0 |
| 2-IBA-Ile-Pro-D-Ala-Asp-Orn | 757.2296 | 758.2376 | 780.2188 | 758.08 | 0 |
| 2-IBA-Ile-Pro-D-Ala-Asp-Thr | 744.198 | 745.206 | 767.1872 | 745.26 | 8.1 |
| 2-IBA-Nle-Pro-D-Ala-Orn-Ala | 713.2398 | 714.2478 | 736.229 | 714.14 | 3.4 |
| 2-IBA-Nva-Pro-D-Ala-Orn-Ala | 699.2241 | 700.2321 | 722.2133 | 700.53 | 0 |
| 2-IBA-Abu-Pro-D-Ala-Asp-Dap | 701.167 | 702.175 | 724.1562 | 702.26 | 10.4 |
| 2-IBA-Ile-Pro-D-Ala-Asp-Leu | 756.2344 | 757.2424 | 779.2236 | 757.84 | 3.2 |
| 2-IBA-hPhe-Pro-D-Ala-Orn-Phe | 837.2711 | 838.2791 | 860.2603 | 838.17 | 5.1 |
| 2-IBA-Ile-Pro-D-Ala-Asp-Nle | 756.2344 | 757.2424 | 779.2236 | 757.08 | 7 |
| 2-IBA-Ile-Pro-D-Ala-Asp-Val | 742.2187 | 743.2267 | 765.2079 | 743.67 | 10.2 |
| 2-IBA-hPhe-Pro-D-Ala-Orn-Orn | 804.282 | 805.29 | 827.2712 | 805.13 | 8.6 |
| 2-IBA-hPhe-Pro-D-Ala-Tyr-Ala | 810.2238 | 811.2318 | 833.213 | 811.71 | NP |
| 2-IBA-hPhe-Pro-D-Ala-Phg-Nle | 822.2602 | 823.2682 | 845.2494 | 823.18 | 5.8 |
| 2-IBA-hPhe-Pro-D-Ala-Phg-His | 846.235 | 847.243 | 869.2242 | 847.83 | 6.7 |
| 2-IBA-hPhe-Pro-D-Ala-Phg-Val | 808.2445 | 809.2525 | 831.2337 | 809.25 | 3.5 |
| 2-IBA-Thr-Pro-D-Ala-tPhe-Abu | 804.2707 | 805.2787 | 827.2599 | 805.17 | 5.4 |
| 2-IBA-Val-Pro-D-Ala-hPhe-Phg | 822.2602 | 823.2682 | 845.2494 | 823.82 | 2.8 |
| 2-IBA-Orn-Pro-D-Ala-Ile-Tle | 755.2867 | 756.2947 | 778.2759 | 756.47 | 48 |

Table B2: Peptides Screened in the $\alpha$-Oxytosylation of 1-Indanone from the Optimization of Peptide **III-10**

| Sequence | Exact Mass | Calc. [M+H]+ | Calc. [M+Na]+ | Observed [M+H]+ or [M+Na]+ | % *ee* of II-8 |
|---|---|---|---|---|---|
| 2-IBA-Orn-Pro-D-Ala-Ile-Ile | 755.2867 | 756.2947 | 778.2759 | 778.59 | 32 |
| 2-IBA-Orn-Pro-D-Ala-Ile-Val | 741.2711 | 742.2791 | 764.2603 | 764.43 | 28 |
| 2-IBA-Orn-Pro-D-Ala-Ile-Phe | 789.2711 | 790.2791 | 812.2603 | 812.83 | 0 |
| 2-IBA-Orn-Pro-D-Ala-Ile-Dap | 728.2507 | 729.2587 | 751.2399 | 751.59 | 21 |
| 2-IBA-Orn-Pro-D-Ala-Ile-Asp | 757.2296 | 758.2376 | 780.2188 | 780.38 | 3 |
| 2-IBA-Orn-Pro-D-Ala-Ile-Abu | 727.2554 | 728.2634 | 750.2446 | 750.46 | 30 |
| 2-IBA-Orn-Pro-D-Ala-Ile-tPhe | 845.3337 | 846.3417 | 868.3229 | 868.42 | 26 |
| 2-IBA-Orn-Pro-D-Ala-Ile-Gln | 770.2612 | 771.2692 | 793.2504 | 793.74 | 19 |
| 2-IBA-Orn-Pro-D-Ala-Ile-Ser | 729.2347 | 730.2427 | 752.2239 | 752.49 | 23 |
| 2-IBA-Orn-Pro-D-Ala-Ile-Ala | 713.2398 | 714.2478 | 736.229 | 736.09 | 27 |
| 2-IBA-Orn-Pro-D-Ala-Ile-Trp | 828.282 | 829.29 | 851.2712 | 851.12 | 20 |
| 2-IBA-Orn-Pro-D-Ala-Ile-Glu | 771.2453 | 772.2533 | 794.2345 | 794.55 | 25 |
| 2-IBA-Orn-Pro-D-Ala-Ile-Nva | 741.2711 | 742.2791 | 764.2603 | 764.80 | 26 |
| 2-IBA-Orn-Pro-D-Ala-Ile-Leu | 755.2867 | 756.2947 | 778.2759 | 778.09 | 29 |
| 2-IBA-Orn-Pro-D-Ala-Ile-Bip | 865.3024 | 866.3104 | 888.2916 | 888.16 | 15 |
| 2-IBA-Orn-Pro-D-Ala-Ile-His | 779.2616 | 780.2696 | 802.2508 | 802.76 | 25 |
| 2-IBA-Orn-Pro-D-Ala-Ile-Asn | 756.2456 | 757.2536 | 779.2348 | 779.82 | 20 |
| 2-IBA-Orn-Pro-D-Ala-Ile-Tyr | 805.266 | 806.274 | 828.2552 | 828.52 | 25 |
| 2-IBA-Orn-Pro-D-Ala-Ile-Phg | 775.2554 | 776.2634 | 798.2446 | 798.64 | 24 |
| 2-IBA-Orn-Pro-D-Ala-Ile-Thr | 743.2503 | 744.2583 | 766.2395 | 766.59 | 15 |
| 2-IBA-Orn-Pro-D-Ala-Ile-Lys | 770.2976 | 771.3056 | 793.2868 | 793.18 | 12 |
| 2-IBA-Orn-Pro-D-Ala-Ile-Nle | 755.2867 | 756.2947 | 778.2759 | 778.59 | 18 |
| 2-IBA-Orn-Pro-D-Ala-Ile-Orn | 756.282 | 757.29 | 779.2712 | 779.92 | 20 |
| 2-IBA-Orn-Pro-D-Ala-Ile-hPhe | 803.2867 | 804.2947 | 826.2759 | 826.59 | 20 |
| 2-IBA-Orn-Pro-D-Ala-Ile-dPhe | 865.3024 | 866.3104 | 888.2916 | 888.16 | 17 |
| 2-IBA-Orn-Pro-D-Ala-Ile-1-Nap | 839.2867 | 840.2947 | 862.2759 | 862.59 | 26 |
| 2-IBA-Orn-Pro-D-Ala-Ile-4-Pya | 790.2663 | 791.2743 | 813.2555 | 813.75 | 30 |
| 2-IBA-Orn-Pro-D-Ala-Ile-2-Nap | 839.2867 | 840.2947 | 862.2759 | 862.59 | 24 |
| 2-IBA-Orn-Pro-D-Ala-Ile-3-Pya | 790.2663 | 791.2743 | 813.2555 | 813.55 | 24 |
| 2-IBA-Orn-Pro-D-Ala-Ile-2-Pya | 790.2663 | 791.2743 | 813.2555 | 813.43 | 28 |
| | | | | | |
| 2-IBA-Orn-Pro-D-Ala-Val-Tle | 741.2711 | 742.2791 | 764.2603 | 764.03 | 38 |
| 2-IBA-Orn-Pro-D-Ala-Phe-Tle | 789.2711 | 790.2791 | 812.2603 | 812.87 | 28 |
| 2-IBA-Orn-Pro-D-Ala-Dap-Tle | 728.2507 | 729.2587 | 751.2399 | 751.63 | 28 |

| | | | | | |
|---|---|---|---|---|---|
| 2-IBA-Orn-Pro-D-Ala-Asp-Tle | 757.2296 | 758.2376 | 780.2188 | 780.08 | 32 |
| 2-IBA-Orn-Pro-D-Ala-Abu-Tle | 727.2554 | 728.2634 | 750.2446 | 750.46 | 0 |
| 2-IBA-Orn-Pro-D-Ala-tPhe-Tle | 845.3337 | 846.3417 | 868.3229 | 868.42 | 41 |
| 2-IBA-Orn-Pro-D-Ala-Gln-Tle | 770.2612 | 771.2692 | 793.2504 | 793.74 | 24 |
| 2-IBA-Orn-Pro-D-Ala-Ser-Tle | 729.2347 | 730.2427 | 752.2239 | 752.39 | 33 |
| 2-IBA-Orn-Pro-D-Ala-Ala-Tle | 713.2398 | 714.2478 | 736.229 | 736.49 | 35 |
| 2-IBA-Orn-Pro-D-Ala-Trp-Tle | 828.282 | 829.29 | 851.2712 | 851.82 | 4.6 |
| 2-IBA-Orn-Pro-D-Ala-Glu-Tle | 771.2453 | 772.2533 | 794.2345 | 794.45 | 6.2 |
| 2-IBA-Orn-Pro-D-Ala-Nva-Tle | 741.2711 | 742.2791 | 764.2603 | 764.03 | 0 |
| 2-IBA-Orn-Pro-D-Ala-Leu-Tle | 755.2867 | 756.2947 | 778.2759 | 778.64 | 27 |
| 2-IBA-Orn-Pro-D-Ala-Bip-Tle | 865.3024 | 866.3104 | 888.2916 | 888.16 | 26 |
| 2-IBA-Orn-Pro-D-Ala-Tle-Tle | 755.2867 | 756.2947 | 778.2759 | 778.59 | 25 |
| 2-IBA-Orn-Pro-D-Ala-His-Tle | 779.2616 | 780.2696 | 802.2508 | 802.78 | 24 |
| 2-IBA-Orn-Pro-D-Ala-Asn-Tle | 756.2456 | 757.2536 | 779.2348 | 779.58 | 23 |
| 2-IBA-Orn-Pro-D-Ala-Tyr-Tle | 805.266 | 806.274 | 828.2552 | 828.52 | 6 |
| 2-IBA-Orn-Pro-D-Ala-Phg-Tle | 775.2554 | 776.2634 | 798.2446 | 798.66 | 0 |
| 2-IBA-Orn-Pro-D-Ala-Thr-Tle | 743.2503 | 744.2583 | 766.2395 | 766.35 | NS |
| 2-IBA-Orn-Pro-D-Ala-Lys-Tle | 770.2976 | 771.3056 | 793.2868 | 793.18 | 6.8 |
| 2-IBA-Orn-Pro-D-Ala-Nle-Tle | 755.2867 | 756.2947 | 778.2759 | 778.59 | 15 |
| 2-IBA-Orn-Pro-D-Ala-Orn-Tle | 756.282 | 757.29 | 779.2712 | 779.32 | 28 |
| 2-IBA-Orn-Pro-D-Ala-hPhe-Tle | 887.2867 | 888.2947 | 910.2759 | 910.59 | 37 |
| 2-IBA-Orn-Pro-D-Ala-dPhe-Tle | 865.3024 | 866.3104 | 888.2916 | 888.16 | 27 |
| 2-IBA-Orn-Pro-D-Ala-1-Nap-Tle | 839.2867 | 840.2947 | 862.2759 | 862,99 | NP |
| 2-IBA-Orn-Pro-D-Ala-4-Pya-Tle | 790.2663 | 791.2743 | 813.2555 | 813.55 | 9.3 |
| 2-IBA-Orn-Pro-D-Ala-2-Nap-Tle | 839.2867 | 840.2947 | 862.2759 | 862.59 | 5.6 |
| 2-IBA-Orn-Pro-D-Ala-3-Pya-Tle | 790.2663 | 791.2743 | 813.2555 | 813.54 | 0 |
| 2-IBA-Orn-Pro-D-Ala-2-Pya-Tle | 790.2663 | 791.2743 | 813.2555 | 813.75 | 20 |
| | | | | | |
| 2-IBA-Ile-Pro-D-Ala-Ile-Tle | 754.2915 | 755.2995 | 777.2807 | 777.17 | 17 |
| 2-IBA-Val-Pro-D-Ala-Ile-Tle | 740.2758 | 741.2838 | 763.265 | 763.85 | 10 |
| 2-IBA-Phe-Pro-D-Ala-Ile-Tle | 788.2758 | 789.2838 | 811.265 | 811.05 | NP |
| 2-IBA-Dap-Pro-D-Ala-Ile-Tle | 727.2554 | 728.2634 | 750.2446 | 750.46 | 5.7 |
| 2-IBA-Asp-Pro-D-Ala-Ile-Tle | 756.2344 | 757.2424 | 779.2236 | 779.43 | NP |
| 2-IBA-Abu-Pro-D-Ala-Ile-Tle | 726.2602 | 727.2682 | 749.2494 | 749.04 | NP |
| 2-IBA-tPhe-Pro-D-Ala-Ile-Tle | 844.3384 | 845.3464 | 867.3276 | 867.76 | 0 |
| 2-IBA-Gln-Pro-D-Ala-Ile-Tle | 769.266 | 770.274 | 792.2552 | 792.72 | 25 |
| 2-IBA-Ser-Pro-D-Ala-Ile-Tle | 728.2394 | 729.2474 | 751.2286 | 751.86 | 20 |

| | | | | | |
|---|---|---|---|---|---|
| 2-IBA-Ala-Pro-D-Ala-Ile-Tle | 712.2445 | 713.2525 | 735.2337 | 735.37 | 10 |
| 2-IBA-Trp-Pro-D-Ala-Ile-Tle | 827.2867 | 828.2947 | 850.2759 | 850.59 | 20 |
| 2-IBA-Glu-Pro-D-Ala-Ile-Tle | 770.25 | 771.258 | 793.2392 | 793.52 | 9.4 |
| 2-IBA-Nva-Pro-D-Ala-Ile-Tle | 740.2758 | 741.2838 | 763.265 | 763.85 | 16 |
| 2-IBA-Leu-Pro-D-Ala-Ile-Tle | 754.2915 | 755.2995 | 777.2807 | 777.17 | 22 |
| 2-IBA-Bip-Pro-D-Ala-Ile-Tle | 864.3071 | 865.3151 | 887.2963 | 887.13 | 0 |
| 2-IBA-Tle-Pro-D-Ala-Ile-Tle | 754.2915 | 755.2995 | 777.2807 | 777.76 | 15 |
| 2-IBA-His-Pro-D-Ala-Ile-Tle | 778.2663 | 779.2743 | 801.2555 | 801.55 | 14 |
| 2-IBA-Asn-Pro-D-Ala-Ile-Tle | 755.2503 | 756.2583 | 778.2395 | 778.95 | 19 |
| 2-IBA-Tyr-Pro-D-Ala-Ile-Tle | 804.2707 | 805.2787 | 827.2599 | 827.79 | 5 |
| 2-IBA-Phg-Pro-D-Ala-Ile-Tle | 774.2602 | 775.2682 | 797.2494 | 797.45 | 19 |
| 2-IBA-Thr-Pro-D-Ala-Ile-Tle | 742.2551 | 743.2631 | 765.2443 | 765.63 | 4.5 |
| 2-IBA-Lys-Pro-D-Ala-Ile-Tle | 769.3024 | 770.3104 | 792.2916 | 792.16 | 14 |
| 2-IBA-Nle-Pro-D-Ala-Ile-Tle | 754.2915 | 755.2995 | 777.2807 | 777.17 | 0 |
| 2-IBA-hPhe-Pro-D-Ala-Ile-Tle | 802.2915 | 803.2995 | 825.2807 | 825.14 | 16 |
| 2-IBA-dPhe-Pro-D-Ala-Ile-Tle | 864.3071 | 865.3151 | 887.2963 | 887.13 | 23 |
| 2-IBA-1-Nap-Pro-D-Ala-Ile-Tle | 838.2915 | 839.2995 | 861.2807 | 861.17 | 4.2 |
| 2-IBA-4-Pya-Pro-D-Ala-Ile-Tle | 789.2711 | 790.2791 | 812.2603 | 812.83 | 18 |
| 2-IBA-2-Nap-Pro-D-Ala-Ile-Tle | 838.2915 | 839.2995 | 861.2807 | 861.17 | 0 |
| 2-IBA-3-Pya-Pro-D-Ala-Ile-Tle | 789.2711 | 790.2791 | 812.2603 | 812.08 | 21 |
| 2-IBA-2-Pya-Pro-D-Ala-Ile-Tle | 789.2711 | 790.2791 | 812.2603 | 812.65 | 8.6 |